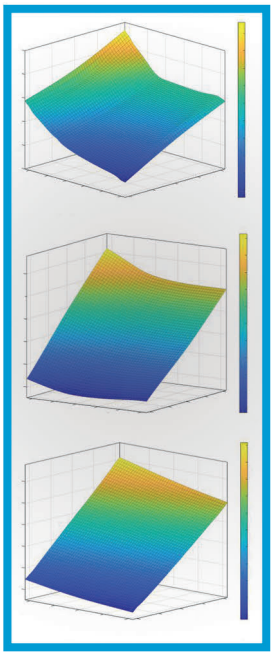

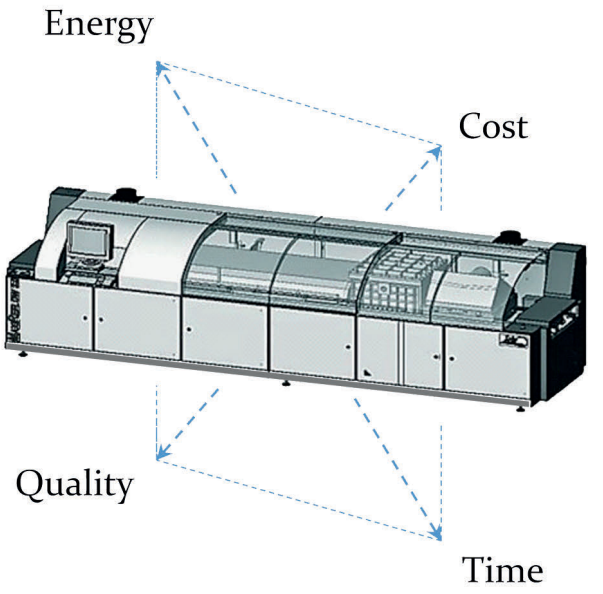

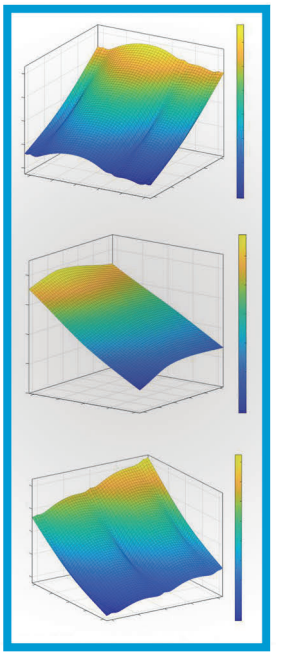

FAU Studien aus dem Maschinenbau 358

Alireza Esfandyari

Multi-Objective Process Optimization for Overpressure Reflow Soldering in Electronics Production

FAU UNIVERSITY PRESS

Alireza Esfandyari

Multi-Objective Process Optimization for Overpressure Reflow Soldering in Electronics Production

FAU Studien aus dem Maschinenbau

Band 358

Herausgeber der Reihe:

Prof. Dr.-Ing. Jörg Franke
Prof. Dr.-Ing. Nico Hanenkamp
Prof. Dr.-Ing. habil. Marion Merklein
Prof. Dr.-Ing. Michael Schmidt
Prof. Dr.-Ing. Sandro Wartzack

Alireza Esfandyari

Multi-Objective Process Optimization for Overpressure Reflow Soldering in Electronics Production

Dissertation aus dem Lehrstuhl für Fertigungsautomatisierung und Produktionssystematik (FAPS)
Prof. Dr.-Ing. Jörg Franke

Erlangen
FAU University Press
2020

Bibliografische Information der Deutschen Nationalbibliothek:
Die Deutsche Nationalbibliothek verzeichnet diese Publikation in der Deutschen Nationalbibliografie; detaillierte bibliografische Daten sind im Internet über http://dnb.d-nb.de abrufbar.

Bitte zitieren als
Esfandyari, Alireza. 2020. *Multi-Objective Process Optimization for Over-pressure Reflow Soldering in Electronics Production.* FAU Studien aus dem Maschinenbau Band 358. Erlangen: FAU University Press. DOI: 10.25593/ 978-3-96147-383-0.

Verlag und Auslieferung:
FAU University Press, Universitätsstraße 4, 91054 Erlangen

Druck: docupoint GmbH

ISBN: 978-3-96147-382-3 (Druckausgabe)
eISBN: 978-3-96147-383-0 (Online-Ausgabe)
ISSN: 2625-9974
DOI: 10.25593/ 978-3-96147-383-0

Multi-Objective Process Optimization for Overpressure Reflow Soldering in Electronics Production

Multikriterielle Prozessoptimierung beim Überdruck-Reflowlöten in der Elektronikproduktion

Der Technischen Fakultät
der Friedrich-Alexander-Universität
Erlangen-Nürnberg

zur
Erlangung des Doktorgrades Dr.-Ingenieur

vorgelegt von

MSc. Alireza Esfandyari
aus Teheran

Als Dissertation genehmigt
von der Technischen Fakultät
der Friedrich-Alexander-Universität Erlangen-Nürnberg

Tag der mündlichen Prüfung:	24.09.2020
Vorsitzender des Promotionsorgans:	Prof. Dr.-Ing. habil. Andreas Paul Fröba

Gutachter: Prof. Dr.-Ing. Jörg Franke
Prof. Dr.-Ing. Marcus Reichenberger
Prof. Dr.-Ing. Jürgen Karl

Preface

The present dissertation originated during my work as a research associate at the Institute for Factory Automation and Production Systems (FAPS) at the Friedrich-Alexander-Universität Erlangen-Nürnberg in Germany.

I would like to thank Prof. Dr.-Ing. Jörg Franke, the chairman of the Institute FAPS, and the first reviewer of this dissertation, for the scientific freedom, benevolent support and the trust given to me for carrying out this work. I would also like to sincerely thank him for taking over the presidency during my doctoral examination. Prof. Dr.-Ing. Jürgen Karl, the chairman of the Institute for Chair of Energy Process Engineering at the FAU Erlangen-Nuremberg, and Prof. Müller, I thank for their acceptance and support as reviewer for the doctoral thesis.

I would like to thank Prof. Dr.-Ing. Reichenberger at the University of Applied Sciences Nürnberg for his sincere support, and my colleagues especially at the research group of electronics production at FAPS, for the productive cooperation, the constructive professional discussions, the great willingness to help and the mutual support in the numerous projects. I would like to emphasize in this context mainly Dr. Andreas Reinhardt, Dr. Aarief Syed-Khaja, Dr. Christopher Kästle, Martin Müller, Alexander Hensel, Dr. Thomas Reitberger, Dr. Rene Schramm, Johannes Hörber, Dr. Stefan Härter and Dr. Bassim Bachy. For the collective experimental work and support, I thank Denis Kozic, Horst Schuster, Gerald Gion. Furthermore, I would like to thank all students and the student assistants for their dedication, which helped me with the research work and the realization of numerous ideas. My many thanks goes to the Michael Pfeffer, Thomas Kuhn, and Dr. Christian Goth for their contributions at the Institute.

Last but most important, my heartfelt thanks go to my mother. Thanks to their ongoing consideration and support, they have made the successful completion of this work possible.

Nürnberg, in 23.10.2020 Alireza Esfandyari

Table of Contents

List of Abbreviations and Symbols

Abbreviations

AC	Air Conditioning
ANN	Artificial Neural Network
ANOVA	Analysis of Variance
APC	Automatic Process Control
BP	Backpropagation
BR	Bayesian Regularization Backpropagation
CIP	Continuous Improvement Process
CGB	Conjugate Gradient Backpropagation
DT	Decision Trees
DOE	Design of Experiment
DES	Discrete Event Simulation
EEG	Erneuerbare Energien Gesetz
GA	Genetic Algorithms
GDM	Gradient Descent with Momentum
KPI	Key Performance Indicator
LED	Light-emitting Diode
LM	Levenberg-Marquardt backpropagation
LMS	Last Mean Square
IMC	Intermetallic Crystal
MES	Manufacturing Execution System
MIS	Management Information System
MLPs	Multilayer Perceptrons
MSE	Mean of Squared Errors
OSP	Organic Protection Passivation
PCB	Printed Circuit Board
PNN	Probabilistic Neural Networks
REA	Renewable Energy Act
RMS	Root Mean Square
RSM	Response Surface Method
RST	Rough Sets
SCG	Scaled Conjugate Gradient method backpropagation
SMCs	Surface Mounted Components
SMD	Surface Mounted Device
SOM	Self-organizing Maps

SMT	Surface Mounted Technology
SPC	Statistical Process Control
SVM	Support Vector Machine
TAL	Time Above Liquidus
SMCs	Surface Mounted Components
SMD	Surface Mounted Device
THD	Through-Hole Device
THT	Through-Hole Technology
USP	Unique Selling Proposition

Symbols

A	Ampere
c_p	Specific heat constant
°C	Celsius
ϵ	Random experimental error
E	Energy
E_X	Exergy
ε	Specific exergy
ΔG_f°	Gibbs free energy
H	Enthalpy
J	Joule
K	Kelvin
m	Mass
N	Newton
o	Output value
P_0	Ambient pressure
P_i	Pressure at a given state
Q	Heat
$\dot{Q}$	Heat flow
R^2	Absolute fraction of variance
R	Universal gas constant
r	Radius
S	Entropy
sec	Second
t	Target value
T_0	Ambient temperature
$T_{S_{max}}$	Maximum soaking temperature
$T_{S_{min}}$	Minimum soaking temperature
T_L	Liquidus temperature
T_P	Peak temperature
T_i	Temperature at a given state
t_L	Liquidus time
t_S	Soaking time
v	Specific volume
V	Volt
w_{Costs}	Weighting for the cost factor
w_{Energy}	Weighting for the energy factor
$w_{Quality}$	Weighting for the quality factor

w_{Time}	Weighting for the time factor
X	Atmospheric composition
X_i^e	Local atmospheric mole fraction
x_k	Number of control variables
y	Response of Interest
β	Vector of unknown constant parameters
φ	Relative humidity
$\eta_{Product}$	Actual product exergetic efficiency
$\eta_{net,max}$	Maximum net exergetic efficiency

List of Figures and Tables

Figures

Tables

1 Introduction

The success of a company is dependent on multiple internal and external factors that are classically divided in three categories, which are related to each other: time, costs and quality. The classical management approach to improve manufacturing performance is also built on the time-cost-quality trade-off theory. Those important factors are constantly controlled and evaluated. For time, the production lead-time is measured. For costs, the resource consumption and process dependent cost are considered. For quality, the first pass yield and the delivery quality can be measured. However with the rising importance of energy and resource consumption, the trade-off model was expanded by the factor energy and resource consumption in the frame of green controlling [1].

The desire to produce energy and resource efficiently began to grow caused not only by the rising energy expenses and by the increasing environmental awareness, but also through the legislations in energy policy by the German government. The electricity supply from renewable energy sources is regulated nationwide by the German law for development of renewable energies. The main driver of this development is the Renewable Energy Sources Act (EEG) of 2000, which aims to achieve an 80% share of renewable energies in the electricity mix by 2050. Renewable energy sources like wind power and photovoltaic are dependent on weather and daytime. While coal-fired and nuclear power plants produce electricity constantly, the supply from renewable energy sources is rather unstable. With its rising share, the electricity supply changes. To adapt to these changes, an adjustment in consumer behavior is necessary to ensure the stability of the electricity supply [2] [3] [4]. Beyond the legislations perspective, the annual greenhouse gas emissions shall be reduced by 80% up to 95% until 2050 in comparison to 1990 and Germany will refrain from using nuclear power [5].

For these reasons, the pressure on manufacturing companies for a resource efficient setup began to grow in recent years. Unlike the other factors in management trade-off performance, energy factor is difficult to measure. To determine the energy efficiency of processes, performance key indicators were developed for manufacturing processes with discrete production [6], as well as for energy-intensive industries with continuous production [7]. The exergy method is the most popular which is mostly used to investigate the complex thermodynamic processes such as textile and chemical industries, and less in manufacturing industries such as in

electronics production. Since energy methods only involve the 1st law of thermodynamics and thus ignore the difference between work and heat, these methods lack factors which are required to adequately show a system effectiveness utilizing given energy resources. Exergy methods also take the second law of thermodynamics into account, and therefore, better suited for thermodynamic processes. As for packaging process and electronics assembly, the soldering process is the most energy intensive process, and therefore exergy analysis suits to investigate the heat transfer complexities [8] [9].

Beyond the importance of energy factor, quality factor for electronic products is inevitably improving. Explicitly for modern electronics products increasingly demand the features of lighter weight, smaller size, and higher quality, high pin-count, and various other product configurations. This is particularly evident in mobile and telecommunication devices. Surface mount technology (SMT) is the primary method used to attach electronic components permanently onto the substrate. A crucial improvement in quality of connecting technologies is to avoid heat dissipation through the joints and increase the reliability of connectivity. Less creation of voids (pores) in solder joint obtains this advancement. While a significant level of voiding can be tolerated in solder joints where electrical conductivity is the main requirement, voiding at any level severely compromises thermal conductivity. For instance, in Light Emitting Diode (LED) lighting modules effective conduction of heat through the 1_{st} level die attach to the substrate and then through the 2_{nd} level attach to the heat sink is critical to performance so that voiding in the solder joints at both levels must be minimized. Voids in solder joints are the result of bubbles of gas that do not escape before the solder has solidified [10]. To release the entrapped bubbles several German technology producers have offered new solutions in the market. IBL Tech. combines the advantages of the vapor phase soldering technology with vacuum process. SEHO Systems GmbH offered a soldering oven combined with an overpressure module. These technologies are proving the reduction of voids and hence delivering namely a void-free solder joint.

Any of the four above explained criteria and factors for manufacturing performance of soldering process is solely optimizable. However, by deploying a trade-off decision making approach, a multi-objective optimization solution is obtainable. The decision making is considered as a problem with a finite set of projects, a finite set of criteria, and set of evaluations of projects with respect to criteria. In this study, the decision

projects are evaluated with respect to four criteria and a trade-off between energy, quality, cost and time. The feasibility of a multi-objective optimization and a multiple criterion decision making problem lies on the compromised intermediate preferences with respect to the set of objectives defined by the decision makers.

1.1 Objectives of the Thesis

To build a cumulative multi-objective solution for overpressure soldering process, each energy, quality, cost, and time criterion will be first optimized. First, the quality of soldering process and a void-free solder joint is targeted. The laboratory facilities from FAPS institute are used to conduct the study and acquire the data. The overpressure soldering concept is evidencing the improvement of void fraction reduction, however the process controlling mechanism and the impact on the final result should be furtherly investigated. A set of design of experiments is obtaining the platform to analyze the most influential variables on void reduction. The statistical analysis is obtaining the degree of influence and interaction of variables on the response and the void fraction creation. The variables interaction measure is targeting the overpressure module to realize the best mechanism for a void-free soldering process.

The most influential variables on quality are delivering soldering profiles that are used to investigate the optimization potentials for time, cost and energy factors. Therefore, the soldering process will be simulated to imitate the production lead-time per PCB to consider any non-productive time including the process breakages and non-predictable waiting times. A transparency model for resource flow is developed and the associated resources flow in the simulation model reveals the saving potentials, and it is obtaining the variable cost for the utilized resources per PCB. By development of “is-analysis” for the current resource flow, a method is utilized to investigate the value-added action in soldering process, and therefore defining a Key Performance Indicator (KPI), which is revealing the minimum required resource per PCB. The minimum required resource per each solder profile is statistical analyzed to realize the most influencing variable and therefore the potential saving measures to reduce the resource consumption and the incurred cost.

The variable set of input parameters for each response in the trade-off model for quality, energy, cost and time factor shall be optimized. Therefore, for the sake of comprehensibility and comparability, an intelligence-based algorithm and a mathematics-based model per each

criterion is developed. Further, the intelligence-based models are utilized as tools to predict the response values in the trade-off model. With respect to optimal solutions for each criterion, a holistic solution is not obtainable. Therefore, deployment of a ranking approach along a decision making model is delivering a compromised multi-objective optimization solution for overpressure soldering process.

1.2 Organization of the Dissertation

This study is divided into nine chapters. In the second chapter, the state-of-the-art for advanced soldering technologies for a void-free soldering process is elaborated. Further, the classical project management trade-off model is explained and extended by the energy criterion. The constraints per each criterion are defined, and the overviews of the mathematical methods are presented which are utilized for analysis, modeling and process optimization.

Chapter three introduces primarily an Ishikawa diagram and Five-M diagram for soldering process. A *method* is presented which is formulating the connection of objectives, the trade-off model and the methods that are used to target a multi-objective process optimization. Furthermore, *materials* and *machines* that are utilized to conduct, test and analyze the experimental part of this study are presented. *Manpower* and *mother nature* are excluded in this study.

Chapter four is aiming to study the thermal profiling process in terms of quality criterion optimization. The soldering oven technology integrated with overpressure module is investigated in detail to identify the most influencing variables on quality indicators. These variables are examined as set of experiments in screening process before the full factorial design of experiment due to the sake of cost and time saving. In parallel with the conduction of final design of experiment, the production lead-time and the electrical energy consumption of the oven technology are measured. The data from this set of experiments are utilized for the multi-objective optimization approach.

The chapter five is presenting a control procedure for the resource flow in soldering process. In order to cope with the dynamics of the process chains, simulation method is a promising approach. Therefore, first a transparency model is developed which is illustrating the flow of electrical energy of the oven technology and auxiliary equipment in periphery levels. Then a simulation tool is utilized by means of imitation purposes

in order to consider the predictable and non-predictable process breaks in the total power consumption of the case study soldering process. By realizing the resource flow balance of the process an exergy method is conducted and the investigation is followed by statistical analysis. The analysis is presented by a meta-model to realize the most influencing setup parameters of the oven technology on periphery levels and how to deduce the increase of the exergy efficiency of the process. In the following part of this chapter, the cost analysis is conducted. The cost for the process-related resource flow is elaborated, and the statistical analysis of the total cost is revealing the effect of oven technology setup changes and the respective power consumption interaction on the total cost of the PCB product.

In the chapter six, the soldering process is mathematically modeled for prediction application and to study the behavior of the system. The experimental designs are obtaining the input data for the Artificial Neural Networks (ANN) and Response Surface Method (RSM) models. The ANN model is starting with definition of input and response parameters, creation of the topology and the model architecture. The data training process and the measure of the error given by the verified models are demonstrating the reliability of the ANN model for the given data series. The RSM model is created based on the given solutions by the software, and hence after definition of the problem, input and response data, the reliability of the model is verified by the obtained set of statistical data. Once the reliabilities of models are proven, the experimental input data are used for the prediction application and to check the error deviation. The model with less error ratio is selected for further prediction of input data which are not set in the initial DOE.

In chapter seven, a compromised intermediate equation model is presented which is obtaining a decision-based optimization solution. Finding the optimal solution for all these responses however is possible but not satisfactory, due to the fact that a holistic solution is not obtainable. Therefore, a trade-off performance model is developed that the decision maker is able to achieve the target setup including the boundary of set of optimized performances. A vector-based compromised solution is presented to control the weight of all performances for a multi-objective solution. The optimized solutions are furtherly experimentally verified to prove the accuracy of the developed prediction models.

2 State-of-the-art Technologies, Concerns and Optimization Solutions

This chapter gives an overview on the state of science, technology and methodology, which is necessary to understand this study. Firstly, the electronics production process chain is briefly explained. The focus is on the convection-based reflow soldering process and enhanced technologies to reduce voids in solder joints. Furtherly, the expansion of the classical project management trade-off model by the energy criterion for a comprehensive evaluation and multi-optimization of soldering process is elaborated. Lastly, the mathematical methods utilized for the analysis, modeling and process optimization are discussed.

2.1 Soldering Process Technology and the Mechanisms

2.1.1 Surface Mount Technology (SMT) Assembly

The production of electronic devices usually follows a certain pattern, in which Printed Circuit Board (PCB) assembly is an essential part of the manufacturing process. The Surface Mount Technology (SMT) is an important method used to directly attach the Surface Mounted Components (SMCs) onto the pads of the PCB, as shown in Figure 1.

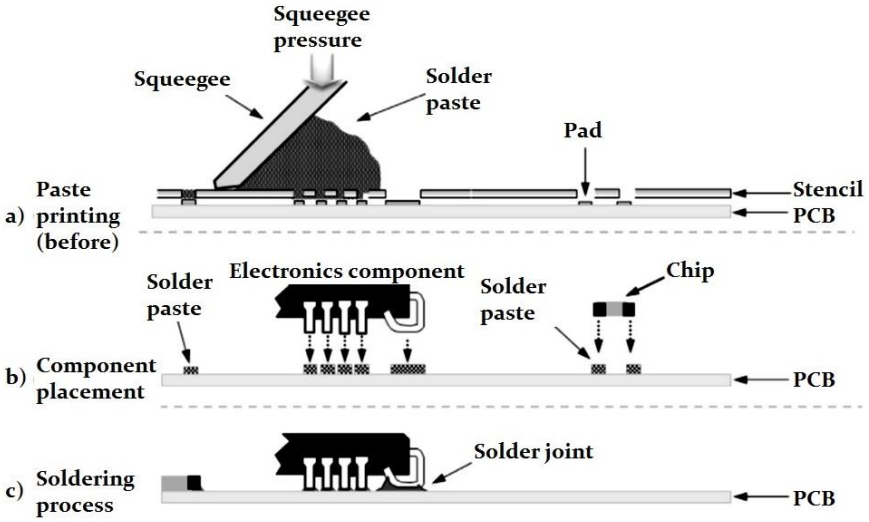

Figure 1: The Surface Mount Technology (SMT) assembly process [11]

The SMT assembly consists of three consecutive process steps: pasting the solder material through stencil printing, component placement process using an automated robotic system, and the soldering process. In Surface Mount Assembly (SMA), the solder paste is first deposited onto the solder pads of the PCB through stencil printing application (Figure 1, a)). In the next step, as shown in Figure 1, b), the SMCs are placed on the substrate using a placing machine. The mounted substrates are then conveyed into a soldering oven to form strong solder joints (Figure 1, c)) [12]. Lastly, the mounted boards are sent to visual inspection process using an Automated Optical Inspection (AOI) system to prove the solder joint quality. If soldering failures or the solder joints defects occur, the defective boards are sent to rework station for correction [13].

2.1.2 Convection-based Soldering Process

The solder reflow process is one of the key determinants of SMT assembly. A thermal profile is indicated by a time-temperature graph that is used to control the heating rate on the PCB product in the reflow oven. The heat in the convection-based reflow soldering oven is generated by reflow convection modules, and a turbulently flowing gas generated via air jets transmits a uniform temperature on the PCB [14].

In the convection-based soldering oven, as shown in Figure 2 for a typical profile for lead-free solder alloys, the substrate and the components are warmed up in the preheating zone, where the temperature quickly rises from ambient temperature to about 160 °C. An increase in temperature to 190 °C activates the flux and it is wetting[1] the metallic surfaces of the solder pads and component leads in the soaking zone in the soaking temperature (T_S). In the reflow zone, the solder particles are melted and liquefied in liquidus temperature (T_L) for the liquidus time (t_L). The PCB is furtherly heated up to the peak temperature (T_P), which is held for the peak time (t_P). During this process, an intermetallic layer between the solder material, the copper and the metal part of electronics component is formed.

[1] Wetting is the ability of a liquid to maintain contact with a solid surface, resulting from intermolecular interactions when the two are brought together.

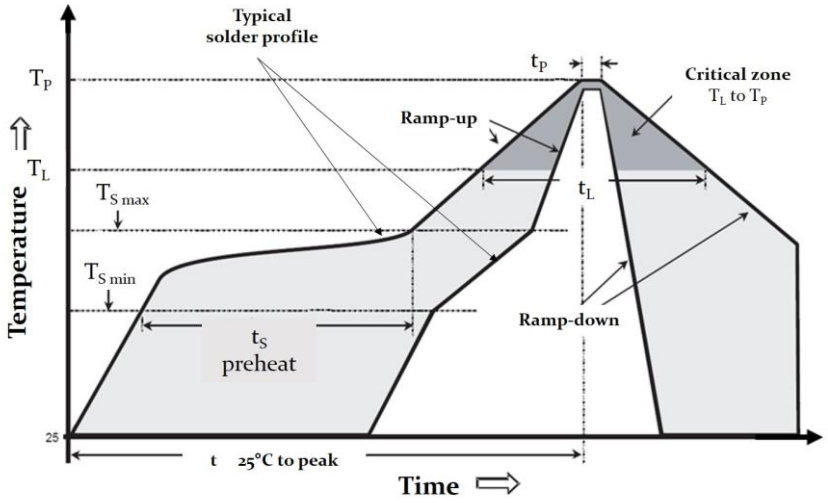

Figure 2: Conventional reflow soldering temperature profile

An Intermetallic Crystal (IMC) is a combination of all base metals that provides the mechanical and electrical integrity of the solder joint. When soldering to a copper substrate with the standard Sn-based solder material, two types of IMCs are formed (Figure 3). The copper-rich Cu_3Sn intermetallic, which melts at 670 °C, is found near the substrate, while the tin-rich Cu_6Sn_5, which melts at 415 °C, is found throughout the joint. As the melting temperatures of these are significantly higher than soldering temperatures, they will not be melted during the reflow process and thus will remain in the joint as occlusions. During soldering, the intermetallic crystals are formed. This IMC will continue to form at a slower rate in the solid phase. The growth as a solid is driven by temperature; as the solder profile approaches its melting point, the rate of IMC growth increases [15].

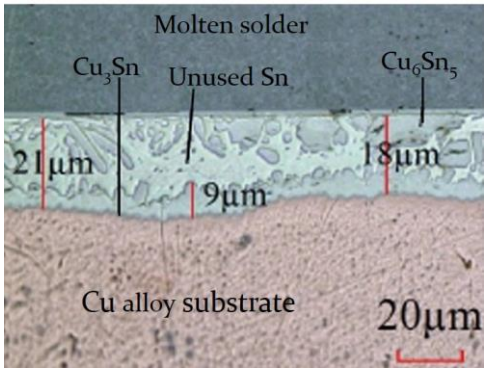

Figure 3: Intermetallic formation between copper and tin [16]

Finally, strong solder joints between component leads and solder pads are formed in the cooling zone of the reflow technology. The heating parameter settings such as working mode of the reflow oven, conveyor speed, solder paste ingredients, and number of components assembled can affect the acceptance of a thermal profile. The use of an inadequate thermal profile can generate numerous soldering failures such as, solder balling, tombstoning, solder voiding, solder bridging, and incomplete solder joints [17] [18] [19].

2.1.3 Solder Joint Defects in Electronics Production

Solder joint quality is extremely important in order to assure the reliability of electronic products in the electronics assembly [20] [21]. The reflow soldering process is recognized as one of the major sources of soldering defects [14]. The thermal profiling and the machine setup is highly dependent on the type of solder alloy material, and hence by the change of product, the oven machine should be reconfigured. The homogeneity and the efficiency of the heat transport have strong influence on the solder joints, because an inhomogeneous temperature profile can cause reflow soldering failures [18] [22]. The common solder joint defects are shown in Figure 4.

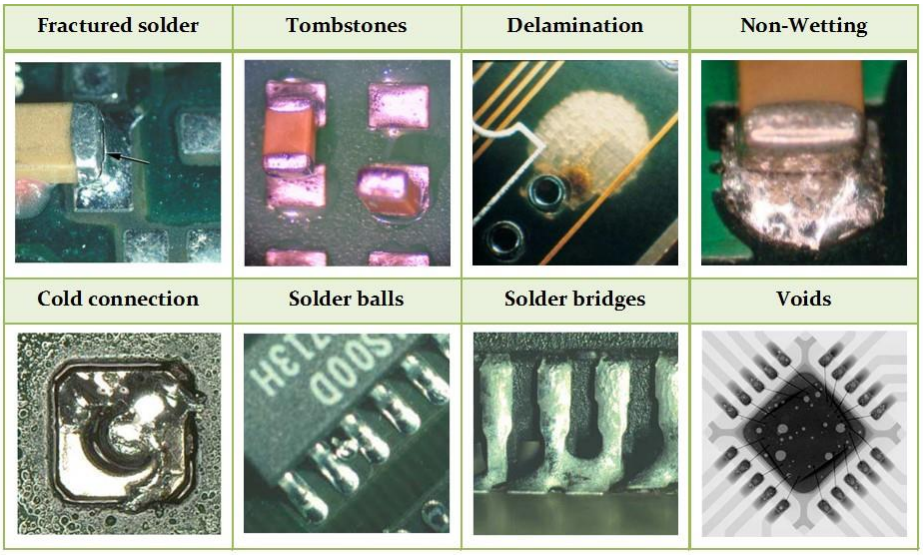

Figure 4: Common solder joint defects [23]

Several studies were conducted to examine the effect of thermal management and heating transfer capability examination of reflow ovens. These are including the application of simple temperature distribution measurements [24] [25], simulation process [26] [26], thermal models of the reflow process[22] [27], heat gas circulation and heat transfer coefficient [22] [28] investigations. In practice, the defect on the PCB as the result of an inhomogeneous heat transfer requires additional repairs and reworking that can cause a loss of productivity of roughly 30–50% of the total manufacturing costs [29], and therefore they should be avoided.

Fractured solder

Fractured solder joints are an uncommon solder joint defect, which is normally caused by thermal expansion of the joint. To keep the mechanical stress as low as possible, the cooling rate should be low. However, the higher the solder joint cooling rate, the higher its strength will be [23] [30].

Tombstones

Tombstones describe an effect when components rise on one side during the soldering process. It occurs especially on small and light two-pole components. The effect arises when one side of the solder liquefies earlier than the other. Reasons for this behavior can be placement process or the temperature profiling. A slow heating in the preheating helps to avoid tombstoning. Depending on the angle, tombstones can be detected visually [23] [31] [32].

Delamination

Delamination is a partial separation of the base material layers. In the delamination area, the material strength is reduced and components might come off. Delamination is caused by excessive thermal stress on the PCB, humidity or impurities in the material. According to the IPC-A-610D, delamination is still acceptable if its ratio is under 30%. To avoid delamination, the soldering process should be shortened or conducted at lower temperatures [23] [32].

Non-wetting

Non-wetting is the incapability of molten solder to engage a metallurgical connection with the basis metal. To avoid non-wetting, the flux should be fully activated. Therefore, the length of temperature profile must be long enough to completely activate the flux, but not too long to avoid consuming its activator too early. Additionally, it must be warm enough

to melt the solder, but not too hot as this can cause unwanted oxidation processes [23] [31].

Cold connection

A cold connection is a poorly wetted solder joint which appears grey. This is caused by inadequate cleaning and lubricated surface before the soldering process and/or insufficient heat supply during the soldering process [23].

Solder balls

Solder balls are balls out of solder, which remain after the soldering process. They can be caused by numerous reasons like spattering, excessive oxidation or poor process conditions causing gassing from the flux. Solder balls are acceptable, if they are embedded, encapsulated, fixed or do not violate the minimum electrical isolation distance. Despite the majority of solder balls is not caused during the soldering process, a slow heating in preheating zone helps to avoid them [23] [31].

Solder bridges

Solder bridges occur when the solder is not able to separate from two or more electrical connections. After the solidification, the unwanted connection might cause short circuits. To avoid solder bridges, a low heating rate is recommended [18] [23].

Voids

Voids are small inclusions of gas or fluid in the solder joint. If the voids are big enough or placed in an unfavorable order, they decrease the mechanical strength of the solder joint. Additionally, voids change the thermal and electrical properties of the solder joint. Voids should be investigated by X-ray technology and it is very difficult to avoid them completely. According to IPC-A-610D, a void ratio of 30% or less is acceptable and a higher fraction is considered as defect. IPC-A-610D is also classifying the electronics products into class 1, 2 and 3, which class 1 allows a void ratio up to 30% for general electronics products application, and class 3 for high-performance electronic devices should be less than 5% and it allows no voids [18] [23] [33] [34]. The void fraction should be directly agreed with the customer.

2.1.4 Mechanism of Void Creation in Solder Joint

The influencing factors on void development can be divided in the four categories: soldering process, PCB, solder paste and electronic components (Figure 5). Diehm et al. [33] investigated the influence of these factors on void creation. Regarding the soldering process it is concluded that the applied soldering technique, the temperature profile, the soldering atmosphere, the soldering temperature, the holding time above the liquidus temperature and the environmental conditions are influencing the void development. Also, the solder paste alloy composition, powder quality, powder size, metal content and flux composition. The substrate material has an influence on void development, as well as the surface metallization, the surface condition, and the solder resist and MicroVia[2] [35] [36].

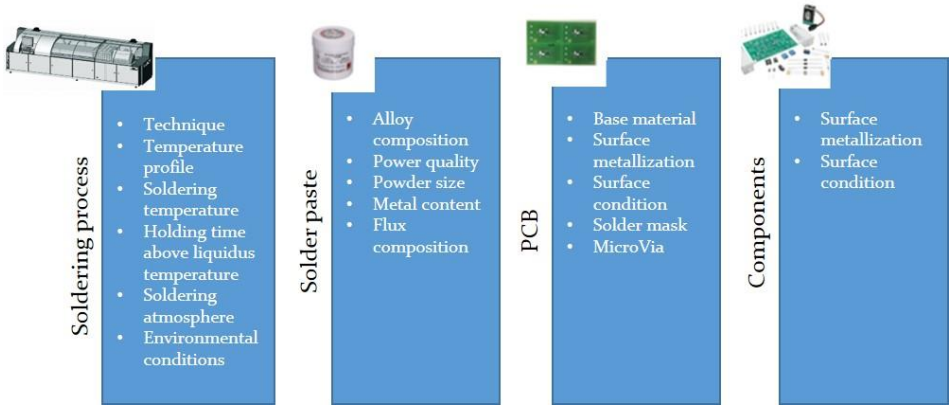

Figure 5: Influential factors on voids development [37]

The homogeneity of the solder joint is crucial for better thermal and electrical performance. Apart from the utilized material, the soldering thermal treatment is changing the form of void creation process. In soldering process, voids formed due to poor wetting of the parent materials or improper outgassing and it impairs the homogeneity and degrade the product service lifetime [16]. Especially in large-area solder connections and power electronics, voids if not outgassed properly result in tilting or even damage of the component. Also, the connection between the size and position of voids in the solder joint may affect the reliability of the solder joint during the use phase of the product life cycle.

[2] Microvias are holes drilled by a laser to generate the electrical connection between the layers in a multilayer circuit board. Via in pad microvias play a decisive role in the miniaturization of circuit boards.

Therefore, commonly the destructive tests such as shear force test are conducted to study the connection of the size and position of voids with the reliability of the solder joint.

Voids in the solder joints are nearly inevitable for common reflow soldering process conditions. As shown in Figure 6, after the placement process of electronic component, the solder material in the reflow oven is starting to melt. First, the solvent material is starting to evaporate, the smaller voids are forming larger voids. If the solder paste is melting sooner than the alloy of the solder balls, the evaporating flux has a chance to escape from solder gap before the balls are melting. Hence, less gases and residues will be enclosed in the solder joints in this case [33]. Therefore, the ingredients of the solder pastes, the evaporation temperature of solvent, which are evaporating during the soldering process, affect the final amount of enclosure gases.

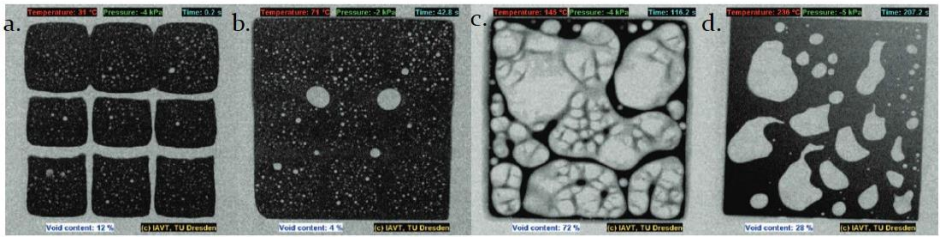

Figure 6: Soldering process from left to right: a. after placement, b. solving agent starts to evaporate, c. solving agent is vaporized, d. gas production after melting of solder [38]

The gas created in molten solder is in a thermodynamically unstable situation. The bubble creates an additional surface in the solder, which means that the free energy of the system is higher than it would be if the gas had escaped. The extra free energy provides a driving force for larger bubbles which have a smaller surface area to-volume ratio, to grow at the expense of smaller bubbles. However, if this occurs only by gaseous diffusion through the liquid the process is very slow. Faster growth can occur by coalescence if the bubbles are being moved by other forces so that they come into contact with other bubbles. In such a contact the micro voids will be absorbed into the macro voids with a net reduction in the area of the gas/solder interface. In reflowing solder paste there is sufficient movement for that to occur so that voiding in solder joints typically occurs as a relatively small number of larger voids [10]. Because of the ambition of gas bubbles and liquid enclosures to minimize their surface, the voids will contract in the solder gap depending on the size. Because the distribution of voids in the solder gap is rarely uniform and

micro voids can cumulate to larger voids, a tilting of component is the result as a rule. A high tilt intensifies inevitably the inhomogeneity, the non-uniform distribution of currents and temperature and the thermomechanical stress [33].

By introduction of lead-free solders with the well-known difficulties of poor wetting and smaller process windows the outgassing process of voids has become more acute. Through wetting balance analysis, a faster wetting and shorter profiles at 10% above the melting point of solder alloy contribute to reduce voids and increase the chance of bubbles leaving the solder joint [33]. The Fraunhofer Institutes IZM and ISiT have investigated the forming and development of voids with more than 200 test boards in a joint research project [39]. Solder joints were observed by X-ray analysis also during the soldering process in this project. It was clearly visible that voids that have already been formed will never escape if keeping the soldering temperature. In addition, the apparent effect can be observed: the voids increase during holding of soldering temperature. However, this is usually caused by the accumulation of several smaller voids, which are under the resolution limit themselves, into larger voids with clearly visible sizes. But there are also some cases, when voids can be formed by dewetting[3] effects of component terminations or outgassing from PCB material during dwelling of soldering temperature [33].

2.1.5 Void Mitigation Strategies in Soldering Process

The Young-Laplace equation is explaining the capillary pressure difference sustained across the interface between static fluids. According to this equation for a particular bubble, assuming the mass of the gas contained is fixed, the size of the bubble at a given temperature depends on the surface tension of the solder and the atmospheric pressure. The tension of the surface behaves against the pressure limiting the size of the bubble can reach for a given constant pressure. It is clear therefore if the surface tension is smaller, the overpressure that can be sustained is reduced, and for a given mass of contained volatiles, the bubble can increase in size [10].

According to this principle, the key elements of void mitigation either could be the alloy combination with the flux and solvent of solder, or the

[3] The terms de- or nonwetting are applied when a surface does not accept the liquid solder. In this case, no diffusional reaction between the liquid solder and the interface of the substrate takes place, and a diffusion layer in the form of an intermetallic zone is not formed.

change of atmospheric soldering process controls. If voids are produced due to improper outgassing process of solvent, then the size of a void that can reach and the ease with which it can break through the surface of the solder and escape is affected by the surface tension of the solder. A lower surface tension of the molten solder is obtaining a larger void, and more likely a higher chance to intersect the solder surface and release of entrapped bubble.

By considering the void mitigation through elimination of solvents from the formulation of the solder paste ingredients, either flux should be not begin to volatile or decompose to create gas until late in the reflow profile. Therefore, the solvent should be completely evaporated in the preheating or just before the reflow phase. However, other ingredients in the flux medium, the resins, activators, thixotropic agents, and stabilizers should remain stable with minimal release of volatiles, particularly during the latter part of the profile when the solder is molten (time above liquidus) [10]. Due to the uncontrollable evaporation of flux, hence it is impossible to assure the complete release of gas before the reflow process. By controlling the atmospheric pressure of the solder material and reducing the surface tension helps the gases trapped in the solder material reaching to the surface. Hence, as shown in Figure 7, a pressure difference between the solvent gas and the environment is demanding when the solder material is in liquid state.

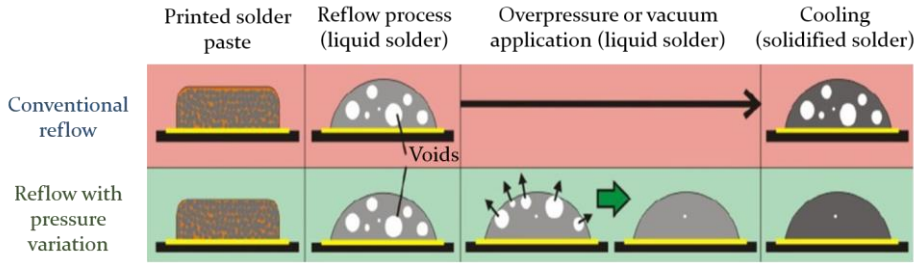

Figure 7: Effects of pressure change during reflow soldering process [40]

2.1.6 Mechanisms of Void-free Soldering Process Technologies

An approach presented for reflow soldering through pressure difference is soldering process combined with a vacuum module. Thereby, the vacuum process is added as module after the peak zone. Vacuum is defined as the state of a gas, when its pressure and thus the particle-number density is lower within than it is outside of its container [41]. Diehm et al. [33] has

suggested that a minimum of 100 mbar pressure difference between inside of void and its environment is necessary to remove gases. This means, that after soldering at normal pressure, the ambient pressure must decrease to 900 mbar or less in order to remove voids. As shown in Figure 7, the gas and flux inclusions in the solder joints expand during the vacuum phase and move out of the joint. The vacuum is generated when the peak temperature is reached. At this point, the solder is liquid. When comparing the temperature profiles of a conventional reflow soldering process and a vacuum reflow soldering process, it is conspicuous that for the vacuum process, the peak temperature needs to be held longer Figure 8, b). This is because the void reduction process must not be run too quickly [42].

There are several disadvantages of a vacuum in soldering process. During the vacuum process, the PCB materials and some components are tending to excessive outgassing. Therefore, the targeted vacuum will be achieved very slowly. In addition, some electrolyte capacitors cannot tolerate the vacuum process because of the hermetically enclosed liquids. Another drawback is that heat cannot be transferred in the vacuum with the usual convection heating but only by means of infrared radiation or heat conduction. Both heating methods are not sufficient for the use on PCBs.

The assemblies have to be heated sufficiently during the soldering process, so that the solder is still liquid in the following vacuum process. To ensure the minimum thermal radiation exposure on the PCB product during the vacuum process, it is essential to achieve a fast transition from the soldering zone into the vacuum area which requires a powerful lock and pump system as well as optimum vacuum pressure process [33]. However, the technology producers are currently convinced that no additional infrared heater is required when the PCB enters the vacuum zone, because the body of the vacuum module is hot enough to radiate the heat onto the substrate and therefore onto the solder material.

Diehm et al. [33] presumed that for the removal of voids, it is not the absolute vacuum pressure that is important, but much more the difference of pressure between void and environment. With this assumption, Klemm et al. [43] conducted a study in a laboratory scale, to investigate the effect of both process types of overpressure and vacuum with In-situ-X-ray-analysis. The results are demonstrating that overpressure Figure 8, c) reduces the solvent gaseous process significantly whereas vacuum Figure 8, b) accelerates it. The melting temperature of the solder is not affected by the pressure change, but the atmospheric

pressure influences the boiling temperature of the solvent significantly. After melting the solder material, the overpressure profiles show a much higher amount of voids in the solder joint than the profiles with negative pressure.

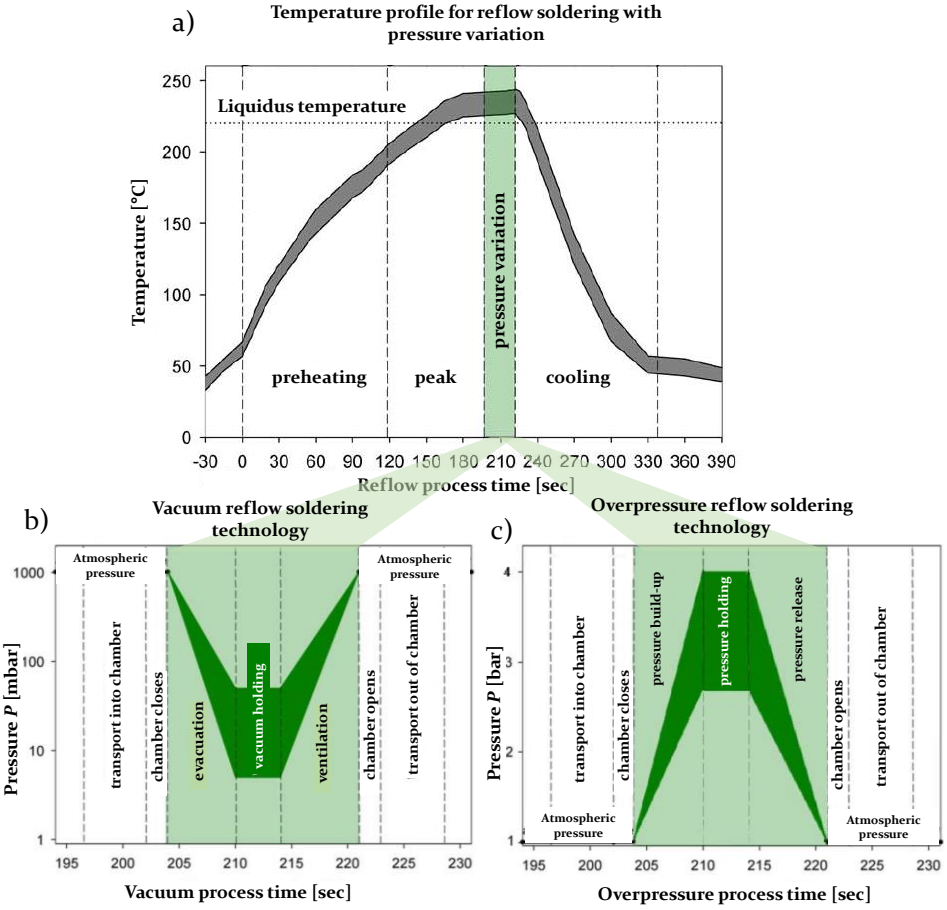

Figure 8: Schematic design of the conventional and the reflow process with pressure variation: a) Soldering with pressure variation, b) Vacuum reflow soldering, c) Overpressure reflow soldering [33] [40]

For both vacuum and overpressure profiles, the number of voids does not change significantly during the pressure release. The observed phenomenon can be explained with Le Chatelier principle. This principle states that the application of pressure on a gas producing chemical reaction slows this reaction down. The higher the pressure, the slower the reaction gets. It means that vacuum process support the reduction of oxides by the flux and overpressure process hinders it. Therefore, vacuum

processes do always exhibit a better wetting behavior of the solder than conventional reflow or overpressure processes. According to Le Chatelier principle it is possible to control the speed of the flux reaction and thereby the intensity of gas production by controlling the atmospheric pressure [43]. The overpressure allows heating of assemblies with forced gas convection, with similar thermal behavior like standard reflow soldering and all its advantages, such as low temperature differences (delta *T*), good heat transfer and controlled heating process [33]. Moreover, outgassing materials and leaking components are not likely to result from a soldering process with elevated pressure. Less mechanical parts construction is needed to reach a high pressure range from 1–4 bar which can be released instantaneously to make voids leave the liquid solder depot [9] [33]. Hence, it is inferred that any of vacuum and overpressure processes for a void-free solder joint has advantages and disadvantages. The focus of this study yields on the soldering process with overpressure module.

2.2 Classical Project Management Trade-Off Model as a Multi-Objective Optimization and Decision Making Method

The classical project management is built on the trade-off theory for time, cost and quality, and it has been investigated as a decision making tool vastly in construction management and project scheduling [44] [45] [46] as well as for manufacturing operation [47] [48]. An approach to provide compromise solutions in the trade-off is using the multi-objective algorithms. The solution methods can be categorized into three main groups, namely, (1) mathematical algorithms, (2) heuristic algorithms, and (3) evolutionary algorithms. Among these groups, evolutionary algorithms and artificial intelligence are the most favorable ones because of the fact that they are capable to deal with more than one objective, easily achieve diverse solutions in complex problems compared to the other algorithms [49].

Another approach for a decision making situation is to find the trade-off between the criteria. The decision making is considered as a problem with a finite set of projects, a finite set of criteria, and set of evaluations of projects with respect to all criteria. In this case, the decision projects are evaluated with respect to three criteria: the project completion time, total cost, and quality. The solution of multiple criterion decision making

problems is possible if the decision maker is able to provide information of his preferences with respect to the set of objectives and consideration.

To build cumulative and lasting manufacturing capability, enhancement should be designed first towards enhancing the time efficiency, shorted lead-time and minimum cost, then while the efforts to enhance time efficiency are further expanded, attention should be paid to improve the quality [50]. While efforts on the previous two are further enhanced, direct attention can be paid to energy efficiency [51]. Energy efficiency is a recent topic highly raised in the attentions which completes the conventional trade-off model and it is addressing the resources as energy and material which are consumed in a manufacturing process. Therefore, as shown in Figure 9, the energy is used as the fourth criterion in the decision making trade-off model [1] [52].

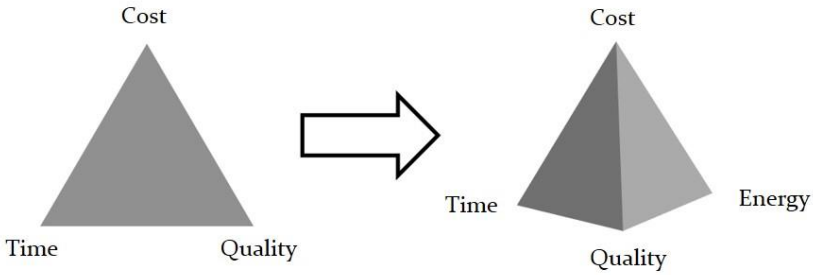

Figure 9: Extended project management trade-off in manufacturing operation [52] [53]

In manufacturing companies the performance of each criterion is controlled by the operation controlling department. The fulfillment of the goals of the company is evaluated and controlled with the help of operation performance indicators. Indicators are crucial performance parameters that represent a specific value over a defined period or unit. Table 1 shows the measured factors, Key Performance Indicators (KPIs), Management Information System (MIS) and Unique Selling Proposition (USP) as evaluation factors for different trade-off criteria of the extended trade-off model [1] [53]. At each level of transparency, there are indicators for evaluation and control which are defined per each criterion. For the measurement there are quantifiable definitions such as production lead-time, material costs, delivery quality or electrical energy consumption. For KPI level, quantifying the relevant proportion per part is illustrating the performance of criteria. In this level, part is chosen as an indicating unit however further dentitions such any value-added benefit could be also utilized upon the requirements of performance evaluation. MIS provide the necessary information to the controlling department and enable a

continuous improvement by using the information flow of process operation. USP is the factor or consideration presented by a seller as the reason that one product or service is different from and better than that of the competition.

Table 1: Levels of transparency for the extended trade-off model [1]

Levels of transparency	Time	Cost	Quality	Energy
Measurements	▪ Production lead-time ▪ Setup time ▪ Delivery time	▪ Material cost ▪ Personnel cost ▪ Capital cost	▪ First pass yield ▪ Delivery quality	▪ Electrical energy Consumption
Key performance indicators (KPIs)	▪ Parts replacement time	▪ Proportion of personnel cost per part	▪ Proportion of warranty cost per part	▪ Energy cost per part
Management information system (MIS)	▪ Machine data collection	▪ Enterprise Resource Planning (ERP)	▪ Production data collection	▪ Green controlling
Unique selling proposition (USP)	▪ Delivery time	▪ Overall operating cost	▪ Durability	▪ Lowest energy use

This work is considering the two transparency level from the measurements and KPIs to define the indicators for each criterion which enable the evaluation and comparison of different soldering process profiles in terms of the trade-off model.

2.2.1 Energy as a Crucial Criterion in Classical Trade-off Model

Industrial activity, and in particular the manufacturing sector, has a large environmental burden associated with it. In the recent years, manufacturing companies started to change their production to produce more resource efficient. This is not only caused by the rising energy expenses and the increasing environmental awareness, but also by the German government energy policy. German manufacturing industries are responsible for about 47% of the total national energy consumption. This makes the energy efficiency in manufacturing systems not only a single company issue but also a national or even global challenge [54].

Therefore, the Co_2 emissions reduction target of at least 40% in 2022 for Germany is impossible to reach without involving the industry sector [55]. Due to these facts, since recent years the German government offered several research programs and incentives to reduce energy consumption in manufacturing sectors.

For instance, several research projects have been launched to reduce the energy consumption in manufacturing industries. EniPROD (Energy Efficient Production Processes) project, which is coordinated by the Technical University of Chemnitz, is aiming is to increase the resource efficiency of the production processes [56]. The SimEnergy project is aiming to predict and optimize the energy usage in automobile industry using Discrete Event Simulation (DES) approaches [57]. EnEffaH (Energy Efficiency in Production in the Drive and Handling Technology Field), is conducted by the Institute for System Dynamics, University of Stuttgart, and it is developing methods, tools and products for an energy efficient automation [58]. Further above, to handle the flexibility of energy sources, the Bavarian Research Foundation provided grants for the project FOREnergy which is aiming to define concepts and solutions for energy flexibility in production. This project started in 2012 and is conducted by several research institutes and partners from industry within the Free State of Bavaria [59]. Further collaborative project granted by the Free State of Bavaria is so-called Green Factory Bavaria (GFB). This project involves several universities and industries in Bavaria (e.g. University of Erlangen-Nuremberg, Technical University of Munich, University of Applied Sciences Nuremberg, Fraunhofer Institute, and industry partners such as Siemens AG and Audi AG, etc.). The core objective of this project is the transfer of knowledge from applied research to industries (mainly small and medium sized companies) to increase energy and resource efficiency of manufacturing processes. To achieve this objective the "Green Factories" in Bavaria are constructed as a demonstration, learning and research platform. Both technical solutions and methodology are developed to reduce energy consumption in production processes [60].

The premier requirement of energy efficiency in manufacturing is to apply methods to transparent the energy consumption along the manufacturing chain. An important part of reducing the energy demand is to effectively measure, calculate, and evaluate the efficiency of production flow in order to realize the optimization potentials. The DIN EN ISO 9000:2005 defines efficiency as follows: "the relationship between the result achieved and the resources used." Following this standard definition, energy efficiency represents the ratio of consumed energy (e.g. kWh) to the generated

benefits (e.g. units produced or value). It corresponds to the productivity that describes the ratio of produced goods (output) to the consumed production resources (inputs) [6]. Another possibility for the definition of energy efficiency in manufacturing is the ratio of the real productivity to the ideal productivity. Here, the question is answered of how the actual produced goods (e.g. the amount) correspond with the defined energy input, i.e. the possible number under ideal conditions [61].

Several strategies are deployed to transparent and control the energy flow of manufacturing processes. As an example in a broader perspective for Manufacturing Execution System (MES) [62], a strategy is developed in which each process is segmented into specific manufacturing operations with a specific energy consumption which is so-called EnergyBlocks [63]. As shown in Figure 10, the energy profile of every manufacturing machine, such as the machining center or transport system, is considered as input data for a defined segment.

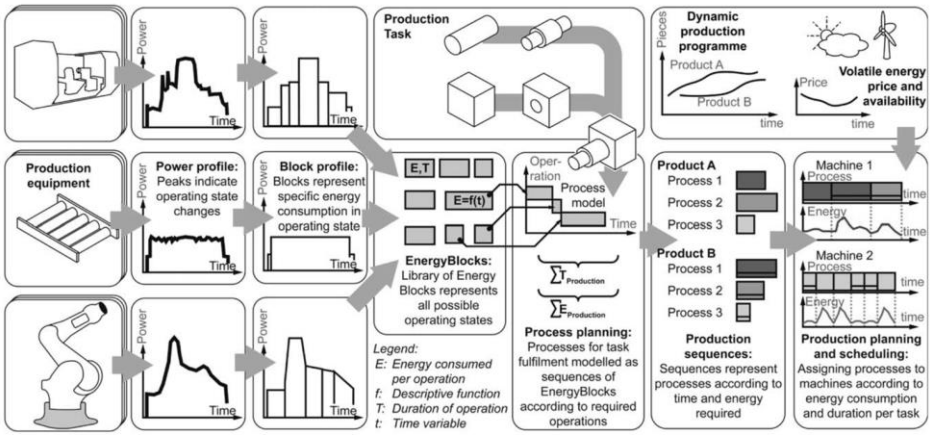

Figure 10: Energy consumption in manufacturing chain blocks [63]

To identify the energy saving potentials, the optimization of the manufacturing sequences are necessary. The key factors to achieve accurate EnergyBlocks data are the data sources and the information flow of the energy profile of every manufacturing machine. The collection, visualization [64] and analysis of the data either could be conducted by modeling and simulation [54] [65], or by mathematical modeling [63]. Such approaches are designed to assist engineers for planning and scheduling handling or assembly processes in order to optimize their energy consumption.

2.2.2 Energy Key Performance Indicators (KPIs)

Key Performance Indicators (KPIs) enable manufacturing companies to keep track of the continuous improvement of a production system, and it avoids uncertainty in the calculations. These KPIs should be defined from the lean concept perspective. The philosophy of lean concept puts the emphasis on the needs of the customers and aims at enhancing productivity. The objective is to create as much value for the customer as possible and continuously improve the value-creating activities. Thus, it is a key to identify what brings value to the customer, and focus on these activities connected to the production of the product or the features the customer is willing to pay for. All other activities are considered as non-value adding steps and referred to as waste. The lean concept reveals bottlenecks, unnecessary activities and optimization potential in order to reduce waste and improve lead-time of production [66]. Hence, quantitatively measuring performance to enable accurate and detailed analyses is essential when it comes to manage the lean Continuous Improvement Process (CIP) [67].

KPIs are crucial performance parameters that represent a specific value over a defined period, and they simply track the values of interest and can be reported in order to show, for instance, deviations above a certain norm [67]. Likewise, for resource efficiency, benchmarking, and energy KPIs in general, is a promising method of comparison that searches for solutions among the strongest competitors and can be used in almost every production unit. KPIs can be used for a comparison of resource efficiency, however, only from specific perspectives. As shown in Figure 11 for the operation processes, the measures should be identified which illustrate the value-added energy into a specific process. Not only the quantity but also the quality of applied energy and resources should be investigated. To do so, the measures and energy indicators should be defined. No instrument for the overall assessment of the energy efficiency in the production exists, mainly because no precise energetic reference points are used or indeed do not yet exist.

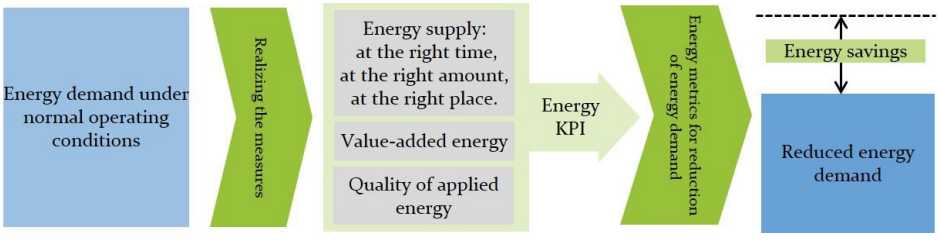

Figure 11: Realization of the measures for energy saving potential

Kreitlein et al. [68] [69] developed a KPI method to show how the energy efficiency can be compared and evaluated during the production of various products. The aim is assessment and evaluation of energy efficiency of the manufacturing processes in the production from the perspective of production planning. Figure 12 illustrate a model for energy efficiency KPIs which was initially developed to quantify the amount of consumed energy for the least energy demand [68]. Further on, the model is developed to investigate the thermodynamic complexity of a production process [70].

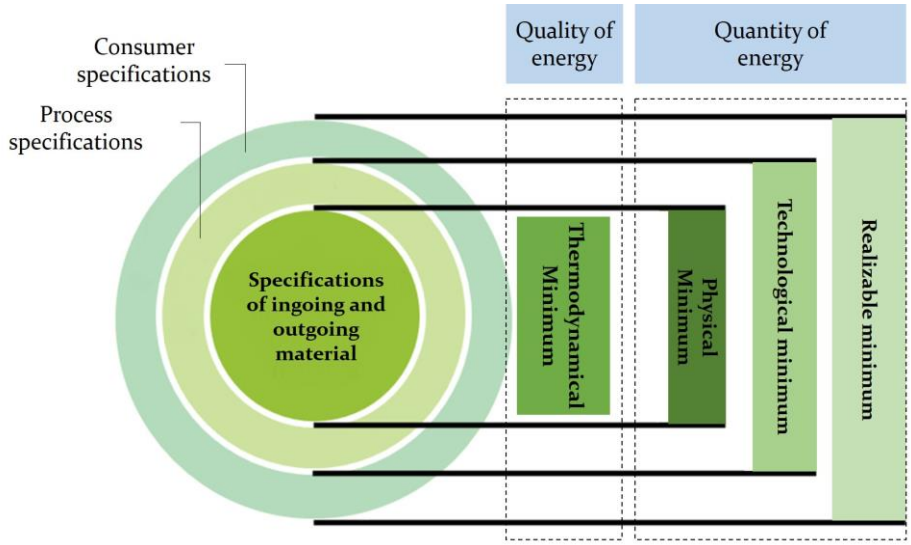

Figure 12: KPIs for energy efficiency of production levels [70]

To quantify the energy efficiency, the least energy demand method is evaluating the energy consumption based on the ratio of the theoretically required electrical energy consumption to the measured electrical energy consumption. Due to its independent comparison basis, the least energy demand method allows for process, product, company, and even cross-industry comparisons. Thus, by means of using KPIs on all levels of the manufacturing process, the method follows the basic intention of making the energy efficiency of a product transparent and ultimately comparable. However, these KPIs in the production process level provide metrics to evaluate the quantity of electrical energy consumption and resources and not the quality of how the resources are consumed in the process.

The quality of resource consumption can be described as the amount of work that can be obtained from a specific amount of available energy.

Thermodynamics provide metrics based on both the first and the second law of thermodynamics to evaluate the quality of energy transformation in a system. Exergy describes the available energy and the exergy analysis identifies the waste of usable energy. The exergy analysis will be used as energy KPI in this study to evaluate the thermodynamic interaction of the used resources in the soldering oven technology.

2.2.3 The 1st Constraint: Exergy Efficiency Analysis to Evaluate the Energy Criterion

Exergy analysis is a tool to realize the minimum energy required doing the work, and this is used as an indicator in the tetrahedron trade-off model. In thermodynamics, exergy is defined as the usable amount of work that can be obtained from a system when it is taken from its current state of thermodynamic balance with the environment, which means exergy is the usable part of energy. An investigation of the energy and resource efficiency is usually performed with a statistical evaluation, however for complex thermal processes exergy methods are established [71]. Since the application of energy methods only involves the 1st law of thermodynamics and therefore ignore the difference between work and heat, these methods lack factors such as the application of material balances, energy balances and equilibrium relationships, which are required to adequately show effectiveness of the system utilizing given energy resources. While energy cannot be destroyed according to the first law of thermodynamics, exergy can be destroyed. The destroyed part is called anergy and cannot be converted back into exergy. Exergy method is also driven from the 2nd law of thermodynamics and it is defined as "The maximum theoretical useful work (shaft work or electrical work) obtainable as the system is brought into complete thermodynamic equilibrium with the thermodynamic environment while the system interacts with this environment only" [72]. The analysis is obtaining also the exergy loss or exergy destruction of the process, and it is indicating that the increase of entropy in a process is proportional to the destruction of exergy [73] [74] [75] [76] [77] [78].

Despite the fact that energy efficiency is currently the most common tool to measure the effectiveness of a process, it might be misleading since it does not assess the energy quality. Another method to analyze the efficiency based on the second law of thermodynamics is entropy analysis. Because entropy analysis delivers results in Joules per temperature change, the exergy analysis delivers its results in energy units and it

enables to compare the interaction of any source of energies in the system. The analysis cannot differ between a resource and waste, and it is identifying and quantifying the types, causes and locations of the losses. Despite the advantages of exergy analysis, it also has some demerits, as the selection of the reference environment is crucial for the analysis [79].

The flexibility of exergy analysis is shown by the large range of fields it has been applied in: industrial systems, evolution theory, social theory, economics, and environmental impact of systems, sustainability, policy and decision making. In the industrial systems emphasis has been placed on applying exergy to sustainability science [80] including studies on the investigation of the relationship between exergy and sustainability and eco-efficiency in manufacturing processes [81], and the critical environmental impact indicators [7]. The common areas of exergy analysis application are mainly in energy intensive systems such as power generation, thermal systems [82], steel industry [83], textile production [84] and a review of the use of exergy in cement manufacturing is given in [85]. According to the basis set by Gyftopoulos and Beretta [74], exergy analysis can be applied to any 'well-defined' system in any state in manufacturing processes as well. The analysis ranging from conventional ones such as machining, casting and molding [86] to advanced processes like PCB assembly production [87], and vapor phase soldering process [88].

Exergy model construction

Before proceeding to the exergy analysis and setting up the specific exergy equations, an understanding of how to balance the exergy is mandatory. For an energy balance in a steady state condition the input energy ($E\ (input)$) has to be the same as the output energy ($E\ (output)$), since energy will neither be created nor destroyed during any kind of process (Eq. 1). Under steady state conditions ($0 = \frac{\Delta E}{\Delta t}$) net energies flowing ($\dot{E}\ (input)$) in and out ($\dot{E}\ (output)$) are equal.

$$E\ (input) = E\ (output) \tag{1}$$

To transform the energy balance to an exergy balance, the destruction of exergy has to be taken into account, and the exergy flowing into the system is not the same as the exergy flowing out. The destroyed exergy is the difference between the exergy input and the exergy output (Eq. 2). The exergy output indicates the exergy that has not been destroyed during the process and could theoretically produce work [89]. Due to the irreversibility of the process, some of the input exergy is always consumed

and destroyed. The exergy loss is the result of friction, diffusion, throttling, combustion processes, absorption or emission of thermal radiations. Only in an ideal, isentropic environment the exergy destruction would be zero [90].

$$Exergy\,(input) = Exergy\,(destroyed) + Exergy\,(output) \quad (2)$$

Since exergy destruction is proportional to the entropy created by the process, losses always occur. So the difference between exergy input and exergy output is the exergy loss ($\dot{E}x_{loss}$). It can be calculated as the product of entropy generated (ΔS) and the environmental temperature (T_0) (Eq. 3). All other losses, such as unutilized resource flows out of the system, contribute to the exergy loss.

$$\dot{E}x_{loss} = T_0 \cdot \Delta S \quad (3)$$

As a result, the exergy destruction ($\dot{E}x_{loss}$) is the difference between the exergy input into the system ($\dot{E}x_{in}$) and the exergy that flows out of the system ($\dot{E}x_{out}$) (Eq. 4).

$$\dot{E}x_{loss} = \dot{E}x_{in} - \dot{E}x_{out} \quad (4)$$

As different forms of energy have different qualities, therefore exergy input and exergy output can have different forms. It can be distinguished between the exergy of the work $\dot{E}x_W$, the exergy of heat $\dot{E}x_Q$, and flow exergy $\dot{E}x_i$ which is the exergy carried by the material flow. Figure 13 shows the exergy model construction and its components. Exergy model consists of physical and chemical exergy. The physical part comprises mechanical and thermomechanical exergy. Mechanical exergy consists of kinetic and potential exergy that are controversial in manufacturing systems. Thermochemical exergy comprises of temperature-based and pressure-based processes. It is addressing the reversible physical processes, and therefore this study is not including thermochemical exergy flow. The chemical part of exergy consists of mixing and separation as well as chemical reactions [74] [76].

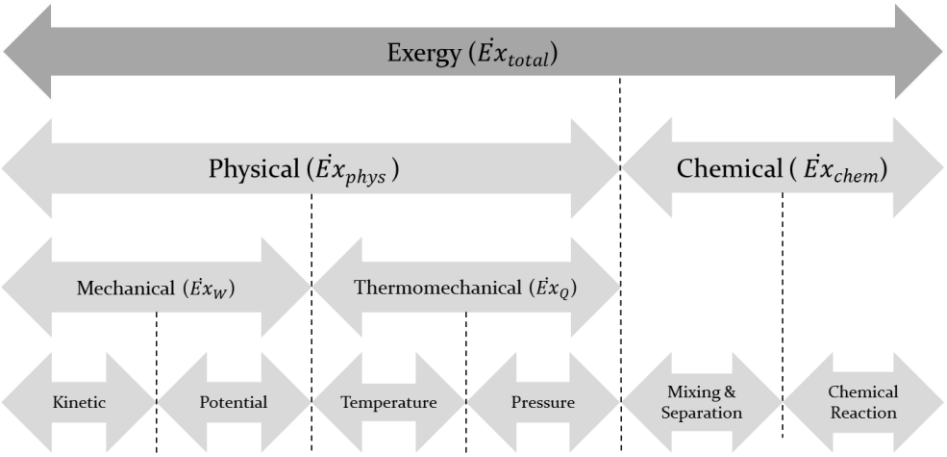

Figure 13: Exergy model construction [74]

Thus, the total exergy flow is composed as followed:

$$\dot{Ex}_{total} = 0 = \Delta\dot{Ex}_{phys} + \Delta\dot{Ex}_{chem} - \dot{Ex}_{loss} \quad (5)$$

In a steady state condition the total exergy flow $\dot{Ex}_{total}$ is zero. In the following, the compound of the total exergy flow is described in detail.

The exergy of the work

For mechanical (potential and kinetic) and electrical work, exergy flow is equal to energy (Eq. 6 and Eq. 7). This means that, under ideal conditions, work flow ($\dot{W}$) could be obtained completely without loss and zero friction [91].

$$\dot{Ex}_{kin} = E = \frac{1}{2}m(v^2 - v_o^2) \quad (6)$$

$$\dot{Ex}_{pot} = E = mg(h - h_0) \quad (7)$$

The exergy flow of work ($\dot{Ex}_W$) flowing into the system is equal to the total of the energy (work) available (Eq. 8).

$$\dot{Ex}_W = E = \dot{W} \quad (8)$$

Heat flow ($\dot{Q}$), on the other hand, is a form of energy that is not fully available to be transformed into work. The exergy flow of heat ($\dot{Ex}_Q$) flowing in or out of the system can be determined in regard to the Carnot's theorem between the temperature of a given state (T_i) and the environmental temperature (T_0) (Eq.9).

$$\dot{Ex}_Q = \left(1 - \frac{T_0}{T_i}\right) \cdot \dot{Q} \tag{9}$$

The Carnot coefficient describes the maximum possible efficiency when transforming heat into usable work [91]. As explained, exergy consists of chemical and physical exergy. Thermomechanical exergy is not deployed which is applicable for reversible processes. The relevance and the calculations are illustrated below.

Physical Exergy

Physical exergy consists of mechanical and thermomechanical exergy. As mechanical exergy in form of kinetic and potential exergy, as described in equation 6 and 7, equals the total quantity of available work, the thermomechanical exergy is a function of entropy (S) and enthalpy (H) from the material at a given state. Therefore, the physical exergy is the maximum available energy in a system until it is brought into equilibrium with the environment. Enthalpy represents the energy content in thermal energy, where entropy describes its unavailability. This results in the fact, that increasing temperature increases the enthalpy of a material flow but also the entropy, which has a reducing effect on the exergy [76] [92]. Accordingly to equation 10, the deltas of entropy and enthalpy at a given state and the environmental state express the physical exergy (or the enthalpy flow $\dot{Ex}_H$) of a material flowing into, or out of the system.

$$\dot{Ex}_H = \Delta H - T_0 \Delta S \tag{10}$$

As shown in equation 11 and equation 12, the enthalpy difference consists of the specific heat constant c_p and the temperature difference between the ambient temperature T_0 and the temperature T_i at a given state. The heat constant c_p is considered to be constant during the entire soldering process. For the entropy difference, there is a distinction between gaseous, liquid and solid substances. While for gaseous substances, the universal gas constant R is used, other substances use the specific volume v. Both equations utilize the pressure difference between the origin P_0 and the given state P_1 [76].

$$\dot{Ex}_{phy,gas} = c_p(T_i - T_0) - T_0\left(c_p \ln\frac{T_i}{T_0} - R \ln\frac{P_i}{P_0}\right) \tag{11}$$

$$\dot{Ex}_{phy,other} = c_p(T_i - T_0) - T_0 c_p \ln\frac{T_i}{T_0} + v(P_i - P_0) \tag{12}$$

Chemical Exergy

Chemical exergy is the maximum useful energy, by means of chemical processes, when the stream is not in a chemical equilibrium. Under

predefined environmental conditions, materials and material compositions have specific chemical exergies ($\varepsilon_{chem,i}$, $\varepsilon_{chem,j}$), such as like the standard chemical exergy by Szargut [93]. If a material specific chemical exergy is not given in any table, it can be calculated using the Gibbs free energy (ΔG_f°) (Eq. 13). The Gibbs free energy is a basic concept of chemical engineering and available in tables for various substances [94]. For atmospheric gases (such as nitrogen) the dead state would be the atmosphere and the mole fractions X_i of the gas (nitrogen). The specific chemical exergy for atmospheric gases ($\varepsilon_{chem,ATMgas}$) depends on the reference temperature and the local atmospheric mole fraction X_i^e (Eq. 14).

$$\varepsilon_{chem,ij} = \varepsilon_{chem,i} + \varepsilon_{chem,j} + \Delta G_f^\circ \tag{13}$$

$$\varepsilon_{chem,ATMgas} = -RT_0 \ln X_i^e \tag{14}$$

The chemical exergy of incompressible substances, such as water, depends on the specific volume v of the material and the pressure difference to the reference state and also the relative humidity φ (Eq. 15).

$$\varepsilon_{chem,water} = v(P_{ATM} - P_{SAT}) - R\,T_0 \ln \varphi \tag{15}$$

In general, the difference of chemical exergy of a substance can be derived from the chemical potential μ_i at the given state and the chemical potential μ_0. In regard to the mole fraction X_i^e and the difference of the chemical potentials the specific chemical exergy can be calculated as shown in equation 16.

$$\varepsilon_{chem,i} = (\mu_i - \mu_0) X_i^e \tag{16}$$

Since for most substances either the specific chemical exergy value or the Gibbs free energy of the formation exists in tables [93] [94], a more detailed explanation on chemical exergy will be referred to the referenced literatures [74].

2.2.4 The 2nd Constraint: The Production Lead-time to Evaluate the Time Criterion

The time criterion in this study is conceived as the production lead-time. The production lead-time is defined as the time an object needs to pass through a system. The setup time is the time, which is necessary to prepare the work. While those two criterion define indicators within the company, the delivery time includes the contact with the customer, as the time from the incoming order to the goods delivery [53] [95]. Likely, the

study is discussing the soldering process that is part of the electronics assembly production, and hence the delivery time is not considered. Furtherly, the focus is on production lead-time of a PCB product, when it enters and leaves the soldering oven technology.

2.2.5 The 3rd Constraint: Economic Perspective to Evaluate the Cost Criterion

Several approaches are reported for the cost analysis in manufacturing companies. Götze, U. [96] defined an economic classification according to the type of goods and consumption as shown in Table 2. Because this study is focusing on the boundaries during the production lead-time of a PCB product, therefore, the analysis are not addressing the non-short-term consumptions, and not the cost for the amortizations, risk costs, taxes, or interest rates.

Table 2: Classification of cost categories according to type of goods and consumption [96]

Type of consumption	Cost categories
I. Short-term consumption: 1. Consumption of material goods 2. Consumption of immaterial goods a) Consumption of own labor services b) Consumption of external labor services c) Consumption of goods based on rights	1. Material cost 2. Personnel cost 3. Cost for external services 4. Cost for legal interests
II. Long-term consumption	5. Amortizations
III. Obligated consumption 1. Technical-economic destruction 2. State and political taxes	6. Risk cost 7. Taxes
IV. Temporal availability consumption	8. Interest rates

When looking at the short-term consumption, only the consumption of process-related material goods, resources, electrical energy consumption are relevant. The cost for personal cost, external services and the cost for legal interest remain unchanged. The change of solder profiles is associated with the variation of production lead-time and therefore it is influencing further alterations in energy and material consumption cost.

2.2.6 The 4th Constraint: Solder Joint Defects to Evaluate the Quality Criterion

The solder joint quality is realized as the quality criterion in the trade-off model. It determines the joint durability and reliability, and it can be

influenced by many factors, among which material ageing, mechanical stress and thermal stress are the most important. When inspected visually, there are three criteria to evaluate the solder joint quality: The wetting of the solder pad and the electronics components metallization, the shape of the solder joint and the condition of the solder surface. During the production of electronic devices, various solder joint defects can occur. Those solder joint defects are all listed in the IPC-A-610D, which contains worldwide-standardized acceptance criteria for electronic assemblies. It features acceptance criteria for all kinds of solder joints and divides the finished electronics in three classes [37]:

- **Class 1: General electronic products** – Main requirement is the functioning of the finished electronic
- **Class 2: Dedicated service electronic products** – Correct functioning, extended durability and uninterruptible service is required, but not critical
- **Class 3: High performance electronic products** – Continuous high performance or vital material supply is required and critical

The criteria are mainly dependent on the quality of soldering process. Special solder surfaces also require special acceptance criteria. The criteria should be based on design, process capability and performance requirements. The solder should achieve a good wetting and form a shallow edge at the to-be-soldered parts. In the end, the parts contour should still be well visible. Since the optimum cannot always be realized, the IPC-A-610D mentions still acceptable criteria in addition to the quality goals. The still accepted criteria cover tolerated deviations in looks, wetting angle of contact and contour visibility. The guideline also differs between leaded and lead-free solder joints. In the following, frequent solder joint defects caused by the soldering process and their respective countermeasures are introduced [37]. This study is addressing the high quality solder joint which could be used for the high-tech products. Hence, the zero-void solder joint is aimed as the main quality measure. A void ratio of 30% or less is acceptable according to IPC-A-610D, but for high-performance electronic devices, it should be even less and under 5% which is the main objective of the quality criterion for the multi-objective process optimization.

2.3 Computational Intelligence for Process Optimization

The volume of data analytics and artificial intelligence grows fast in modern manufacturing establishes the new research expert programs [97] and new applications in industry [98] [99] [100]. The new digital production environments, which exploit technologies such as barcodes, sensors, control systems and vision systems in data acquisition [101]. The data can contain information about design, production, machines, processes, materials or quality. It is stored in databases and often not analyzed because of its large volume or missing values. Modern electronics process equipment can be used to store data whose flexible exploitation is, however, laborious to process experts. It is typical for the production of electronics that practically the only operation using the historical process data is the Statistical Process Control (SPC) [102] [103] [104], whereas the proactive operations for process improvement, such as diagnostics and optimization [19] [105] [106], often lack this valuable and abundant information. In other words, process equipment is regularly used in the production without a thorough analysis of the data that is, or at least could be, stored during the process. Due to the increasing amount of data and technical advances in information technology and computer systems, the process experts need also new and better instruments for process analysis and modeling. The key, in this respect, are automated diagnostics and optimization systems that enable fast and easy access to process data [107].

To enable a systematic analysis approach, a broad range of computational methods is used to analyze and improve processes. The used models vary from simple regression models to complex advanced models. The simple methods are used for analysis, as they are fast and easy to understand and implement. The complex methods are used for difficult optimization problems. If there is only a single optimization objective, the variable is focused. Multi-objective optimization on the other hand do not result in unique optimal solutions, but in optimum ranges for the used variables, the so-called Pareto optimality [108] [109]. The multi-objective optimization methods, as illustrated in Figure 14, can be divided in the categories no-preference methods, a posteriori methods, a priori methods and interactive methods. No-preference methods do not consider the opinion of the decision maker and are therefore used when the decision maker does not have any special requirements. A posteriori methods are used to generate Pareto optimal solutions, which is often computationally

expensive and difficult. The results are presented to the decision maker who selects the most preferred alternative. For a priori methods, the decision maker has to specify his preferences before the solving process, which is difficult as the decision maker does not always know what is possible and realistic. For the interactive methods, the analyst and the decision maker work in cooperation. This has the advantage that only part of the Pareto optimal points has to be generated and evaluated [110].

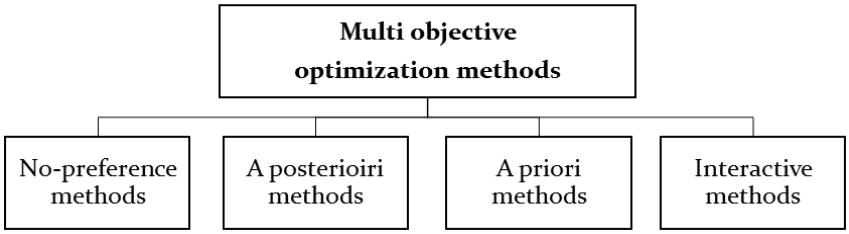

Figure 14: Classification of multi-objective optimization methods [110]

Moreover, the recent applications for computational intelligence has produced new intelligent methods for automated extraction of useful information [111]. Methods such as artificial neural networks, fuzzy sets, rough sets and evolutionary computation, which are generally associated with computational intelligence [112] [113] [114] [115] [116], are nowadays widely used in different industrial environments. Computational intelligence is the study of the design of intelligent agents. What it does is appropriate for its circumstances and its goal, it is flexible to changing environments and changing goals, it learns from experience, and it makes appropriate choices given perceptual limitations and finite computation [117]. Computational intelligence is the base concept with respect to machine learning. Machine learning is the study of computer algorithms that improve automatically through experience. The definition emphasizes the use of computer algorithms in learning and especially the adaptivity, or the ability to improve, of these algorithms. The main goal of the entire concept is thus to create algorithms that utilize past experience, or example data, in solving problems [118]. These methods include decision-based learning algorithms, and methods such artificial neural networks helps to learn from the past experiences, diagnose the problems and predict the future events in production processes.

2.3.1 Intelligent Process Optimization Methods for Soldering Process in High-Volume Electronics Production

Since last years, there have been many studies carried out on the monitoring of reflow soldering process and improvement of soldering process quality. Most of these studies have adopted qualitative defect mechanism analysis and computational simulation models for upgrading the soldering quality through keeping the actual profile at the specified target level [24]. Three commonly used methods have been implemented to achieve this objective [119]:

- Thermal simulation modeling: a computational model with process specifications is used to simulate the shape of the reflow thermal profile. The simulation is performed iteratively until the results agree with the predefined specifications or the shape of the target thermal profile. The final recipe(s) will be used as the oven machine setup [26] [120] [121].
- SPC method: the ingredients of a reflow thermal profile (e.g. setup peak temperature, soaking temperature, preheating slope, and so on) are monitored by traditional control charts with predefined limits to diagnose and identify any variability in the reflow soldering process and reduce the need for post-reflow inspections [122].
- Computational intelligence approach: the computational intelligence approaches are designated to acquire knowledge of the essential factors that influence the performance of the reflow soldering process. Specifications are considered to deduce the most acceptable recipes for achieving homogeneous temperature distribution in soldering process [123].

Computational intelligence approaches in electronics manufacturing is fast growing. Traditionally, the used methods in process improvement through data-driven analysis were statistical linear methods or experimental testing [102] [124]. Liukkonen et al. [109], have conducted a complete review on the application of computational intelligence in mass soldering of electronics. The earliest intelligent applications to mass soldering originate from the early 1990s, including the application of methods such as multilayer perceptron, probabilistic neural networks, self-organizing maps, fuzzy logic and also the first hybrid methods. As a matter of fact, at the beginning of the 1990s the research has been quite active in this field, whereas a reduction can be seen in the published

literature at the turn of the century. Nonetheless, it seems that the range of computational methods has been widened in the 21st century as new methods such as support vectors machines, rough sets, decision trees and genetic algorithms have become a part of the research. More than 60% of all studies were about application of these methods in inspection of solder joints and quality management issues. Shown in Figure 15, multilayer perceptron have been the mostly used intelligent method, covering approximately 50% of the applications. Applications of self-organizing maps, fuzzy methods and hybrid methods have also been reported but the use of methods other than these has been only marginal. 82% of the applications utilize Multilayer Perceptron (MLP) (feedforward artificial neural network models), if the applications of hybrid methods are included. The main conclusion proves the recent trends of applications of Artificial Neural Networks (ANN) in electronic packaging comparing with other computationally intelligent methods explained comprehensively explained by Liukkonen et al. [109].

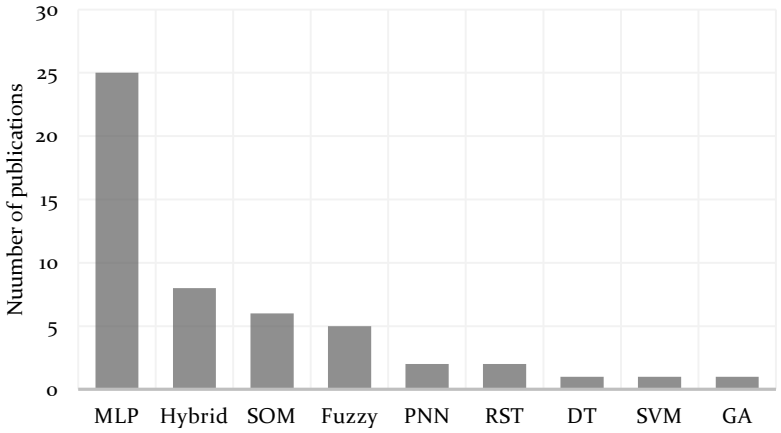

Figure 15: Classification of applications according to computational method. MLP (Multilayer Perceptron), PNN (Probabilistic Neural Networks), SOM (Self-Organizing Maps), RST (Rough Sets), DT (Decision Trees), SVM (Support Vector Machine), GA (Genetic Algorithms) [109]

Comparing with other mathematical optimization methods, ANN require less formal statistical training and it can also implicitly detect complex relations between independent and dependent variables. Another advantage is the ability to detect all possible interactions between the predictor variables. Additionally, it can be developed using various training algorithms, and hence it is relatively easy to use. On the opposite side, ANN method work like a black box and it has a limited ability to

identify possible causal relationships. In addition, the application of this method in some fields is also very difficult. Despite their simple usage, they require greater computational resources than other methods. In addition to that, they are vulnerable to overfitting, which distorts the results. Another disadvantage is the requirement of enough training data if the algorithm obtaining an over-fitted results [125] [126] [127].

2.3.2 Artificial Neural Network (ANN) Principle and Applications Biological Neural Networks

Artificial neural networks are used to capture a relationship between variables which are difficult to relate analytically. They have the ability to learn and to be trained for certain tasks. Thereby, ANNs try to imitate the human brain learning process of biological neuron which is shown in Figure 16. By using neurotransmitters, coded information is sent from the synapses to the axon and the axon transmits the information to other neurons. 100 billion interconnected neurons are organized in groups and subsystems and altogether form the brain [128] [129]. The principle of information handling in brain were used, mathematically modeled, and deployed in industry application for data analytics.

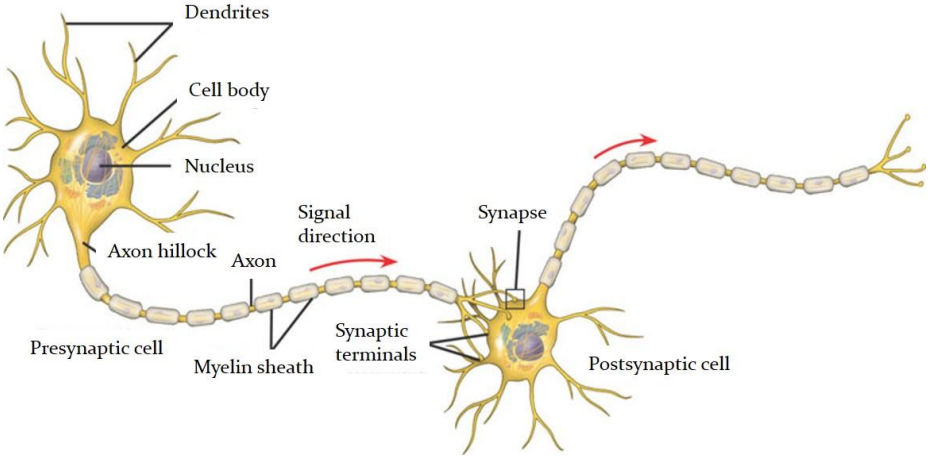

Figure 16: Simplified model of a biological neuron [130]

Mathematical modelling of neural network

According to Figure 17, ANN is a structure which is able to receive input vector $I = [i_1, i_2, \dots, i_n]$, and generate appropriate output vector $O = [o_1, o_2, \dots, o_m]$ [131]. The ANN contains several connected elementary calculation units, which are called neurons. The structure

shows a schematic representation of an artificial neuron with input vector (with r elements) and characteristic structure of the feed forward ANN with k hidden layers. Each of the input elements $x_1, x_2, \dots, x_r$ is multiplied with the corresponding weight of the connection $w_{i,1}, w_{i,2}, \dots, w_{i,r}$. The neuron sums these values and adds a bias b_i (which is not present in all networks). The argument of the function (which is called transfer function) is given as follows [132]:

$$a_i = x_1 w_{i,1} + x_2 w_{i,2} + \cdots + x_r w_{i,r} + b_i \tag{17}$$

while neuron produces output:

$$y_i = f(a_i) \quad = f\left(\sum_{j=1}^{r} x_j w_{i,j} + b_i\right) \tag{18}$$

This output represents an input to the neurons of another layer, or an element of the output vector of the ANN. The whole system is perceived as parallel because many neurons can implement calculations simultaneously. The most important feature of a neural network is the structure of the connected neurons because it determines the way the calculations are performed. Apart from the source layer that receives the inputs and the output layer on which the input layer is mapped, a neural network can have one or more intermediate hidden layers. Furthermore, the types of interneuron connections determine the characteristics of a network and consequently the tasks for which it is designed to be used.

In feed forward networks, data run exclusively from the input units to the output units while in recurrent networks, feedback connections act beneficially for the training process and the behavior of the network. Finally, the algorithm used for the network training affects its performance and effectiveness. The training of neural networks refers to the procedure adopted to achieve a desired behavior by modifying the synaptic weights, which allows them to learn from their environment and improve their performance through time. The various methods of adjusting the connections weights constitute different training algorithms. Each algorithm comprises a well-defined set of rules for solving the training problem and has specific advantages and disadvantages. Depending on the environment of the neural network, three different training methods may be distinguished, namely supervised, unsupervised, and reinforcement learning. In supervised learning, the training is based on examples of desired behavior. The parameters are adjusted according to the training vector and the error

signal between the target values ($t(k)$) and predicted values ($y(k)$) of the network outputs [133].

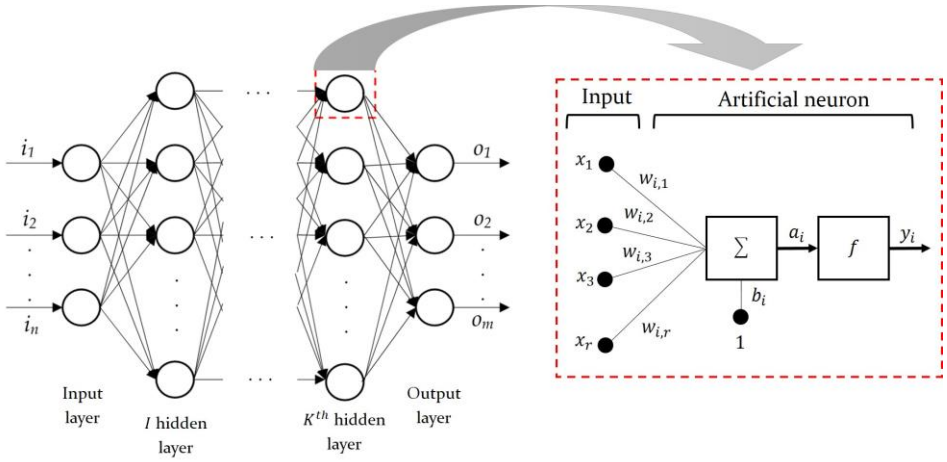

Figure 17: Artificial neuron and the structure of the feed forward artificial neural network [132]

The adjustment of parameters is implemented with an error correction algorithm. It must be pointed out that typical supervised learning neural networks are the feed forward and the radial basis function networks. On the other hand, in unsupervised learning the weights are modified in response to network inputs only. There are no target outputs available. Most of these learning algorithms perform clustering operations. They categorize the input patterns into a finite number of classes. This is especially useful in applications such as vector quantization. Finally, reinforcement learning trains the network with the use of a feedback signal called reinforcement signal, which "awards" the right behavior or "punishes" the wrong behavior of the network. It can be easily understood that the network receives only a training data set without the respective desired outputs and during the training, it tries to find a set of weights that tend to avoid negative reinforcement signals.

Backpropagation (BP) learning algorithm

Backpropagation (BP) algorithm is a supervised learning algorithm that adapts the synaptic weights, aiming to minimize the Mean Squared Error (MSE) between the desired and the actual network outputs after each input vector presentation. Backpropagation (BP) ANNs are the most common than any other kind of networks [134]. Feed-forward perceptrons could be trained with various backpropagation algorithms, such

Conjugate gradient backpropagation, the backpropagation Levenberg–Marquardt algorithm, the backpropagation Bayesian algorithm, and adaption learning function such as adaptive backpropagation algorithm of the steepest descent. Such networks with one or more hidden layers are the Multilayer Perceptrons (MLP). These networks, unlike simple perceptron, are capable of classifying linearly inseparable patterns and can solve complicated problems. They are trained with backpropagation algorithms and the transfer function employed is a differentiable sigmoid function like hyperbolic tangent [133].

Standard backpropagation is a gradient descent algorithm in which the network weights are moved along the negative of the gradient of the performance function. The main idea of the algorithm is that the errors of the hidden layers are specified by the backpropagation of the output neurons errors. The algorithm includes a forward and a backward phase. During the forward phase the input signals "travel" through the network from input to output, layer by layer, generating eventually a certain response and during the backward phase the error signals are back propagated, from the output layer to the input layer resulting in the adjustment of the network parameters by minimizing the Mean Squared Error (mse). Therefore, the synaptic weights are adjusted to minimize the criterion according to equation 19.

$$mse = \frac{1}{Q}\sum_{k=1}^{Q} e(k)^2 = \frac{1}{Q}\sum_{k=1}^{Q}(t(k - y(k))^2 \tag{19}$$

where: Q – number of experiments, $e(k)$ – error, $t(k)$ – target values, $y(k)$ – predicted values

For backpropagation algorithms, the weights are initialized with small random values and a random input pattern is chosen, which is propagated forward through the network. After the errors are calculated, the weights are updated. This procedure is repeated until the output error is below a certain threshold or the maximum number of iterations is reached.

Artificial Neural Network (ANN): state of the art in industry

ANN has yet to have a quantitatively major impact on productivity growth in industry [135]. Besides present day industries are facing new challenges in terms of market demand and competition in various applications. ANN is recently changing known as Industry 4.0. The segments that the manufacturing companies see as offering the greatest potential for benefitting from the digital transformation to industry 4.0 include research and development (in which a total of 78% of companies see great

or very great potential), warehousing and logistics (74%), production (73%), services (72%), procurement and purchasing (69%) and sales (56%) [136].

Integration of ANN with recent emerging technologies such as Industrial Internet of Things (IoT) [137] [138], big data analytics [139] [140] [141] [142], cloud computing [143] [144] and cyber physical systems [145] [146] will enable operation of industries in a flexible, efficient, and sustainable approach. The key elements in ANN application in industry can be characterized by the key elements include analytics technology, big data technology, cloud or cyber technology, domain knowhow and evidence. Analytics is the core of ANN, which can only bring value if other elements are present. Big data technology and cloud are both essential elements, which provide the source of the information and a platform. While these elements are essential, domain knowledge and evidence are also important factors that are mostly overlooked in this context. Domain knowhow is the key element from the following aspects: 1) understanding the problem and use the power of ANN in order to solving it; 2) understanding the system so that right data with the right quality can be collected; 3) understanding the physical meanings of the parameters and how they are associated with the characteristics of a system or process; and 4) understanding how these parameters are influencing the defined objectives. Evidence is also an essential element in validating ANN models and incorporates them with cumulative learning ability. By gathering data patterns and the evidence (or label) associated with those patterns can only we improve the ANN model to become more accurate and comprehensive [140].

ANN is recently applied extensively for prediction applications. One of the recent advancement trends for ANN application refer to autonomous vehicles (self-driving cars). Such vehicles combine a variety of sensors to perceive their surroundings, such as Lidar, sonar, radar, GPS and inertial measurement units [147]. Beyond that, they are equipped with computer (machine vision) that currently is one of the most prominent ANN technologies. Decision-based algorithms based on artificial intelligence used in autonomous transportation can substantially reduce the number of accidents and, as a result, reduce the number of fatalities. Also, ANN systems can contribute to achieving better and more accurate results in health diagnoses [148] [149]. Additionally, the implementation of simple robotics in companies may lead to noticeable savings, not to mention data-driven economy, where the use of ANN solutions plays a significant role [150]. This is a very promising area for European countries startups,

especially in the financial, health sectors, and high-tech industries. In fact, the challenge of making industrial data accessible for reuse is as much imminent as it is inevitable. ANN is all about data-based innovation decision-making and prediction tools, when preparing regulatory impact assessment and this could create new demand in various applications in production industries [97].

Artificial Neural Network (ANN) modeling as a quality management tool in electronics production

Despite the evident advantages and disadvantages of linear and statistical mathematical methods, the use of advanced nonlinear modeling methods, such as ANN, in the process analysis and optimization is mandatory in the electronics production assembly [151]. However, these methods are traditionally considered rather complicated and difficult to use which has limited the applicability of ANNs to real industrial problems. But this is changing, by the trend of development of expert and intelligent systems and data-driven applications in industry. Several studies support the fact that ANN method is a useful and effective means to exploit the process data [152] [153] [154]. ANNs can be used for various tasks. It can classify input patterns to pre-specified classes with feature vectors. With its clustering ability, data mining can be performed. Additionally, ANNs can be used to approximate functions. Another application of ANNs is the prediction ability that is used for the purpose of this work.

Application of ANN method in soldering process has been mainly investigated for: (1) quality control and inspection of solder joints and, (2) quality management for analyzing, predicting and optimizing the soldering process profile [109]. Intelligent detection and diagnose of faulty solder joints is an important part of electronics production, because any flaws cause failures impeding the correct functioning of electronic products. Cho et al. [155], presented a variety of optical inspection systems processing based on neural networks for this purpose. Particularly multilayer perceptrons with backpropagation have been a popular method for inspection [156] [157] [158] [159] and classification of solder joints [160] [161]. Nevertheless, there are also applications based on self-organizing maps and vector-based learning [162] [163], fuzzy logic [164] [165], genetic algorithms [160] [119], and hybrid intelligence [13] [159].

Quality management has been the main application field of intelligent methods with regard to mass soldering process of electronics assembly. Kusiak et al. [166] has investigated some best decision learning algorithms in machine learning and data mining of PCB defects. The earliest

applications investigated the design factors of PCB assembly yield using both regression and neural network models trained with backpropagation [167]. Furthermore, Coit et al. [168] predicted soldering quality in wave soldering using a combination of production data and design of experiment data. A backpropagation algorithm and a network consisting of 13 input variables and two hidden layers were used to produce three outputs: excellent, good and fair solder quality. The results of the study were moderate, i.e. about 80% of classifications were correct, but it was beneficial that in erroneous cases the network predicted a higher defect level rather than a lower one. Yang et al. [169] implemented a neuro-fuzzy system for defect prediction and control of a surface mount assembly line. The system was able to identify all defects, but produced a few false alarms. The authors reported that the downtime inflicted by defects was reduced remarkably by 47% after implementing the system. Tseng et al. [170] used an extended approach based on the rough set theory to a problem of quality control in PCB assembly. They managed to predict 97% of the solder balls, so the method overcame clearly the statistical methods used in their comparative studies.

In the area of improving the product reliability, Lin et al. [171] created a predictive model for the sheer force of reflow soldered joints of ball grid array packages. Their system was based on integrated use of a multilayer feed forward neural network for modeling and sequential quadratic programming for optimization. Zhou et al. [172] combined a back propagating ANN with particle swarm optimization to optimize thermomechanical fatigue reliability of solder joints in Plastic Ball Grid Array (PBGA). Liukkonen et al. [173] [174] exploited several investigations to test multiple linear regression and multilayer perceptron neural network to the variable selection in the wave soldering process profiles. They also proposed a model for variable selection of wave soldering process by using the overall cost of poor soldering quality as the model output. These systems can offer an advantageous automated tool for a quality engineer working for predictive quality management. Alternatively, the process engineers can exploit the system to process optimization in various manufacturing processes. Also, for the optimization of reflow soldering processes, BP algorithm is proposed to predict [175] and improve the optimum soldering temperature profile [176] [177], to improve the online control and Automatic Process Control (APC) [178], and to diagnose the technology setup parameters and predicting the output elements of a reflow temperature profile [119] [179].

2.3.3 Response Surface Method (RSM): Principle and Approach

Response Surface Method (RSM) consists of various mathematical and statistical techniques. It is used to develop a functional relationship between a response of interest y and a number of control variables x_k. In RSM, two important models are generally used to describe the functional relationships: the first-degree model (Eq. 20) and the second-degree model (Eq. 21). ϵ describes a random experimental error and β is a vector of unknown constant parameters.

$$y = \beta_0 + \sum_{i=1}^{k} \beta_i x_i + \epsilon \tag{20}$$

$$y = \beta_0 + \sum_{i=1}^{k} \beta_i x_i + \sum_{i<j}^{k} \sum \beta_{ij} x_i x_j + \sum_{i=1}^{k} \beta_{ii} x_i^2 + \epsilon \tag{21}$$

With these models, it is possible to establish a relationship between the variables which can be used to predict response values. Additionally, it can be used to determine the significance of variables and the optimum variable settings to achieve a certain goal. To set up the model, a series of Design of Experiments (DOEs) should be conducted first. The number of experiments in DOE should follow a $n \times k$ design matrix, whereby n is the number of different factors and k is the number of control variables. Depending on the desired output, various design types can be used. For first-order models, the most common designs are 2^k factorial, Plackett-Burman and simplex designs. Plackett-Burman is a fractional factorial design based on main effects alone. It is a two level screening design that is used to identify significant factors that influence response. Response surface methodology is the follow up of Plackett-Burman or sometimes can be used standalone. It is full factorial design based on main, interaction and quadratic effects. It is three or five level design that is used to optimize significant factors identified by Plackett-Burman method. For second-order models, the most common designs are the 3^k factorial (Full Factorial design), Central Composite and the Box-Behnken designs [180] [181] [182]. These designs are used for optimization purposes, and based on the objectives and cost saving factors, a design will be deployed. Because the Full Factorial design is considering every combination of factor levels, and therefore the experimental conduction is more costly and time taking rather Central Composite and the Box-Behnken designs [183]. To conduct the RSM approach as an optimization method, the following steps should be followed:

1) Independent variables are selected which have major effects on the system. The vital variables from the many using a fractional

factorial or Plackett-Burman design should be identified. These are dependent on the study objective and the researcher experience.

2) The experimental design is chosen and executed according to the experimental matrix. When the experiments are finished, the experimental data is handled with mathematic-statistical treatment.

3) The model fitness is evaluated and it is verified whether performing a displacement to the optimal region is possible and/or necessary.

4) The optimum values for each variable are obtained.

As seen in Figure 18, it is common to perform screening process with first-order to reduce the cost and time. After several iterations towards the desired output, a second-order model is used to determine the final results. The optimization by means of RSM is carried out step by step. For each step, only part of the valid value range is considered. The center of this range is the current center point. Half the width of the range *w* is a relative size and refers to the size of the value range of the respective factor. For better manageability, the factor values are converted from their natural value ranges into coded value ranges without units.

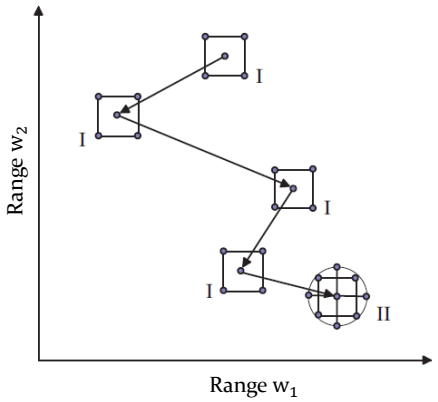

Figure 18: Structure of Response Surface Method (RSM) [184]

To determine the optimum conditions for the control variables over a predefined region, a fitting model is required. For first degree models, the method of steepest ascent can be used, which is an extension of Laplace method to approximate an integral. Usually, the first-degree model is used for the RSM preliminary stage. For second-degree models, the

method of ridge analysis can be used. It optimizes the response of interest subject to x being on a hypersphere surface with the radius r. With the method of Lagrange multipliers, the optimum can be searched [180] [181] [182].

$$\sum_{i=1}^{k} x_i^2 = r^2 \tag{22}$$

The RSM approach provides a numerical approach to deal with discrepancies in the design space. Thereby, it can efficiently smooth out numerical noise. While most optimization methods only vary one factor at a time and keep the others constant, RSM can vary them simultaneously. Another advantage is the progressive change in experimental design until a fitting model is found. It can also help identifying an optimum value beyond the factor levels and therefore determine the future direction of research. Its major disadvantage is a mixing of higher order effects. Designs with only a few points may fit higher order surfaces but the higher order effects will be mixed with other effects resulting in the inability to distinguish the true effects. Another drawback is in the complex problems with long data series which are requiring more sample points. In such cases, the optimization process is costly because each new sample point requires a new calculation of the coefficients of the surrogate problem which entails a high computational burden and a huge memory consumption [180] [184].

2.3.4 Analysis of Variance (ANOVA) Approach

Minitab® software is a statistic and analysis package developed by Pennsylvania University. With its modular structure, it enables the Analysis Of Variance (ANOVA) to identify the significance of the model and to calculate the effects and interactions of the process parameters on various dependent variables. For each of the effects and interactions, Minitab calculates an F-value (ratio of variance) and a P-value (significance value). The logical analysis of these two factors indicates whether the results are random or not. Additionally, the mean value is calculated for the data as well as the standard deviation. Minitab uses the F-value to calculate the P-value, which you use to make a decision about the statistical significance of the terms and model. The F-value is the test statistic used to determine whether the term is associated with the response. A sufficiently large F-value indicates that the term or model is significant.

The significance value, which is often called P-value, describes the probability of an observed data situation under the null hypothesis. The null hypothesis is the assumption that a certain effect does not exist in the data. If the P-value is small enough, it can be assumed that the effect exists. The smaller the P-value is, the stronger the significance. If the P-value is below 0.05%, it is statistically significant. Often the P-value is marked with stars to illustrate the strength of significance of the data situation. When the P-value is between 0.05 and 0.01, the effect is marked with *. When it is between 0.01 and 0.001, the effect is marked with ** and if it is below 0.001 it is marked with *** [185] [186].

3 Description of the Applied Methodology and the Utilized Machines and Materials

This chapter is going to illustrate the material and the applied methodology in this study. In order to collect the data corresponding to criteria defined in the trade-off model, conduction of a set of experiments is required. There are management tools utilized in business organizations to prepare for the experiments. Cause and effect diagram, Ishikawa or Fishbone diagram is one of such management tool to elaborate influencing factors on a certain process. Thereby, in Ishikawa diagram, the causes are divided in 5 to 6 root-cause categories, which all start with 'M'. As explained for the objectives definition in chapter 1.1, the quality criterion optimization is considered as the preliminary aim of this study due to the fact that the inherence of novelty of the studied oven technology is addressing the quality improvement for soldering process in SMT industry. Figure 19 shows that the quality root-causes for soldering process are the *method*, *machinery, mother nature* (environment), *manpower* and *material*. Herewith all causes are kept constant as to avoid unwanted distortions, and defects caused by printing and placement machine. Because the main focus lies on soldering process and hence further influences by other processes in the production chain should be kept minimum as possible.

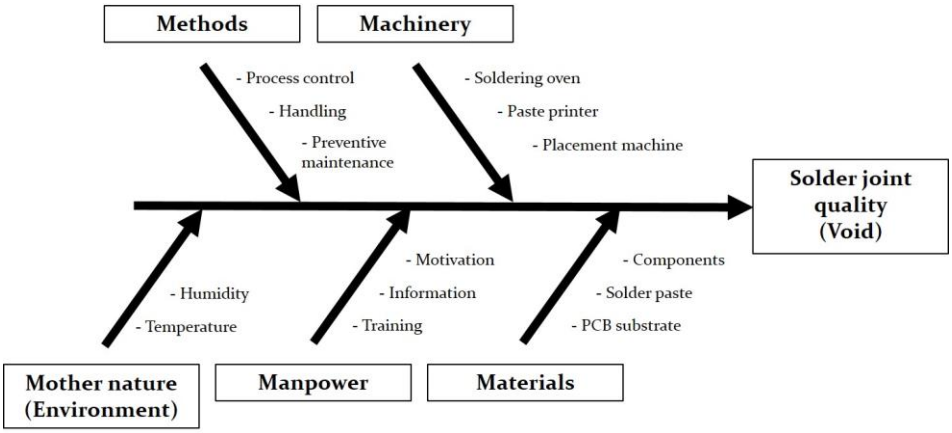

Figure 19: Ishikawa diagram for soldering process quality caused by Five-M, according to [34] [187]

The Ishikawa diagram for soldering process is obtaining a big picture to structure the breakdown of root-causes for a void-free solder joint. Each root cause is therefore elaborated in detail. For the methodology, a road map is presented which is formulating the connection of objectives, the trade-off model and the methods which are used to target a multi-objective process optimization. Furtherly, the materials and machines regarded for the experimental study are presented. These are comprised of the oven technology, the experimental demonstrator, the measurement instruments and the quality inspection devices. The Manpower and Mother Nature is assumed to be constant factors.

3.1 Methodology for the Multi-objective Process Optimization

The production of electronic products is intensively trending to decrease the production cost while the product quality is increasing. Additionally, the products become more and more technical and miniaturized, and the offered solutions to manufacture them are becoming more complex. In the recent years, application of intelligence-based methods by means of process analysis, control and optimization is not evitable. Especially computational intelligence and its applications have been used, as they are able to learn from the data and experience, to self-organize, to adapt in response to dynamically changing conditions and to solve real world problems. This study is utilizing the statistical and mathematical methods to analyze the data, building up the models to control the process, and configuring the intelligence-based algorithm for further usages as prediction, diagnose, and optimization tool. These methods however are used previously in various case studies in electronics production, but in this study, all are configured as a set of solution in the trade-off model.

The proposed roadmap for a multi-objective optimization problem is illustrated using a case study for an overpressure soldering technology. Furthermore, this work is defining a mechanism for the void-free overpressure soldering process. Figure 20 shows the flowchart roadmap of the optimization process. A set of experimental data was collected from the oven technology. To obtain the most influencing variables on voiding process, a screening study is conducted before the full factorial Design of Experiment (DOE), and the meta-models are illustrating the measure of influences. The same approach is conducted for energy, time and cost criteria in the trade-off model. For the energy factor, exergy is utilized to evaluate the thermodynamic interaction of various resources used in the

process. First, the power consumption is measured, and the consumed auxiliary resources are defined. Furtherly, the power consumption of periphery instruments for the oven are modelled and simulated. The time factor should be minimized, and the cost factor comprise of several parameters that have to be calculated individually.

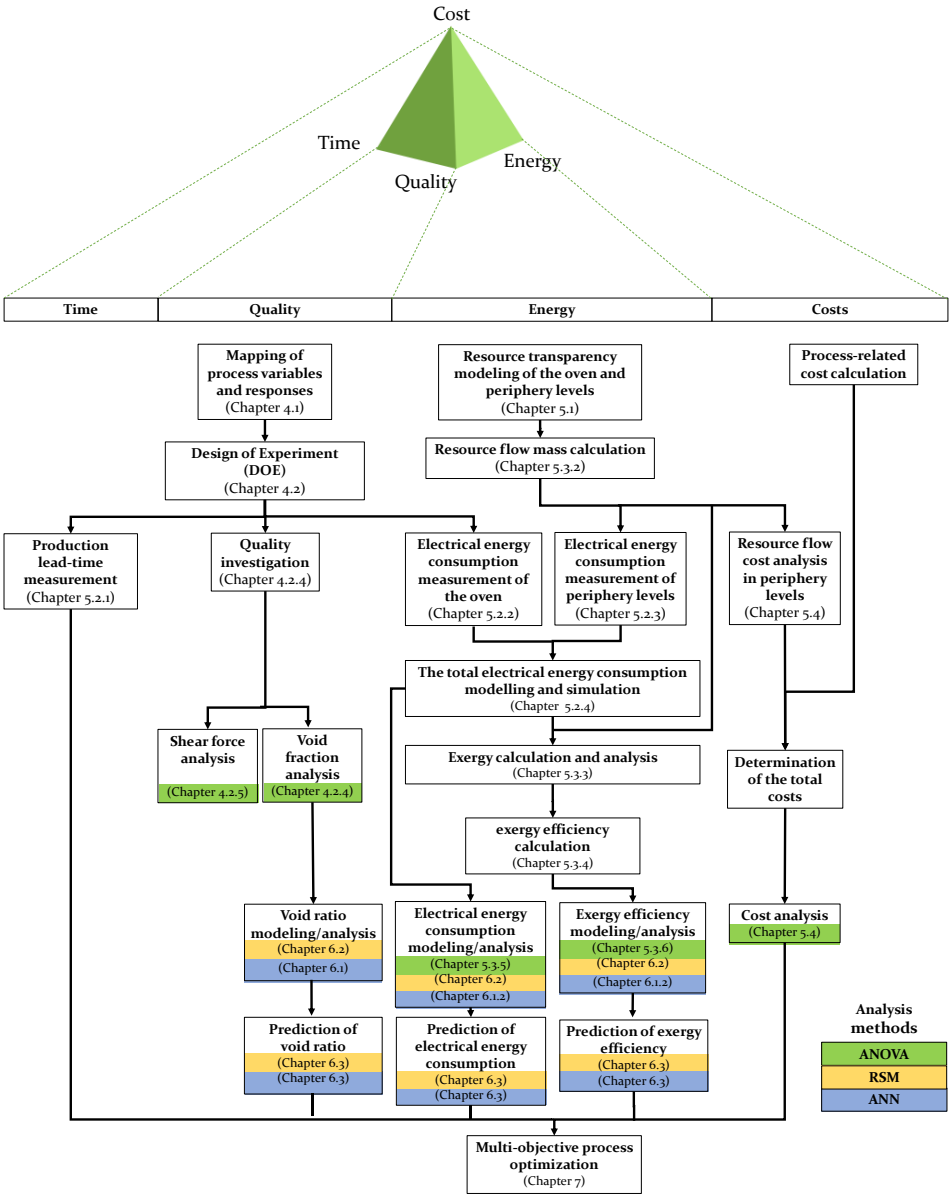

Figure 20: Flowchart roadmap for the multi-objective process optimization

The Analysis of Variance (ANOVA) is used for the data analytics and to find the effects and interactions of the process parameters. The Response Surface Methodology (RSM) is employed to acquire the optimal heating parameters, while the Artificial Neural Networks (ANNs) – Backpropagation Network (BPN) algorithm is utilized to formulate nonlinear cause-and-effect relationships of the process factors and responses by learning from the experimental dataset. These algorithms are used as the means of optimization and diagnose tool for the multi-objective process. In parallel, both the RSM and ANN methods are compared for their prediction accuracy as if to investigate the best applied method in this case study. Including the multi-objective process, a ranking approach and decision making method is developed which is offering a compromised solution based vectors for the trade-off model.

3.2 Utilized Machines and Soldering Oven Integrated With an Overpressure Module

To conduct the experimental work, a surface mounted demonstrator board is assembled utilizing the solder printing machine, electronic component placement machine (mounter), and soldering oven technology. The SMT assembly process is already shown in Figure 1. The solder paste was applied by a stencil printer of type Horizon 03iX (ASM Assembly Systems GmbH & Co. KG, Munich) on substrate. The machine is able to apply a pressure from 0 to 20 kg at a printing pace from 2 to 300 mm per second. In this study, the stencil printing was done with aluminum blade squeegee with 45° angle, stencil thickness of 110 µm, print force of 4.0 kg and 35 mm/sec print velocity. In the next step, the electronic components were placed by a SIPLACE SX2 (ASM Assembly Systems GmbH & Co. KG, Munich) placement machine. It has a theoretical placement rate of 67,750 components per hour at a placement accuracy of ± 22 µm, ± 0.05°/(3sec). In the third step, the substrate-mounted components will be sent to the soldering oven. Figure 21 shows the reflow oven used in this study, which is manufactured by Seho Systems GmbH (SEHO Systems GmbH, Kreuzwertheim). This oven is equipped with an overpressure chamber module in the peak zone with a total volume of 240 liter, and it is designed to build the overpressure up to maximum standard of 4.2 bar using compressed air or nitrogen. For the proper transport of PCBs during the soldering process in the oven a metal carrier frame is used which is ensuring a safe delivery of substrate from the preheating zone to overpressure module and along the entire process.

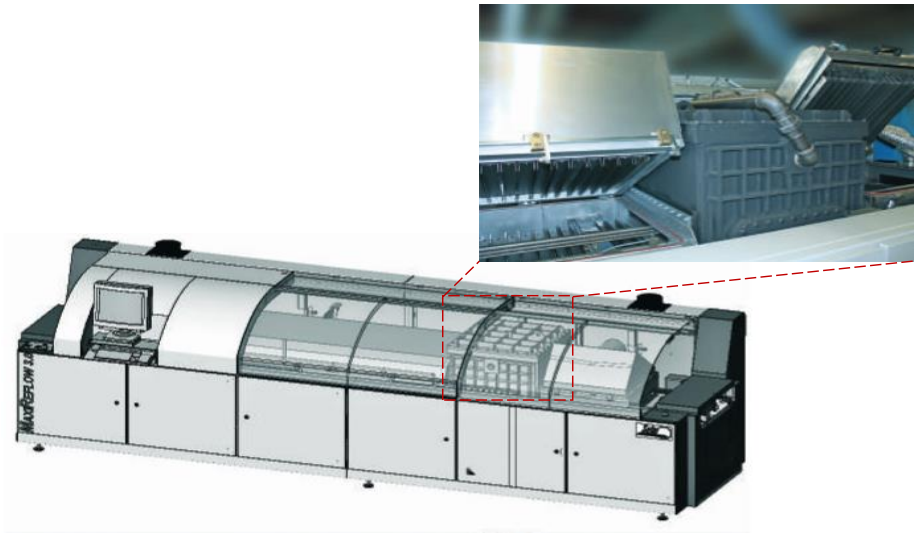

Figure 21: MaxiReflow 3.0 HP integrated with overpressure module [188]

The main function of MaxiReflow 3.0 HP is to ensure a void-free soldering process using the integrated technology module. The main focus of this work is elaborating a multi-objective optimization solution utilizing the Seho soldering oven, and therefore a comprehensible explanation on the detail functional configuration of this technology is presented in chapter 4.

3.3 Material, Measurement Tools and Instruments

The surface mounted PCBs are processed according to the solder profiles for the experimental study. Each profile is designed with a specific oven machine setup, hence the power monitor instrument is utilized to measure, and therefore to study the influence of setup configuration changes on the power consumption. By means of investigating the heat transfer efficiency, online temperature of components material and the input data for resource consumption and efficiency analysis, a thermal profiler, KIC Profiler X5, is utilized to collect the online temperature of thermal points on one PCB per each profile. The utilized instruments and the demonstrator are presented in Figure 22.

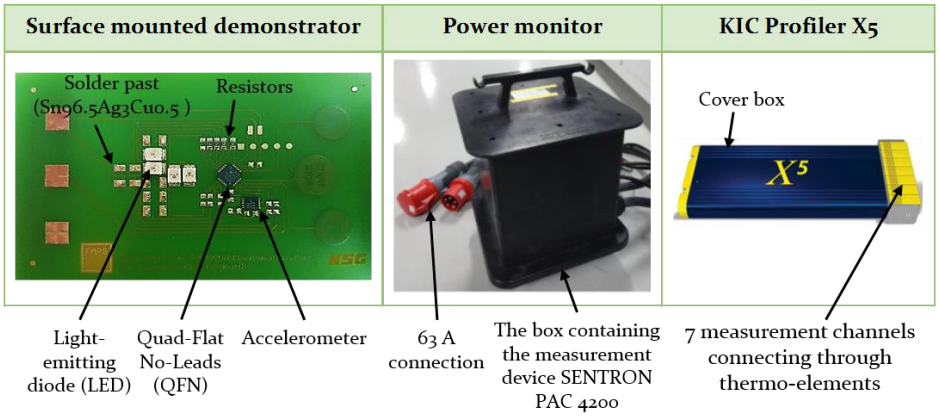

Figure 22: Material and measurement instruments

Surface mounted demonstrator: The surface mounted PCB shown in Figure 22 is one out of four PCBs in a multi-block panel. In order to increase the throughput of PCB assembly in SMT lines, PCBs are often designed in panels so that they consist of many smaller individual PCBs. The size of the panel is 370mm long and 200mm wide and all four PCBs are assembled with same electronic components with the same layout. The thickness of PCB is 1.5 mm, and the copper thickness of 35 µ. Each PCB is mounted with one Quad-Flat No-Leads (QFN), one accelerometer, four Light-Emitting Diodes (LED) and four resistors. For the means of void investigation, only the QFN solder joint is studied and the analysis is elaborated in chapter 4.2.1.

The compounding material portion of the electronic components are investigated from the suppliers of the components and the summary is presented in Table 12.The PCB substrate contains the largest proportion with 45.77 gram of Fr4. The second largest proportion is the copper layer with 5.17 g of copper. A lead-free solder paste type of series F640 (Heareus GmbH, Hanau) is utilized with melting point of 217 °C, chemical compound of *Sn96.5Ag3Cu0.5* and with particle size of 25 to 45 microns in a spherical shape. The solder paste contains 11% of flux, and the metal part is about 88 ± 1% with a viscosity of 130 ± 40 pascal-second.

Power monitor: The collection of the current electrical energy consumption per each solder profile is followed by installation of power monitor instrument with 63 A connection between the oven machine and electrical energy source. The measurement device SENTRON PAC 4200 from SIEMENS Company does the record of the measurement values. The device is following the performance accuracy class according to IEC

61557-12 with a deviation of 0.2% from the measurement values. With the current configuration of the device, the measurement range is 2 A–200 A per phase, between 0 V–400 V [189]. The recording and presentation of the measured values are done through a LAN-interface with an external computer. The measurement device is continuously measuring the current values every 200 ms for active power, apparent power, and reactive power. It is important to notice the timestamp to record the right process duration. The series of data are transportable to an Excel page and hence it could be presented as a data series chart [190]. The current power consumption per measuring time point is calculated by multiplying the measuring time interval by the measured current value of the active power. The approach for electrical energy consumption analysis is furtherly explained in the chapter 5.2.2.

Thermal profiling measurement instrument: The temperature of heat source and the desired temperature value on the surface of substrate in the soldering process is always changing and the heat transfer coefficient is controlling the transfer ratio. Further factors such as the size of the electronic components also affecting on the consistency of heat transfer, and therefore it causes the variation of the temperature value on different spots on the surface of the substrate. Therefore, KIC Profiler X5 (KIC, San Diego, USA) is utilized to acquire the real-time temperature values in the soldering process and to control the thermal process. The device has seven measurement channels to measure and acquire the temperature values in the range of -150 °C and 1050 °C, and accuracy of ± 0.5 °C. The instrument is able to measure a temperature value every 0.1 seconds. To ensure the KIC Profiler functionality, it has to be isolated to maintain its working temperature between 0 °C and 85 °C. During the conduction of experiments, the thermocouples are attached to three points on PCBs. The first one on the PCB substrate, the second one on the solder joint material, and the third one is so attached to measure the reflow air temperature one centimeter above the surface of the substrate. The profiler is then connected to the PC software to read and to plot the time-based temperature dataset during the soldering process.

3.4 Quality Inspection Instruments and the Machine for Destructive and Non-destructive Tests

A primary feature of solder joint quality is visually inspecting the occurred defects through non-destructive tests. Hence, a microscope is utilized as the traditional visual inspection tool to inspect the optical failures. An

X-ray machine form Nordson Dage is utilized for an inter-core inspection of solder joints and therefore the size of voids. The shear tester from XYZTEC is used to conduct the destructive tests to investigate the strength of sheer force of the solder joints. The shear test by itself is not evaluating the defects but the connection between the size and position of voids in the solder joint may affect the reliability of the solder joint during the use phase of the product life cycle. Therefore, this test is also conducted to investigate the correlation with voids fraction. The utilized instruments and machines for quality inspections are shown in Figure 23.

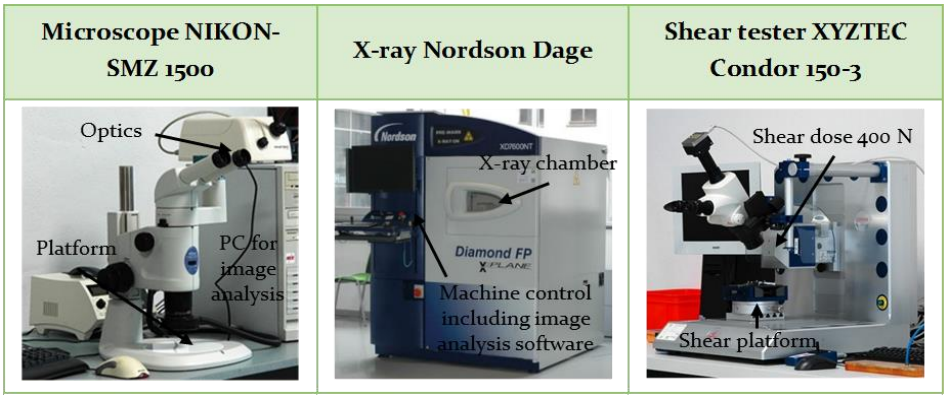

Figure 23: Quality inspection instruments and machines

Microscope instrument: Many of the possible solder joint defects are investigable through optical inspection of the surface of the solder joints. Therefore, a stereomicroscope type SMZ 1500 (Nikon Corporation, Tokyo, Japan) is used. The microscope has a resolution of 3840 x 3072 pixels, a zoom ratio of 15 to 1 and a zoom range from 0.75x to 11.25x. The PC software connected to the instrument enables the image processing. The microscope is mainly used for the general investigation of solder defects and the investigations are furtherly explained in chapter 4.2.6.

X-ray machine: The XD7600NT Diamond FP (Nordson Corporation, Westlake, USA) X-ray machine is utilized to capture the images in order to investigate the measure of voids fraction in solder joints. The XD7600NT scanner is a 2D radiography inspection device with a DAGE NT100 sealed-transmissive 160kV X-ray tube and a DAGE 3 CMOS flat panel detector. The inspection device was fitted with the DAGE µCT inspection option which provides CT functionality by adding a rotation stage and a CT reconstruction workstation. The machine has a resolution of 1940 x 1530 pixels, a geometric magnification of 2500x, a system magnification of 7100x and a digital zoom magnification of 35000x. The

µCT option allows easy installation and removal of the rotation stage and thus provides fast switching between 2D and 3D inspection tasks. The void fraction analysis approach is furtherly explained in chapter 4.2.1.

Shear test instrument: Shear testing is performed to determine the shear strength of a material. It measures the maximum shear stress that may be sustained before a material will rupture. The strength of the solder joints in the context of this work are measured with the help of the shear tester XYZTEC Condor 150-3 (XYZTEC, Panningen, Netherlands). The instrument is doing the pull and shear tests with the measurement accuracy of 0.1% for the substrates with the maximum size of 140 mm x 100 mm. The axis is motioning up to 5 mm/sec with the accuracy of 0.5µm, and it is able to conduct the shear testing in the range of 8N and 400N. This instrument is used to investigate the shear strength of four resistors in each PCB, and the analyses are furtherly explained in chapter 4.2.5

4 Quality Investigation for Overpressure Soldering Process through Design of Experiments (DOE)

This chapter is aiming to build a full factorial DOE by means of preparing the dataset for this study, and the focus initially lies on quality factor for soldering process. First, the soldering technology is introduced, and the soldering process is explained in detail to identify the most influencing variables on quality and a void-free solder joint. These variables are sorted out by a screening study before the full factorial DOE for the sake of cost and time effectiveness. Further, the set of parameters defined in the DOE is utilized to conduct the study for other criteria in the trade-off model including time, cost, and energy.

4.1 Mapping of Process Variables and Responses for Solder Profiling With Overpressure Module

An inherent part of conducting a design of experiment is to identify the process variables which are producing the response factors. There is a relation between the setup configuration of oven, heat transfer coefficient, and the temperature measures on the PCB components. To understand the thermal profiling, the process variables and setup configuration of the oven are studied. Combination of these variables is obtaining the profile and therefore the thermal gradient which is treating the PCB components.

4.1.1 Description of the Soldering Machine

In order to understand the mechanism of temperature profiling combined with the overpressure function, first a detailed explanation on the technical configuration of the soldering oven is presented. Subsequently by realizing the machine configuration, the technology constraints to setup the soldering process are elaborated. Hence, it derives a framework by which the design of experiment of this work is constructed.

Figure 24, a) shows the schematic construction of reflow oven technology with overpressure module. The preheating stage uses convection to transfer the heat. The preheating stage is divided into six independently adjustable heating zones. Separate heating of the top or bottom of the mounted PCB product is possible. The top side of the sixth zone is

designed so that a selective infrared soldering process is optionally applicable. In the overpressure chamber, convection flow principle is used to transfer heat to the printed circuit assembly, and quartz (infrared) heater is used to apply additional heat to the unit. The combination of convection and quartz heating during overpressure process ensures stable and reproducible temperature conditions. The overpressure chamber is equipped with two heating zones.

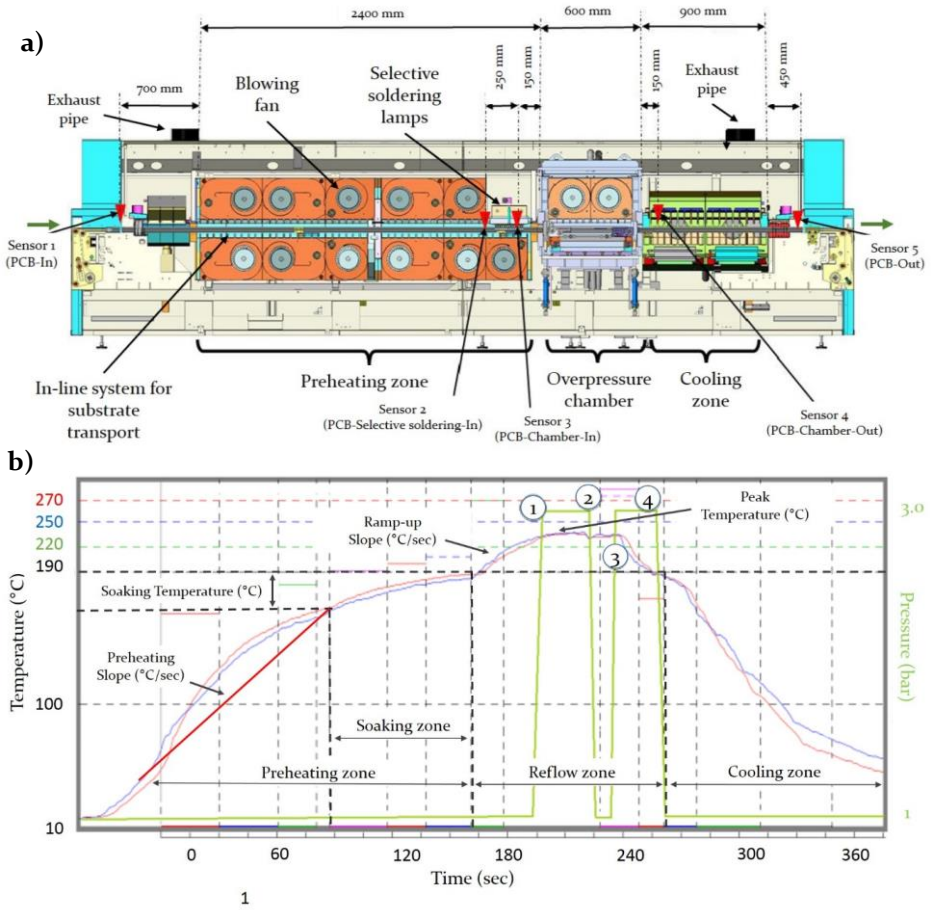

1. The liquid solder is exposed to the first overpressure.
2. Pressure is released to remove the trapped air or voids.
3. The liquid solder is exposed to overpressure for the second time.
4. Pressure is released as soon as the alloy has solidified.

Figure 24: Reflow oven integrated with overpressure chamber: a) the technology schematic design, b) the heating requirement for temperature profile with overpressure function in reflow zone [188]

As shown in Figure 24, b), after a short time at peak temperature and natural outgassing of evaporated volatiles , Nitrogen gas (N_2) is pumped from an external intermediate cylinder into the chamber, and pressure is built-up to hold and suppress the solder joint against formation of new voids in the solder joint. By instantly releasing the pressure, the recent formed voids are outgassed. To freeze the void-free solder joint, the pressure is built up again and held until the joint is slowly cooled. This is done by the clocked conveyor travers system, which transports the product to the second convection zone of the hyper pneumatic chamber. At the second position, the joint is simultaneously completely cooled and the pressure is completely released. The nominal temperature in the second zone is already set to a value below the liquidus temperature of solder alloy, which allows the solder to solidify while under pressure. This squeeze-release process mechanism forces voids to gas out of the solder connections. Then, the PCB is delivered to the cooling zone, where two individual cooling stages use running water and air as a coolant [188] [191].

4.1.2 Description of the Solder Profiling

The reflow soldering process is thermally treating the substrate assembled with electronic components in a specific temperature level, for a specified period of time, at a proper heating gradient. A thermal profile time-temperature curve is commonly generated to adjust the heating parameters and to control the thermal effects on the assembled boards. As illustrated in Figure 24, b), the timestamps of reflow thermal profile separated into 4 process zones in which the heat for each zone is independently controllable. These are preheating, soaking, reflow (peak) and cooling zones. Each heating zone is controlled with a heating gradient rate and elapse time, and the function mechanism of each zone is explained in detail in the following.

Preheating zone

Generally the solder material is heated to its liquidus temperature. The preheating time not only defines the time that takes during the preheating zone, but also defines the time between the initial temperature and the melting temperature. It is crucial not to exceed the maximum permissible load temperature and the processing time. If the process is too slow in the preheating zone, there is a risk that the flux will be consumed completely, and if it is too fast, the flux activation is not taking place. Furtherly the blowing fan power is regulating the efficiency of convectional heat transfer from the zones onto the substrates.

Therefore, a well-defined heating gradient in preheating zone is assuring a qualitative soldering process. The heating gradient of 0.5 °C/sec–1 °C/sec is recommended in the preheating zone [12], and it can be calculated by equation 23. The initial temperature is 25 °C which is the ambient temperature. 210 °C is selected as the outlet temperature before the PCB enters into the overpressure chamber. The length of preheating zone is 2400 mm, and hence according to the recommended gradient in the literature, the transport band speed is calculated between 39 cm/min–78 cm/min.

$$Heating\ gradient = \frac{\left(Intial\ temperature\ in\ preheating\ zone\ (°C) - Outlet\ temperature\ (°C)\right)}{Length\ of\ conveyor\ belt\ (mm)/Transport\ speed\ (mm/min)} \quad (23)$$

The purpose of preheating is to allow the solvents to evaporate and to activate the flux. An increment part of preheating zone is soaking zone. The soak zone brings the temperature of all components and board areas to an equal level. Due to differences in thermal inertia and thermal capacity of materials, components do not heat up at the same speed. This is especially the reason of infrared heating before the peak zone. However, uneven absorption of infrared energy is deduced due to color and surface reflectivity of components in demonstrators with thru-hole components. As shown in Figure 25, in the preheating zone, the PCB material and solder joint temperature curves are showing a temperature-increase up to 150 °C. Subsequently in the soaking zone, the temperatures of these components are demonstrating a close and similar behavior as the air temperature in the oven. It is inferred that the materials that are absorbing the heat reference with delay, then losing it slower.

Peak zone

In the reflow zone, the temperature rises at a rate of approximately 2 °C/sec to a temperature above the melting point (the temperature above liquidus).The desired fast soldering process requires a minimum soldering temperature of 10% above melting point (based on Kelvin scale), independent from the solder alloy. This is because solder both joins better with the copper and wets the pads and component pins better when it is hotter, and thereby it is creating better solder joint. On the other hand, high temperatures are usually prohibited for assembly processes because of sensitive components and printed circuit board materials. The temperature above liquidus should be held for 40 to 80 seconds, so that an intermetallic compound is able to form [33].

In addition of considerations for the peak zone in classical soldering ovens, the pressure build up process in the oven in this study is influencing the thermal behavior of materials in the peak zone. Additional mechanical function of pressure build-up is affecting the elongation of reflow time and the process details are illustrated in Figure 25. The setup peak temperature for this profile is 285 °C. When the PCB is entering into the overpressure chamber, the solder material will be in molten state. However, as like the function of soaking zone in preheating zone, the material of different electronic components are requiring an elapsing time to reach to peak temperature. The solder material is requiring a waiting time at normal pressure to ensure complete natural outgassing of the gasses formed. Then, the PCB is subject to overpressure, which is decelerating the new gas formations in the solder joint. In the next step, the pressure is released, and the existing voids or the trapped gases are exhausted out of the solder joint during the pressure release leading to reduce voids. The overpressure and release process can be repeated up to two times to ensure the completion of gas exhaust from the solder joint (multiple Squeeze-Release) and it follows with the final pressure built-up (Squeeze).

As illustrated in Figure 25, the PCB is moved into the second zone in overpressure chamber for solidification, which is setup with a temperature below the liquidus temperature of solder material (Freeze). An important step here is that before releasing the final pressure, the components are to be moved into the second position to ensure a void-free solder connection. During this process, there are six quartz-based heaters in the bottom side of the chamber which is homogenizing the heat treatment and therefore the incident temperature differences due to the overpressure build-ups. The pressure build-up cause a sudden temperature drop, and subsequently the quartz heaters immediately are compensating the heat drop by an incident increase of heat source under the substrate, which is demonstrated as peaks in the air temperature curve in Figure 25. In contrary by the overpressure release, the air temperature is also showing an incident drop in the curve which is compensated immediately by the quartz heaters.

Cooling zone

The time between the solidification point of the solder and the reaching of the final temperature is defined in the literature as the cooling time, which should be kept as short as possible [12]. In the cooling zone, two situations could occur. During rapid cooling, a fine-grained structure can

form which is positively influencing on the stability of the solder joint. On the other hand, a fast rapid cooling cause the stress and damage of components due to the different expansion coefficients [18] [192]. In the literature, the value for the cooling time for electronics production has been recommended between 40 and 60 seconds [179]. The cooling zone is equipped with cooling water pipes. Two convectional blowing fans are continuously exchanging the heat source in this zone with the environment. The substrates are nearly reaching to the ambient temperature when they are leaving the reflow oven.

4.1.3 Process Variables and Responses

Previous studies for reflow soldering process in SMT assembly are confirming that there should be an agreement between the design of the assembly, settings of the reflow oven, and the heating requirements for obtaining an acceptable reflow thermal profile [22] [24]. For the sake of efficiency, accuracy, and economical reasons, domain experts evaluated the collection of variables and chose ones that would be fruitful to an experimental design. Therefore, the process setup variables selection of the soldering process is based on the recommendations from literature review of this work, the screening process, and the field knowledge of veteran experts.

The process setup variables are producing the heating requirements, and thermal profiling is controlling the quality of voiding process. The heating requirement for solder profiling in preheating zone associated with overpressure function are shown in Figure 24, b). Figure 25 is detailing the process variables in overpressure module. These variables specifically are associating a big influence on voiding process mechanism in the first zone of overpressure module. By control of these variables, the responses could be controlled. The soldering oven technology with overpressure function is proven for the minimization of void fraction, but the setup function (combination of the setup variables of the machine technology) and the mechanism of the overpressure module is not scientifically investigated yet.

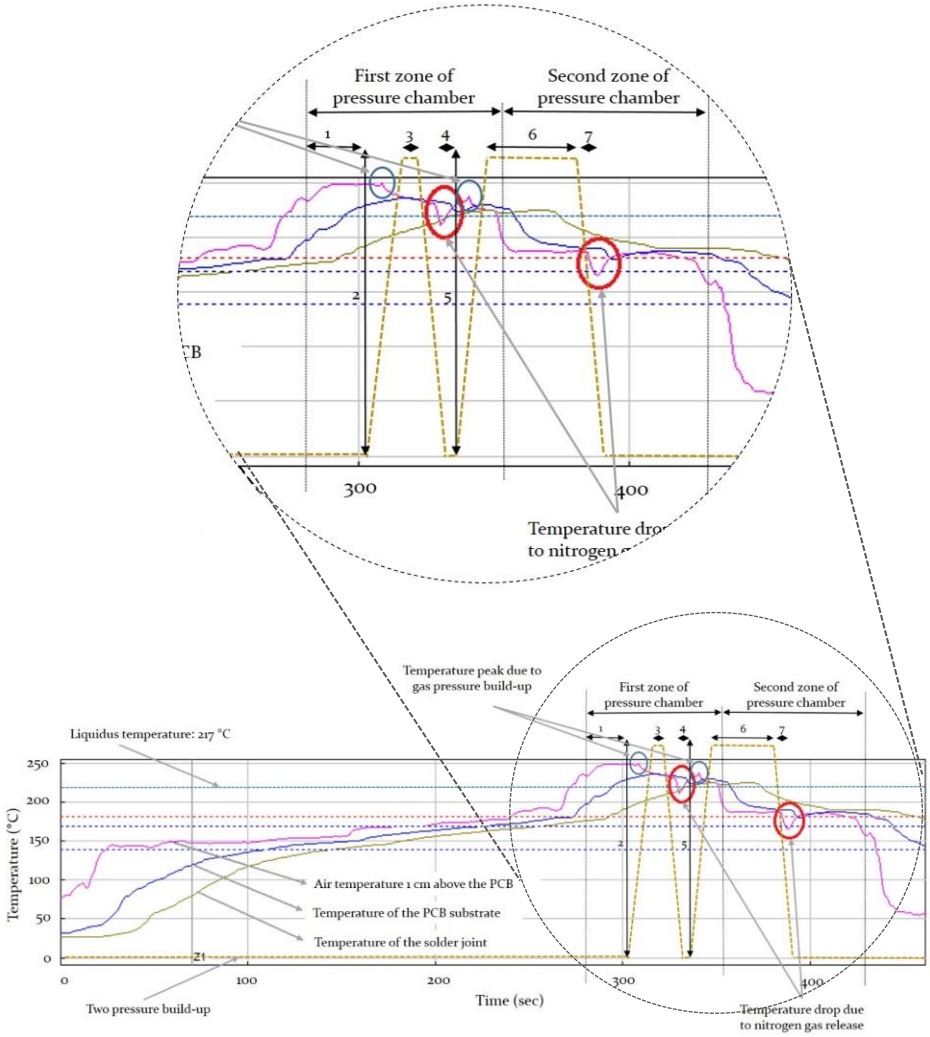

1. Waiting time until the first pressure build-up
2. Measure of the first pressure build-up
3. The first pressure holding time
4. Waiting time in between of the pressure build-ups
5. Measure of the second pressure build-up
6. The second pressure holding time
7. Pressure release time

Figure 25: Process variables for overpressure module in soldering oven

Figure 26 is showing the input setup variable and heating requirement responses for overpressure reflow profile. The input is comprised of the settings of the reflow oven for the preheating zone, overpressure chamber

(peak zone), and cooling zone, as well as PCB flow pitch. The conveyor speed and temperature (°C) setup are defining the responses including the slope (°C/sec) and the measure of heating or cooling rates. The setup parameters in overpressure chamber, as seen in Figure 25, is the combination of the gas pressure build-up, the measure of the pressure and the in-between process waiting times. These parameters are crucial because they are defining the thermal treatment for a void-free soldering process under the overpressure and above the liquidus temperature. Given the same temperature settings, the PCB flow gap also should be defined so that the pace of process flow in the oven kept constant. The throughput time in the overpressure chamber is always lower than the preceding process flow in the preheating zone. Hence, the PCB gap between two consecutive boards (the input PCB into the oven) should be so designed that it obtains a continuous flow process in the entire oven. Furthermore, the air fans power are setup for the maximum configurable measure because it obtains the maximum heat transfer coefficient on substrate.

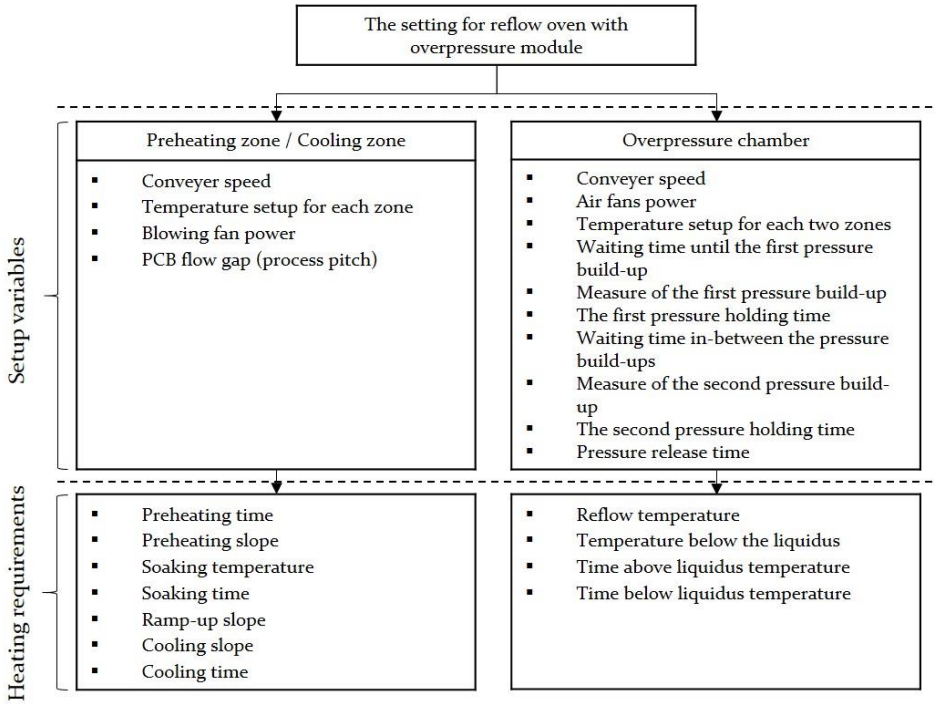

Figure 26: Process setup variables and heating requirement responses for overpressure reflow profile

4.2 Design of Experiment (DOE) and Quality Assessment Approach

To conduct the RSM approach, first a Design of Experiment (DOE) design should be implemented. The DOE is the design of a framework that aims to describe or explain the variation of information under conditions that are hypothesized to reflect the variation. The variation of information are usually rather complex and hence difficult to control. To cope with these difficulties and overcome the complexities, the variables should be discovered which have the most influence on response and therefore the cost of the experimental design also will be reduced. All process variables are introduced in Figure 26.

As explained in chapter 2.3.3, for the first step, a set of 2^k experiments should be conducted which are usually referred to as screening designs. The 2^k refers to designs with k factors where each factor has just two levels. These designs are created to explore a large number of factors, with each factor having the minimal number of levels, just two. By screening we are referring to the process of screening a large number of factors related to study. Due to efficiency, cost factor and accuracy, the collection of all variables could not be included in the design of experiment and those ones should be chosen that are fruitful with the most interactive effect on responses. More important factors are sorted out and used for the second-order models. After the screening the variables, the full factorial 3^k design is used to analyze them to understand the actual response functions. The results are statistically analyzed and the interaction effect of variables on void creation is studied by application of RSM approach. Apart from void ratio investigation, the average of shear force for resistor components is investigated and the general optical inspection is conducted for further solder joint defects. In parallel, the power consumption of the oven technology during each experiment is measured and the results are used for resource consumption analysis.

4.2.1 Void Ratio Investigation for Solder Joints

To investigate the void fraction of solder joints, an image analysis approach is employed. The solder joint connection of a Quad-Flat No-Leads (QFN), as shown in Figure 27, is considered for void formation investigation per each solder profile, because in the larger area of a solder joint larger inclusions of void can form. The X-ray images are captured with X-ray system, XD7600NT from Nordsen Dage (Figure 27, a)) and then they are analyzed for the void ratio analysis using the software

ImageJ (Figure 27, b)). The software *ImageJ* is used as the means of color recognition tool, in which the voids appear with bright gray color from X-ray images. The software *ImageJ* determines the threshold of the brighter and darker pixels, and it is coloring the darker area in red (Figure 27, b)). Using the tracing tool of the software, the pad area of the QFN that is soldered is being captured and it is shown in yellow border. This procedure is necessary because the image analysis requires the largest possible area, which has a uniform brightness level. By realizing the portion of the area with red pixels in yellow border, the void fraction is obtained by the software. The setup Macro for all images are kept constant and all reported fraction by the software are controlled again for the sake of the result accuracy.

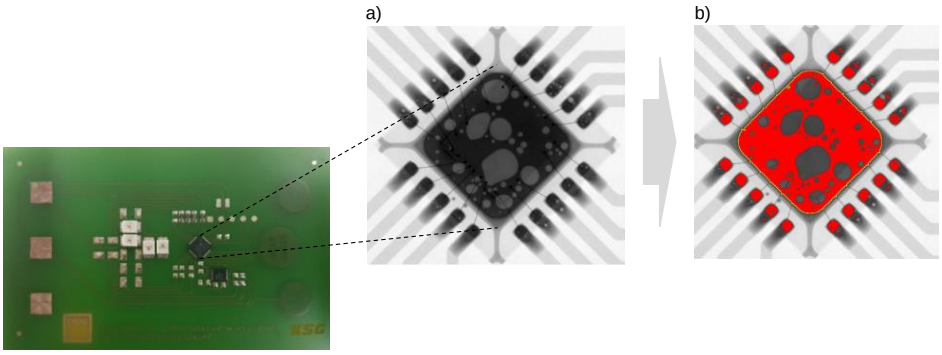

Figure 27: Void ratio analysis a) original image from X-ray system b) image for threshold analysis using ImageJ software

4.2.2 Screening Process for the Most Influential Variables on Void Formation

The screening process for the most influential variables is divided into three analysis steps in three individual zones for preheating, overpressure chamber and cooling zones. In each step, the void portion as the main objective of quality factor is investigated and analyzed for variables interaction. The starting point is proposition of a temperature setup created based on the thermal profiling constraints for process variables and responses as discussed in chapter 4.1.3.

Because the Time Above Liquidus (TAL) is proven to be the most essential factor on void formation [10], the first attempt refers to the influential variables on void fraction in the first and second zone in the overpressure chamber. The applied solder material has a melting point of 217 °C. The recommended peak temperature in classical soldering process is 10%

above the melting point of solder material. Due to additional overpressure function and unknown behavior of heating gradient of nitrogen gas during the overpressure process, the peak temperature in this study is setup 30% above the melting point and therefore 285 °C. The temperature in the second zone of overpressure chamber is set below the melting point of solder material and therefore 212 °C. The transport band speed is 60 cm/min and the current setup power for the blowing fans is 70%. Waiting time between the pressure build-ups is kept minimum as possible so that the solder joint have less outgassing chance for further void formation. The second overpressure holding time should be long enough so that the PCB is moved to the second zone of chamber and subsequently cooled down below the liquids temperature. The speed of transport traverse band in the chamber is not crucial, and it should be configured at the highest speed. Lastly, the solder joint for an assured duration of waiting time in the second zone of chamber is cooled down after the second overpressure. Table 3 is showing the first setup attempt in screen process.

Table 3: Temperature profile setup for overpressure chamber in screening process

Preheating						Overpressure		Cooling	
Zone 1	Zone 2	Zone 3	Zone 4	Zone 5	Zone 6	Zone 1	Zone 2	Zone 1	Zone 2
150 °C	150 °C	160 °C	170 °C	180 °C	210 °C	285 °C	212 °C	25 °C	25 °C

Transport band speed in preheating zone and cooling zone	Blowing fan power for all zones	Waiting time until the first overpressure build-up	Measure of overpressure	The first overpressure holding time
60 cm/min	70%	20 sec / 50 sec	2 bar / 4 bar	5 sec / 20 sec

Waiting time after the first overpressure	The second overpressure holding time	Transport band traverse speed in overpressure zone	Waiting time after the second overpressure
5 sec	45 sec	75 cm/min	20 sec

Based on the results with the lowest void portion in the screening process for overpressure chamber, these parameters are adopted for the subsequent experimental design in the preheating zone and the second zone in the chamber. The complete combination of the setup parameters fully determines the interactions between the parameters within a zone. However, at the current state of the study, it is not possible to make any statements about the interactions of the setup parameters across zones.

In the profile setup in Table 3, there are 3 factors that are considered for changes in two levels, and therefore 8 ($=2^3$) experiments are conducted.

The profile with the waiting time of 20 seconds before the first pressure build-up, 4 bar overpressure, and 5 seconds of pressure holding time is showing the best void fraction of 4.89%. In average for the examined DOE, the profiles with 20 seconds of waiting time, 4 bar overpressure are showing 50%, and profiles with 5 seconds of pressure holding time 25% less void fraction in compare with other profiles. The biggest void fraction among all profile is 15.60%.

For the investigation of preheating zone, the preheating slope, soaking temperature and soaking time are targeted. In addition of thermal profile alteration, the conveyor speed is changed to study the thermal gradient of profiles. Table 4 is showing the profile setup for preheating zone.

Table 4: Temperature profile setup for preheating zone in screening process

Preheating						Overpressure		Cooling	
Zone 1	Zone 2	Zone 3	Zone 4	Zone 5	Zone 6	Zone 1	Zone 2	Zone 1	Zone 2
Temperature profile 1 (T1)									
150 °C	150 °C	160 °C	170 °C	180 °C	210 °C	285 °C	212 °C	25 °C	25 °C
Temperature profile 2 (T2)									
112 °C	132 °C	160 °C	210 °C	200 °C	210 °C	250 °C	203 °C	25 °C	25 °C

Transport band speed in preheating zone and cooling zone	Blowing fan power for all zones	Waiting time until the first overpressure build-up	Measure of overpressure	The first overpressure holding time
60 cm/min / 90 cm/min	70% / 100%	20 sec	4 bar	5 sec

Waiting time after the first overpressure	The second overpressure holding time	Transport band traverse speed in overpressure zone	Waiting time after the second overpressure
5 sec	45 sec	75 cm/min	20 sec

The measures for the best results in the first zone of overpressure chamber are presumed and the transport band speed, temperature, and the power of blowing fans are changed in two levels. In addition of the attempted thermal profile (T_1), the second profile (T_2) is proposed. A good and fast wetting is helpful for minimizing the amount of voids. A fast wetting which is able to transport the developing gases and residues out of the solder joints needs a certain minimum soldering temperature.

Karaalioglu [193] reported that for an efficient heat transfer rate for Seho oven, the peak temperature should be at least 10% above melting point,

and therefore 250 °C is determined as the minimum peak temperature setup. For both profiles, the temperature is reaching from 25 °C to 210 °C before the peak zone. If the transport band is configured for 60 cm/min, the preheating gradient including the soaking zone is 0.76 °C/sec, and the maximum theoretical preheating gradient is 1.15 °C/sec if the band speed is setup for 90 cm/min. The PCB flow gap is neglected for further discussion at the current stage of the study; however, its importance will be illustrated when the overpressure chamber is defining the production pace of preceding process in the preheating zone.

An experimental design with three variables including 8 (= 2^3) experiments is conducted. By the change of blowing fan power, however the heating rate is changing [26], but the result for void fraction in these profiles are not demonstrating a significant difference. The average difference of void portion for profiles with 70% fan power (5.62%) and 100% fan power (5.78%) is only about 0.16%. The combination of T_1 thermal profile and 60 cm/min obtains preheating slope of 1.56 °C/sec and it follows with 160 seconds of soaking time. If the speed is increased up to 90 cm/min, a steeper preheating slope of 2.3 °C/sec and 107 seconds of soaking time is obtained. The T_2 profile and 60 cm/min combination is deriving a preheating slope of 1.25 °C/sec and 140 seconds of soaking time. If the speed of transport band is increased up to 90 cm/min, the preheating slope is increasing to 1.88 °C/sec and the soaking time is shortened to 93 seconds. This profile is obtaining the best result with 3.87% void fraction.

Comparing with other profiles, a fast preheating slope before the soaking zone, allow activating the flux, and the shortest soaking time illustrate adequate duration to forbid extra release of volatiles. In contrary, the combined T_1 thermal profile with 90 cm/min demonstrates the worst result (7.70% void fraction). This is because the flux is activated much sooner and the solvents in higher temperature have faster gaseous activity. The analysis are explaining the void fraction reduction by a fast preheating slope before soaking zone and shortened soaking time. In addition, a smoother thermal process start aids the uniform treatment of PCB components material due to thermal inertia.

In the final step of screening process, the setup factors within the second zone of chamber are investigated. In this zone, the solder material is cooled down under overpressure below the liquidus temperature, before it is completely cooled down in the cooling zone. From the recent results, the profile setup for T_2 thermal profile with 100% blowing fan power and

90 cm/min transport band speed is considered. If the first zone is setup for 250 °C, the minimum temperature in the second zone due to temperature balance of adjacent zones will be 203 °C. Also an alternative temperature of 212 °C which is very close to liquidus temperature is examined in the second zone. As mentioned before, solder material in the second zone is cooled below the liquids temperature and there should be enough time so that the solder joint, during overpressure, is moved from the first to the second zone. Once the overpressure is released, a fast cooling is required and hence two alternative measures are examined for the waiting time after the second pressure release. Table 5 is showing the setup profile for screening process in the second zone.

Table 5: Temperature profile setup for the second zone of overpressure chamber in screening process

Preheating						Overpressure		Cooling	
Zone 1	Zone 2	Zone 3	Zone 4	Zone 5	Zone 6	Zone 1	Zone 2	Zone 1	Zone 2
Temperature profile									
112 °C	132 °C	160 °C	210 °C	200 °C	210 °C	250 °C	203 °C / 212 °C	25 °C	25 °C

Transport band speed in preheating zone and cooling zone	Blowing fan power for all zones	Waiting time until the first overpressure build-up	Measure of overpressure	The first overpressure holding time
90 cm/min	100%	20 sec	4 bar	5 sec

Waiting time after the first overpressure	The second overpressure holding time	Transport band traverse speed in overpressure zone	Waiting time after the second overpressure
5 sec	45 sec / 30 sec	75 cm/min	20 sec / 35 sec

For the current experiments, three variables are changed and therefore eight experiments are conducted. The impact of current variables on the result is much higher than previous experiments. The profiles with temperature of 203 °C are demonstrating significantly lower average void fraction (13.38%) compare with the temperature level of 212 °C (18.88%). Longer overpressure holding time for 45 seconds obtains better result with an average void fraction of 12.88%. 30 seconds of overpressure holding time shows the average void fraction of 19.38%. The waiting time after the second pressure build-up for 20 seconds delivers 14.51% of void portion comparing with 35 seconds that obtains 17.74%. Therefore, the profile setup of 203 °C, 45 seconds of holding time and 20 seconds of waiting time is showing the best void portion of 4.56%. The worst result is demonstrated by setup of 212 °C, 30 seconds of holding time and 35

seconds of waiting time after the second pressure build-up with void fraction of 22.43%.

4.2.3 Development and Conduction of full factorial Design of Experiment (DOE)

From the screening process in previous chapter, the independent variables that have vital effect on the soldering process are identified through a 2^k design. For a comprehensive conduction of DOE, considering all variables, which are interacting on responses, are mandatory. However, there is a consideration of trade-off between data collection cost and sample size. To minimize the design deflection, Franklin [194] has provided an introduction to generate a 3^K orthogonal array with k design parameter. Orthogonal array testing is a systematic and statistical way of a black box testing technique used when number of inputs to the application under test is small but too complex for an exhaustive testing of every possible input to the system. 3^K design will be used to find the optimal solution from the major factors which are identified in screening process.

The screening process excluded the reflow zone, and it will be considered in Full Factorial design shown in Table 6. Some variables are realized with negligible influence and therefore they are set at their minimum value. Some variables are identified with their optimum value and hence they are set as constant in the DOE. 90 cm/min combined with T_2 thermal profile derives a good preheating gradient and soaking time. The power of blower fans is set at its maximum. The first pressure build-up suppresses further creation of voids in the peak zone, and the release of pressure hence releases the voids created before the pressure build-up. The holding time and the waiting time after the first overpressure, is kept as minimum. 45 seconds is long enough so that the transport band in the chamber is moving the substrate from the first to the second zone, which is set below the liquidus temperature. The waiting time after the second overpressure is set according to the best result in screening process. Therefore, a set of configuration is tabulated below for a Full Factorial design of 27 run.

Table 6: Temperature profile setup for the full factorial DOE

Preheating						Overpressure		Cooling	
Zone 1	Zone 2	Zone 3	Zone 4	Zone 5	Zone 6	Zone 1	Zone 2	Zone 1	Zone 2
Temperature profile									
112 °C	132 °C	160 °C	210 °C	200 °C	210 °C	250 °C / 285 °C / 300 °C	203 °C	25 °C	25 °C

Transport band speed in preheating zone and cooling zone	Blowing fan power for all zones	Waiting time until the first overpressure build-up	Measure of overpressure	The first overpressure holding time
90 cm/min	100%	20 sec / 40 sec / 60 sec	0 bar / 2 bar / 4 bar	5 sec

Waiting time after the first overpressure	The second overpressure holding time	Transport band traverse speed in overpressure zone	Waiting time after the second overpressure
5 sec	45 sec	75 cm/min	20 sec

Setup variables in full factorial design

Profile	1	2	3	4	5	6	7	8	9	10	11	12	13	14	15	16	17	18	19	20	21	22	23	24	25	26	27
Temperature	250	250	250	250	250	250	250	250	250	285	285	285	285	285	285	285	285	285	300	300	300	300	300	300	300	300	300
Pressure	0	0	0	2	2	2	4	4	4	0	0	0	2	2	2	4	4	4	0	0	0	2	2	2	4	4	4
Waiting time	20	40	60	20	40	60	20	40	60	20	40	60	20	40	60	20	40	60	20	40	60	20	40	60	20	40	60

The heat absorption rate varies from component to component. The heat rate for a larger component (such as a quad flat package QFP component or substrate material) is slower than those for a smaller sized one (i.e., resistor chips/capacitor chips or solder joint). As seen in Figure 25, the components temperatures after entering into the first zone in the chamber are not uniform and they are depending on the temperature value and the waiting time before the first overpressure. Especially for the solder material and the heat absorption duration that has a big influence on the void formation in parallel with the overpressure function.

Therefore, additional measure of reflow temperature of 300 °C is considered in the full factorial DOE. Furthermore, according to the screening process, the waiting time until the first overpressure (the time above the liquidus) and the measure of overpressure level are demonstrated with significant interaction on void ratio creation. These three variables are considered for the DOE, and the setup profile is shown in Table 6. According to orthogonal array testing If we have 3 parameters, each can have 3 value level then the possible number of tests using conventional full factorial method is 27 ($=3^3$). The experiments are conducted and the results are discussed in the following session.

4.2.4 Void Ratio Result, Statistical Analysis and Meta-model Development

The optical inspection for all electronic components is conducted and four QFN packages per each profile are investigated for void fraction. The utilized solder material $Sn96.5Ag3Cu0.5$ exhibits a non-eutectic behavior. Soldering process will be complicated if the solder alloy does not behave as a eutectic[4] and solidifies over a range of temperature with more than one stage of solidification. The solder joint might be formed at the lowest possible temperature of solidification for any mixture of specified constituents. Solidification begins at around 219 °C with the growth of primary tin (Sn) dendrites which continue to grow as the solder cools to 217 °C when the remaining liquid, enriched in silver (Ag) and copper (Cu), solidifies as a eutectic [10]. The molten solder is isolated within the network of primary tin dendrites and therefore the solidification and reduction of the volume delivers accommodated voids. Voids created in this process are obtained irregular shape that reflects the shape of the solidification front that formed them. If the reduction of volume is extreme, the shrinkage of the voids could intersect the surface of the solder joint which appears as crack cavity or shrink hole. However, no crack is observed in the solder joints as defects. This is because the void size in the preceding process in the peak zone is reduced under overpressure before creation of macro voids.

In interval plot shown in Figure 28, the void fractions are plotted and the average result per each solder profile are shown. Individual standard deviations were used to calculate the intervals. The ANOVA analysis is

[4] Relating to or denoting a mixture of substances (in fixed proportions) that melts and solidifies at a single temperature that is lower than the melting points of the separate constituents or of any other mixture of them.

performed with Minitab software, which is already introduced in chapter 2.3.4. The regression analysis demonstrates R^2 value of 81.40%. R-squared explains the variability of the response data around its mean. Hence, in this case, this value explains that the model 81.40% fits the void ratio data well. This ratio could be improved if the standard deviation would be less for the results of profile numbers such as 12, 22, 23, and 25. By the decrease of Individual standard deviations in each profile, R^2 is increasing, however in a dynamic and qualitative process like void formation, this value is considered as a good fit value. Temperature profile 7 (250 °C, 4 bar, 20 sec) with lowest standard deviation shows the lowest average void ratio of 4.54%, and temperature profile 3 (250 °C, 0 bar, 60 sec) demonstrate the largest void ratio of 28.34%.

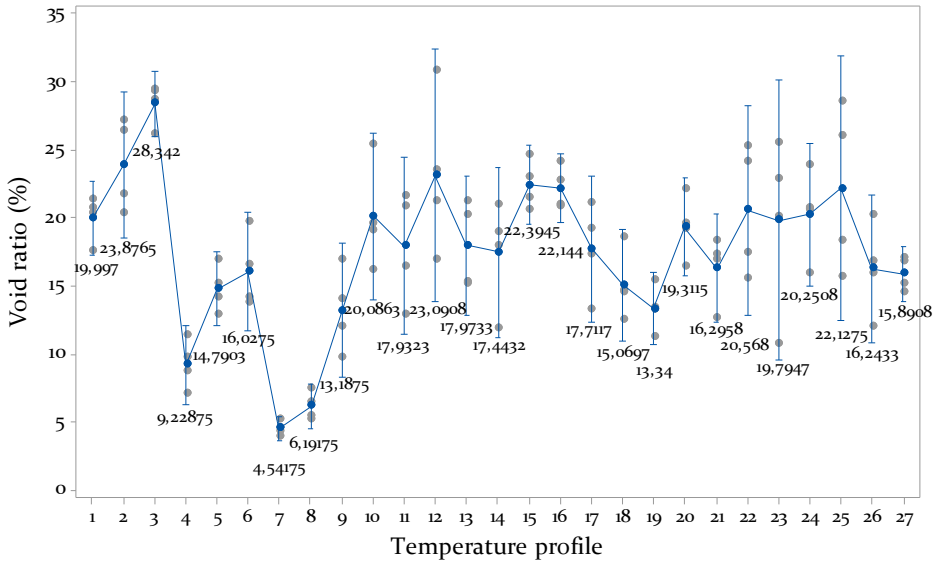

Figure 28: Interval plot for void ratio per each profile

After data collection, they should be checked for model adequacy using the residual plots. A high R^2 value demonstrated with good results from residual plot is proving the reliability of the model. If the normality assumption is not violated, the conclusion reached by a regression analysis in which normality is assumed will generally be reliable and accurate. From the normal probability plot, to determine whether the void ratio data follow the distribution, the P-value is compared to the significance level. Usually, a significance level of 0.05 (5%) is reliable. If the P-value is larger than the significance level, the decision is to fail to reject the null hypothesis because there is not enough evidence to

conclude that the data do not follow the distribution. Hence, a significance level of 0.05, indicates on the risk that the data do not follow the distribution is 5%. The probability plot assesses how closely the data points follow the fitted distribution line. If the specified theoretical distribution is a good fit, the data points fall closely along the straight line. As shown in Figure 29, the void ratio in the normal probability plot follows the fitted line well. In addition, the null hypothesis states that the data follow a normal distribution. Because the P-value is 0.192, which is greater than the significance level of 0.05, the decision is to fail to reject the null hypothesis. It cannot be conclude that the data do not follow a normal distribution.

A residual versus fitted values plot is used to check if the variances of the error terms are constant and they must have a mean of zero. If this is not the case, your model may not be valid. To check these assumptions, as shown in Figure 29, the points on the plot appear to be randomly scattered around zero, so assuming that the error terms have a mean of zero is reasonable. The vertical width of the scatter does not appear to increase or decrease across the fitted values, so we can assume that the variance in the error terms is constant, and the model is reliable.

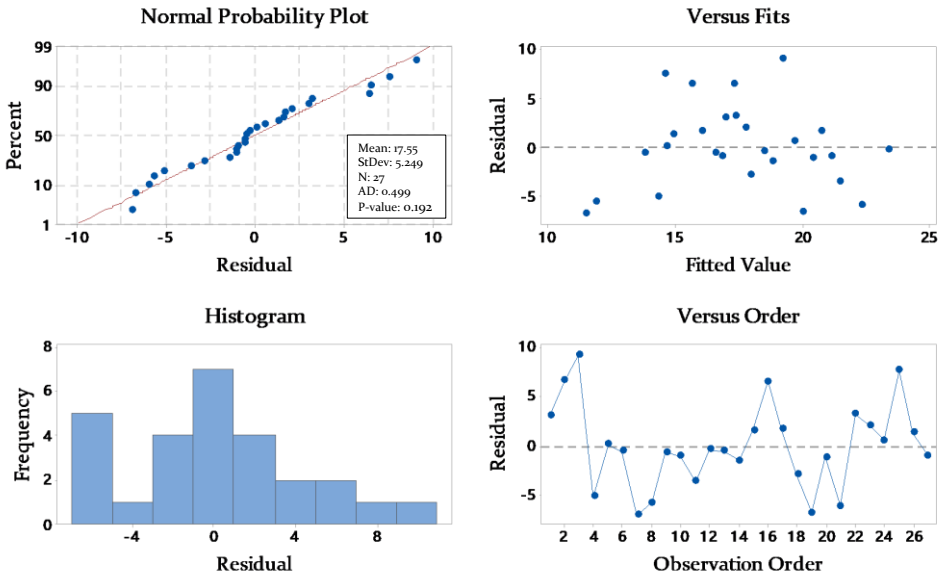

Figure 29: Residual plots for void ratio (%)

A histogram is most effective when there are approximately 20 or more data points. As for this study, the histogram for 27 profiles are not

showing a long tail in one direction, or a bar that is far away from the other bars, and hence the model does meet the model assumptions.

The residuals versus order plot mean to verify the assumption that the residuals are independent from one another and to detect the time dependence of the residuals. The demonstrated plot shows the randomly distribution of residuals around the centerline, and also no trends or patterns when displayed in time order.

After results verification, an analysis with Full Factorial design is conducted to investigate the significance level. The deployed design is a second-order model but the analysis are conducted for linear and interaction of factors on responses. Table 7 shows the effects (F-value) and significances (P-value) of the setup parameters on void ratio. Pressure parameter demonstrate that it has the highest statistically significance associated effect on the void ratio with F-value of 29.39, which is proved by P-value of 0.000. Temperature and waiting time parameters are also showing their significance by P-values of 0.007 and 0.028 in the next levels. The analyses of parameters interaction illustrate the highest significance of temperature and pressure effect on each other with F-value of 39.52. The pressure and waiting time interaction is showing the lowest effect because the waiting time occurs before the pressure build-up in the process.

Table 7: The significance analysis for void ratio

Factor	F-value	P-value
Temperature	9.15	0.007**
Pressure	29.39	0.000***
Waiting time	5.60	0.028*
(Temperature) * (Pressure)	39.52	0.000***
(Temperature) * (Waiting time)	10.68	0.004**
(Pressure) * (Waiting time)	4.50	0.047*
Regression Equation in Uncoded Units: Void ratio (%) = -7.1 + 0.0789 Temperature – 25.19 Pressure + 1.457 Waiting time + 0.0913 Temperature*Pressure – 0.00474 Temperature*Waiting time – 0.0395 Pressure*Waiting time		

By using the main effects plot, the differences between level means for one or more factors is examined. There is a main effect when different levels of a factor affect the response differently. A main effects plot graphs the response mean for each factor level connected by a line. As shown in

Figure 30, the increase of pressure shows a significant difference in the magnitude of the effect on reduction of void ratio. The significance analysis also proves this fact. In addition, the increase of waiting time demonstrates the increase of void ratio formation. Although the increase of temperature shows the increase of void formation up to 285 °C but the further temperature raise up to 300 °C consumes the solder volatiles completely.

Using an interaction plot, shown in Figure 31, infers that how the relationship between a parameter setup and void ratio depends on the value of the second parameter setup factor. This plot displays means for the levels of one factor on the X-axis and a separate line for each level of another factor. For some parameters, the lines are rather parallel and no interaction occur, however for the temperature and pressure parameters, the most nonparallel lines are illustrating the magnificent of strength of the interaction. The significance of interaction is illustrated in Table 7, and this fact is proven by the highest F-value. The pressure and waiting time combination are displayed with rather parallel line with a slight interaction. At the temperature of 250 °C, the increase of waiting time significantly effect on the increase of void ratio; however the waiting time has not much effect on void formation increase in other two temperature levels. Likewise, the pressure increase straightly decrease the void fraction at the temperature of 250 °C, however the effect of pressure changes in other two temperature levels are not much significant on void formation.

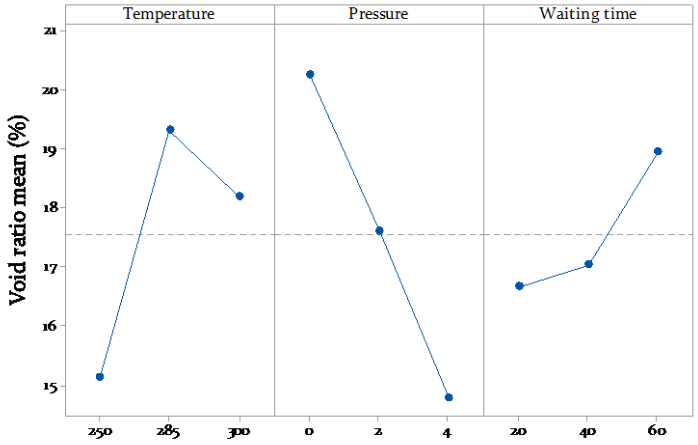

Figure 30: Main effects plot for void ratio

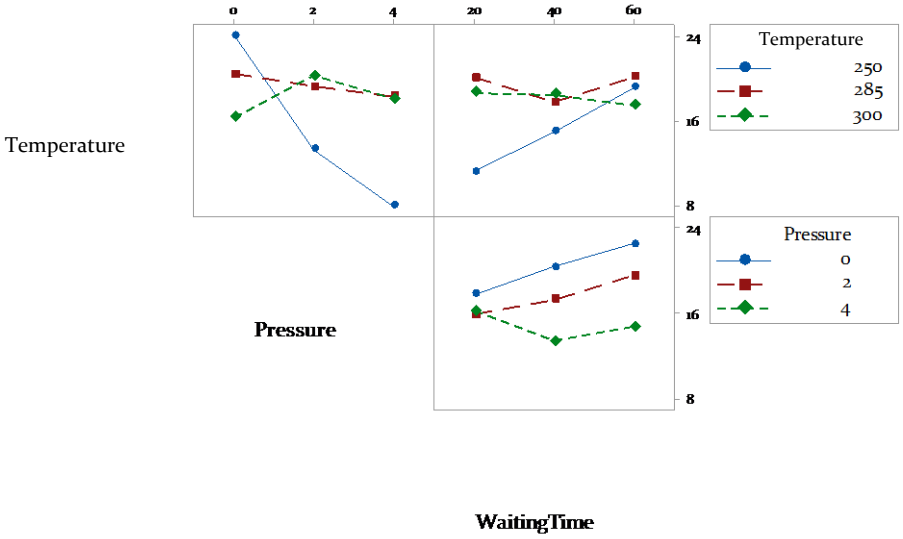

Figure 31: Interaction plot for void ratio

The interaction effect diagrams for all profiles with the respective setup parameters are plotted by MATLAB software and they are shown in Figure 32. The curve fitting tool is used to interpolate the data by Thin-plate spline method. From Figure 32, a), it is inferable that respect to the significant interaction of temperature and pressure, the void ratio by increase of pressure and decrease of temperature is highly decreasing. However, the associated technology limit for overpressure chamber (the maximum allowed overpressure setup up to 4 bar), and the limitation for the minimum heat transfer coefficient (the minimum setup temperature for the oven (250 °C) respect to solder material with melting temperature of 217 °C), does not enable further investigations beyond this setup measures to investigate more extended interaction of these factors.

The pressure of inside void bubble gas is contributed directly by the evaporation of flux and associated solvent and it depends on the temperature. The pressure of atmosphere is prohibiting the void to grow, and on the other hand, if the temperature of flux is reaching to the equilibrium, it stops evaporating and hence the void stops growing. Therefore, the void ratio is less at the waiting time of 20 seconds comparing with 60 seconds. In addition, by increase of overpressure level in the machine, voids are stopping growing, and by the release of overpressure, the macro voids are tending to escape. A higher

overpressure gives the voids a higher chance and longer time to release. As shown in Figure 32, a), if this fact is combined with lower temperature at 250 °C where the solvents have even less chance of creation of more gas, then it obtains the best results. The best void ratio is achieved at a peak temperature of 250 °C, waiting time of 20 seconds, and pressure of 4 bar. The results for 300 °C at different levels of overpressure are rather similar because the flux volatiles are already consumed before the overpressure changes make a significant effect on voids release.

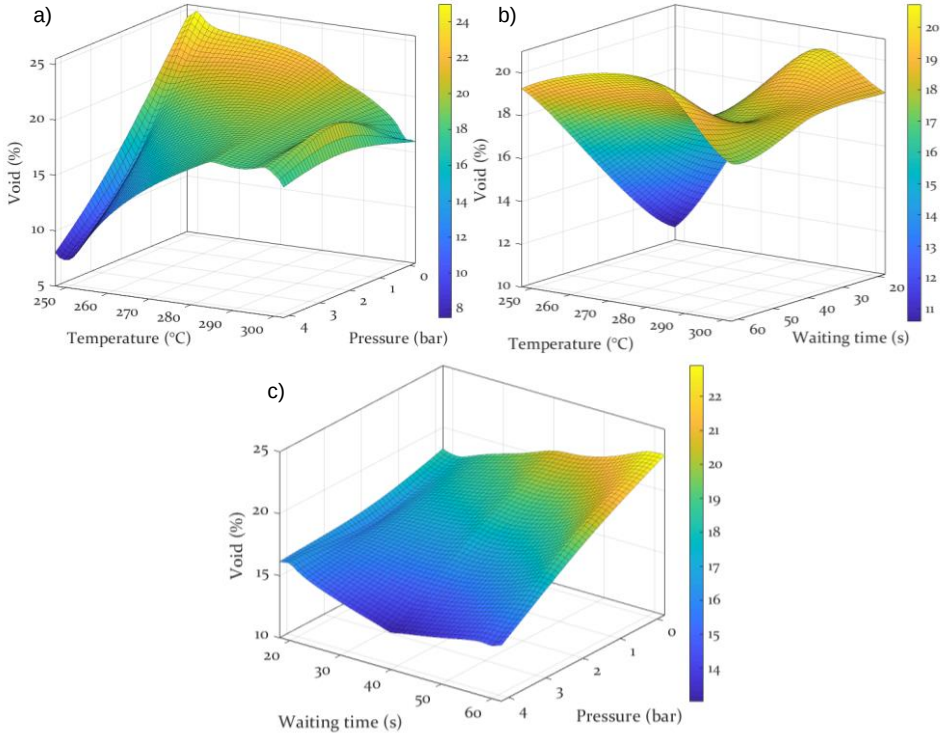

Figure 32: Surface plot for interaction effects on void ratio for: a) temperature and pressure b) temperature and waiting time c) waiting time and pressure

Figure 32, b) demonstrate that by increase of the waiting time (reflow time and/or time above liquidus) and temperature (peak temperature), the void formation is progressing, because the micro-voids have more time to form the bigger voids as well as the flux evaporation is prolonged. If the bigger voids have enough reflow time to reach the surface, and/or if the temperature is increasing to certain state, bigger voids are able to escape and hence the incidence of voiding is reduced. The high incidence of voiding with the lower temperature is thought to be due to the inferior

wetting that left a lot of non-wetted areas to which a bubble could attach and less time for the trapped bubble to escape from the molten solder during the time above liquidus. In contrary, the higher incidence of voiding with the high reflow profile is thought to be due to the higher incidence of non-wetted areas because of the exhaustion of flux activity during the longer TAL. This is also inferred in Figure 30 for the temperature effect on void fraction changes. The largest void ratio is achieved at a peak temperature of 285 °C, waiting time of 60 seconds, and pressure of 0 bar. However, by increase of temperature up to 300 °C, the void ratio begins decreasing. The waiting time and pressure factors are associating the lowest interaction significance, and hence their influence on void ratio should be interpreted separated. In Figure 32, c), the void ratio is not considerably changing, however the pressure build-up assist the voids to be minimized. The pressure influence on void ratio appears almost linear. Higher pressure obtains lower void ratio. The interaction of the pressure with the waiting time shows a simple pattern.

4.2.5 Shear Force Investigation of Solder Joints, Statistical Analysis and Results

The shear force test is conducted based on 2^k design to investigate the main effects of 3 main variables are defined in Table 6. Therefore, per each profile, 8 measures are required for this test. The average of shear force for two resistors per each single PCB is calculated, and hence four PCB in one panel obtains four average values. Figure 33 plotted the 4 mean of measures and the total average per each profile. The best shear force is addressed by the profile 7 (250 °C, 4 bar, 20 sec) with the measure of 37.81 N, and the weakest at temperature profile 23 (300 °C, 2 bar, 40 sec) with the measure of 26.69 N. The analysis of variance shows standard deviation of 2.46, and shear force average of 30.73 N. The R^2 value of 43.25% and R^2 prediction value of 3.50% illustrate that the regression fitted model hardly explains the distribution of results around its mean. However, the low R^2 prediction and big deviation from R^2 value shows that the model is not reliable for further prediction usage, and it cannot be interpreted through three major variables. Therefore, the shear force data are not furtherly analyzed for their significance and variance. From the results it could be drawn that by increase of temperature the shear force is intensively decreasing, and by increase of waiting time, shear force rather increasing. In all profiles the shear force shows a linear increase from 2 to 4 bar.

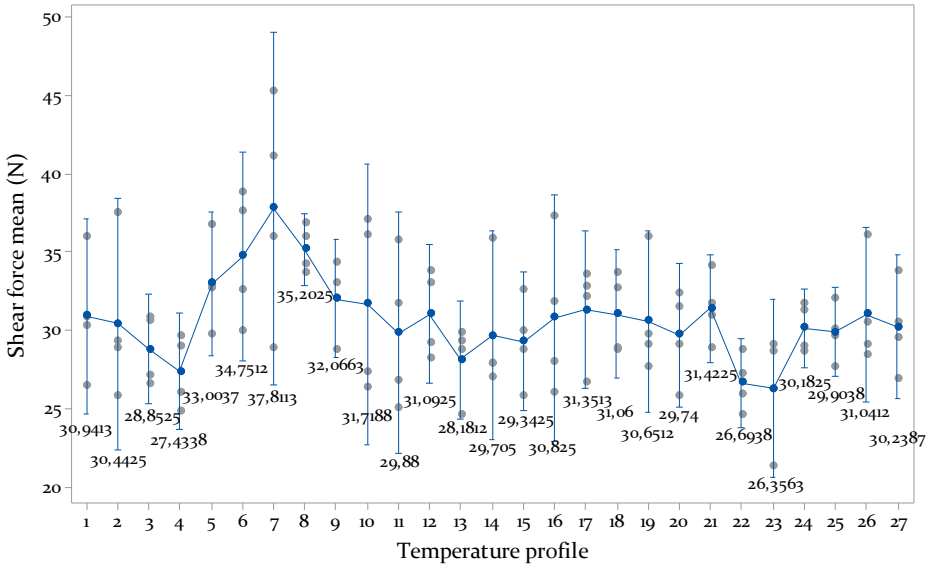

Figure 33: Interval plot for shear force per each profile

4.2.6 Further Solder Joint Defects

All demonstrators are optically inspected for any anomalies and defects listed in chapter 2.3.1. There are a constant number and size of solder balls are seen across the solder joints of resistors and none on the other electronic components. Too high heating gradient cause the creation of solder balls in soldering process, however, solder balls are detected in profiles with low heating gradients in this study. It is inferred that solder paste residues in stencil printing should be the main reason. The solder balls do not harm the electrical minimum isolation distance and therefore no short circuit detected. In all profiles, no further defects are detected.

4.3 Conclusion

In this chapter, a controlling procedure for voids minimization (quality criterion) in soldering process using overpressure module is elaborated. There is an agreement between the setup configuration of oven, heating transfer factors, and temperature measured on the substrate components. A detail study on the soldering oven technology and the controlling mechanism for thermal profiling is obtaining the process setup variables and heating requirement responses. There are a set of variables, which are demonstrating the significance on the quality of soldering process. A set

of experimental design followed by statistical analysis shows the vital parameters influencing a void-free soldering process and hence the significance of effect.

From this chapter, the following conclusions are drawn:

- According to the investigated experiments, reflows peak temperature, waiting time until the first overpressure (TAL), and the measure of overpressure level are demonstrated with significant interaction on void ratio. The regression analysis demonstrates R^2 value of 81.40%. This value explains that the model including the studied process variables (deduced from DOE) with the highest significance and coincidence measure of 81.40% fits the void ratio data well. 18.60% are influencing variables such as the solder printing machines and the dynamic process variables in soldering process, which are not considered in this study.
- Temperature profile 7 (250 °C, 4 bar, 20 sec) with lowest standard deviation shows the lowest average void ratio of 4.54%, and temperature profile 3 (250 °C, 0 bar, 60 sec) demonstrate the largest void ratio of 28.34%.
- The first overpressure build-up is decelerating the new gas formations in the solder joint, and by the pressure release, the existing voids or the trapped gases are exhausted out of the solder joint leading to reduce voids. The significance analysis demonstrates that pressure has the highest significance in the magnitude of the effect on reduction of void ratio. Temperature and waiting time parameters are also showing their significance in the next levels.
- The pressure of inside void bubble gas is contributed directly by the evaporation of flux and associated solvent and it depends on the temperature. The pressure of atmosphere is prohibiting the void to grow, and on the other hand, if the temperature of flux is reaching to the equilibrium, it stops evaporating and hence the voids stop growing. Therefore, the void ratio is less at the waiting time of 20 seconds comparing with 60 seconds.
- At the temperature of 250 °C, the increase of waiting time significantly effect on the increase of void ratio, however the waiting time has not much effect on void formation increase in other two higher temperature levels. Likewise, the pressure

increase straightly decrease the void fraction at the temperature of 250 °C, however the effect of pressure changes in other two temperature levels are not much significant.

- If the bigger voids have enough reflow time to reach the surface, and/or if the temperature is increasing to certain state, bigger voids are able to escape and hence the incidence of voiding is reduced. The high incidence of voiding with lower temperature is thought to be due to the inferior wetting that left a lot of non-wetted areas to which a bubble could attach and less time for the trapped bubble to escape from the molten solder during the time above liquidus. In contrary, the higher incidence of voiding with the high reflow profile is thought to be due to the higher incidence of non-wetted areas because of the exhaustion of flux activity during the longer TAL. However, by the extensive increase of waiting time above liquidus at higher temperature (300 °C, 60 sec) deduce the decrease of void ratio.
- For the shear force test, the statistical fit general linear model analysis is explaining the 43.25% of variation of shear force results, and hence the model does not demonstrate a linear interrelation with void ratio for further interpretation. The solder joints for resistors are might be too small to follow the mechanisms of void formation. Most research agrees that voids by themselves are not a reliability concern but rather the location of the voids within the solder joint that determines their negative impact, if any, on the reliability of the joint. Voids forming at the intermetallic layers and interfacial surfaces near the base metals of the component metal can be the stress concentration points for cracking during aging or shear force test [195].
- The optical inspection of solder joints demonstrates a constant number and size of solder balls across the joints of resistors and non on the other electronic components. Solder balls could be caused by a too high heating gradient. However other relevant defects caused by this flaw are not seen, and therefore, solder paste residues caused by stencil printing machine should be the main reason.

An alternative technology for overpressure soldering to target the voids creation below 5% is vacuum vapor phase technology. It is inferred that overpressure reduces the outgassing of voids significantly whereas the negative pressure and vacuum process accelerates it. The melting

temperature of the solder is not affected by the pressure change, but the atmospheric pressure influences the boiling temperature of the solvent significantly. After melting the solder material, the overpressure profiles show a much higher amount of voids in the solder joint than the profiles with negative pressure. For both vacuum and overpressure profiles, the number of voids does not change significantly during the pressure release. The higher the pressure, the slower the reaction gets. Therefore, vacuum support the reduction of oxides by the flux and overpressure process hinders it. It is inferred that vacuum processes exhibit a better wetting behavior of the solder than overpressure processes.

A pressure change does not stop the chemical reaction of the flux and thus the production of gas. The formation of new voids does only stop when either one of the reactants is empty or the joint is cooled below melting temperature, and the cooling of the solder joints causes the voids to shrink. The results for overpressure soldering demonstrated that a smaller void area can be achieved with shorter TAL as this minimizes the vaporization of flux volatiles during the reflow stage of the profile. The results for ramp to peak in reflow zone and short TAL profiles indicated that preheat appears to be effective in reducing the incidence of voiding as this allows excess volatiles to escape before reflow begins. Therefore, as expected, a shorter TAL and a lower peak reflow temperature might well minimize the likelihood of gas being generated by decomposition of flux constituents in voids trapped at non-wetted areas.

The influence of overpressure process during the complete peak time accelerated the IMP formation rate compared to vacuum vapor phase soldering. Though vacuum process soldering demonstrate advantages with void reduction, overpressure soldering emerges as a dominant mechanism for both void reduction and IMP formation at the same time [196]. In addition, the linear reduction of void ratio by the increase of overpressure shows that even the application of overpressure more than 4 bar could reduce the voids less than 4%.

The drawbacks for vacuum soldering refers to the selection of solder material, because some flux ingredients incline to extreme foaming so that the components can be uplifted or replaced. Also, PCB materials and also some components are tending to excessive outgassing in vacuum. Some electrolyte capacitors cannot tolerate the vacuum process because of the hermetically enclosed liquids. Another drawback is that heat transfer in the vacuum soldering cannot be done with the usual convection heating but only by means of infrared radiation or heat

conduction. The assemblies have to be heated sufficiently during this soldering process, so that the solder is still liquid in the following vacuum process. The overpressure soldering process allows heating of assemblies with forced gas convection, low temperature differences (delta *T*), and a controlled heating process. Moreover, outgassing materials and leaking components are not likely to result from a soldering process with elevated pressure. Less mechanical technology construction is required to reach overpressure range from 1–4 bar, and hence void release.

Similar for vapor phase technology principles, there are recent advancements for reflow soldering oven combined with vacuum modules. In this technology, to ensure a minimum thermal exposure it is essential to achieve a fast transition from the preheating zone into the vacuum area, which requires a powerful lock, and pump system as well as optimum vacuum pressure during the time when the solder material is still above the liquidus. Hence, it is inferred that any of vacuum and overpressure processes for a void-free solder joint has advantages and disadvantage which a compromised decision defines the best solution.

5 Controlling Procedure for Resource Consumption of Soldering Process

The resource consumption of a specific process is dynamic and highly depending on the process configuration of the machine. The cumulative load profiles of all machines in the production line are defining the total resource consumption for the product. However, the specific power consumption behavior of a process chain can be significantly influenced by its specific technical configuration and the process setup and control [54]. This includes the individual machine chain, their interlinkage (e.g. process chain structure, buffers) as well as aspects like planning, scheduling of orders (e.g. start time, capacity allocation) or flow of production. In addition to the production chain there is auxiliary equipment that is supporting the main body of the process chain. Also for the soldering process technologies, the dynamics of the interlinked production process and the interdependency of auxiliary equipment should be measured, analyzed and hence controlled.

Analysis of the resource flow for the machine and the auxiliary equipment in the process however is illustrating the quantity of the flow and hence the measure of consumption, but it does not illustrate the quality of resource transformation in the soldering process. Exergy analysis method is used to study the minimum amount of the required resources to complete the soldering process. Therefore, first, a transparency model is developed which is illustrating the flow of electrical energy of the oven technology and periphery equipment. To build such a model for soldering process, a keen understanding of the technical process systems and the technology is mandatory. Then, a simulation tool is utilized by means of imitation purposes in order to consider the predictable and non-predictable process breaks in the total power consumption of soldering process in this case study. By realizing the resource flow balance of the process, an exergy method is conducted and the investigation is followed by statistical analysis. The analysis is presented by a meta-model to discuss the most significant parameters which are influencing on the final resource consumption on periphery levels. This enables the saving potentials for resource consumption of the soldering process.

5.1 Development of Resource Transparency Model for Soldering Process

To assist in the effort to transparent the resource flow model, the soldering process is broken into 'levels of study' across four levels, as shown in Table 8. The elements in these levels are illustrating the equipment that is directly and indirectly connected with the material transformation in soldering process. Furtherly, the study of resource consumption for periphery levels is combined with a model proposed by Schenk et al. [197] which is elaborating the transparency model shown in Figure 34. For soldering process, including not only the oven itself, but also the auxiliary surrounding equipment obtains a big picture for the resource flow transparency. Therefore, it is necessary to investigate all supporting facilities of the peripheral systems of the oven, and thus their electrical energy consumption and the supplied resources.

Table 8: Resource consumption levels for soldering process

Level	Description
Product level	The resource input for the material transformation in the **soldering process,** e.g. heaters that are generating the thermal process.
Periphery 1	The mechanical parts power consumption of the **oven technology**, e.g. convection fans and blowers, and transportation bands.
Periphery 2	The auxiliary-specific power consumption of equipment, which are supplying the **auxiliary resources**, e.g. gas compressors.
Periphery 3	The power consumption of supporting **facilities** in factory level, e.g. environment humidity and air conditioning system.

In the 'product level', the exergy method is used to illustrate the minimum energy input needed to perform the material transformation in soldering process. The 'first periphery' is illustrating the resource transparency for the mechanical part of the oven, which mostly have to do with the kinetic of the oven technology. The 'second periphery' is considering the auxiliary equipment of the oven, which are supplying mainly the resources into the technology. The analysis of this periphery mainly yields the power consumption of the auxiliary equipment, which are affected massively by the production states (time-based power consumption variables) and energy states (power requirement intensity) of the oven. The 'third periphery' is addressing the electrical energy

consumption of facilities, which are supporting the air conditioning, and illumination of the other peripheries.

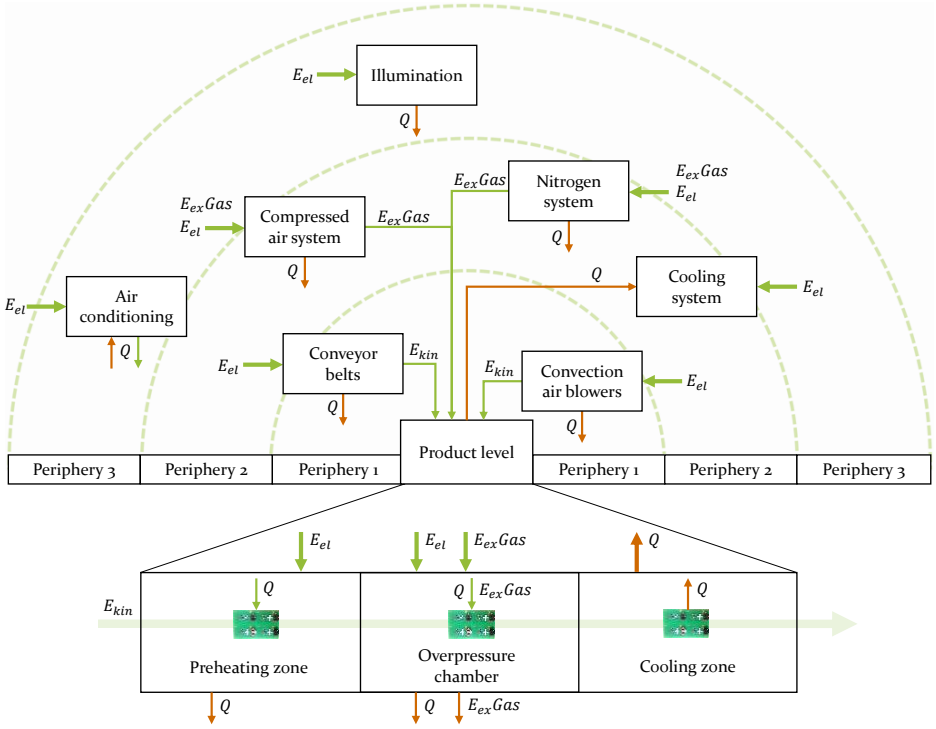

Figure 34: The resource transparency model for soldering process

The resource transparency model reveals the resource flow dependency on the oven production state and the power consumption of the auxiliary equipment. Using this model and a simulation tool the power consumption in all peripheries will be measured and calculated.

5.2 Analysis of the Electrical Energy Consumption

The periphery auxiliary equipment is consuming electrical energy to supply the demanded resources by the oven. The accumulation of auxiliary power consumption for the oven technology is obtaining the total power consumption of the system. The total power consumption is correlated to production lead-time per product. Hence, by mapping the resource flow into the oven, the corresponding electrical energy consumption of the supply systems in the periphery levels are investigated, and the analysis is followed by the cost calculation per PCB.

5.2.1 Measurement of Production Lead-time for Soldering Process

The resource consumption is correlated with the increment of production lead-time. There are many definitions of production lead-time, but in the present work, it is defined as when the PCB goes into the oven in the first zone and it is delivered after the cooling zone. The lead-time in the oven is depending on the setup parameter for the speed of transport bands and waiting time in the overpressure chamber. As shown in Figure 35, the transport bands speed for all profiles are constant; however, they are changing corresponding with the change of waiting time in the peak zone. The production lead-time in the overpressure chamber is the 'process pacemaker'[5]. Reduction of processing time in the chamber is reducing the entire production lead-time for soldering process and hence the time for the entire production line. The given production lead-time does not consider the profiles setup time and warm-up process time, however they are considered for electrical energy consumption analysis in the simulation process when the production status is changing.

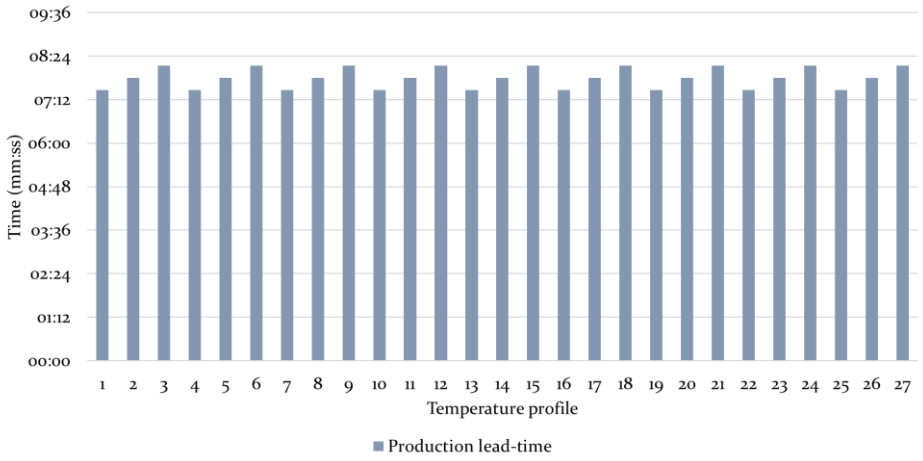

Figure 35: Production lead-time per PCB

[5] Any process along a value stream that sets the pace for the entire stream. (The pacemaker process should not be confused with a bottleneck process, which necessarily constrains downstream processes due to a lack of capacity.) This point is called the pacemaker process, because how you control production at this process sets the pace for all the upstream processes [193].

5.2.2 Analysis of the Oven Technology for Electrical Energy Utilization

The power consuming components of the oven consists of 11 heaters in preheating zone, two heaters and 6 quartz auxiliary heaters in the peak zone, and 15 motors for convection blowers and three transport bands. After that the oven is turned-on, the power consumption during the warm-up process decreases by 80% of the initial consumption after 110 minutes. During the warm-up process, each heater runs with nearly the maximum power consumption possible to reach the setup temperature. The temperatures in preheating zones reach the setup temperatures after 9 to 12 minutes, and thereafter a rapid reduction of the total energy consumption is measured. The setup temperature in the peak zone is being reached after 30 minutes of warm-up process. As soon as the temperature at each zone reaches 10 °C less than the setup temperature, the heater starts to oscillate and hence consumes less and less electrical energy. Subsequent to the initial state of the oven, the total electrical energy consumption reaches a constant value after 110 minutes. The completion of warm-up process illustrates that the oven is in operational state. The measured values by the power monitor are plotted using the excel tool. Figure 36 is showing the load profiles for the temperature profiles 25 and 19.

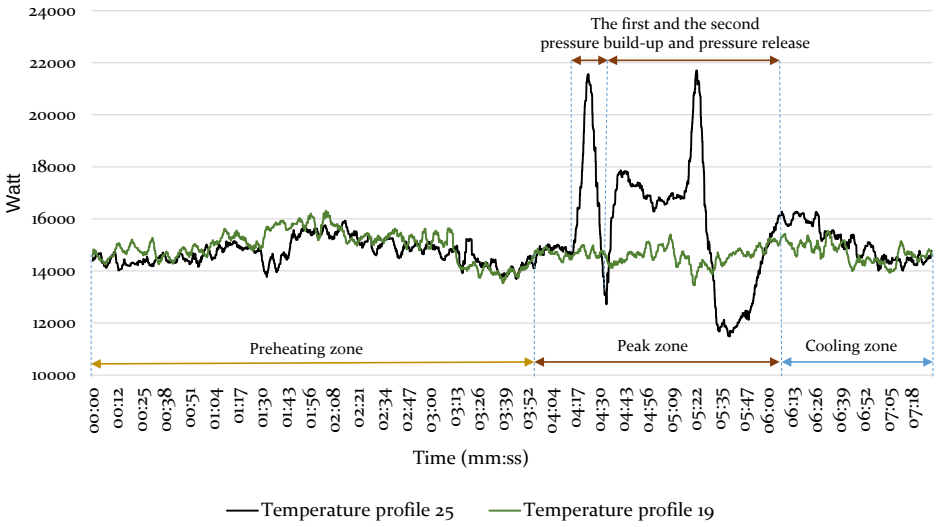

Figure 36: Load profiles for two temperature profiles

These two profiles are demonstrating the same machine setup with different pressure build-up. The two incident increase of peak consumptions are illustrating the electrical consumption due to two pressure build-up and pressure release for profile 25, however the profile 19 presents no pressure change and hence the electrical energy load stays rather constant.

Due to specific thermal treatment process of overpressure chamber, this zone yields the longest throughput time in the oven and therefore it is the pacemaker process. The production lead-time of the entire soldering process is mainly affected by the waiting time in the chamber. Depending on the changes from 20, 40, and 60 seconds of waiting time, therefore the number of PCB products that could be processed in the preceding preheating zone is changing. The total numbers of PCBs, which are processed at the same time in the oven, are correspondent to the waiting time setup and therefore 2.95, 2.72 and 2.54 PCBs. The measured power consumption for a specific production time hence is divided into the corresponding number of PCBs in the oven, and the electrical energy consumption per each profile and per each zone is shown in Figure 37. The overpressure zone/peak zone, in average, consumes 62% of the total electrical energy. The preheating zone consumes 27% and the cooling zone 12% of the total power consumption respectively.

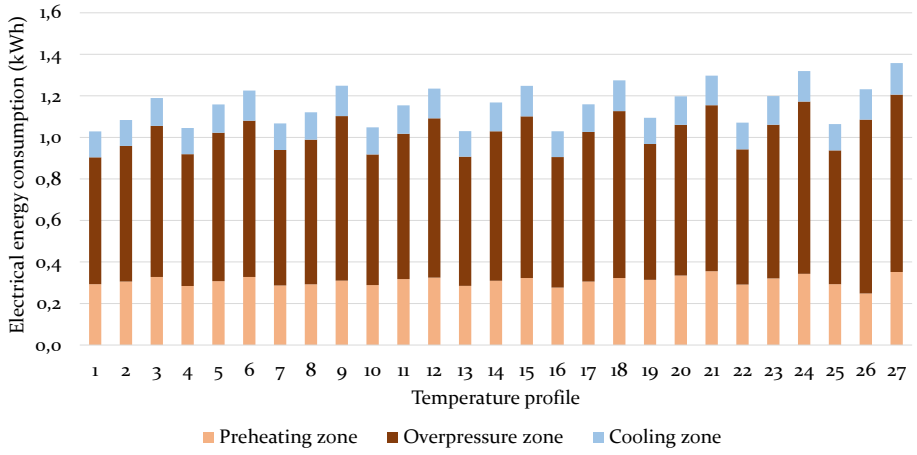

Figure 37: Oven technology electrical energy consumption per each zone for each temperature profile and per one PCB

5.2.3 Analysis of the Periphery Levels for Resource Flow-Related Electrical Energy Consumption

The electrical energy usage of auxiliary equipment in periphery levels of the machine for lighting, compressed air, nitrogen, air conditioning, and the cooling water systems are included in the total power consumption analysis. The lighting and air conditioning power consumptions are calculated per area in which the oven is installed, and other resources are calculated per production lead-time. To calculate the electrical energy utilized by periphery auxiliaries, first the resource mass consumption ratio per PCB should be calculated and the respective dynamic electrical energy consumption by the equipment is obtained through the simulation model in the next chapter.

Two ceiling lamp panels illuminate the oven; each consists of 6 fluorescent tubes with 49 watt output. These are switched-on during the entire production process simulation. The consumption of air conditioning system is depending on the season to automatically regulate the standard temperature in the production hall. Because the air conditioning system is only available for the entire building, therefore a tool is used to calculate the power consumption per volume of the used space by the oven [199]. The water is used as a cooling medium to cool down the cooling zone and it is supplied via a cooling tower on the roof of the building. The power consumption of the cooling tower is not clear, and hence, a cooling system with a similar cooling capacity is considered to calculate the average power consumption of this periphery. A closed circuit cooler, MCC-MCE A1/A4 cooling tower [200], from Mita Company, is considered to estimate the electrical energy consumption value. To investigate the utilized cooling water entering into the oven, an ultrasonic flow meter is used to measures the velocity of input volume. Using ultrasonic transducers, the flow meter can measure the average velocity of cooling water along the path of an emitted beam of ultrasound, by averaging the difference in measured transit-time between the pulses of ultrasound propagating into and against the direction of the water flow. The measured flow rate supply of cooling water is about 1.15 m^3/h.

The compressed air supply of the oven is controlled centrally. The compressed air system consists of two compressors and two dryers. The bigger compressor supplies 1000 liter of compressed air per minute and the smaller one 500 l/min. The volume of the air pressure tank is 500 liter, and the compressors are switched on automatically when the pressure in the tank falls below 6 bar, and it goes to standby when the pressure of the

tank reaches 45 bar. Also, for the nitrogen gas supply of the system, an all-in-one nitrogen skid, from Atlas Copco Company [201], is utilized as a guideline. The unit has a tank volume of 1000 liter which is filled with 45 bar gas pressure. The mass of nitrogen gas input is calculated per number and measure of pressure build-up for each profile multiplied by the 240 liter capacity of the chamber. The air pressure input that is used for pneumatic function of the chamber and the mass consumption is negligible.

Figure 38 shows the resource mass consumption per PCB. Because the water flow has a rational dependency on production lead-time, it shows a similar pattern as the power consumption. The nitrogen gas consumption is dependent on the pressure in the overpressure zone; hence it follows the pattern per profile setup. When the cooling water accounts for almost 90% of the mass consumption, nitrogen represents 9.6% and the air pressure 0.5%.

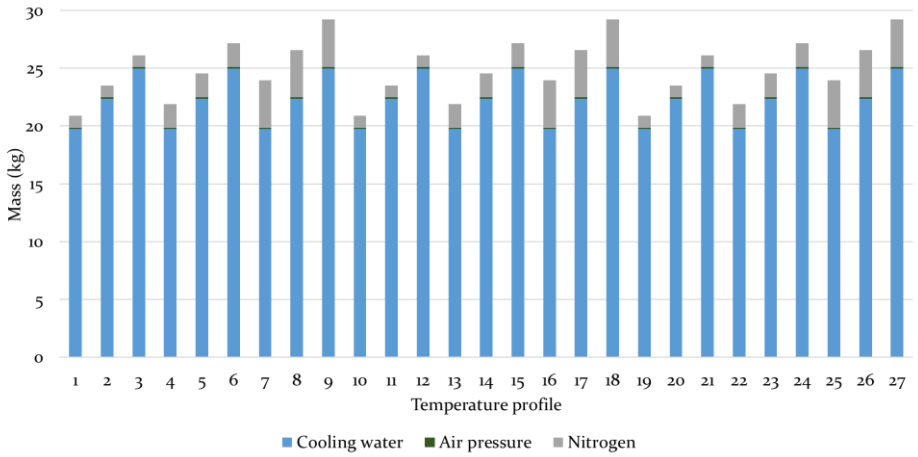

Figure 38: Resource mass consumption per PCB

5.2.4 Development of the Model and Simulation Process to Evaluate the Total Electrical Energy Consumption

In order to control and cope with the dynamics of the process chains, simulation method is a promising approach. Discrete Event Simulation (DES) could be utilized for a single machine or a highly interactive process chain to control the interdependency of the resource flow [202] [203] [204]. Three paradigms are introduced in the area of application of DES to control the resource flow in manufacturing systems. As shown in

Figure 39, these paradigms vary depending on the embedding of evaluation schemes and/or the interfaces with other simulation tools. The particular logic of each approach obtains distinctive advantages and disadvantage. According to paradigm A, the simulation approaches is offering relatively good coverage of resource flows, comprehensive evaluation schemes with relatively low modeling/simulation complexities and good transparency for the process. As a drawback, this paradigm cannot consider a certain resource oriented dynamics and interdependencies in detail. In contrary, paradigm B derives very detailed analysis of subsystems and fields of action. However, this approach leads to quite complex models which are requiring efforts for transferability. Paradigm C as a 'one-stop solution' can basically overcome some disadvantages of the other two paradigms. As a drawback, this approach is potentially restricted by possible limitations of the utilized simulation environment. Therefore, combination of the necessary logic to integrate the dynamic resource consumption and the strong discrete event and material flow oriented perspective is difficult [54].

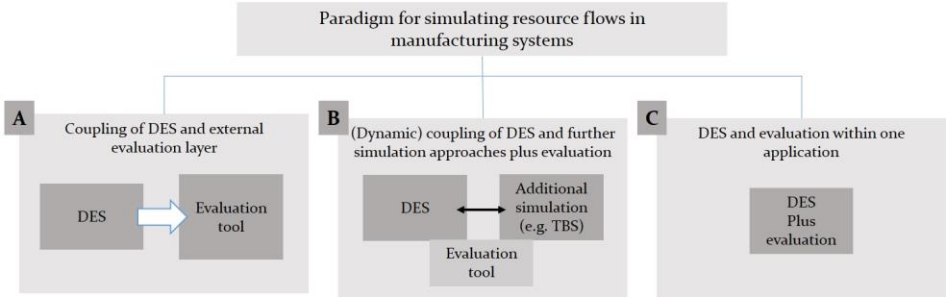

Figure 39: Paradigms for simulating resource flow in manufacturing systems [54]

This study is utilizing the paradigm C to transparent and controls the dynamic of the resource flow and to evaluate the power consumption of the oven technology and interlinked auxiliary equipment which are supporting the main technology during the process. The chosen paradigm extends the existing categorization with another aspect: transparency/analysis and presentation.

With the application of such simulation, the series of the data can be presented directly in the simulation software or external software plotters. On the other hand, the results can be exported into a spreadsheet program to use its special features such as graphical representation. Essentially, exporting the results has the benefit of further analysis without the need for expensive simulation program licenses. Due to the

proliferation of spreadsheet software, this presentation of results is easier. However, the resulting data can be very large when using load profiles with a high temporal resolution. The present approach therefore is able to analyze the data internally and export the results; however the export function aggregates the records to a maximum size.

Simulation Process in Tecnomatix® Plant Simulation 12

Tecnomatix® Plant Simulation software enables the simulation, visualization, analysis and optimization of production systems and logistics processes. Plant Simulation enables to optimize material flow, resource utilization and logistics for all levels of plant planning, from global facilities and local plants to specific production lines. Users can choose from predefined resources, order lists, operation plans and control rules. In the present approach, the discrete event simulation framework Plant Simulation is chosen as the core software due to its modular expansion options. The extension is implemented as a modular library as well as for the energy module. After adding the power module to an existing material flow model, all components can be configured with a setup dialog of the energy module. In order to implement the desired energy simulation, the network oriented modeling of Plant Simulation is utilized. In the given context, the term network is defined as the summary of several basic elements to a superior object. Using this structure, different hierarchical levels of the model network interlinked with the resource flow can be simulated.

As shown in Figure 40, the oven technology is separated into three zones modules, and each zone is connected with relevant resource module according to transparency model in Figure 34. These modules are modeled as a network or a basic material flow element given by Plant Simulation. This hierarchical structure is taken advantage of by extending Plant Simulation with energy aspects. Hereby the key element is the energy module, which is a network consisting of all required elements and matching methods to administrate specific power or resource profiles, to calculate the total resource consumption of the technology and periphery. Once the resource modules have been added to an existing network, all relevant material flow elements, located in the same network, are automatically detected and linked to the tool. Starting the simulation, not only the material flow, but additionally the resource profiles of the linked network are protocolled. To fulfill this purpose, observer procedures are used which are automatically invoked if changes in the material flow simulation occur. Thus, they allow the calculation of resource data

without changing already existing methods as well as for the material flow model.

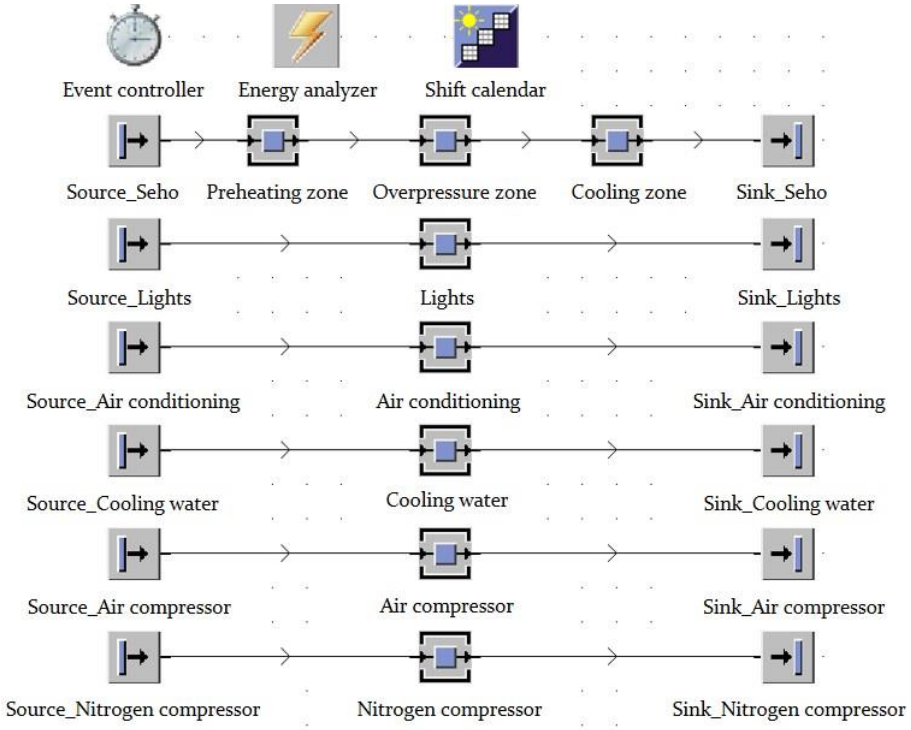

Figure 40: The simulation process model for the total power consumption

The event controller is used to start the simulation and to set the speed and scheduling. The energy analyzer makes it possible to analyze the resource consumption of the individual systems in the model. The production run and scheduling, as well as breaks, are defined by the shift calendar. The simulation is planned for five weeks, starts on Monday at 6:00 am and ends on Saturday at 6:00 am, each day three shifts, and one hour break time is scheduled per each shift. In the simulation model, the source is defined for the oven that supplies the machine with the product and a sink for the finished goods. The source is controlled via delivery list to show the entry times of the various production events based on the production lead-time of temperature profiles. For each zone in the oven, the power consumption is defined according to the measured values. Additionally, a distinction is made between the various production states of the oven: Working, Setting-up, Operational, Failed, Standby, and Off. During the setup, the oven goes to the 'Setting-up' state and 'Failed' in case of disturbance or breakage. After setup, the machine is ready for

operation. In this state, it is waiting until a PCB arrives. During the working process, the status of the oven changes to 'Working' and then to the 'Operational' state. The machine goes to the 'Standby' state during the intermittent periods and break times, and for a non-working weekend, the oven is in 'Off' state and consume no resource. Hence, the individual states of the oven are considered for the simulation application and not the average power consumption.

For the periphery levels in the simulation model only two states where applied. The 'Working' state and 30% of this value, which is used for 'Operational' state. The cooling water system in the simulation process is supplying at intervals of each 3.66 hours during working production process. The compressed air unit has a power demand of 13 kW during the production process and 3.9 kW in standby state of the unit. The compressed air supply in simulation process is operating each 0.96 hours during the working production state. The nitrogen supply system has a power demand of 26 kW during the production process and 7.8 kW in standby state. Figure 41 shows the total power consumption of the peripheral equipment for each temperature profile per PCB. In average, the air compressor unit is consuming 56.4%, and the nitrogen compressor unit 43.4% of the total peripheral power consumption and the influence of waiting time in all profiles are significant. The average power consumption for cooling water accounts for 0.19% of the total consumption, whereas the lights and air conditioning are negligible with a share less than 0.01%.

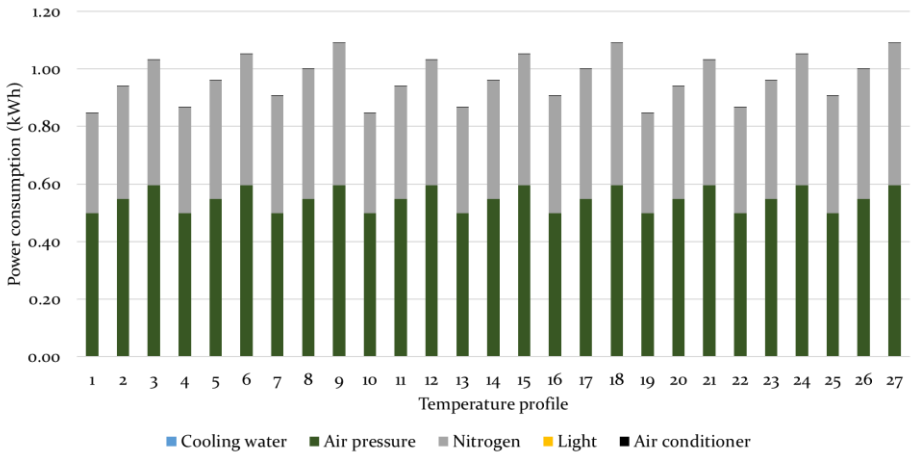

Figure 41: The peripheries power consumption per PCB

5.3 Thermodynamic Process Investigation of the Energy Efficiency Using Exergy Analysis

After analysis of power consumption for the oven technology and the peripheries, exergy method is employed to investigate the quality of resource transformation in soldering process in the product level. To enable an exergy analysis, the comparison with a reference environment is initially necessary. The reference environment is comprised of temperature, pressure, atmospheric compositions and other reference values. To conduct the calculations, as shown in Table 9, a reference temperature of 25 °C, an atmosphere pressure of 1.01325 bar, a relative humidity of 70% and an atmospheric composition of N_2, O_2 and others are setup [90] [205].

Table 9: Reference values for exergy analysis, according to [90] [205]

Properties	Value
Temperature T_0	298.15 K (25 °C)
Pressure P_0	101325 Pa
Relative humidity φ	70%
Atmospheric composition X	N_2: 78.084 mole% O_2: 20.947 mole% Others: 0.969 mole%

5.3.1 Defining the Resource Flow for the Subsystem Boundaries

Exergy value only exists in comparison to the reference state, the setup of the system and subsystem boundaries. Hence, as shown in Figure 42, the oven technology is divided in three zones; Preheating zone, overpressure chamber and cooling zone. Environment is also regarded as the fourth subsystem. Each subsystem is investigated for the resource input and output, and the values are shown in Table 10. The parameters in the preheating and cooling zones are remaining constant; however, values in overpressure zone are varying according to the setup parameters defined in the DOE in chapter 4.2.3.

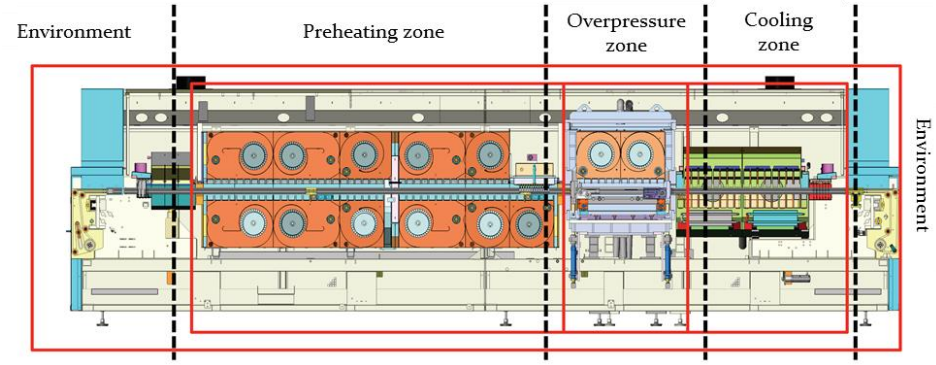

Figure 42: Subsystems boundaries of the oven technology

Table 10: Input and output resource parameter per each subsystem

Zone	Input			Output		
	Resource	Temperature (°C)	Pressure (bar)	Resource	Temperature (°C)	Pressure (bar)
Preheating zone	PCB	25	-	PCB	220	-
	Air	25	1.01325	Air	35	1.01325
	Electrical energy	-	-	-	-	-
Overpressure zone	PCB	220	-	PCB	203	-
	Nitrogen gas	20	6.8	Nitrogen gas	203 and 250 203 and 285 203 and 300	1.01325 2 4
	Electrical energy	-	-	Flux vapor	203 and 250 203 and 285 203 and 300	1.01325 2 4
Cooling zone	PCB	203	-	PCB	25	-
	Cooling water	10	-	Cooling water	16	-
	Electrical energy	-	-	-	-	-

5.3.2 Calculation of the Resource Mass and Exergy Flow

All the resource supply including material, electrical energy, and PCB components entering and leaving the oven carry exergy into and out of the system. Before calculating the exergy flow and balancing it, it is necessary to determine the type of exergy which is carried by each resource. As with many other production machines, the reflow oven does neither produce electrical work nor obtain it. It is also assumed that the heat transfer across system boundaries does not occur in the reflow oven. The exceptions are losses due to insufficient isolation or radiation, which is included in the total exergy loss.

A comprehensive explanation on the exergy calculation procedure is given in chapter 2.2.3. To calculate the exergy of resource input and output, their specific exergy values are calculated. These values differ for each temperature profile because of the pressure and temperature differences as well as due to the difference of resource flows. The actual exergy is determined by multiplying the mass of a resource type with their standard exergy values [93].

Chapter 5.2.3 is explaining the calculation approach for the resource flow, and the resource flow Sankey diagram for temperature profile 1 is shown in Figure 43. From this diagram, it defers that water has by far the largest proportion. This also applies for other temperature profiles. Nitrogen gas and compressed air is the product of supply systems and the compressors. The mass of nitrogen gas is dependent on the applied pressure and it changes from 1 kg to 4 kg. The mass of compressed air flow is not changing but its pressure. The mass of PCB and the electronic components remain constant.

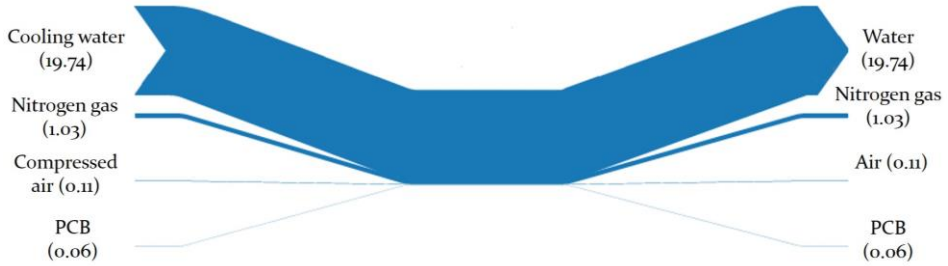

Figure 43: Resource flow for temperature profile 1 (kg)

The exergy of material resources and PCB is the sum of the chemical and physical exergy of its individual components. Once the resource flow for all profiles are realized, the input and output values should be studied. The chemical and physical exergy of the corresponding resources will be calculated referring to their flow amount.

The nitrogen and compressed air supplier systems are consuming electrical energy (100% exergy), to deliver the input nitrogen and pressurized air gases. The total exergy balances for these resource gases are calculated. For instance, a detailed example for exergy analysis of resource material for temperature profile 1 is tabulated in Table 11. Also by utilizing the specific chemical exergy of the PCB assembly chemical components in Table 12, the total exergy of PCB product is calculated.

Table 11: Exergy flow of resource material for temperature profile 1

Resource	Mass (kg)	$E_{chem,in}$ (kJ)	$E_{chem,out}$ (kJ)	$E_{phys,in}$ (kJ)	$E_{phys,out}$ (kJ)
Compressed air	0.112	0	0	0	~0
Nitrogen gas	1.025	26.3	26.3	172.7	51.0
Cooling water	19.74	507.4	507.4	32.3	52.3

Table 12: The mass and chemical exergy of the PCB electronic components, according to [93]

Material	Mass (g)	Specific heat capacity (kJ/kgK)	Density (g/cm³)	Specific chemical exergy (kJ/kg)	Chemical exergy (kJ)
Al2O3	0.028608	0.718	3.95	147	0.0042
Aromatic polymer	0.16	1.4	1.13	23000	3.6800
Carbon	0.000258	0.71	1.8	34127	0.0088
Copper	5.175511	0.385	8.96	2112	10.9307
Epoxy	0.38346	1	1.2	35195	13.4959
Fr4	45.775	0.6	1.8	29045	1329.5349
Iron	0.001548	0.449	7.87	6702	0.0104
Nickel	0.001136	0.444	8.902	3952	0.0045
Silica	0.272152	0.750	2.2	37	0.0138
Silicon	0.007568	0.705	2.33	30434	0.2303
Silver	0.0151892	0.235	10.49	651	0.0099
Tin	0.289677	0.228	7.31	4649	1.3467
Total	52.11				1370.16

5.3.3 Balancing and Calculation of the Exergy Loss and Destruction

After all resource flows are determined, an exergy balance is conducted to make the exergy loss visible by adding up the differences of electrical work, physical and chemical exergy. The chemical exergy loss is considered zero, as the mass flow is constant in the system. The electrical exergy provided to the process is converted primarily into heat and mechanical work, and during the energy conversion process a big amount of useful energy is dissipated as heat and friction, and hence it is directly accounted to the loss. The exergy loss is calculated by the equation 24.

$$E_{X_{loss}} = \Delta E_{X_W} + \Delta E_{X_{i,phys}} + \Delta E_{X_{i,chem}} \quad (24)$$

Figure 44 shows the exergy Sankey diagram for the temperature profile 1. This diagram shows the sum of physical and chemical exergy per each resource input and output described in Table 11 and Table 12. During the reflow soldering process, little to no chemical reaction takes place, and no material is added onto the PCB during the solder process. Therefore, the chemical exergy for material streams flowing into the system is 1370.16 kJ and it is calculated as to be the same as the chemical exergy flowing out of the system. Because the PCB enters the oven with ambient temperature, and cooled down at the end of the process to nearly the same temperature. Therefore, as shown in Table 13, the PCB obtains 351.70 kJ exergy in the first zone, and it is changing during the process in the next zones, however it carries almost no physical exergy when it leaves the oven.

Table 13: The physical exergy flow of the PCB in oven zones for profile 1 (kJ)

Preheating						Overpressure		Cooling	
Zone 1	Zone 2	Zone 3	Zone 4	Zone 5	Zone 6	Zone 1	Zone 2	Zone 1	Zone 2
351.70938	505.28939	717.99665	1132.945	1247.251	1365.4369	1739.0571	1164.1202	0	0

For a unit PCB assembly, the total electrical energy of 3247.9 kJ is consumed to produce about 199.04 kJ of nitrogen and 0 kJ air pressure. The efficiency of auxiliary gas suppliers for profile 1 is 6.5% (for all profiles are shown in Table 14). The exergy carried by the nitrogen gas into the oven is 199.04 kJ, and it is reduced to 77.34 kJ after utilization in reflow soldering. Air output obtains a very small fraction of physical exergy which is neglected as zero exergy. In addition, 3703.7 kJ of electrical energy is fully utilized by the oven in soldering process to produce the thermal process. The electrical energy used by the oven and periphery are simulated and calculated in capital 5.2.4, and it is mainly constituting the exergy loss after exergy balancing.

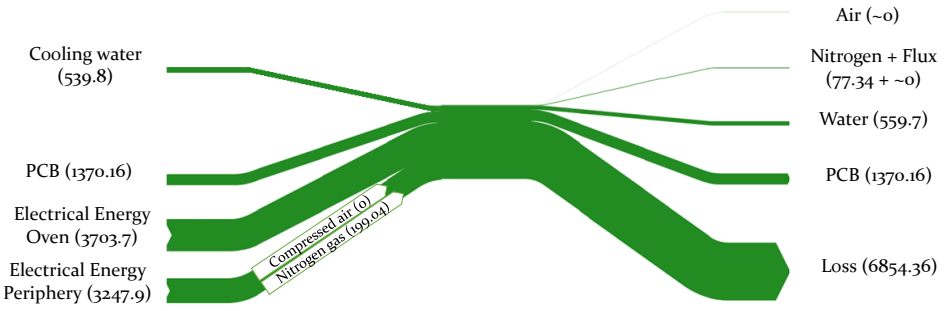

Figure 44: Exergy flow for temperature profile 1 (kJ)

For cooling water, the exergy content remains almost intact, with a small exergy obtain of 19.9 kJ. Cooling water is recycled but the exergy of air and nitrogen stream carry their resource intensities, which may cause local disturbances when dumped into the environment. Since physical exergy of water constitutes a small value, the most of their exergy would be reutilized. But the exergy of the exhausted air or nitrogen are transferred to the surroundings often without any use. The exergies of the compressed air out may include a very small portion of physical exergy (chemical exergy will not significantly differ at the exit from the value at the inlet) which may indicate a measure of a resource spent (availability of compressed air used for the process).

5.3.4 Definition of Exergy Efficiency Indicators and Analysis

Once the exergy balance of resource flows is illustrated, the efficiency definition is deployed to define the exergy efficiency indicators. The sum of associated exergy input carried by nitrogen and air to total electrical energy consumed by the supply systems and compressors are delivering the exergy efficiency of these systems. 5.1% is the minimum and 19.6% is the maximum obtained efficiency.

In the case of the exergy efficiency of the soldering oven, two types of efficiencies are considered. The total exergy efficiency ($\eta_{net,max}$), which is the ratio of the exergy flowing out of the system and the accumulation of all exergy flowing into the system (Eq. 25). This takes all exergy streams into account, such as the exergy carried by PCB and cooling water when entering and leaving the system boundaries. Nitrogen gas and pressurized air is the product of supplier systems, and hence the total electrical energy consumption of periphery is included as the exergy input.

$$\frac{E_{X_{Total,Out}}}{E_{X_{Total,In}} + Electrical\ Energy\ consumption\ by\ Oven\ and\ periphery} = \eta_{net,max} \qquad (25)$$

The product exergy efficiency ($\eta_{Product}$) is based on the amount of exergy carried by the PCB. This efficiency describes how much of the entire exergy input into the oven is utilized by the final product (Eq. 26). This indicator illustrates the minimum amount of available energy which the PCB is requiring during the soldering process, and hence the rest are considered as non value-added available energy.

$$\frac{E_{X_{Product,Out}}}{E_{X_{Total,In}} + Electrical\ Energy\ consumption\ by\ Oven\ and\ periphery} = \eta_{Product} \qquad (26)$$

The efficiency indicators for all profiles are shown in Table 14. This table illustrates that the lowest total exergy efficiency is 20.3% for temperature profile 21 (300 °C, 0 bar, 60 sec), and the highest value is obtained by the temperature profile 16 (285 °C, 4 bar, 20 sec) with the efficiency of 28.6%. The product exergy efficiency shows the lowest value of 11.7% for the profile 27 (300 °C, 4 bar, 60 sec), and 15.4% as the highest value for the profile 1 (250 °C, 0 bar, 20 sec).

Table 14: Exergy efficiency indicators per each temperature profile

Profile	Exergy efficiency of nitrogen and air pressure suppliers (%)	Total exergy in (kJ)	Total exergy out (kJ)	Electrical energy consumption oven (kJ)	Electrical energy consumption periphery (kJ)	Total exergy efficiency (%)	Product exergy efficiency (%)
1	6.1	1909.9	1966.4	3703.7	3247.9	22.7%	15.4
2	5.6	1981.7	2035.4	3901.9	3585.3	22.0%	14.4
3	5.1	2053.0	2104.0	4282.5	3912.0	21.0%	13.3
4	11.3	1909.9	2167.1	3762.9	3519.2	24.0%	14.9
5	10.3	1981.7	2236.1	4171.7	3855.8	22.8%	13.6
6	9.5	2053.0	2304.7	4411.5	4181.9	22.1%	12.8
7	19.6	1909.9	2696.6	3842.5	4061.7	27.9%	13.9
8	18.1	1981.7	2765.6	4034.6	4397.0	27.0%	13.1
9	16.9	2053.0	2834.2	4495.4	4721.8	25.6%	12.1
10	6.1	1909.9	1974.8	3774.6	3247.9	22.6%	15.3
11	5.6	1981.7	2043.8	4154.8	3585.3	21.5%	14.0
12	5.1	2053.0	2112.3	4446.4	3912.0	20.7%	13.1
13	11.3	1909.9	2183.8	3707.9	3519.2	24.3%	15.0
14	10.3	1981.7	2252.8	4204.4	3855.8	22.9%	13.6
15	9.5	2053.0	2321.4	4494.3	4181.9	22.1%	12.7
16	19.6	1909.9	2730.0	3705.7	4061.7	28.6%	14.1
17	18.1	1981.7	2799.0	4174.0	4397.0	26.9%	12.9
18	16.9	2053.0	2867.6	4588.0	4721.8	25.6%	12.0
19	6.1	1909.9	1978.5	3940.4	3247.9	22.2%	15.0
20	5.6	1981.7	2047.5	4311.5	3585.3	21.2%	13.8
21	5.1	2053.0	2116.1	4670.8	3912.0	20.3%	12.8
22	11.3	1909.9	2191.4	3856.5	3519.2	24.0%	14.7
23	10.3	1981.7	2260.4	4317.1	3855.8	22.7%	13.4
24	9.5	2053.0	2328.9	4748.6	4181.9	21.6%	12.4
25	19.6	1909.9	2745.1	3830.8	4061.7	28.4%	13.9
26	18.1	1981.7	2814.1	4434.5	4397.0	26.4%	12.6
27	16.9	2053.0	2882.7	4887.8	4721.8	25.1%	11.7

5.3.5 Statistical Analysis and Meta-model Development for Electrical Energy Consumption

The statistical analysis using Minitab software is conducted to investigate the effect of parameter setup and their interactions on the electrical

energy consumption of the oven technology and its peripheries. The significance analysis results are shown in Table 15. The electrical energy consumption meta-model for the oven technology shows that the measurements with the accuracy of 95.50% (R^2 value) are explaining the fitted model. From the analysis, R^2 prediction value of 91.85% is close enough to R^2 value to emphasize on the reliability of the model for further prediction usage. As a rule of thumb, if the R^2 value is more than 0.90 and the value of the adjusted or predicted R^2 is more than 0.80, the fitted model will be considered adequate and each model provides sufficient explanation capability. According to the analysis, the waiting time factor is statistically significant with the highest effect, and temperature in the next level with lower effect. The pressure parameter is statistically less significant. By the prolongation of waiting time in the process, the electrical energy consumption linearly is increasing. The interaction of waiting time with temperature is however significant but with less effect on the electrical energy of the oven.

The fitted model for the electrical energy consumption of auxiliary equipment in peripheries, indicating the R^2 value of 99.63% and R^2 predication value of 99.36%. Therefore, the given data for this model are highly reliable for analysis of variance and significance analysis. Temperature is showing absolutely no significance because the electrical energy consumption of the oven has no effect on the electrical energy consumption in periphery level. The pressure and waiting time factors with the highest effect are highly statistically significant. The compressors in periphery level with considerable electrical energy consumption support the nitrogen production. By the increase of waiting time, the cooling water consumption and therefore the corresponding equipment electrical energy consumption is increasing. The interactions of setup parameters in periphery levels are absolutely not significant.

The cumulative electrical energy consumption of all peripheries and the oven technology level is shown in total electrical energy in Table 15. The R^2 value of 98.62% is describing that all considered parameters in all peripheries are very well explaining the value of total electrical energy consumption, and the R^2 predication value of 97.46% illustrates the reliability of the model for further predictions and interpretation purposes. The significance analysis deduces that all setup parameters are highly statistically significant, and elongation of waiting time is extremely influencing on the total electrical energy consumption. The interaction of waiting time with other two factors however is significant but less effective.

Table 15: The significance analysis for electrical energy consumptions

	Oven technology electrical energy/power consumption		Periphery electrical energy/power consumption		Total electrical energy/power consumption	
Factor	**F-value**	**P-value**	**F-value**	**P-value**	**F-value**	**P-value**
Temperature	34.99	0.000***	0.00	1.000	39.23	0.000***
Pressure	5.55	0.029*	526.67	0.000***	59.49	0.000***
Waiting time	344.37	0.000***	4740.00	0.000***	1258.63	0.000***
(Temperature) * (Pressure)	1.45	0.242	0.00	1.000	1.20	0.287
(Temperature) * (Waiting time)	8.34	0.009**	0.00	1.000	7.15	0.015*
(Pressure) * (Waiting time)	3.82	0.065	0.00	1.000	4.49	0.047*
Regression Equation in Uncoded Units Oven technology electrical energy consumption = 0.942 + 0.000069 Temperature + 0.0374 Pressure - 0.00599 Waiting time - 0.000160 Temperature*Pressure + 0.000038 Temperature*Waiting time + 0.000333 Pressure*Waiting time						
Regression Equation in Uncoded Units Periphery electrical energy consumption = 0.7567 - 0.000000 Temperature + 0.01500 Pressure + 0.004500 Waiting time + 0.000000 Temperature*Pressure + 0.000000 Temperature*Waiting time + 0.000000 Pressure*Waiting time						
Regression Equation in Uncoded Units Total electrical energy consumption = 1.655 + 0.000224 Temperature + 0.0463 Pressure - 0.00048 Waiting time - 0.000142 Temperature*Pressure + 0.000035 Temperature*Waiting time + 0.000354 Pressure*Waiting time						

Metamodeling typically involves studying the output, input relationships, and then fitting right meta-models to represent that behavior. As shown in Figure 45, the fitted surface plots present the interaction of parameters and rational changes as already discussed for the statistical analysis. Likewise, temperature and pressure are illustrating rather same significance and effect. As shown in Figure 45, a), by the change of any factor, the other factor displays a rational increase or decrease. The significance analysis shows that the effect of waiting time factor on responses and specifically the effect on the response in periphery level is about 9 times higher than pressure effect and the effect on the total electrical energy or power consumption is about 25 times higher than other two parameters. Therefore the two contours in Figure 45, b), and Figure 45, c) are illustrating similar behavior for the other two factors when the waiting time measure is increasing.

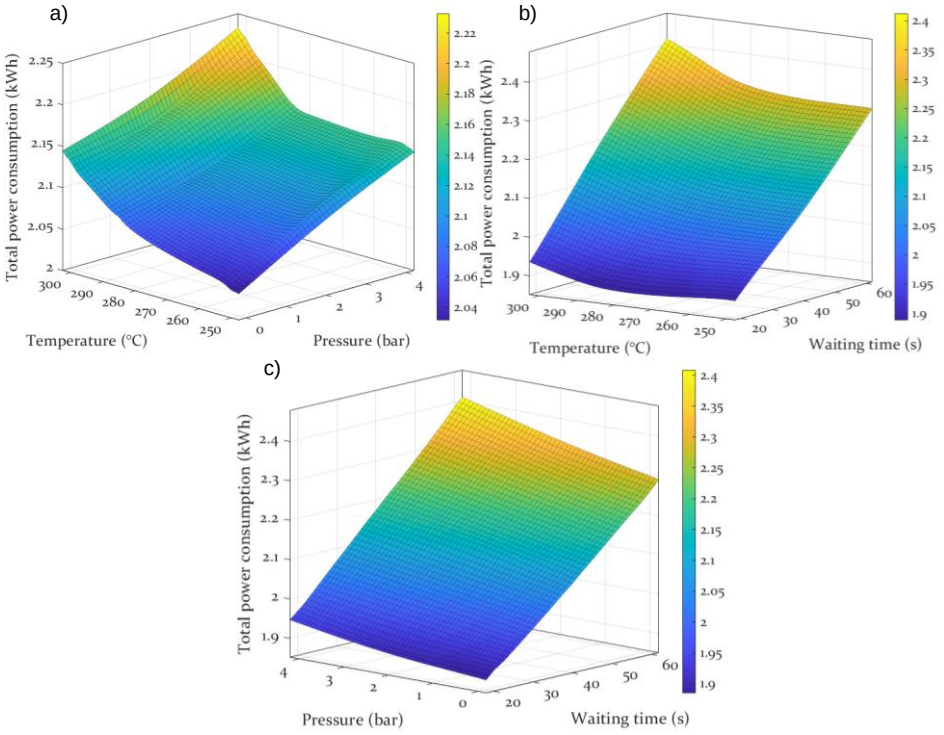

Figure 45: Surface plot for interaction effects on total electrical energy consumption for: a) temperature and pressure b) temperature and waiting time c) pressure and waiting time

5.3.6 Statistical Analysis and Meta-model Development for Exergy Efficiency

Energy is not fully available to do useful work. The real amount of available energy will depend on some aspects that it is not feasible to energy model. Therefore, the exergy efficiency is revealing the measure of efficiency indicator of available energy to benchmark different setup profiles. The indicator for the total exergy efficiency is revealing a comparison measure for all profiles, and the product exergy efficiency is used to investigate the efficiency of the applied resources for the PCB product. From the ANOVA analysis for the total exergy efficiency of 27 profiles, it is inferred that the fitted model is obtaining R^2 value of 93.58% and R^2 predication value of 89.21%. Therefore, the fitted model for the exergy efficiency is valid for further explanation. As shown in Table 16, the pressure and waiting time are statistically significant; however, no significance is realized by the temperature parameter. The pressure factor is illustrating the highest effect because the energy intensive compressors

in periphery level support this factor. The waiting time factor is influencing on the working time of all periphery levels. Therefore, it has the highest effect on the electrical energy and equivalent to 100% exergy.

Table 16: The significance analysis for exergy efficiency

	Product exergy efficiency		Total exergy efficiency	
Factor	**F-value**	**P-value**	**F-value**	**P-value**
Temperature	20.19	0.000***	0.54	0.470
Pressure	289.62	0.000***	234.85	0.000***
Waiting time	870.15	0.000***	42.24	0.000***
(Temperature) * (Pressure)	1.71	0.206	0.40	0.532
(Temperature) * (Waiting time)	2.38	0.138	0.44	0.517
(Pressure) * (Waiting time)	0.38	0.544	1.69	0.209
Regression Equation in Uncoded Units Product exergy efficiency = 17.30 - 0.00318 Temperature - 0.634 Pressure - 0.0183 Waiting time + 0.001102 Temperature*Pressure - 0.000130 Temperature*Waiting time + 0.00067 Pressure*Waiting time				
Regression Equation in Uncoded Units Total exergy efficiency = 22.24 + 0.0007 Temperature + 0.88 Pressure + 0.031 Waiting time + 0.00259 Temperature*Pressure - 0.000268 Temperature*Waiting time - 0.00677 Pressure*Waiting time				

The product exergy efficiency is indicating on the exergy carried/utilized by the PCB product when it is completing the soldering processed. The fitted model for product exergy efficiency is explaining the 98.39% of data variation, and the R^2 predication of 97.26% which is close enough to R^2 value for further prove of the model reliability. This efficiency is considering the product material components. As seen in Table 16, all factors are statistically significant on the product exergy efficiency. The chemical exergy of PCB individual substances and therefore the total exergy of PCB product for each individual profile are identical and it shows the resource intensity of the product. It is assumed that the individual PCB components and elements are not chemically interacting with each other. But in a reality, it may not be the case. The substances react with each other and form intermetallic or intermediate compounds at the regions of contact. Moreover, a detail about the kind and intensities of the interactions possible within the stream (inside components or PCB assembly) is not available. Considering the quantity of the chemicals/substances involved, the impact of these quantities in total exergy is negligible. The material chemical exergy by the change thermal

treatment in different profiles are changing and it obtains a comparable efficiency metric for different thermal profiles.

As opposed to other studied performance factors, the total exergy efficiency should be maximized. From the surface plots in Figure 46, it is inferred that the change of temperature is not affecting on the efficiency, but the increase of pressure has rather a linear effect. In addition, the figures are explaining that how the decrease of waiting time is affecting positively on the efficiency response. The pressure factor points out the most effective significance at 4 bar and the combination with 20 seconds of waiting time for efficiency increase in Figure 46, c) is noticeable.

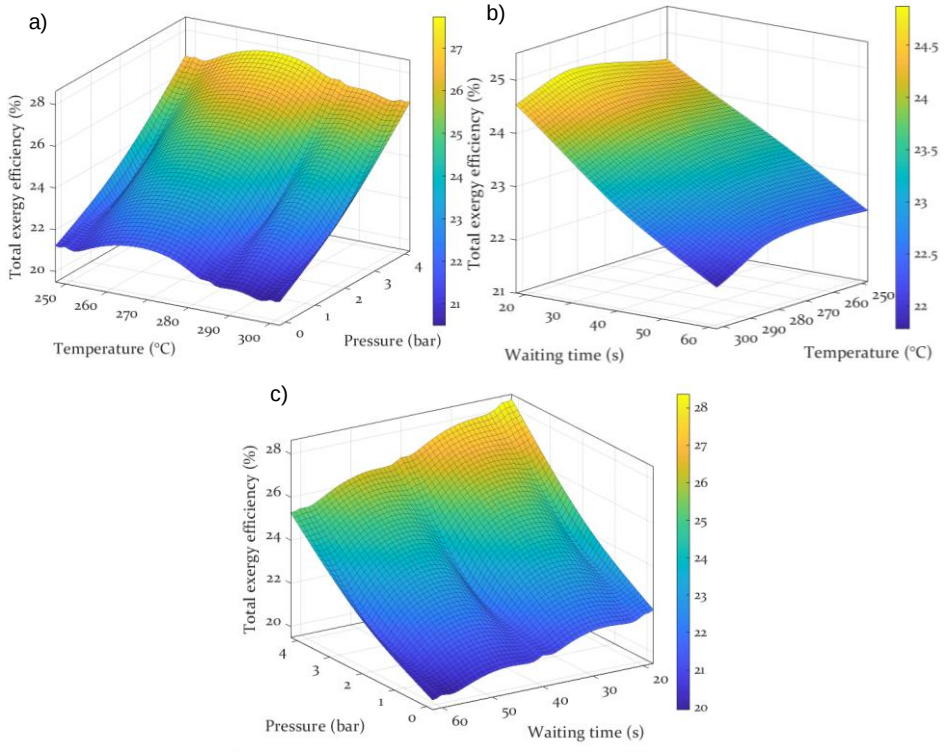

Figure 46: Surface plot for interaction effects on exergy efficiency for: a) temperature and pressure b) temperature and waiting time c) waiting time and pressure

The multi-vari chart in Figure 47 is illustrating that the magnitude of exergy efficiency is slightly increasing when the waiting time is shortened. The gradient of the green line is proving this fact. The red lines are illustrating that the efficiency magnitude is extensively changing when the pressure level is increasing. This fact is proven also by the significance

analysis of pressure parameter. The statistical analysis depicts that the pressure changes and waiting time changes have the most significant effect on the total exergy efficiency, however the pressure effect is about 6 times higher than waiting time factor. From the multi-vari chart it is perceptible that the highest exergy efficiency for temperatures of 250 °C and 285 °C at different levels of pressure are closely changing. The profile for 285 °C, 4 bar, and 20 seconds of waiting time obtains the highest exergy efficiency of 28.6%.

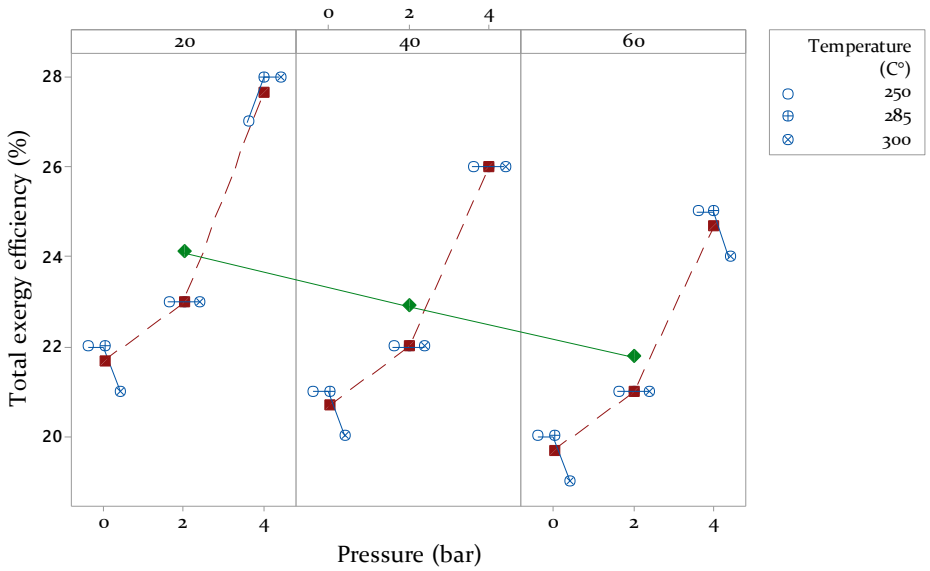

Figure 47: Multi-Vari chart for total exergy efficiency by temperature - waiting time and panel variable of waiting time

5.4 Calculation and Statistical Analysis of the Total Cost for Soldering Process

As discussed in chapter 2.2.5, when looking at the short-term consumption, only the consumption of process-related material goods, resources, electrical energy consumption are relevant. Therefore, the cost for the associated resource consumption per one PCB production is calculated. The statistical analysis is followed for the cost factor and the influencing factors are discussed.

The total cost for soldering process is comprised of the process-related resource consumption, which are changing by the change of temperature profiles. The cost for cooling water, 0.001963 € per liter, is calculated

according to Erlanger Stadtwerke (ESTW) [206]. The cost for electrical energy consumption of lights, air conditioner, and the water cooling system are negligible. The total cost for cooling water, nitrogen and air pressure supply systems, and electrical energy consumption per PCB are calculated based on the analysis in chapter 5.2.2 and 5.2.4 and illustrations are shown in Figure 48.

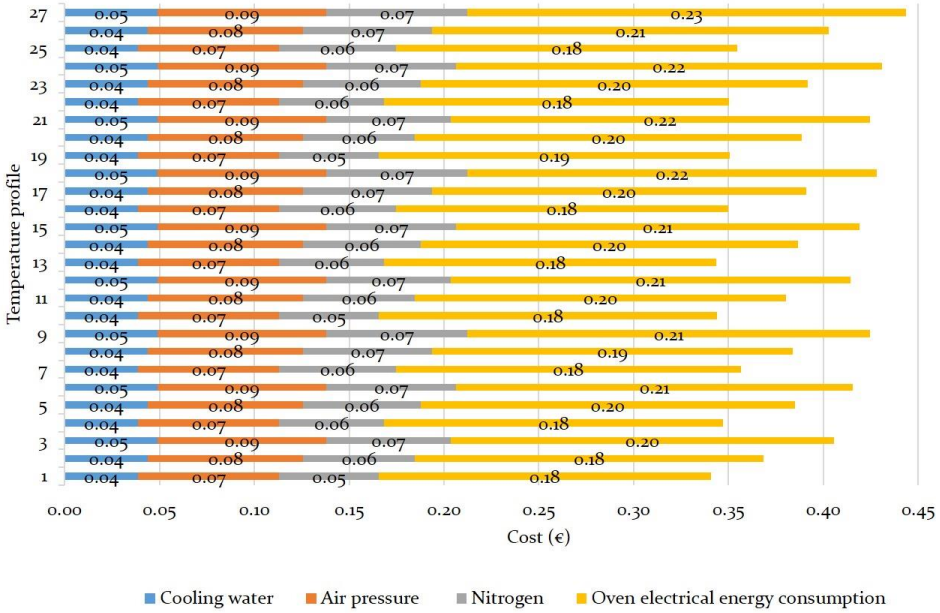

Figure 48: Total process cost per PCB product

The price for electrical energy consumption for industry is about 0.17 € per kWh. This price is used to calculate the electrical energy consumption costs. Nitrogen and air pressure are the product of supply systems and hence the associated power consumption cost for the supply systems are representing the price of these resources. The resources for all profiles are obtained an accumulative cost from 0.34 € to 0.44 €. The power consumption cost for soldering process per PCB, in average, is comprised of 51% for oven, 15% for nitrogen supply system, 20% for air pressure supply system, and near 10% for cooling water system [207]. This obtains a good overview on the cost for overpressure soldering process in SMT production industry. The statistical analysis of the total cost is revealing the effect of oven setup changes and the respective electrical energy/power consumption on the total process cost (Table 17).

Table 17: The significance analysis of the factors affecting on the total process cost

	Total process cost	
Factor	**F-value**	**P-value**
Temperature	1.55	0.237
Pressure	11.52	0.005**
Waiting time	214192.80	0.000***
Oven technology power consumption*	32060784.51	0.000***
Periphery power consumption **	1701615.63	0.000***
(Temperature) * (Pressure)	5.83	0.033*
(Temperature)*(Waiting time)	6.33	0.027*
(Temperature)*(Oven technology power consumption)	0.26	0.618
(Temperature)*(Periphery power consumption)	6.82	0.023*
(Pressure)*(Waiting time)	237.72	0.000***
(Pressure)*(Oven technology power consumption)	60.61	0.000***
(Waiting time)*(Oven technology power consumption)	121.52	0.000***
(Waiting time)*(Periphery power consumption)	7722.57	0.000***
(Oven technology power consumption)*(Periphery power consumption)	121.96	0.000***
*according to Table 8, it refers to "product level" ** according to Table 8, it refers to "periphery 1, 2, 3"		
Regression Equation in Uncoded Units Total cost = 0.03559 + 0.000011 Temperature + 0.000104 Pressure + 0.000441 Waiting time + 0.161562 Oven technology power consumption + 0.14496 Periphery power consumption + 0.000000 Temperature*Pressure + 0.000000 Temperature*Waiting time - 0.000000 Temperature*Oven technology power consumption - 0.000014 Temperature*Periphery power consumption + 0.000001 Pressure*Waiting time - 0.000177 Pressure*Oven technology power consumption - 0.000050 Waiting time*Oven technology power consumption - 0.000132 Waiting time*Periphery power consumption + 0.01131 Oven technology power consumpti*Periphery power consumption		

Comparing with the Table 8, the cost for auxiliary resources is accumulated as periphery cost. By including the setup factors and the cost as the response in the analysis, waiting time and pressure are statistically significant, and waiting time interaction is contributing 99.21% on the total cost of the product. Due to the big contribution of the waiting time factor, the setup factors are associated with oven technology and periphery cost factors for significance analysis. As shown in Table 17, waiting time is highly statistically significant and electrical energy

consumption of the oven and periphery level is rather equally sharing the same strong effect on the final cost. The temperature factor is statistically insignificant as well as the interaction of this factor with other effective factor on the final cost. The pressure factor also is statistically significant, but it yields the least effect on the final cost.

5.5 Conclusion

This chapter presented a control procedure for the resource flow in the overpressure soldering process, and the cost is evaluated. First, a transparency model is developed which is illustrating the flow of electrical energy of the oven technology and auxiliary equipment in four periphery levels. It is inferred that:

- The transparency model identified the magnitude of resource flow for nitrogen gas, compressed air, cooling water, and the associated electrical energy cost of the supplier units. Furtherly, the electrical energy consumption for air conditioning and the plant illumination is studied. PCB product and personnel are considered as constant resource consumption factors.
- The analysis of oven technology is illustrating that once the machine is turned-on, the power consumption during the warm-up process decreases by 80% of the initial consumption after 110 minutes. The oven is in operational state when the warm-up process is ending. During the warm-up process, each heater runs with nearly the maximum power consumption possible to reach the setup temperature. The temperature in preheating zones reach the setup temperatures after 9 to 12 minutes, and it leads to a rapid reduction of the total energy consumption. The setup temperature in the peak zone is being reached after 30 minutes of warm-up process.
- In the product level for the oven technology, the overpressure zone/peak zone, in average, consumes 62% of the total electrical energy. The preheating zone consumes 27% and the cooling zone 12% of the total power consumption per PCB product.
- In the periphery level, for all consumed resources in unit of kilogram, 90% cooling water, 9.6% nitrogen, and 0.5% air pressure are consumed per PCB product.

Then, a simulation tool is utilized by means of imitation purposes in order to consider the predictable and non-predictable process breaks in the total power consumption of the soldering process. It is inferred that:

- In average, the air compressor unit is consuming 56.4%, and the nitrogen compressor unit 43.4% of the total peripheral power consumption. The average power consumption for cooling water unit accounts for 0.19% of the total consumption, whereas the lights and air conditioning are negligible with a share less than 0.01%.
- From the statistical analysis, R^2 value of 98.62% is describing that the considered setup parameters (deduced from DOE study) in all peripheries are very well explaining the value of total power consumption response, and the R^2 predication value of 97.46% illustrates the reliability of the model for further predictions and interpretation purposes. The effect of waiting time factor on responses in the periphery level is about 9 times higher than pressure effect. The effect of waiting factor on the total power consumption is about 25 times higher than temperature and pressure parameters.

By realizing the resource flow balance of the process, an exergy method is conducted and the investigation is followed by statistical analysis. Energy can be consumed and conserved but not all that energy is available to do useful work. Therefore, the exergy efficiency is revealing the measure of efficiency indicator of available energy to benchmark different setup profiles. It is inferred that:

- During the reflow soldering process, little to no chemical reaction takes place, and no material is added during the solder process. Therefore, the chemical exergy for material streams flowing into the system is considered to be the same as the chemical exergy flowing out of the system. Because the PCB demonstrator is cooled down at the end of the process to nearly the reference temperature, and therefore the final product carries almost no physical exergy.
- Unlike the material flow, the electrical energy, which is 100% available form of exergy, is completely consumed in the process. Therefore, the electrical energy/ power consumption of the oven technology and auxiliary equipment supplying the resources are

interacting significantly on the exergy flow of the process. Electrical energy is directly converted to exergy loss.

- From the statistical analysis for the total exergy efficiency, it is inferred that the fitted model is obtaining R^2 value of 93.58% and R^2 predication value of 89.21%. Therefore, the fitted model for the exergy efficiency is valid for further explanation. The pressure and waiting time are statistically significant; however, no significance is realized by temperature parameter. The statistical analysis depicts that the pressure changes and waiting time changes have the most significant effect on the total exergy efficiency.
- The highest exergy efficiency of 28.6% is obtained by the profile with setup profile of 285 °C, 4 bar, and 20 seconds of waiting time. The obtained exergy value and the associated setup may point out the directions for further technology development.

Lastly the associated cost for the resource flow per PCB product is conducted and the statistical analyses are illustrating the most influential factors in overpressure soldering process. Hence, It is inferred that:

- The resources for all profiles are obtained an accumulative cost from 0.34 € to 0.44 €. The power consumption cost for soldering process per PCB, in average, is comprised of 51% for oven, 15% for nitrogen supply system, 20% for air pressure supply system, and 10% for cooling water system.
- Waiting time and in the next level, pressure are statistically significant. However, waiting time factor demonstrates 99.21% of interaction contribution on the oven and periphery supply systems and therefore on the total process cost. The comparative analysis of waiting time in different profiles indicates on efficiency of overpressure oven technology during the active production phases. Comparing with the recent advanced soldering techniques such as laser soldering, conductive adhesives which are featuring the least resource consumption; this study is a leap forward that may impact in diverse domains of sustainability and economic impact of overpressure soldering technology.

6 Development of Mathematical Prediction Models for Solder Profiles

The aim of this chapter is to develop reliable models using the DOE data input to predict the responses. Hence, the error analysis is conducted and the comparison of models is defining the reliable models. The reliable models with acceptable errors are deployed, and by the given input setup parameters are predicting optimized responses. Predication, optimization, and experimental verification of predicted responses are conducted in chapter 7.

The intelligent process optimization methods are reviewed and discussed in chapter 2.3. The RSM is a series of mathematical and statistical techniques useful for the modeling and analysis of problems in which the responses of interest are influenced by several influential factors, and the main objective is to optimize their responses. In addition, the ANN is obtained trending attention for solving the multi-objective optimizations. An ANN method which is also a computational model mimics the decision making process through the data learning process. This method is used for an approximate mapping of nonlinear relationship between the parameter setups and responses considering a randomized distribution of data learning process. The ANN and RSM methods firstly are utilized for prediction process, and secondly the results are used for comparison purposes to check the reliability of any of these methods for the current case study application. Any of these methods are following different modeling topology process, as illustrated in Figure 49.

In chapter 4.2.3, the responses of interests including the quality and resource efficiency for soldering process through conduction of DOE are collected and mathematically modeled. The ANN model is starting with definition of input and response parameters, creation of the topology and the model architecture. The data training process and the measure of the error given by the verified models are demonstrating the reliability of the ANN model for the given data series. The RSM model is created based on the given solutions by the software, and hence after definition of the problem, input and response data, the reliability of the model are verified by the obtained set of statistical data. Once the reliabilities of models are proven, the experimental input data are used for the prediction application. The deviations of the predicted values with the results from experiments are demonstrating the error ratios of developed model. Upon

the accuracy of the developed model, it may help to explain the soldering process system and to study the effects of different components, and to make predictions about the profiling behavior.

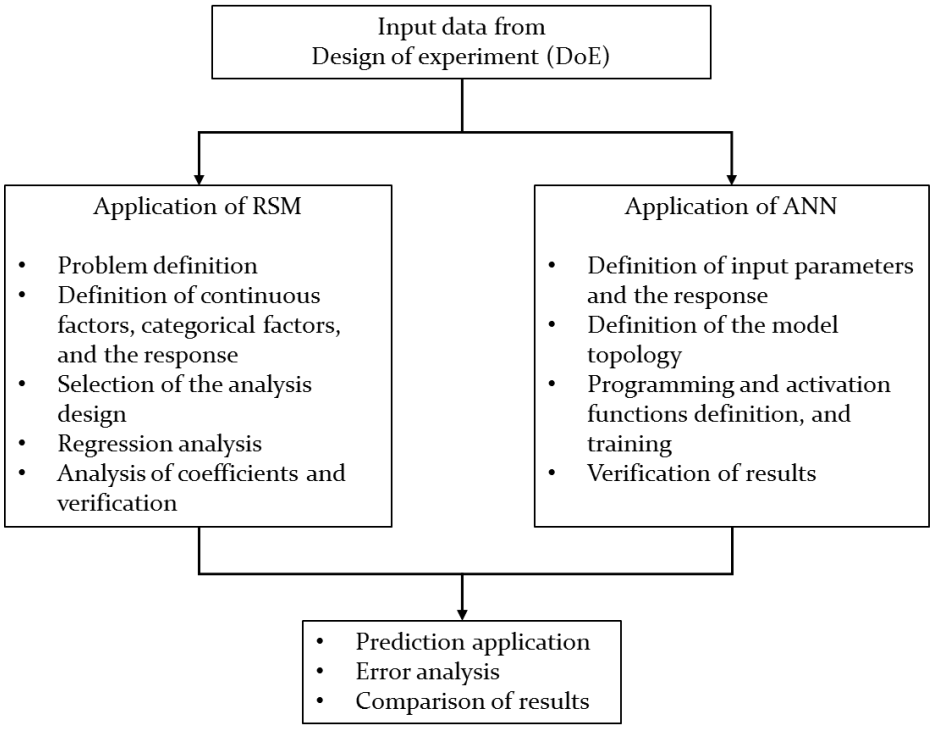

Figure 49: The structure of the mathematical modeling approach

6.1 Modeling of the Criteria using Artificial Neural Network (ANN) Method

ANN is used, first, to optimize the relation between the input parameters and responses in soldering process. Three models are individually developed for the void ratio, total electrical energy consumption and the exergy efficiency. The verified reliable models are utilized for prediction applications and to prove the optimized parameters setup. To build up the ANN model, a set of requirements are fulfilled which are discussed in the next subchapter.

6.1.1 Development of the ANN Models

The neural network modeling requires several parameters to adjust the topology of the network. According to the steepest gradient along the

error surface, Backpropagation Neural Network (BPN) is the best-known supervised technique for adjusting randomized weights during the data-learning phase. As shown in Figure 50, the BPN has input, hidden, and output layers. In order to design a BPN model, parameters should be defined including: the number of data-learning iterations; the learning rate; momentum; the number of hidden layers; and the number of processing elements in the hidden layer. There are some general recommendations on the setup of these parameters, but there is no universally proven criterion to define an appropriate network topology. Defining a high performance ANN design is not straightforward and it depends on the appropriate selections of network topology and parameters, and therefore there is a trade-off between mapping performance and computational complexity of the model. The profiling of the reflow soldering process is nonlinear and complex, and hence feedforward BPN algorithm is useful to map the cause and effect relationship of input setups and responses (void ratio, total power consumption, and total exergy efficiency). A high performance ANN model is used for further prediction purposes that are attributed with an acceptable error, a good performance, and an acceptable response data regression.

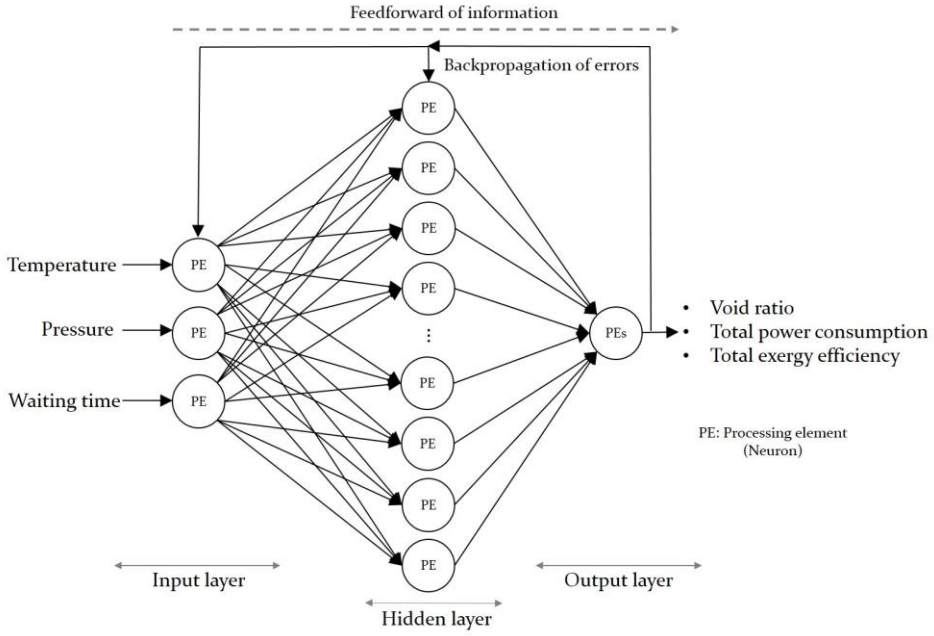

Figure 50: Architecture of ANN model for soldering process profiling

Temperature, pressure, and waiting time are defined as three input neurons. Depending on which response is going to be modeled, any of void ratio, or power consumption, or total exergy efficiency is chosen as the response neuron. As the rule of thumb, the number of hidden layers should be somewhere between the number of input and output layer, and in most problems one hidden layer is optimal. The number of neurons for the hidden layer also should not exceed twice the number of input nodes; otherwise an overfitting will be experienced at this point. However, these rules are not universal and a set of trial and error tries are revealing the best models with the least occurred error. For all models, Conjugate Gradient Backpropagation (CGB) with powell-beale restarts algorithm is selected as training function and Gradient Descent with Momentum (GDM) weight and bias learning function with default Momentum constant of 0.9 and Learning rate of 0.01.

The MATLAB® software package is utilized to develop the ANN architecture and model. The neural network toolbox is used to set up and find the best training dataset. The input data and response are defined. The given data for 27 experiments were randomly separated into three groups; 70% for training the data, 15% for testing samples, and 15% for validation. A final ANN topology for the hidden layers and neurons and an output layer with the Sigmoid transfer function is designated to train and test the experimental data with a limit of 10,000 epochs for all models. According to the trial and error experiments for any of the responses, one hidden layer and 4 neurons are identified for the best model performance before overfitting occurs. The Figure 51 is illustrating the training process flow chart for ANN modeling.

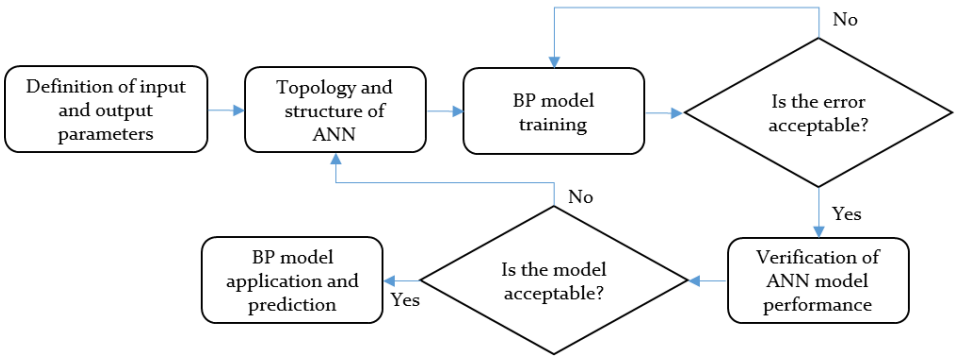

Figure 51: Training process flow chart for ANN modeling

After training the model, the Mean of Squared Errors (MSE) is checked for the network performance function measure. By the evaluation of different

trial and error setups for the ANN topology, the least MSE value should be realized and hence it verifies the model if the performance of the model is acceptable or not. In parallel, the regression plot (Figure 52) for the trained data is proving the verification of the final model. If the regression is acceptable and therefore if the regression accuracy is high enough, the model is reliable for further prediction applications.

6.1.2 Application and Verification of ANN Models

To develop the ANN model, three input parameters are chosen, and responses are selected according to the aim of the study. First, the void ratio is selected as the response for the first model. One hidden layer and four hidden neurons are defining the topology of the model. The model for this topology will be several times trained to obtain the best validation performance with the MSE of 0.13872. In parallel, as shown in Figure 52, the regression plots are examined to check if the training performance of the data in this model is satisfactory.

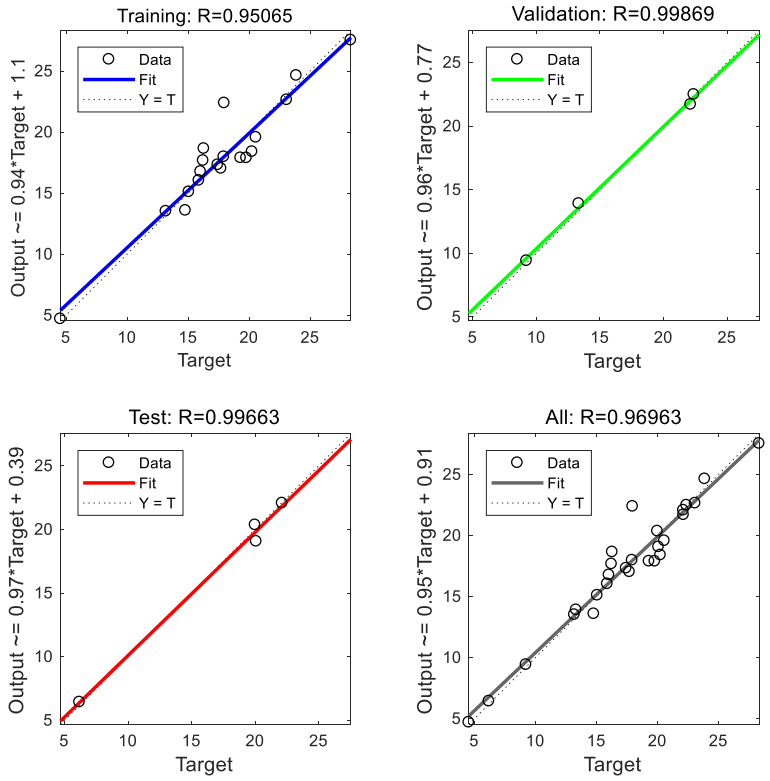

Figure 52: Regression plot of training, validation and test

In each plot, the dashed line represents the perfect result, i.e. outputs equal targets, whereas the solid line corresponds to the best-fit linear regression. As R-*value* approaches to one, then there is an exact linear relationship. The regression results (R-value) for training, validation and test are 0.95065, 0.99869 and 0.99663, respectively. Those results were corresponding to a total regression of 0.96963. The high accuracy of trained model associated with low MSE demonstrates the reliability of this model for prediction application.

The above explained process approach for modeling and verification of the ANN models for all three responses are performed and the results are shown in Table 18. The verified models with demonstrated MSEs are conforming to the reliability of the ANN models for further prediction applications.

Table 18: ANN model verification for all responses

Response	All: R-value	Mean Squared Error (MSE)
Void ratio	0.96963	0.13872
Total power consumption	0.99531	$7.8079*10^{-5}$
Total exergy efficiency	0.99287	0.0061449

6.2 Modeling of the Criteria using Response Surface Method (RSM) and Verification of Models

In the optimization process, likewise ANN approach, RSM quantifies the relationship between the input variables and the response surfaces, and it finds the optimal solution sets with the highest desirability according to the given response surface design. RSM method is following three solution approaches. In comparison with Central Composite design, the Box-Behnken design is considering combinations that are at the midpoints of the edges of the experimental space and it requires at least three continuous factors. Central Composite designs usually have axial points that may not be in the region of interest, or may be impossible to conduct because they are beyond safe operating limits. The Box-Behnken design is identifying all design points fall within the safe operating zone. In comparison with the two above, the third solution, the Full Factorial design is the most useful and powerful in explorations of the factor space to identify the region of optimal response because it is considering every combination of factor levels. Through the screening process, the safe

operation zones for overpressure soldering oven are known, and they are identified with the maximum, minimum and midpoint for each parameter. This study deployed the Full Factorial design to create and analyze the response surface.

Minitab® software is utilized to conduct the RSM. After identifying the designs for which the experimental data should be analyzed, the continuous factors (input process parameters), categorical factors (categorical classification of data), as well as the responses are defined. The RSM is producing a mathematical model, which correlate the input parameters and responses according to a polynomial equation. This equation is containing coefficients, which are describing the size and direction of the relationship between a term in the model and the response variable. To minimize multicollinearity among the terms, the coefficients are all in coded units, and they are shown in Table 19.

Table 19: Coded coefficients for the process responses

Term	Void ratio	Total power consumption	Total exergy efficiency
Constant	17.311	2.12297	23.369
Temperature	1.792	0.03330	-0.122
Pressure	-3.341	0.04262	2.643
Waiting time	1.457	0.19601	-1.121
(Temperature) * (Pressure)	4.564	-0.00712	0.129
(Temperature) * (Waiting time)	-2.373	0.01741	-0.134
(Pressure) * (Waiting time)	-1.580	0.01417	-0.271

In a polynomial equation of a response, the coefficient for a term represents the change in the mean response associated with an increase of one coded unit in that term, while the other terms are held constant. The sign of the coefficient indicates the direction of the relationship between the term and the response. As for the void ratio in Table 19, the coefficient for interaction of pressure among other continuing factors is the highest and then pressure has the highest effect. Interaction of temperature and pressure is proving their high effect comparing with other interaction terms. These analyses are confirming the significance analysis discussed in chapters 4.2.4, 5.3.5, and 5.3.6. The associated analysis from analysis of variance, significance analysis and demonstrated coefficients for RSM model responses are aligned with each other, and hence it is inferring the validity of the RSM models for further prediction applications.

6.3 Prediction Application and Comparison of ANN and RSM Models

After that the validation of both ANN and RSM models are demonstrated, the input parameters are used to predict the responses. The MATLAB® software is directly calculating the error percentages for ANN models, however for RSM models, the error ratio is manually calculated by the difference of approximate prediction and the exact values to realize the reliability of predicted responses comparing with the experimental measures. As illustrated in Figure 53, Figure 54, Figure 55, the error variation for each response is highly different. There is no universal measure of acceptable error ratio, but it will be defined by the goal setup of the study and the space scale of the response. For the basic variables and for the measures which are following a linear equation, such as power consumption, of course the individual error is quite low. In such cases the analysis are followed with an intensive standard deviation analysis and analysis of variance. However, for qualitative measures such as void ratio which is the product of a dynamic process, there are non-controllable influencing parameters on the response. In the discussed statistical analysis for void fraction, the ratio of variance and the adjusted R^2 is proving the reliability of data series and therefore the minimality of non-controllable parameters.

Figure 53 is displaying the void ratio prediction for both models and the corresponding errors. The RSM model for void ratio is obtaining a higher variation of error occurrence up to 30%. It explains the development of a qualitative model in which some influencing factors are unknown or if the preceding processes should be investigated to find the influential factors. The errors occurred for void ratio, also is corresponding to the explanations in the statistical analysis of the input parameters with R^2 value of 81.40%. In comparison, the ANN model is showing much less error variation, and therefore the predicted void ratio is following the experimental measurement. In contrary with void ratio model, the errors shown in Figure 54 and Figure 55, are depicting much less error fluctuation, and therefore a higher accuracy of predicted responses. The error for RSM model in Figure 55 is revealing an error-trend that is occurred by the change of pressure setup, and therefore it shows a lower accuracy of predicted measures for the profiles with pressure of 2 bar.

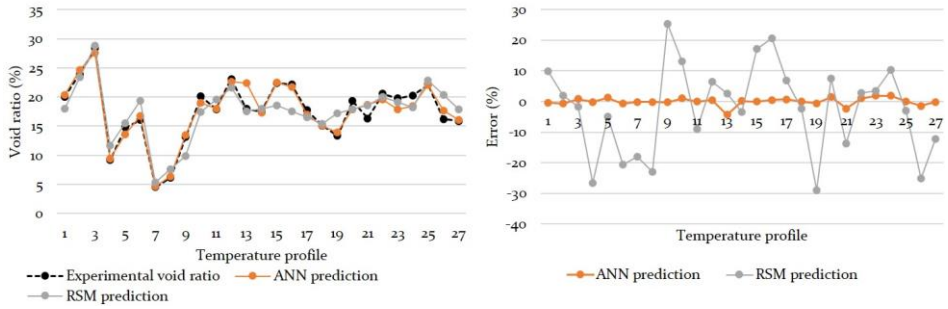

Figure 53: Void ratio and error comparison for ANN and RSM models

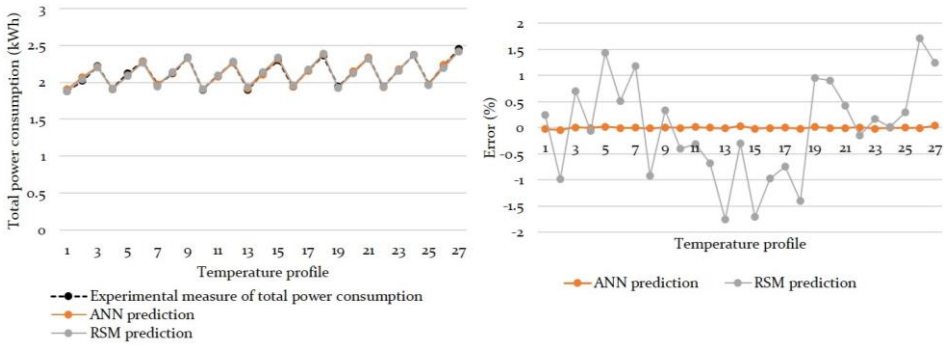

Figure 54: Total power consumption and error comparison for ANN and RSM models

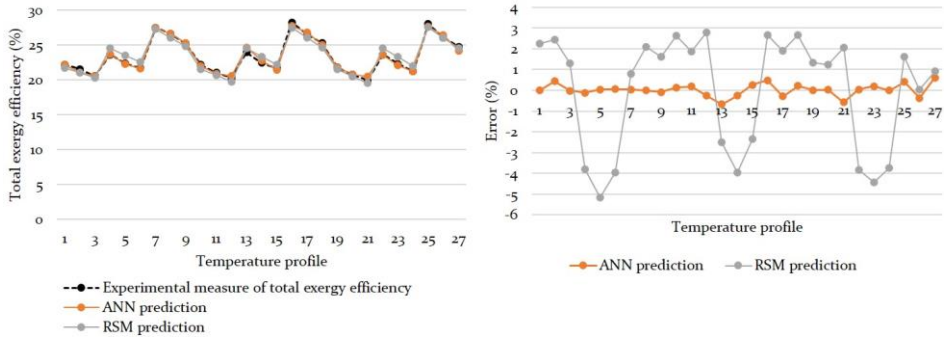

Figure 55: Total exergy efficiency and error comparison for ANN and RSM models

Both well trained ANN and RSM models were compared with their predictive capability. The average error for ANN as well as the RSM models per each response is tabulated in Table 20. Considerably, the average error for void ratio is much higher than for other two responses, and the error obtained by the RSM method is much higher comparing to ANN approach. The results illustrating that the ANN model has higher

modeling ability rather than the RSM models for soldering process. The ANN model predictions are corresponding much closer to the line of perfect prediction than the RSM models. Thus, the ANN model shows a significantly higher generalization capacity than the RSM models.

Table 20: The average error for ANN and RSM models

Response	Average Error for ANN (%)	Average Error for RSM (%)
Void ratio	0.84365356	11.8735271
Total power consumption	0.01241887	0.75977458
Total exergy efficiency	0.21701782	2.44004546

6.4 Conclusion

In this chapter, the soldering process is mathematically modeled for prediction application and to study the behavior of the profiling system. The ANN and RSM methods firstly are employed to build up the models for prediction applications, and secondly the results are used for comparison purposes to check the reliability of any of these methods for the current case study application. It is inferred that:

- One hidden layer and four hidden neurons are defining the topology of the ANN models. The model for this topology is used for void ratio, total power consumption and total exergy efficiency. These three models after several repetition of training are obtaining the best validation performance with the MSE of near zero. The regression results (R value) for training, validation, test, and the total regression are showing accuracy over 95%. The high accuracy of trained model associated with low MSE demonstrates the reliability of these models for prediction application.
- The safe operation zones for soldering oven are known, and to conduct a comprehensive experimental design, the Full Factorial design is used to create the RSM model. The associated analysis from analysis of variance, significance analysis and demonstrated coefficients for RSM model responses are conforming to each other, and hence it is inferring the validity of the RSM models for further prediction applications.

- The comparison of average errors for the each model are illustrating that the ANN model has higher modeling ability rather than the RSM models for soldering process.

Deduced from the implemented models in this study, the higher predictive accuracy of the ANN can be attributed to its universal ability to approximate the nonlinearity of the system, whereas the RSM is restricted to a second-order polynomial. It is experienced that the generation of ANN model requires a large number of iterative calculations and to check the overfitting process. Therefore ANN model may require a high computational time to create and more costly, whereas it is only a single step calculation for a response surface model. Comparing the overall facts for the mathematical modeling, ANN is realized as a convincing modeling approach for further prediction application in soldering process.

7 Multi-Objective Optimization of the Trade-Off Model Using a Decision Making Approach for Soldering Process

In this chapter, a multi-criterion optimization approach is applied first to investigate the compromised optimum solution for the experimental result, and hence later for the predicted result. The multi-objective optimization approach is shown in Figure 56. As shown in this roadmap, the first step is to define the criteria according to the setup framework of the decision maker. As known, the void ratio is representing the quality factor and the production lead-time for time factor. For the energy factor, the power consumption of the oven technology and periphery equipment, and the exergy efficiency of utilized resources are elaborated. To calculate the cost factor, consumed resources and materials are furtherly investigated.

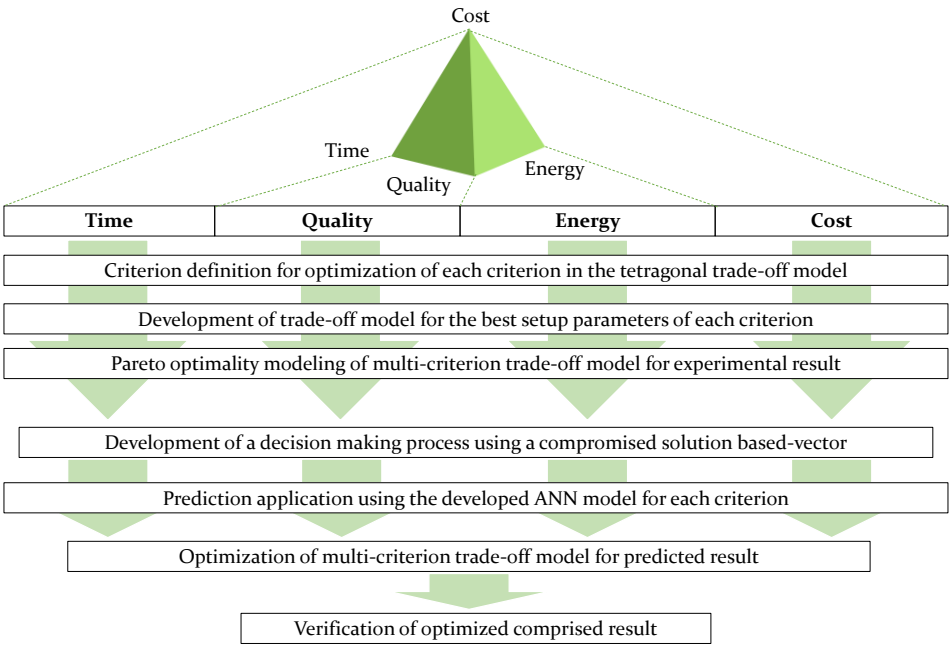

Figure 56: Multi-criterion optimization roadmap approach

Elaboration of the optimal solution considering all these criteria however is possible but it is not satisfactory, because a holistic solution is not obtainable. Therefore, a trade-off model is developed that the decision

maker is able to achieve the target setup including the boundary of set of optimized performances. A vector-based solution is presented to control the weight and importance of each criterion for a multi-objective solution for the experimental DOE. The trained ANN algorithms will be used for prediction applications and to prove the best parameters setups which are not experimentally verified. The optimized comprised solutions from experiments and predictions are furtherly experimentally verified to prove the accuracy of the developed prediction models.

7.1 Development of Trade-Off Model for the Best Setup Parameters of Each Criterion

The statistical and significance analysis are preparing for an approach to rank the strength of accumulative influencing factors on the final responses. The measures of effect of these factors on response are statistically realized but the decision maker according to the multi-objective optimization solution will define the positive or negative desire.

The difficulty of multi-objective or multi-criterion lies in the fact that the objectives are in conflict with each other and an improvement of one objective may lead to the reduction of other objectives. Therefore, obtaining the global optimum in all objectives at the same time is impossible. The goal of a multi objective solution is a compromise between different objectives in order to get the balance and to achieve optimum for every objective as much as possible. There are many methods such as multi-objective weighted method, hierarchical optimization method, objective programming, and hybrid programming method [208]. These methods are obtaining efficient solutions for decision makers to reach the objective. Theoretically most accepted approach is to find effective solutions frontier of multi-objective programming which is called Pareto efficient solution set. But in general there are infinitely many Pareto optimal solutions which lead to the complexity of algorithm and the large amount of calculation. This study is using Pareto optimality as a multi-criterion solution to seek a trade-off between all objectives. These objectives relating to their significance on responses are aimed to be maximized or minimized.

In chapters 4.2.4, 5.3.6, 5.4.2, the statistical and significance analysis are conducted, and the effects of input parameters on responses are evaluated. According to these analyses, a criterion definition in trade-off model is given in Table 21. For time factor, the waiting time is relevant

because other factors are not significantly effective on production lead-time. The waiting time is highly statistically significant and it should be reduced for all criteria. The cost factor is including the cost for the resources, energy and the material flow in the process, and it should be minimized. The process cost for resources are changing according to profile setup. The effect of pressure and waiting time on the periphery power consumption, and the temperature and waiting time on the power consumption of the oven are statistically highly significant. The effect of temperature on final production cost is not statistically significant, but other factors are. Furthermore, waiting time is highly statistically significant on the process cost, and the optimality criteria tending this response to be reduced minimally.

Respect to criteria definition, the quality factor should be optimally maximized as possible. The analysis of variance illustrate that shear test results are not valid for further analysis, however the void ratio is considered as the profounding indicator for the quality criterion. Pressure is demonstrating the biggest significance on void creation, and to achieve the minimum ratio, the highest measure of pressure, lower temperature, and a shorter waiting time is targeted.

Table 21: Criterion definition in trade-off model

Factor	Time (↓)	Cost (↓)	Quality (↑)	Energy	
				Total power consumption (↓)	Total exergy efficiency (↑)
Temperature	→	↓	↓**	↓***	↑
Pressure	→	↓**	↑***	↓***	↑***
Waiting time	↓***	↓***	↓*	↓***	↓***

↕*** extensively significant
↕** significant
↕* less significant
↕ no significance
→ no interaction

For the energy factor, the widespread target is the reduction/minimization of the consumed resources in the production process. The total power consumption is representing the electrical energy consumption of the oven technology and the periphery equipment. All factors are highly significant, and as for the criterion

definition, the reduction of temperature and waiting time is reducing the electrical energy of the oven and periphery equipment as well as a significant reduction for the power consumption of compressors which are supplying the nitrogen gas and hence the pressure build-up. The pressure and temperature are the main parts of thermomechanical exergy. Therefore, for the total exergy efficiency, the pressure interaction, which is contributing for more than 80% of the exergy efficiency, should be extensively increased; however, the temperature does not prove a significant effect. Electrical energy that is 100% exergy, by longer production lead-time will be converting more into exergy loss, and hence reduction of waiting time increases the total exergy efficiency.

According to the criterion definition in the trade-off model, Figure 57 illustrates the Pareto optimality model for all profiles. All the best performances are obtained by profiles with the waiting time of 20 seconds. Some associated profiles are creating the surface plots for a best specific performance. Nine profile coordinators are creating the green surface plot which is demonstrating the profiles with the lowest cost and production lead-time. Among the nine profiles, four profile coordinators shown in the corners of the black surface plot is showing the profiles with the highest quality and exergy efficiency, and lowest total power consumption. It is inferred that at any of these surface plots, any profile coordinators in these surface could be associated with a specific best performance. All profile coordinates in green surface plot showing the minimum production lead-time of 448 seconds and the lowest process cost about 0.35 €. Only one profile coordinate is demonstrating the best quality and lowest void ratio of 4.54%. One profile coordinate in the model is proving the highest exergy efficiency of 28.6%. Four profile coordinates in the black surface are showing the profiles for the lowest total power consumption of 1.88 kWh, 1.90 kWh, and 1.91 kWh.

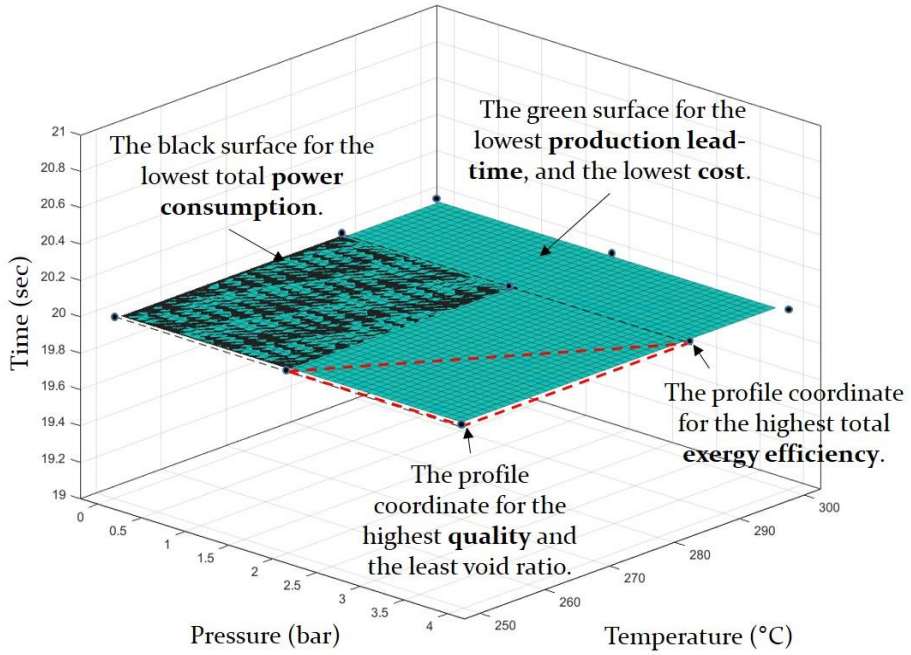

Figure 57: Trade-off model for the best extreme points of experimental design

7.2 Development of Decision Making Process for the Multi-objective Solution

The lowest costs with the shortest production lead-time solution is best suited for mass soldering of high-tech electronic devices, as for the time and cost is the most important factor. When a company is producing high performance electronics, the highest quality should be the primary objective. For green companies, the solution with the highest exergy efficiency is suggested. The best profiles for each objective are shown in the trade-off model; however no profile is identified which is satisfying a multi-objective solution. Therefore, compromised solution-based vector is introduced to apply on the trade-off model for a multi-objective decision making process.

The comprised solution is requiring the extreme coordinates/optimized solutions per each objective. The extreme coordinates for quality and exergy efficiency is determined, and any compromised solution for these objectives are satisfying the decision for the lowest cost and production lead-time. However, the extreme point for the total power consumption is not yet clear. Thereby, by applying the criterion definitions from Table 21

on the surface plot of power consumption in the trade-off model, the setup profile for 250 °C, 2 bar, and 20 seconds is determined as the extreme coordinate/optimized solution. Moreover, this profile is realized with the best exergy efficiency and better quality comparing with other four profiles in the surface plot. The extreme coordinates for three objectives are illustrated in red dash-line in Figure 57, and any coordinate in the surface boundary of the selected area is partially satisfying all the objectives in the trade-off model. To control the measure of importance, a weight is given to any of these objectives. The sum of the weights, as shown in equation 27, should be one. The parameter settings for the compromise solution were calculated utilizing a vector-based equation (Eq. 28). With the help of the extreme points of vectors and weights, other intermediate solutions can be calculated. Depending on the predefined scenario and associated objective, these weights using the pairwise comparison are determining the final decision on the setup parameters.

$$w_{Exergy} + w_{Power} + w_{Quality} = 1 \tag{27}$$

$$\begin{pmatrix} Peak\ temperature_{Compromise} \\ Pressure_{Compromise} \\ Waiting\ time_{Compromise} \end{pmatrix} = w_{Exergy} * \begin{pmatrix} 285\ °C \\ 4\ bar \\ 20\ sec \end{pmatrix} + w_{Power} * \begin{pmatrix} 250\ °C \\ 2\ bar \\ 20\ sec \end{pmatrix} + w_{Quality} * \begin{pmatrix} 250\ °C \\ 4\ bar \\ 20 sec \end{pmatrix} = \begin{pmatrix} 261.6\ °C \\ 3.32\ bar \\ 20\ sec \end{pmatrix} \tag{28}$$

To verify the above vector-based equation a compromised intermediate (equal importance of given weights) solution for the extreme points of the red dash-line in Figure 57 is calculated. Hence, w_{Exergy} equals 0.33, w_{Power} equals 0.33, and 0.33 is defined for $w_{Quality}$, and the result are experimentally verified in Table 22.

7.3 Prediction Application and Experimental Result Verification for the Trade-Off Model

The calculated compromised solution from the trade-off performance is experimentally verified and the measures are demonstrated as if the expectation from each criterion is equal. Moreover than verification applications, further experiments are conducted to prove the quality of developed models for prediction usage. Form the conclusion in chapter 6,

it is concluded that the developed ANN model are reliable for prediction application, and therefore these models are deployed to investigate the optimized compromised solutions.

First, the input variables out of the boundary of the given input parameters in experimental design are defined. Two constraints are defining the boundaries of the input variables. The first constraint is the technology, material, and technical concerns. If the peak temperature is set below the liquidus temperature, the solder material does not melt, and if it sets too high, the flux vaporizes too fast. These concerns are combined with the constrain criterion in Table 21, and hence a set of input variables are designed to predict the responses. Thereby, 250 °C is the minimum and the desired temperature, and it is set to be increased incrementally by 5 °C up to 300 °C. Zero bar is the minimum and 4.2 bar is set as the maximum technical overpressure measure. Likewise, from the criterion definition, 10 seconds is proven as the desired measure for the waiting time. These measure levels are used as the input variables for further prediction applications. The prediction values for cost, quality and exergy efficiency were obtained utilizing the ANN models and the production lead-time was interpolated utilizing the experimental values. 1.88 kWh is calculated for the total power consumption of all profiles. In addition, it is inferred that the total process cost is decreasing from 0.02 € to 0.01 € per 5 seconds decrease of waiting time. However, these changes are negligible and it does not identify the predicted profile with the lowest cost. The exergy efficiency will be increasing 0.02% if the pressure changes from 4 bar to 4.2 bar. The exergy efficiency for most of profiles is showing the fluctuations from 27% to 28%. The given parameters for 265 °C, 4.2 bar and 10 seconds are illustrating the highest predictive exergy efficiency of 28.7%. The setup profile of 250 °C, 4.2 bar and 10 seconds present the lowest void ratio of 4.05%.

The predicted input variables for the optimized exergy efficiency and quality are used for the compromised intermediate solution in equation 29. The decision made in this scenario is deploying an equal weight; w_{Exergy} equals 0.5 and $w_{Quality}$ equals 0.5. The verified result for the comprised intermediate predictive solution is presenting the optimized setup parameters, which are addressing 5.4% of void ratio and 28.6% for exergy efficiency. The verified result is conforming to the verified predictive solutions, and it demonstrates the reliability of optimization equation model.

$$\begin{pmatrix} Peak\ temperature_{Compromise} \\ Pressure_{Compromise} \\ Waiting\ time_{Compromise} \end{pmatrix} = w_{Exergy} * \begin{pmatrix} 265\ °C \\ 4.2\ bar \\ 10\ sec \end{pmatrix} + w_{Quality} * \begin{pmatrix} 250\ °C \\ 4.2\ bar \\ 10 sec \end{pmatrix} = \begin{pmatrix} 257.5\ °C \\ 4.2\ bar \\ 10\ sec \end{pmatrix} \quad (29)$$

Table 22: Solutions and additional experimental verification

Solution type	Temperature profile	Production Lead-time (sec)		Process cost (€)		Power consumption (kWh)		Exergy efficiency (%)		Average void ratio (%)	
		predicted	verified	predicted	verified	predicted	verified	predicted	verified	predicted	verified
Comprised intermediate solution	261.6 °C, 3.32 bar, 20 sec	-	448	-	0.34	-	1.9	-	26.61	-	7.6
Predictive solution	250 °C, 4.2 bar, 10 sec (Highest quality)	438	438	0.34	0.34	1.88	1.88	28.6	28.6	4.05	4.42
	265 °C, 4.2 bar, 10 sec (Highest exergy efficiency)	438	438	0.34	0.34	1.88	1.88	28.7	28.7	6.5	6.48
Comprised intermediate predictive solution	257.5 °C, 4.2 bar, 10 sec	-	438	-	0.34	-	1.88	-	28.6	-	5.4
Additional experiments	250 °C, 4.2 bar, 20 sec	-	448	-	0.35	-	1.91	-	27.9	-	4.43
	250 °C, 4.2 bar, 25 sec	-	453	-	0.36	-	1.90	-	27.8	-	4.64
	250 °C, 4.2 bar, 30 sec	-	458	-	0.36	-	1.93	-	27.6	-	5.17

The verified prediction solutions for production lead-time, cost and power consumption are identical and for the exergy efficiency and void ratio are attained with a high accuracy. The vector-based model is utilized for further prediction application of desired solutions for setup temperature

profiles of the reflow oven with overpressure chamber. Depending on the decision strategy for the chosen weights for quality and exergy efficiency, the desired solutions in parallel are satisfying the optimization objectives for the lowest production lead-time, lowest cost, and lowest power consumption.

The comprised intermediate predictive solution is presenting the reliable solution, which is experimentally proven. By comparing the result from this solution with comprised intermediate solution, the optimized intermediate solution for all criteria in the trade-off model is explicitly perceptible. Further above explained verifications, three profiles from predicted performances are experimentally examined as the means of comparison to check the effect of waiting time changes with the highest possible technical overpressure measure. In these experiments, the void ratio is not presenting a higher void fraction when the waiting time is increasing. In contrary the exergy efficiency for these profiles are rationally high due to the fact that the overpressure is setup at the highest possible technical value. The results are summarized and the experimental verifications for these profiles are shown in Table 22.

7.4 Conclusion

The improvement and optimization of the overpressure reflow soldering process is critical in order to achieve high quality and reliable solder joints, which in turn increases the yield of the downstream stages of the PCB assembly. The reflow soldering process integrated with overpressure module furtherly involves multiple performance characteristics including resource, cost, and time efficiency, and is nonlinear in nature.

In this chapter, a compromised intermediate equation model is presented which is obtaining a decision-based optimization solution. A vector-based compromised solution is requiring the extreme coordinates of the trade-off model, and by the given weight, the performances for a multi-objective solution is controlled. As an example, to obtain the highest quality of solder joint with the least void ration for class 3 and high-tech electronic devices, the given weight for quality factor will be 1, and in contrary 0 is given to other factors in the trade-off model. The optimized comprised solutions from experiments and predictions are furtherly experimentally examined to prove the accuracy of the developed prediction models. It is inferred that:

- According to criterion definition, for reduction of time, cost, total power consumption, the widespread target is the reduction/minimization of the waiting time, temperature, and pressure factors. However, to optimize the total exergy efficiency and quality, overpressure should be maximized.
- After verification of results, the compromised solution based-vectors is proven as a reliable solution for a multi-objective decision making process.
- The total process cost in the soldering process is decreasing from 0.02 € to 0.01 € per 5 seconds decrease of waiting time.
- The exergy efficiency will be increasing 0.02% if the pressure changes from 4 bar to 4.2 bar. The given parameters for 265 °C, 4.2 bar and 10 seconds are illustrating the highest predictive attainable exergy efficiency of 28.7%.
- The best quality with the lowest void ratio of 4.05% is presented by the setup profile of 250 °C, 4.2 bar and 10 seconds. 10 seconds is the minimum waiting time until the first overpressure (TAL) before the first pressure build-up is assuring that bigger voids reach the surface. By applying 4.2 bar, the highest technical overpressure measure, the void grow is reaching to minimum rate.
- Given an equal importance for all factors in the trade-off model for the full factorial DOE, the setup profile of 261.6 °C, 3.32 bar, 20 seconds waiting time is realized as a compromised intermediate solution. By including the technical extreme points, 257.5 °C, 4.2 bar, 10 seconds are obtaining the compromised intermediate solution for the optimized exergy efficiency of 28.6% and the void ratio of 5.4%.

By the given setup information for the full factorial DOE in Table 6, and the concluded result for compromised intermediate solution for the temperature in first zone of overpressure chamber, the overpressure measure, and the waiting time until the first overpressure build-up, Table 23 is showing the optimized profile for the best compromised performance. When it is not possible to eliminate voids, they should be minimized by a systematic approach based on controlling the factors involved in the generation of voiding and their mitigation. The smaller preheating slope and a rather constant soaking temperature (210 °C) drive the optimized profile. The results show that a smaller void area can

be achieved with shorter ramp to peak and TAL (10 seconds) as this minimizes the vaporization of flux volatiles during the reflow stage of the profile. Therefore, as expected, for small solder joints, a shorter TAL and a lower peak reflow temperature might well minimize the likelihood of gas being generated by decomposition of flux constituents in voids trapped at non-wetted areas.

Table 23: The compromised intermediate multi-objective optimization profile

Preheating						Overpressure		Cooling	
Zone 1	Zone 2	Zone 3	Zone 4	Zone 5	Zone 6	Zone 1	Zone 2	Zone 1	Zone 2
Temperature profile									
112 °C	132 °C	160 °C	210 °C	200 °C	210 °C	257.5 °C	203 °C	25 °C	25 °C

Transport band speed in preheating zone and cooling zone	Blowing fan power for all zones	Waiting time until the first overpressure build-up	Measure of overpressure	The first overpressure holding time
90 cm/min	100%	10 sec	4.2 bar	5 sec

Waiting time after the first overpressure	The second overpressure holding time	Transport band traverse speed in overpressure zone	Waiting time after the second overpressure
5 sec	45 sec	75 cm/min	20 sec

By increase of temperature from 250 °C to 257.5 °C, exergy efficiency is reaching to a comprised intermediate trade-off with other factors. 4.2 bar overpressure build-up is giving the highest chance to the trapped voids in the solder joints to escape. 5 seconds is the minimum duration for overpressure holding time and waiting time after the first overpressure so that to keep the TAL at its minimum at this stage of the process. Hence it reduces the production lead-time, cost, and power consumption, and it delivers higher exergy efficiency. An important step for the second overpressure is that before releasing the pressure, the components are to be moved into the second position to ensure a void-free solder connection, and 45 seconds is long enough so that the solder joints are solidified below the liquidus temperature. 20 seconds is set as the minimum waiting time after the second overpressure to deliver the PCB into the cooling zone. The designation of this temperature profile can

help the overpressure soldering process to achieve a multi-objective optimization of soldering process as specified in the Six Sigma management paradigm and continuous improvement program.

8 Summary

Surface mount technology (SMT) is the primary method used to attach electronic components permanently onto the substrate. A crucial improvement in quality of connecting technologies is increasing the reliability of solder joint and less heat dissipation due to poor connectivity. While a significant level of voiding can be tolerated in solder joints where electrical conductivity is the main requirement, voiding at any level severely compromises thermal conductivity. The voids are generally considered to come mainly from the flux medium by volatilization of solvents and as the result of reactions with metal oxides, and from decomposition of resins and other constituents of the material. To avoid the voiding deficiencies and increase the reliability of the solder joints, controlling the release process of voids are mandatory. By controlling the atmospheric pressure of the solder and reducing the surface tension helps the gases trapped in the solder material reaching to the surface. The recent advanced soldering technologies are offering the solutions to control the pressure between void and environment differences by vacuum or overpressure module concepts. Any of these technology concepts however are accompanied by advantages and disadvantages. The soldering oven technology combined with an overpressure module is offering a void-free solder joint solution, however the configuration of the mechanism related to the process is not comprehensively investigated yet. Furthermore, the offered technology concept in the market is inherently energy intensive and a deep study on the resource flow into the process is mandatory if the minimization of the consumption is required.

To cope with the above explained complications, a multi-objective optimization solution is offered which is based on a multi-criterion trade-off model for quality, energy, cost and time criterion. The constraints per each criterion and the Five-M are explaining the tools which enable the conduction of this study. The comprehensive analysis of the soldering oven technology obtain the input variables which lead to control the heating factors and gradients of the reflow process and therefore the delivered solder joint quality and the resource consumption. For the sake of cost and time saving, the Design of Experiment (DOE) is separated into four steps to realize the most influential setup parameters of the oven technology on void creation process. Deducing from the screening process, the waiting time until the first pressure build-up, the

temperature in the first zone of the over pressure chamber and measure of overpressure are realized as the most influential parameters on the voiding process. The full factorial DOE is conducted to examine the void-free soldering process. In parallel, the production lead-time and the resource consumption of the oven technology are measured. In order to control the resource flow of the oven technology, a transparency model is developed which is dividing the resource consumption of the oven and the auxiliary equipment in three levels. The resource flow into the oven technology is simulated to consider the none value-adding process time (e.g. non-predictable waiting time) and the correlated resource consumption. This obtains the total electrical energy consumption including none value-adding operations.

The simulation results are showing that 54% of electrical energy is consumed by the oven technology and 46% by the periphery levels. The periphery level is sharing the electrical energy consumption as for the air compressor 56.4%, the nitrogen compressor 43.4%, and the cooling water 0.19%, whereas the lights and air conditioning are negligible with a share under 0.01%. The statistical analysis and fitted models developed for electrical energy consumption of technology level and periphery levels demonstrate the reliability of the input data, and hence, waiting time is realized with the highest significance on these levels.

The exergy efficiency is calculated as the means of energy Key Performance Indicator (KPI) for the resource flow in the soldering process. The pressure change is the most influential factor on the physical exergy and hence the total exergy efficiency in soldering process until it is brought into equilibrium with the environment. The cost analysis for all experimental profiles are illustrating that the waiting time factor is significantly influencing on the final total costs as well as interacting with the power consumptions in the oven and periphery levels.

After the conduction of measurement, calculation and analysis of indicators for quality, resource, time and cost, these criteria are mathematically modeled for further prediction and optimization application. This study compares the performance of Response Surface Method (RSM) and Artificial Neural Network (ANN) methodologies with their modeling, prediction, and generalization capabilities using the experimental data based on the Full Factorial design. The ANN model indicates that it is much more robust and accurate in estimating the values of dependent variables when compared with the RSM models. The structured nature of the RSM is useful to exhibit the factors contributions

from the coefficients in the regression models. This ability is powerful in identifying the insignificant main factors and interaction factors or insignificant quadratic terms in the model and thereby can reduce the complexity of the problem. However, ANN has consistently performed better than the RSM in all aspects for each criterion.

The approach to find the optimal solution for each criterion however is possible but a holistic multi-criterion solution is not obtainable. According to the significance analysis, a criterion approach is defined for the setup parameters to maximize or minimize each objective/criterion. A trade-off model is developed that the decision maker is able to achieve the setup target including the boundary set of optimized performances. The presented vector-based solution controls the weight of all performances for a multi-objective solution, and hence it achieves a compromised intermediate solution. ANN model is used to predict the responses for the input variables which are not experimentally examined. The verified results for the predicted and compromised intermediate solutions are conforming to the fact that the ANN model is a reliable application solution in soldering process. If the quality is addressed as for the highest priority, the minimum technical temperature setup of 250 °C, the maximum technical pressure setup of 4.2 bar, and the minimum setup waiting time of 10 seconds derives the minimum void ratio. According to vector based solution, given an equal importance for all factors in the trade-off model for the given data from the full factorial DOE, the setup profile of 261.6 °C, 3.32 bar, 20 seconds of waiting time is realized as a compromised intermediate solution. By including the technical extreme points, 257.5 °C, 4.2 bar, 10 seconds are obtaining the compromised intermediate solution for the optimized exergy efficiency and 5.4% of void ratio for overpressure soldering process.

The outlook of this work is mainly focusing on two main topics. Void-free overpressure soldering process, and the widespread application of the developed trade-off model to consider the economic aspects of similar void-free soldering technologies. In soldering process, since the wetting of solder on a copper substrate is irreversible these voids have to have been there since the beginning of the soldering process. They only needed enough time to grow to detectable sizes. In addition, it is likely that most of the voids remaining after overpressure reflow are those attached to non-wetted areas. This raises the question why and where voids do form generally, and this requires more investigations on a real-time based monitoring of voids creation. Because, all void ratio investigation in this study are conducted through a 2D X-ray analysis and hence the volume of

bubble voids are not calculated. A 3D volume analysis of solder joints obtains an accurate forming behavior of voids fraction.

Klemm et al. [43] [38], have conducted In-Situ X-ray investigation to achieve the lowest final pore contents of < 1 % by applying the combined soldering profiles with vacuum and overpressure steps in laboratory scale. Also, Syed-Khaja [209] introduced the technology concepts that the pressure variation with combination of multiple vacuum and overpressure obtains excellent void content with negligible defects and full IMP growth. These technologies are delivering paternoster systems, which can be installed flexibly according to the profile with the lowest void ratio. Such technology concepts are deriving the maximum solder quality, however their long thermal process handling illustrate the necessity of application of the developed trade-off model to transparent the economic aspects for a successful concept introduction to the market.

9 Zusammenfassung

Die Surface Mount Technology (SMT) ist das primäre Verfahren, um elektronische Komponenten dauerhaft auf dem Substrat zu befestigen. Eine entscheidende Verbesserung der Qualität der Verbindungstechnologien wird durch die Erhöhung der Zuverlässigkeit der Lötverbindung und eine geringere Wärmeabstrahlung erzielt aufgrund schlechter Konnektivität. Während bei Lötverbindungen, bei denen die elektrische Leitfähigkeit die Hauptforderung ist, ein gewisses Maß an Porenbildung toleriert werden kann, ist die Wärmeleitfähigkeit bei Porenbildung stark beeinträchtigt. Es wird allgemein davon ausgegangen, dass die Poren hauptsächlich aus dem Flussmittel durch Verflüchtigung von Lösungsmitteln und als Ergebnis von Reaktionen mit Metalloxiden sowie durch Zersetzung von Harzen und anderen Bestandteilen des Materials stammen. Um Poren zu vermeiden und die Zuverlässigkeit der Lötstellen zu erhöhen, ist es zwingend erforderlich, den Entstehungsprozess der Lötstellen zu kontrollieren. Durch die Kontrolle des atmosphärischen Drucks des Lotes und die Reduzierung der Oberflächenspannung werden jene im Lötmaterial eingeschlossenen Gase an die Oberfläche geleitet, die die Poren bei Nichtentweichen verursachen. Die neuesten fortschrittlichen Löttechnologien bieten Lösungen, um den Druck zwischen den Gasen innerhalb der Poren und der Umgebung des Bauteils mittels Vakuum- oder Überdruckmodulkonzepte zu kontrollieren. All diese Methoden sind jedoch mit Vor- und Nachteilen verbunden. Die Lötofentechnik in Kombination mit einem Überdruckmodul ermöglicht Voidfreie Lötstellen. Jedoch ist die Konfiguration des prozessbezogenen Mechanismus noch nicht vollständig untersucht. Darüber hinaus ist die auf dem Markt angebotene Methode energieintensiv, und eine eingehende Untersuchung des Ressourcenflusses in den Prozess ist zwingend erforderlich, wenn eine Minimierung des Verbrauchs erreicht werden will.

Um die oben erläuterten Komplikationen zu beherrschen, wird in dieser Arbeit eine multikriterielle/gesamtheitliche Optimierungslösung angeboten, die auf einem Trade-off-Modell für Qualitäts-, Energie-, Kosten- und Zeitkriterien basiert. Die Rahmenbedingungen für jedes Kriterium und die Five-M erklären die Werkzeuge, die die Durchführung dieser Studie ermöglichen. Die umfassende Analyse der Lötofentechnik liefert die Eingangsgrößen, die zur Steuerung der Heizfaktoren und zu den Gradienten des Reflow-Prozesses und damit der gelieferten Lötstellenqualität und dem Ressourcenverbrauch führen. Aus Gründen der Kosten- und

Zeitersparnis wird ein Design of Experiment (DoE) durchgeführt, welches sich in vier Abschnitte unterteilt, um die wirkungsvollsten Setup-Parameter der Ofentechnologie für den Prozess der Reduktion der Porenbildung zu ermitteln.

In der ersten Phase des DoE werden die Wartezeit bis zum ersten Druckaufbau, die Temperatur in der ersten Zone der Überdruckkammer und die Messung des Überdrucks als die wichtigsten Einflussgrößen auf den Porenbildungsprozess identifiziert. Das anbschließende DoE wird durchgeführt, um den lunkerfreien Lötprozess zu untersuchen. Parallel dazu werden die Produktionsvorlaufzeit und der Ressourcenverbrauch der Ofentechnologie gemessen. Um den Ressourcenfluss der Ofentechnik zu steuern, wird ein Transparenz-Modell entwickelt, das den Ressourcenverbrauch des Ofens und der Hilfseinrichtungen in drei Ebenen unterteilt. Der Ressourcenfluss in die Ofentechnik wird unter Berücksichtigung der nicht wertschöpfenden Prozesszeit (z.B. nicht vorhersehbare Wartezeit) und des damit verbundenen Ressourcenverbrauchs simuliert. Dies ergibt den gesamten elektrischen Energieverbrauch einschließlich der nicht wertschöpfenden Tätigkeiten.

Die Simulationsergebnisse zeigen, dass 54 Prozent der elektrischen Energie durch die Ofentechnik und 46 Prozent durch die Peripherie verbraucht werden. Die Peripherieebene teilt sich den elektrischen Energieverbrauch. Dieser ergibt sich aus den Verbrauchern Luftkompressor (56,4 Prozent), Stickstoffkompressor (43,4 Prozent) und Kühlwasser (0,19 Prozent), während die Beleuchtung und Klimatisierung mit einem Anteil unter 0,01 Prozent vernachlässigbar sind. Die statistischen Analysen und angepassten Modelle, die für den elektrischen Energieverbrauch auf Technologie- und Peripherieebene entwickelt wurden, zeigen die Zuverlässigkeit der Eingangsdaten, so dass auf diesen Ebenen Wartezeiten mit höchster Bedeutung realisiert werden.

Die Exergieeffizienz wird als Mittel der Energiekennzahl (KPI) für den Ressourcenfluss im Lötprozess berechnet. Die Druckänderungen sind der wichtigste Faktor für die physikalische Exergie und damit für die gesamte Exergieeffizienz im Lötprozess. Die Exergieeffizienz wäre bei Absenkung des Drucks auf Umgebungsdruck am größten bis er mit der Umgebung ins Gleichgewicht gebracht wird. Die Kostenanalyse für alle Versuchsprofile zeigt, dass der Wartezeitfaktor die endgültigen Gesamtkosten erheblich beeinflusst und mit den Leistungsverbräuchen in der Ofen- und Peripherieebene zusammenwirkt.

Nach der Durchführung von Messungen, Berechnungen und Analysen von Indikatoren für Qualität, Ressourcen, Zeit und Kosten werden diese Kriterien mathematisch modelliert, um sie für weitere Prognose- und Optimierungsanwendungen zu nutzen. Diese Studie vergleicht die Leistung der Methoden der Response Surface Methodik (RSM) und des Künstlichen Neuronalen Netzwerks (ANN) mit ihren Modellierungs-, Vorhersage- und Verallgemeinerungsfunktionen unter Verwendung der experimentellen Daten, die auf der Designmethode Full Factorial basieren. Das ANN-Modell zeigt, dass es viel robuster und genauer bei der Bewertung der Werte abhängiger Variablen im Vergleich zu den RSM-Modellen ist. Der strukturierte Charakter der ANOVA und des RSM ist nützlich, um die Faktorenbeiträge aus den Koeffizienten in den Regressionsmodellen darzustellen. Diese Fähigkeit ist stark bei der Identifizierung der unbedeutenden Hauptfaktoren und Interaktionsfaktoren oder unbedeutenden quadratischen Faktore im Modell und kann dadurch die Komplexität des Problems reduzieren. ANN hat jedoch in allen Aspekten für jedes Kriterium stets besser abgeschnitten als das RSM.

Der Ansatz, für jedes Kriterium die optimale Lösung zu finden, ist möglich. Eine ganzheitlich optimierte Mehrkriterienlösung ist hingegen nicht möglich. Entsprechend der Signifikanzanalyse wird ein Kriterienansatz für die Setup-Parameter definiert, um jedes Ziel/Kriterium zu maximieren oder zu minimieren. Es wird ein Kompromissmodell entwickelt, mit dem der Entscheidungsträger in der Lage ist, das Setup-Ziel unter bestmöglicher Berücksichtigung der teilweikonträren Anforderungen zu erreichen. Die vorgestellte vektorbasierte Lösung steuert das Gewicht aller Leistungen für eine Mehrzwecklösung und erreicht damit eine Zwischenlösung. Das ANN-Modell wird verwendet, um die Antworten für die Eingangsgrößen vorherzusagen, die nicht experimentell untersucht werden. Die verifizierten Ergebnisse für die vorhergesagten und noch nicht final optimierten Zwischenlösungen entsprechen der Tatsache, dass das ANN-Modell eine zuverlässige Anwendungslösung im Lötprozess ist. Wird die Qualität mit der höchsten Priorität adressiert, ergibt sich aus der minimalen technischen Temperatureinstellung von 250 °C, der maximalen technischen Druckeinstellung von 4,2 bar und der minimalen Haltezeit von 10 Sekunden das minimale Voidverhältnis. Entsprechend der vektorbasierten Lösung, die für alle Faktoren im Trade-Off-Modell für die gegebenen Daten aus dem finalen DoE gleich wichtig ist, wird das Setup-Profil von 261,6 °C, 3,32 bar, 20 Sekunden Wartezeit als Kompromiss ermittelt. Durch die Einbeziehung der technischen Extrempunkte, 257,5 °C, 4,2 bar,

10 Sekunden erhalten Sie die Zwischenlösung für den optimierten Exergiewirkungsgrad und 5,4 Prozent Voidanteil beim Überdrucklötprozess.

Die Perspektive dieser Arbeit konzentriert sich hauptsächlich auf zwei Hauptthemen. Voidfreies Überdrucklötverfahren und die weit verbreitete Anwendung des entwickelten Trade-Off-Modells zur Berücksichtigung der wirtschaftlichen Aspekte ähnlicher Voidfreier Löttechnologien. Da die Benetzung von Lot auf einem Kupfersubstrat irreversibel ist, müssen diese Hohlräume im Lötprozess seit Beginn des Lötprozesses vorhanden sein. Sie brauchten nur genug Zeit, um auf erkennbare Größen zu wachsen. Außerdem ist es wahrscheinlich, dass die meisten der nach dem Überdruck-Rückfluss verbleibenden Hohlräume diejenigen sind, die an nicht benetzten Stellen angebracht sind. Dies wirft die Frage auf, warum und wo sich Voids im Allgemeinen bilden, und dies erfordert weitere Untersuchungen über eine echtzeitbasierte Überwachung der Voidbildung. Da alle Untersuchungen des Voidverhältnisses in dieser Studie durch eine 2D-Röntgenanalyse durchgeführt werden, wird das Volumen der Blasenhohlräume nicht berechnet. Eine 3D-Volumenanalyse von Lötverbindungen ergibt ein genaues Umformverhalten des Voidanteils. Zukünftige Forschung sollte sich demnach darauf konzentrieren, die Entstehungsorte und -zeitpunkte zu identifizieren und klassifizieren sowie die Geometrie der Gasblasen über die Zeit zu untersuchen.

Klemm et al. [43] [38], haben In-Situ-Röntgenuntersuchungen durchgeführt, um den niedrigsten Voidanteil von < 1 % zu erreichen, indem sie die kombinierten Lötprofile mit Vakuum- und Überdruckstufen im Labormaßstab applizierten. Syed-Khaja [209] stellte außerdem die Technologiekonzepte vor, dass die Druckvariation mit der Kombination von Mehrfachvakuum und Überdruck einen ausgezeichneten Voidanteil mit vernachlässigbaren Fehlern und vollem IMP-Wachstum erzielt. Diese Technologien liefern Paternostersysteme, die je nach Profil mit dem niedrigsten Voidanteil flexibel installiert werden können. Solche Technologiekonzepte leiten die maximale Lötqualität ab, aber ihre lange thermische Prozessführung verdeutlicht die Notwendigkeit der Anwendung des entwickelten Trade-off-Modells, um die wirtschaftlichen Aspekte für eine erfolgreiche Markteinführung des Konzepts transparent zu machen.

Bibliography

[1] RACKOW, T., P. SCHUDERER and J. FRANKE. Green Controlling–Ressourcenorientierte Steuerung von Unternehmen. *ZWF Zeitschrift für wirtschaftlichen Fabrikbetrieb,* 2013, 108(10), P. 773-777

[2] WOSNITZA, F. and H.G. HILGERS. *Energieeffizienz und Energiemanagement: Ein Überblick heutiger Möglichkeiten und Notwendigkeiten:* Springer-Verlag, 2012. ISBN 3834886718

[3] KOHL, J. *Automatisierte Datenerfassung für diskret ereignisorientierte Simulationen in der energieflexiblen Fabrik.* Dissertation. Erlangen, 2016

[4] BORNSCHLEGL, M. *Methods-Energy Measurement – Eine Methode zur Energieplanung für Fügeverfahren im Karosseriebau.* Dissertation. Bamberg: Meisenbach, 2016. Fertigungstechnik - Erlangen. 285. ISBN 9783875254099

[5] QUASCHNING, V. *Erneuerbare Energien und Klimaschutz. Hintergründe-Techniken und Planung-Ökonomie und Ökologie-Energiewende:* Carl Hanser Verlag GmbH Co KG, 2013. ISBN 3446437371

[6] KREITLEIN, S., N. EDER, A. SYED-KHAJA and J. FRANKE. Comprehensive Assessment of Energy Efficiency within the Production Process. *World Academy of Science, Engineering and Technology, International Journal of Mechanical, Aerospace, Industrial, Mechatronic and Manufacturing Engineering,* 2015, 9(7), P. 1359-1366

[7] AO, Y., L. GUNNEWIEK and M.A. ROSEN. Critical review of exergy-based indicators for the environmental impact of emissions. *International Journal of Green Energy,* 2008, 5(1-2), P. 87-104

[8] ESFANDYARI, A., D. SATTLER, A. SYED-KHAJA and J. FRANKE. A Lean-Based Key Performance Analysis for a Resource Efficient Soldering Oven in Electronics Production. *Applied Mechanics & Materials,* 2017, 856

[9] ESFANDYARI, A., A. SYED-KHAJA, T. JAVIED and J. FRANKE. Energy Efficiency Investigation on High-Pressure Convection

Reflow Soldering in Electronics Production. *Applied Mechanics and Materials,* 2014, 655, P. 95

[10] SWEATMAN, K., T. NISHIMURA, K. SUGIMOTO and A. KITA. Controlling Voiding Mechanisms in the Reflow Soldering Process. *Proceedings of IPC APEX Expo,* 2016

[11] SCHEEL, W., Hg. *Baugruppentechnologie der Elektronik. Montage.* 2., aktualisierte und erw. Aufl. Berlin: Verl. Technik, 1999. ISBN 3341012346

[12] LEE, N.-C. Optimizing the reflow profile via defect mechanism analysis. *Soldering & Surface Mount Technology,* 1999, 11(1), P. 13-20

[13] TSAI, T.-N. Development of a soldering quality classifier system using a hybrid data mining approach. *Expert Systems with Applications,* 2012, 39(5), P. 5727-5738

[14] PRASAD, R.P. One solder profile for all board. *Surface Mount Technology Magazine,* 2002, P. 11-14

[15] SURASKI, D. *Reflow Profiling: Time above Liquidus* [online]. 2007 [Access on: September 2019]

[16] KHAJA, A.S., C. KAESTLE, A. REINHARDT and J. FRANKE, Hg. *Optimized thin-film diffusion soldering for power-electronics production:* IEEE, 2013. ISBN 1479900362

[17] TSAI, T.-N. Modeling and optimization of stencil printing operations: A comparison study. *Computers & Industrial Engineering,* 2008, 54(3), P. 374-389

[18] BELL, H. *Reflowlöten. Grundlagen, Verfahren, Temperaturprofile und Lötfehler ; mit 41 Tabellen.* Bad Saulgau: Leuze, 2005. ISBN 9783874802024

[19] RÖSCH, M. *Potenziale und Strategien zur Optimierung des Schablonendruckprozesses in der Elektronikproduktion.* Dissertation. Bamberg: Meisenbach, 2011. Fertigungstechnik - Erlangen. 221. ISBN 9783875253191

[20] CHANSA-NGAVEJ, C. and J. KASEMSOMPORN, Hg. *Optimization of reflow-thermal profile by design of experiments with response surface methodology for minimizing solder-ball defects:* IEEE, 2008. ISBN 1424423295

[21] PAN, E.S., Y. JIN, H. XU and W.Z. LIAO, Hg. *Forecasting and parameters optimization of reflow soldering profile based on BPNN and GA:* Trans Tech Publ, 2010. 139. ISBN 0878492267

[22] ILLÉS, B. Distribution of the heat transfer coefficient in convection reflow oven. *Applied Thermal Engineering,* 2010, 30(13), P. 1523-1530

[23] IPC, A. 610D. *Revision DE: Acceptability of Electronic Assemblies / Abnahmekriterien für elektronische Baugruppen,* 2014

[24] GAO, J., Y. WU and H. DING. Optimization of a reflow soldering process based on the heating factor. *Soldering & Surface Mount Technology,* 2007, 19(1), P. 28-33

[25] ROSU, B., P. REYES-TURCU and D. SIMION-ZANESCU, Hg. *Thermal management system for reflow oven:* IEEE, 2003. ISBN 0780380029

[26] ESFANDYARI, A., B. BACHY, S. RAITHEL, A. SYED-KHAJA and J. FRANKE. Simulation, Optimization and Experimental Verification of the Over–Pressure Reflow Soldering Process [online]. *Procedia CIRP,* 2017, 62, P. 565-570. ISSN 22128271. Available on: doi:10.1016/j.procir.2016.06.092

[27] LAU, C.-S., M.Z. ABDULLAH and F. CHE ANI. Three-dimensional thermal investigations at board level in a reflow oven using thermal-coupling method. *Soldering & Surface Mount Technology,* 2012, 24(3), P. 167-182

[28] ILLÉS, B. and I. BAKÓ. Numerical study of the gas flow velocity space in convection reflow oven [online]. *International Journal of Heat and Mass Transfer,* 2014, 70, P. 185-191. ISSN 00179310. Available on: doi:10.1016/j.ijheatmasstransfer.2013.10.075

[29] FELDMANN, K. and J. STURM. Closed loop quality control in printed circuit assembly. *IEEE Transactions on Components, Packaging, and Manufacturing Technology: Part A,* 1994, 17(2), P. 270-276

[30] N.N. *Epec-build to print electronics* [online] [Access on: April 2017]. Available on: http://www.epectec.com/pcb/

[31] BIOCCA, P. Lead-free SMT Soldering Defects How to Prevent Them. *Global SMT and Packaging, Lead-Free Resource Guide,* 2005, P. 11-14

[32] N.N. *TechnoLab* [online]. *Qualifying and testing solutions* [Access on: April 2017]. Available on: http://www.technolab.de/_de/loetlexikon/index.php

[33] DIEHM, R., M. NOWOTTNICK and U. PAPE. Reduction of voids in solder joints an alternative to vacuum soldering. *Proc. of the IPC APEX EXPO, San Diego, CA,* 2012, 28

[34] RAUER, M. *Der Einfluss von Poren auf die Zuverlässigkeit der Lötverbindungen von Hochleistungs-Leuchtdioden.* Dissertation. Bamberg: Meisenbach Verlag, 2018. Fertigungstechnik - Erlangen

[35] WABLE, G.S., S. CHADA, B. NEAL and R.A. FOURNELLE. Solidification shrinkage defects in electronic solders. *JOM Journal of the Minerals, Metals and Materials Society,* 2005, 57(6), P. 38-42

[36] HELO, P. Managing agility and productivity in the electronics industry [online]. *Industrial Management & Data Systems,* 2004, 104(7), P. 567-577. ISSN 02635577. Available on: doi:10.1108/02635570410550232

[37] WEGE, S., R. DIEHM and V. LIEDKE, Hg. *Prozesstechnologien für hochzuverlässige, elektronische Baugruppen. MARITIM Hotel & Congress Centrum Bremen.* Bremen, September 2013

[38] KLEMM, A., M. OPPERMANN and T. ZERNA, Hg. *Analysis of soldering processes using in-situ X-Ray observations:* IEEE, 2015. ISBN 095680862X

[39] NOWOTTNICK, M., A. NOVIKOV and U. PAPE. » Material-und Prozesseinflüsse auf die Herstellung porenarmer Lötverbindungen «. *SMT/HYBRID/PACKAGING Tutorial 11; Nuremberg,* 2007

[40] ULZHÖFER, C. *Vacuum reflow. A simple approach for void reduction by means of an inline reflow system.* Wertheim, 2012

[41] PANTAZICA, M., P. SVASTA, H. WOHLRABE and K.-J. WOLTER. Factors influencing the formation of voids in chip component solder joints. In: *2013 IEEE 19th International Symposium for Design and Technology in Electronic Packaging (SIITME). 24 -27 Oct. 2013, Galați, Romania.* Piscataway, NJ: IEEE, 2013, P. 277-282. ISBN 9781479915552

[42] ÖTTL, H. *What are the benefits of soldering with vacuum profiles?* [online]. 2012 [Access on: May 2017]. Available on: www.rehm-group.com

[43] KLEMM, A., P. JAHNGEN, M. OPPERMANN and T. ZERNA. In-situ-X-Ray investigation on pressure release during conventional and diffusion soldering. In: *2013 IEEE 15th Electronics Packaging Technology Conference (EPTC 2013):* IEEE, 2013, P. 821-826. ISBN 9781479928347

[44] POLLACK-JOHNSON, B. and M.J. LIBERATORE. Incorporating Quality Considerations into Project Time/Cost Tradeoff Analysis and Decision Making [online]. *IEEE Transactions on Engineering Management,* 2006, 53(4), P. 534-542. ISSN 00189391. Available on: doi:10.1109/TEM.2006.883705

[45] HERAVI, G. and S. FAEGHI. Group decision making for stochastic optimization of time, cost, and quality in construction projects. *Journal of Computing in Civil Engineering,* 2012, 28(2), P. 275-283

[46] TAVANA, M., A.-R. ABTAHI and K. KHALILI-DAMGHANI. A new multi-objective multi-mode model for solving preemptive time–cost–quality trade-off project scheduling problems. *Expert Systems with Applications,* 2014, 41(4), P. 1830-1846

[47] HO, W., X. XU and P.K. DEY. Multi-criteria decision making approaches for supplier evaluation and selection [online]. A literature review. *European Journal of Operational Research,* 2010, 202(1), S. 16-24. ISSN 03772217. Available on: doi:10.1016/j.ejor.2009.05.009

[48] YURDAKUL, M. AHP as a strategic decision-making tool to justify machine tool selection [online]. *Journal of Materials Processing Technology,* 2004, 146(3), P. 365-376. ISSN 09240136. Available on: doi:10.1016/j.jmatprotec.2003.11.026

[49] SHANKAR, N.R., M.M.K. RAJU, G. SRIKANTH and P.H. BINDU. Time, cost and quality trade-off analysis in construction of projects. *Contemporary Engineering Sciences,* 2011, 4(6), P. 289-299

[50] EVERSHEIM, W. *Organisation in der Produktionstechnik.* bearbeitete and korrigierte Auflage. Berlin: Springer, 2002. ISBN 3540420169

[51] WESTKÄMPER, E. *Einführung in die Organisation der Produktion:* Springer-Verlag, 2006. ISBN 3540307648

[52] KHALAF, S. *Entwicklung eines Vorgehensmodells zur Erstellung energieeffizienter Fertigungsstrategien für verkettete Fertigungssysteme:* Shaker, 2012. ISBN 3844014845

[53] RACKOW, T. *Erweiterung des Unternehmenscontrollings um die Dimension Energie.* Dissertation. Erlangen, 2016

[54] HERRMANN, C., J. HESSELBACH, R. BOCK and T. DETTMER. Coolants made of native ester—technical, ecological and cost assessment from a life cycle perspective. *Advances in Life Cycle Engineering for Sustainable Manufacturing Businesses,* 2007, P. 299-303

[55] BMWI. *Zahlen and Fakten Energiedaten. Struktur des Energieverbrauchs.* Deutschland, 3. März 2014

[56] *eniPROD - Energieeffiziente Produkt- und Prozessinnovationen in der Produktionstechnik* [online] [Access on: May 2017]. Available on: http://www.eniprod.tu-chemnitz.de/index.php

[57] *SimEnergy - Simulationsgestützte Planung und Bewertung der Energieeffizienz für Produktionssysteme in der Automobilindustrie* [online] [Access on: May 2017]. Available on: https://www.uni-kassel.de/projekte/simenergy/

[58] *EnEffaH - Energieeffizienz in der Produktion im Bereich Antriebs- und Handhabungstechnik* [online] [Access on: May 2017]. Available on: https://www.eneffah.de/

[59] *FOREnergy - Die energieflexible Fabrik* [online] [Access on: May 2017]. Available on: http://forenergy.de/

[60] *Green Factory Bavaria* [online] [Access on: May 2017]. Available on: http://www.greenfactorybavaria.de/

[61] KHALAF, S. Bewertung und Optimierung von Produktionsprozessen. *Ruhr-Universität Bochum. Lehrstuhl für Produktionssysteme.* 2013, 21

[62] LANGER, T., A. SCHLEGEL, J. STOLDT and M. PUTZ. A Model-based Approach to Energy-saving Manufacturing Control Strategies [online]. *Procedia CIRP,* 2014, 15, P. 123-128. ISSN 22128271. Available on: doi:10.1016/j.procir.2014.06.019

[63] WEINERT, N., S. CHIOTELLIS and G. SELIGER. Methodology for planning and operating energy-efficient production systems [online]. *CIRP Annals - Manufacturing Technology,* 2011, 60(1), P. 41-44. ISSN 00078506. Available on: doi:10.1016/j.cirp.2011.03.015

[64] EBERSPÄCHER, P., P. SCHRAML, J. SCHLECHTENDAHL, A. VERL and E. ABELE. A model-and signal-based power consumption

monitoring concept for energetic optimization of machine tools. *Procedia CIRP,* 2014, 15, P. 44-49

[65] PARYANTO, P., A. HETZNER, M. BROSSOG and J. FRANKE. A Dynamic Simulation Model of Industrial Robots for Energy Examination Purpose [online]. *Applied Mechanics and Materials,* 2015, 805, P. 223-230. ISSN 16627482. Available on: doi:10.4028/www.scientific.net/AMM.805.223

[66] OHNO, T. *Toyota production system: beyond large-scale production:* CRC Press, 1988. ISBN 0915299143

[67] ISSAR, G. and L.R. NAVON. *Operational Excellence: A Concise Guide to Basic Concepts and Their Application:* Springer, 2016. ISBN 3319206990

[68] KREITLEIN, S., S. SCHWENDER, T. RACKOW and J. FRANKE. E|Benchmark-A Pioneering Method for Energy Efficient Process Planning and Assessment along the Life Cycle Process. *Procedia CIRP,* 2015, 29, P. 56-61

[69] KREITLEIN, S., S. SPRENG and J. FRANKE. E|Benchmark – A Pioneering Method for Process Planning and Sustainable Manufacturing Strategies [online]. *Procedia CIRP,* 2015, 26, P. 150-155. ISSN 22128271. Available on: doi:10.1016/j.procir.2014.07.070

[70] ESFANDYARI, A., S. KREITLEIN, E. SCHMIDT and J. FRANKE, Hg. *Thermodynamic and theoretical-based modeling and assessment of an energy-efficient performance measurement system in the soldering process:* IEEE, 2016. ISBN 1509052089

[71] SÖZEN, A. and E. ARCAKLIOĞLU. Exergy analysis of an ejector-absorption heat transformer using artificial neural network approach. *Applied Thermal Engineering,* 2007, 27(2), P. 481-491

[72] TSATSARONIS, G. Definitions and nomenclature in exergy analysis and exergoeconomics. *Energy,* 2007, 32(4), P. 249-253

[73] SZENDIUCH, I. and M. NOVOTNÝ. Lead-free Solder Joint Quality Investigation. *Acta Electrotechnica et Informatica, 2006,* 6(1), p.4.

[74] BAKSHI, B.R. *Thermodynamics and the destruction of resources.* Cambridge: Cambridge University Press, 2013. ISBN 0521884551

[75] GUNDERSEN, T. An introduction to the concept of exergy and energy quality. *Department of Energy and Process Engineering Norwegian University of Science and Technology,* 2011, 4

[76] QUEROL, E., B. GONZALEZ-REGUERAL and J.L. PEREZ-BENEDITO. *Practical approach to exergy and thermoeconomic analyses of industrial processes:* Springer Science & Business Media, 2012. ISBN 1447146220

[77] TALBI, M.M. and B. AGNEW. Exergy analysis: an absorption refrigerator using lithium bromide and water as the working fluids. *Applied Thermal Engineering,* 2000, 20(7), P. 619-630

[78] ZAHORANSKY, R. *Energietechnik: Systeme zur Energieumwandlung; Kompaktwissen für Studium und Beruf:* Springer-Verlag, 2009. ISBN 3834804886

[79] DEWULF, J., H. VAN LANGENHOVE, B. MUYS, S. BRUERS, B.R. BAKSHI, G.F. GRUBB, D.M. PAULUS and E. SCIUBBA. Exergy: its potential and limitations in environmental science and technology. *Environmental Science & Technology,* 2008, 42(7), P. 2221-2232

[80] GUTOWSKI, T.G., D.P. SEKULIC and B.R. BAKSHI, Hg. *Preliminary thoughts on the application of thermodynamics to the development of sustainability criteria:* IEEE, 2009. ISBN 1424443245

[81] THARUMARAJAH, A. and P. KOLTUN, Hg. *An exergy-based environmental indicator for manufacturing systems:* IEEE, 2007. ISBN 142440990X

[82] DINCER, I. and M.A. ROSEN. *Exergy: energy, environment and sustainable development:* Newnes, 2012. ISBN 0080970907

[83] SUN, W.-q., J.-j. CAI, T. DU and D.-w. ZHANG. Specific Energy Consumption Analysis Model and Its Application in Typical Steel Manufacturing Process [online]. *Journal of Iron and Steel Research, International,* 2010, 17(10), P. 33-37. ISSN 1006706X. Available on: doi:10.1016/S1006-706X (10)60180-X

[84] KHATTAK, S.H., R. GREENOUGH and N. BROWN, Hg. *Suitability of exergy analysis for industrial energy efficiency, manufacturing and energy management:* Eceee, 2012

[85] MADLOOL, N.A., R. SAIDUR, N.A. RAHIM, ISLAM and M.S. HOSSIAN. An exergy analysis for cement industries: an overview. *Renewable and sustainable energy reviews,* 2012, 16(1), P. 921-932

[86] BRANHAM, M., T.G. GUTOWSKI, A. JONES and D.P. SEKULIC, Hg. *A thermodynamic framework for analyzing and improving manufacturing processes:* IEEE, 2008. ISBN 1424422728

[87] SAIGANESH, S. *Sustainable resource utilization in manufacturing of printed circuit board assembly: exergy analysis of the process*. Dissertation. University of Kentucky Master's Theses. 34. 2010

[88] ESFANDYARI, A., A. SYED-KHAJA, M. HORVATH and J. FRANKE, Hg. *Energy Efficiency Analysis of Vapor Phase Soldering Technology through Exergy-Based Metric:* Trans Tech Publ, 2015. 805. ISBN 3038356468

[89] SHUKUYA, M. and A. HAMMACHE. *Introduction to the Concept of Exergy. for a Better Understanding of Low - Temperature - Heating and High - Temperature - Cooling Systems.* IEA ANNEX37 _ Low Exergy Systems for Heating and Cooling of Buildings, 2002

[90] SZARGUT, J. *Exergy method: technical and ecological applications:* WIT press, 2005. 18. ISBN 1853127531

[91] KUGELER, K. and P.-W. PHLIPPEN. *Energietechnik: technische, ökonomische und ökologische Grundlagen:* Springer-Verlag, 2013. ISBN 3662070294

[92] SAIGANESH, S. and D.P. SEKULIC, Hg. *Balancing material and exergy flows for a PCB soldering process: Method and a case study:* IEEE, 2010. ISBN 1424470951

[93] SZARGUT, J. Standard Chemical Exergy of Some Elements and Their Compounds, Based upon the Concentration in Earth's Crust. *Bulletin of the Polish Academy of Sciences, Technical Sciences,* 1987, 35(1-2), P. 53-60

[94] SZARGUT, J., D.R. MORRIS and F.R. STEWARD. Energy analysis of thermal, chemical, and metallurgical processes, 1988

[95] LÖDDING, H. Verfahren der Fertigungssteuerung: Grundlagen, Beschreibung, Konfiguration (2., erw. Aufl.). *Berlin [ua]: Springer,* 2008

[96] GÖTZE, U. *Kostenrechnung und Kostenmanagement:* Springer-Verlag, 2010. ISBN 3642118240

[97] N.N. *acatech.de* [online] [Access on: September 2019]. Available on: https://www.acatech.de/dialog/acatech-horizonte/

[98] BAKAKEU, J., S. TOLKSDORF, J. BAUER, H.-H. KLOS, J. PESCHKE, A. FEHRLE, W. EBERLEIN, J. BÜRNER, M. BROSSOG, L. JAHN and J. FRANKE. An Artificial Intelligence Approach for Online Optimization of Flexible Manufacturing Systems [online]. *Applied*

Mechanics and Materials, 2018, 882, P. 96-108. ISSN 16627482. Available on: doi:10.4028/www.scientific.net/AMM.882.96

[99] YOO, I.S., M. LANDGRAF, S. REITELSHÖFER and J. FRANKE. Soft Robotics mit DEA. Künstliche Muskeln für Roboterkollegen. *Handling,* 2015, P. 50-51

[100] MAYR, A., M. WEIGELT, M. MASUCH, M. MEINERS, F. HÜTTEL and J. FRANKE. Application Scenarios of Artificial Intelligence in Electric Drives Production [online]. *Procedia Manufacturing,* 2018, 24, P. 40-47. ISSN 23519789. Available on: doi:10.1016/j.promfg.2018.06.006

[101] CHOUDHARY, A.K., J.A. HARDING and M.K. TIWARI. Data mining in manufacturing: a review based on the kind of knowledge. *Journal of Intelligent Manufacturing,* 2009, 20(5), P. 501-521

[102] SAUER, W., M. OPPERMANN, G. WEIGERT, S. WERNER, H. WOHLRABE, K.-J. WOLTER and T. ZERNA. *Electronics process technology: Production modelling, simulation and optimisation:* Springer Science & Business Media, 2007. ISBN 184628354X

[103] SMITH, J.A. and F.B. WHITEHALL. *Optimizing quality in electronics assembly: A heretical approach:* McGraw-Hill Professional, 1997. ISBN 0070592292

[104] BIEHLER, H.-M. *Optimierungskonzepte für Qualitätsdatenverarbeitung und Informationsbereitstellung in der Elektronikfertigung.* Dissertation. Bamberg: Meisenbach, 1999. Fertigungstechnik - Erlangen. 94. ISBN 3875251261

[105] ZÖLLNER, B. *Adaptive Diagnose in der Elektronikproduktion.* Dissertation. München, 1995. Fertigungstechnik - Erlangen. 45. ISBN 3446183086

[106] STURM, J. *Prozeßintegrierte Qualitätssicherung in der Elektronikproduktion.* Dissertation. Bamberg: Meisenbach, 1996. Fertigungstechnik - Erlangen. 60. ISBN 3875250826

[107] LIUKKONEN, M., E. HAVIA, H. LEINONEN and Y. HILTUNEN. Expert system for analysis of quality in production of electronics. *Expert Systems with Applications,* 2011, 38(7), P. 8724-8729

[108] LIUKKONEN, M. *Intelligent Methods in the Electronics Industry:* University of Eastern Finland, 2010. ISBN 9526102819

[109] LIUKKONEN, M., E. HAVIA and Y. HILTUNEN. Computational intelligence in mass soldering of electronics–A survey. *Expert Systems with Applications,* 2012, 39(10), P. 9928-9937

[110] MIETTINEN, K. *Nonlinear multiobjective optimization:* Springer Science & Business Media, 2012. 12. ISBN 1461555639

[111] WANG, K. Applying data mining to manufacturing: the nature and implications. *Journal of Intelligent Manufacturing,* 2007, 18(4), P. 487-495

[112] PAL, N.R. and S. PAL. Editorial. *International Journal of Pattern Recognition and Artificial Intelligence,* 2002, 16(07), P. 773-779

[113] MOSLEMIPOUR, G., T.S. LEE and D. RILLING. A review of intelligent approaches for designing dynamic and robust layouts in flexible manufacturing systems [online]. *The International Journal of Advanced Manufacturing Technology,* 2012, 60(1-4), P. 11-27. ISSN 02683768. Available on: doi:10.1007/s00170-011-3614-x

[114] CHEN, Y. and B. PENG. Multi-objective optimization on multi-layer configuration of cathode electrode for polymer electrolyte fuel cells via computational-intelligence-aided design and engineering framework [online]. *Applied Soft Computing,* 2016, 43, P. 357-371. ISSN 15684946. Available on: doi:10.1016/j.asoc.2016.02.045

[115] GEN, M. and L. LIN. Multiobjective evolutionary algorithm for manufacturing scheduling problems [online]. State-of-the-art survey. *Journal of Intelligent Manufacturing,* 2014, 25(5), P. 849-866. ISSN 09565515. Available on: doi:10.1007/s10845-013-0804-4

[116] ZHANG, Y., A. BERNARD, R. HARIK and K.P. KARUNAKARAN. Build orientation optimization for multi-part production in additive manufacturing [online]. *Journal of Intelligent Manufacturing,* 2015, 47(3), P. 593. ISSN 09565515. Available on: doi:10.1007/s10845-015-1057-1

[117] DAVID, P., M. ALAN and G. RANDY. Computational intelligence: A logical approach, published by Oxford University Press, New York. 1998. ISBN-13: 9780195102703

[118] MITCHELL, T.M. Evaluating hypotheses. *Machine Learning*, WCB, 1997, P.128-153

[119] TSAI, T.-N. Thermal parameters optimization of a reflow soldering profile in printed circuit board assembly: A comparative study. *Applied Soft Computing,* 2012, 12(8), P. 2601-2613

[120] GONG, Y., Q. LI and D.G. YANG, Hg. *The optimization of reflow soldering temperature profile based on simulation:* IEEE, 2006. ISBN 1424406196

[121] ALVAREZ, C. *Simulationsgestützte Methoden zur effizienten Gestaltung von Lötprozessen in der Elektronikproduktion.* Dissertation. Bamberg: Meisenbach, 2008. Fertigungstechnik - Erlangen. 194. ISBN 9783875252774

[122] LI, C.-q. and Z.-h. WU, Hg. *SPC system analysis and design of reflow soldering process:* IEEE, 2006. ISBN 1424406196

[123] ZHONG, J., X. HU, J. ZHANG and M. GU, Hg. *Comparison of performance between different selection strategies on simple genetic algorithms:* IEEE, 2005. 2. ISBN 0769525040

[124] CASTILLO, E.D. *Process Optimization. A Statistical Approach.* Boston, MA: Springer Science+Business Media, LLC, 2007. International series in operations research and management science. 105. ISBN 0387714359

[125] RAJAGOPALAN, R. and P. RAJAGOPALAN, Hg. *Applications of neural network in manufacturing:* IEEE, 1996. 2. ISBN 0818673249

[126] TU, J.V. Advantages and disadvantages of using artificial neural networks versus logistic regression for predicting medical outcomes. *Journal of clinical epidemiology,* 1996, 49(11), P. 1225-1231

[127] ZUPAN, J. Introduction to artificial neural network (ANN) methods: what they are and how to use them. *Acta Chimica Slovenica,* 1994, 41, P. 327

[128] GUPTA, N. Artificial neural network. *Network and Complex Systems,* 2013, 3(1), P. 24-28

[129] JAIN, A.K., J. MAO and K.M. MOHIUDDIN. Artificial neural networks: A tutorial. *Computer,* 1996, 29(3), P. 31-44

[130] KALOGIROU, S.A. Artificial neural networks in renewable energy systems applications: a review. *Renewable and sustainable energy reviews,* 2001, 5(4), P. 373-401

[131] SANTOCHI, M. and G. DINI. Use of neural networks in automated selection of technological parameters of cutting tools. *Computer Integrated Manufacturing Systems,* 1996, 9(3), P. 137-148

[132] TANIKIĆ, D. and V. DESPOTOVIC. *Artificial intelligence techniques for modelling of temperature in the metal cutting process:* INTECH Open Access Publisher, 2012. ISBN 9535107364

[133] MARKOPOULOS, A.P., S. GEORGIOPOULOS and D.E. MANOLAKOS. On the use of back propagation and radial basis function neural networks in surface roughness prediction. *Journal of Industrial Engineering International,* 2016, 12(3), P. 389-400

[134] AL HAZZA, M.H.F. and E.Y.T. ADESTA, Hg. *Investigation of the effect of cutting speed on the Surface Roughness parameters in CNC End Milling using Artificial Neural Network:* IOP Publishing, 2013. 53. ISBN 1757899X

[135] HOUSE, W. Artificial intelligence, automation, and the economy. *Executive office of the President.* Available on: https://obamawhitehouse.archives.gov/sites/whitehouse.gov/files/documents/Artificial-Intelligence-Automation-Economy.*PDF,* 2016

[136] FINANCE, A.T.C.C. Industry 4.0 Challenges and solutions for the digital transformation and use of exponential technologies. *Finance, Audit Tax Consulting Corporate: Zurich, Swiss,* 2015

[137] DA XU, L., W. HE and S. LI. Internet of things in industries. A survey. *IEEE Transactions on industrial informatics,* 2014, 10(4), P. 2233-2243

[138] KAESTLE, C., H. FLEISCHMANN, M. SCHOLZ, S. HAERTER and J. FRANKE. Cyber-physical electronics production. In: *Industrial Internet of Things:* Springer, 2017, P. 47-78

[139] LEE, J., E. LAPIRA, B. BAGHERI and H.-a. KAO. Recent advances and trends in predictive manufacturing systems in big data environment. *Manufacturing letters,* 2013, 1(1), P. 38-41

[140] LEE, J., H. DAVARI, J. SINGH and V. PANDHARE. Industrial Artificial Intelligence for industry 4.0-based manufacturing systems. *Manufacturing letters,* 2018, 18, P. 20-23

[141] SHI, J., J. WAN, H. YAN and H. SUO, Hg. *A survey of cyber-physical systems:* IEEE, 2011. ISBN 1457710102

[142] LEE, J., H.D. ARDAKANI, S. YANG and B. BAGHERI. Industrial Big Data Analytics and Cyber-physical Systems for Future Maintenance & Service Innovation [online]. *Procedia CIRP,* 2015, 38, P. 3-7. ISSN 22128271. Available on: doi:10.1016/j.procir.2015.08.026

[143] ZHANG, L., Y. LUO, F. TAO, B.H. LI, L. REN, X. ZHANG, H. GUO, Y. CHENG, A. HU and Y. LIU. Cloud manufacturing [online]. A new manufacturing paradigm. *Enterprise Information Systems,* 2012, 8(2), P. 167-187. ISSN 17517575. Available on: doi:10.1080/17517575.2012.683812

[144] DITTER, A., D. FEY, J. BÜRNER and J. FRANKE, Hg. *Smarteco. An integrated solution from load balancing between the grid and consumers to local energy efficiency:* IEEE, 2015. ISBN 0769556973

[145] FLEISCHMANN, H., J. KOHL and J. FRANKE. A reference architecture for the development of socio-cyber-physical condition monitoring systems. In: *SoSE and cyber physical systems (CPS), from academia to application and back. 2016 11th Systems of Systems Engineering Conference (SoSE), IEEE : June 12-16, 2016, Kongsberg Kunnskap og kulturpark, Kongsberg, Norway.* Piscataway, NJ: IEEE, 2016, P. 1-6. ISBN 9781467387279

[146] BRANDMEIER, M., E. BOGNER, M. BROSSOG and J. FRANKE. Product Design Improvement through Knowledge Feedback of Cyber-physical Systems [online]. *Procedia CIRP,* 2016, 50, P. 186-191. ISSN 22128271. Available on: doi:10.1016/j.procir.2016.05.026

[147] ANDRÉ, Q., Z. CARMON, K. WERTENBROCH, A. CRUM, D. FRANK, W. GOLDSTEIN, J. HUBER, L. VAN BOVEN, B. WEBER and H. YANG. Consumer choice and autonomy in the age of artificial intelligence and big data. *Customer Needs and Solutions,* 2018, 5(1-2), P. 28-37

[148] MADDOX, T.M., J.S. RUMSFELD and P.R.O. PAYNE. Questions for artificial intelligence in health care. *Jama,* 2019, 321(1), P. 31-32

[149] PANCH, T., P. SZOLOVITS and R. ATUN. Artificial intelligence, machine learning and health systems. *Journal of global health,* 2018, 8(2)

[150] PANESAR, S., Y. CAGLE, D. CHANDER, J. MOREY, J. FERNANDEZ-MIRANDA and M. KLIOT. Artificial intelligence and the future of surgical robotics. *Annals of surgery,* 2019, 270(2), P. 223-226

[151] SEIDEL, R., A. MAYR, F. SCHAFER, D. KISSKALT and J. FRANKE. Towards a Smart Electronics Production Using Machine Learning Techniques. In: *2019 42nd International Spring Seminar on Electronics Technology (ISSE).* [Piscataway, New Jersey]: [IEEE], 2019, P. 1-6. ISBN 9781728118741

[152] HARDING, J.A., M. SHAHBAZ and A. KUSIAK. Data mining in manufacturing: a review. *Journal of Manufacturing Science and Engineering,* 2006, 128(4), P. 969-976

[153] HAYKIN, S.S. *Neural networks and learning machines:* Pearson Upper Saddle River, NJ, USA, 2009. 3

[154] KOHONEN, T., SCHROEDER, T.S. HUANG and S.-O. MAPS. Springer-Verlag New York. *Inc., Secaucus, NJ,* 2001, 43, P. 2

[155] CHO, H. and W.S. PARK, Hg. *Neural network applications in automated optical inspection: state of the arts:* International Society for Optics and Photonics, 2002

[156] ACCIANI, G., G. BRUNETTI and G. FORNARELLI. Application of neural networks in optical inspection and classification of solder joints in surface mount technology. *IEEE Transactions on industrial informatics,* 2006, 2(3), P. 200-209

[157] EDINBAROUGH, I., R. BALDERAS and S. BOSE. A vision and robot based on-line inspection monitoring system for electronic manufacturing. *Computers in Industry,* 2005, 56(8), P. 986-996

[158] MEYER, S., H. WOHLRABE and K.-J. WOLTER. Neural network modeling to predict quality and reliability for BGA solder joints. In: *2010 Proceedings 60th Electronic Components and Technology Conference (ECTC):* IEEE, 2010, P. 1596-1603. ISBN 9781424464104

[159] WU, W.-Y., C.-W. HUNG and W.-B. YU. The development of automated solder bump inspection using machine vision techniques. *The International Journal of Advanced Manufacturing Technology,* 2013, 69(1-4), P. 509-523

[160] HAO, W., Z. XIANMIN, K. YONGCONG, O. GAOFEI and X. HONGWEI. Solder joint inspection based on neural network combined with genetic algorithm. *Optik-International Journal for Light and Electron Optics,* 2013, 124(20), P. 4110-4116

[161] WU, H., X. ZHANG, H. XIE, Y. KUANG and G. OUYANG. Classification of Solder Joint Using Feature Selection Based on

Bayes and Support Vector Machine [online]. *IEEE Transactions on Components, Packaging and Manufacturing Technology,* 2013, 3(3), P. 516-522. ISSN 21563950. Available on: doi:10.1109/TCPMT.2012.2231902

[162] WU, F. and X. ZHANG. An inspection and classification method for chip solder joints using color grads and Boolean rules. *Robotics and Computer-Integrated Manufacturing,* 2014, 30(5), P. 517-526

[163] LIAO, C.-T., W.-H. LEE and S.-H. LAI. A Flexible PCB Inspection System Based on Statistical Learning [online]. *Journal of Signal Processing Systems,* 2012, 67(3), P. 279-290. ISSN 19398018. Available on: doi:10.1007/s11265-010-0556-8

[164] ACCIANI, G., G. FORNARELLI and A. GIAQUINTO. A fuzzy method for global quality index evaluation of solder joints in surface mount technology. *IEEE Transactions on industrial informatics,* 2011, 7(1), P. 115-124

[165] TSAI, T.-N. and J.-H. YEH. Identification and risk assessment of soldering failure sources using a hybrid failure mode and effect analysis model and a fuzzy inference system. *Journal of Intelligent & Fuzzy Systems,* 2015, 28(6), P. 2771-2784

[166] KUSIAK, A. and C. KURASEK. Data mining of printed-circuit board defects [online]. *IEEE Transactions on Robotics and Automation,* 2001, 17(2), P. 191-196. ISSN 1042296X. Available on: doi:10.1109/70.928564

[167] MAHAJAN, R.L. optimization and control in. *Manufacturing Challenges in Electronic Packaging,* 2012, P. 185

[168] COIT, D.W., B.T. JACKSON and A.E. SMITH. Neural network open loop control system for wave soldering. *Journal of Electronics Manufacturing,* 2002, 11(01), P. 95-105

[169] YANG, T. and T.-N. TSAI. Modeling and implementation of a neurofuzzy system for surface mount assembly defect prediction and control. *Iie Transactions,* 2002, 34(7), P. 637-646

[170] TSENG, T.-L.B., M.C. JOTHISHANKAR and T.T. WU. Quality control problem in printed circuit board manufacturing—An extended rough set theory approach. *Journal of manufacturing systems,* 2004, 23(1), P. 56-72

[171] LIN, Y.-H., W.-J. DENG, J.-R. SHIE and Y.-K. YANG. Optimization of reflow soldering process for BGA packages by artificial neural network. *Microelectronics international,* 2007, 24(2), P. 64-70

[172] ZHOU, J.-c., X.-q. XIAO, Y.-f. EN, N. CHEN and X.-z. WANG. Thermo-mechanical fatigue reliability optimization of PBGA solder joints based on ANN-PSO. *Journal of Central South University of Technology,* 2008, 15(5), P. 689-693

[173] LIUKKONEN, M., T. HILTUNEN, E. HAVIA, H. LEINONEN and Y. HILTUNEN. Modeling of soldering quality by using artificial neural networks. *IEEE Transactions on electronics packaging manufacturing,* 2009, 32(2), P. 89-96

[174] LIUKKONEN, M., E. HAVIA, H. LEINONEN and Y. HILTUNEN. Quality-oriented optimization of wave soldering process by using self-organizing maps. *Applied Soft Computing,* 2011, 11(1), P. 214-220

[175] GUO, Y., Z.-L. SUN, E.-S. PAN and Q. YANG. Forecast of SMT reflow soldering profile based on improved artificial neural network. *Dongbei Daxue Xuebao/Journal of Northeastern University,* 2011, 32(12), P. 1749-1752

[176] CANG, T., E.-S. PAN and M.-x. ZHANG, Hg. *Optimization study of reflow soldering profile for Surface Mount Technology:* IEEE, 2011. 3. ISBN 1457715872

[177] GREENE, C.M. and P. DAMODARAN, Hg. Artificial neural networks for reflow profiles in electronics assembly, In *IIE Annual Conference. Proceedings*, *Institute of Industrial and Systems Engineers (IISE)*, 2007, P. 1249

[178] GUO, Y., Z.-L. SUN and E.-S. PAN. Online control and optimization strategy of technological parameters of reflow soldering [online]. *Dongbei Daxue Xuebao/Journal of Northeastern University,* 2014, 35(4), P. 555-558. Available on: doi:10.3969/j.issn.1005-3026.2014.04.023

[179] TSAI, T.-N. and C.-W. TSAI. Development of a closed-loop diagnosis system for reflow soldering using neural networks and support vector regression. *International Journal of Industrial Engineering : Theory Applications and Practice,* 2014, 21(1), P. 18-32

[180] ZANGENEH, N., A. AZIZIAN, L. LYE and R. POPESCU, Hg. Application of response surface methodology in numerical

geotechnical analysis*,* In *Proc. 55th Canadian Society for Geotechnical Conference, Hamilton*, 2002

[181] MYERS, R.H. Response surface methodology--current status and future directions. *Journal of Quality Technology,* 1999, 31(1), P. 30

[182] KHURI, A.I. and S. MUKHOPADHYAY. Response surface methodology. *Wiley Interdisciplinary Reviews: Computational Statistics,* 2010, 2(2), P. 128-149

[183] FUKUDA, I.M., C.F.F. PINTO, C.d.S. MOREIRA, A.M. SAVIANO and F.R. LOURENÇO. Design of Experiments (DoE) applied to pharmaceutical and analytical Quality by Design (QbD). *Brazilian Journal of Pharmaceutical Sciences,* 2018, 54(SPE)

[184] MÜLLER, D., M. STÖBER and A. THÜMMLER. *Einsatz der Response-Surface-Methode zur Optimierung komplexer Simulationsmodelle:* SFB 559, 2005

[185] KORNER, F. Bedeutung einiger häufig gebrauchter statistischer Kennzahlen and Begriffe and ihre Interpretation. *Der Ornithologische Beobachter,* 2006, P. 1-4

[186] RÖßLER, I. and A. UNGERER. *Statistik für Wirtschaftswissenschaftler: eine anwendungsorientierte Darstellung:* Springer-Verlag, 2016. ISBN 3662484129

[187] GERHARD, M. *Qualitätssteigerung in der Elektronikproduktion durch Optimierung der Prozeßführung beim Löten komplexer Baugruppen:* Meisenbach, 1997. ISBN 3875251032

[188] N.N. *Seho Systems GmbH* [online]. *SEHO MaxiReflow - HP High-End Reflow Oven* [Access on: May 2017]. Available on: http://www.esd-center.se/fileadmin/user_upload/esd_center/pdf_produkter/Kretsteknik/Seho/Brochure_MaxiReflow_HP.pdf

[189] SIEMENS AG. *Multifunktionsmessgerät SENTRON PAC4200* [online]. *Systemhandbuch,* 2009

[190] SPRENG, S., J. KOHL and J. FRANKE, Hg. *Development of an adjustable measuring system for electrical consumptions in production:* Trans Tech Publ, 2014. 655. ISBN 3038352837

[191] ESFANDYARI, A., A. SYED-KHAJA, T. LANDSKRONE and J. FRANKE, Hg. *An Exergy-Based Analysis of Temperature Profiles for an Over-Pressure Reflow Oven Technology:* American Society of Mechanical Engineers, 2015

[192] BRIGGS, E. and R. LASKY. Best practices reflow profiling for lead-free SMT Assembly. *Indium Corporation Tech Paper,* 2012, P. 1-8

[193] FRANKLIN, M.F. Constructing tables of minimum aberration pn–m designs. *Technometrics,* 1984, 26(3), P. 225-232

[194] COYLE, R., H. MCCORMICK, P. READ, R. POPOWICH and J. OSENBACH, Hg. *The Influence of Solder Void Location on BGA Thermal Fatigue Life,* 2010. 15

[195] SYED-KHAJA, A. and J. FRANKE. Investigations on advanced soldering mechanisms for transient liquid phase soldering (TLPS) in power electronics. In: *Electronics System-Integration Technology Conference (ESTC), 2014. 16 - 18 Sept. 2014, Helsinki.* Piscataway, NJ: IEEE, 2014, P. 1-7. ISBN 9781479940264

[196] SCHENK, M., S. WIRTH and E. MÜLLER. *Fabrikplanung und Fabrikbetrieb: Methoden für die wandlungsfähige, vernetzte und ressourceneffiziente Fabrik:* Springer-Verlag, 2013. ISBN 3642054595

[197] SHOOK, J. and C. MARCHWINSKI. *Lean Lexicon. A graphical glossary for Lean Thinkers:* Lean Enterprise Institute, 2014. ISBN 1934109460

[198] N.N. *Leistungsberechnung von Klimageräten* [online] [Access on: September 2017]. Available on: https://de.trotec.com/tkl-mieten/infocenter/kapazitaetsberechnungen/leistungsberechnung-von-klimageraeten/?tx_tklinfo_tklinfopi[action]=airconditioning&tx_tklinfo_tklinfopi[controller]=Calculator&cHash=223bd78013ddc04e47c92abc0d22f197

[199] N.N. *MCC-MCE: Corrosion-free Closed Circuit Cooling Towers* [online] [Access on: April 2018]. Available on: www.mita-tech.it

[200] N.N. *Atlas Copco* [online]. *All-in-one Nitrogen and Oxygen Skid* [Access on: April 2018]. Available on: www.atlascopco.com

[201] KOHL, J., S. SPRENG and J. FRANKE. Discrete event simulation of individual energy consumption for product-varieties. *Procedia CIRP,* 2014, 17, P. 517-522

[202] WOHLRABE, H., H. FRITZSCHE and S. LUNGEN. Simulation based optimization of a SMD-assembling process. In: *2016 39th International Spring Seminar on Electronics Technology (ISSE). 18-22 May 2016.* Piscataway, NJ: IEEE, 2016, P. 226-231. ISBN 9781509013890

[203] PARYANTO, P. *Mechatronic simulation approach for the process planning of energy efficient handling systems.* Dissertation. Bamberg: Meisenbach, 2017. Fertigungstechnik - Erlangen. 297. ISBN 9783875254242

[204] SZARGUT, J., A. VALERO, W. STANEK and A. VALERO. Towards an international legal reference environment. *Proceedings of ECOS,* 2005, 2005, P. 409-420

[205] N.N. *Erlanger Stadtwerke (ESTW)* [online]. *energy price calculator* [Access on: October 2017]. Available on: http://www.estw.de

[206] JING, W., Z. YONGSHENG, Y. HAOXIONG and Z. HAO, Hg. *A Trade-off pareto solution algorithm for multi-objective optimization:* IEEE, 2012. ISBN 1467313653

[207] SYED-KHAJA, A. *Diffusion Soldering for the High-temperature Packaging of Power Electronics.* Erlangen: FAU University Press, 2019. FAU Studien aus dem Maschinenbau. 315. ISBN 3961471622

Publications within the scope of the presented research topics

[P1] ESFANDYARI, A., B. BACHY, S. RAITHEL, A. SYED-KHAJA and J. FRANKE. Simulation, Optimization and Experimental Verification of the Over–Pressure Reflow Soldering Process [online]. *Procedia CIRP,* 2017, 62, P. 565-570. ISSN 22128271. Available on: doi:10.1016/j.procir.2016.06.092

[P2] ESFANDYARI, A., D. SATTLER, A. SYED-KHAJA and J. FRANKE. A Lean-Based Key Performance Analysis for a Resource Efficient Soldering Oven in Electronics Production [online]. *Applied Mechanics and Materials,* 2016, 856, S. 91-98. ISSN 16627482. Available on: doi:10.4028/www.scientific.net/AMM.856.91

[P3] ESFANDYARI, A., S. KREITLEIN, E. SCHMIDT and J. FRANKE. Thermodynamic and theoretical-based modeling and assessment of an energy-efficient performance measurement system in the soldering process. In: *2016 Electronics Goes Green 2016+ (EGG):* IEEE, 2016, P. 1-6

[P4] ESFANDYARI, A., S. HÄRTER, T. JAVIED and J. FRANKE. A Lean Based Overview on Sustainability of Printed Circuit Board Production Assembly [online]. *Procedia CIRP,* 2015, 26, P. 305-310. ISSN 22128271. Available on: doi:10.1016/j.procir.2014.07.059

[P5] ESFANDYARI, A., A. SYED-KHAJA, T. LANDSKRONE and J. FRANKE. An Exergy-Based Analysis of Temperature Profiles for an Over-Pressure Reflow Oven Technology. In: *Proceedings of the ASME International Mechanical Engineering Congress and Exposition - 2015. Presented at ASME 2015 International Mechanical Engineering Congress and Exposition, November 13-19, 2015, Houston, Texas, USA.* New York, N.Y.: The American Society of Mechanical Engineers, 2016, V06BT07A019. ISBN 9780791857441

[P6] ESFANDYARI, A., A. SYED-KHAJA, M. HORVATH and J. FRANKE. Energy Efficiency Analysis of Vapor Phase Soldering Technology through Exergy-Based Metric [online]. *Applied Mechanics and Materials,* 2015, 805, P. 196-204. ISSN 16627482. Available on: doi:10.4028/www.scientific.net/AMM.805.196

[P7] ESFANDYARI, A., A. SYED-KHAJA, T. JAVIED and J. FRANKE. Energy Efficiency Investigation on High-Pressure Convection Reflow Soldering in Electronics Production. *Applied Mechanics and Materials,* 2014, 655, P. 95

[P8] ESFANDYARI, A., T. JAVIED, F. REISSMANN and J. FRANKE. A standby strategy model for an energy efficient soldering oven machine. In: *2016 IEEE Conference on Technologies for Sustainability (SusTech). 9-11 Oct. 2016.* Piscataway, NJ: IEEE, 2016, P. 47-51. ISBN 9781509041589

Publications on the other topics

[P9] SYED-KHAJA, A., J. STECHER, A. ESFANDYARI, S. KREITLEIN and J. FRANKE. Energy Efficient Manufacturing of Power Electronics Substrates through Selective Laser Melting Technology [online]. *Applied Mechanics and Materials,* 2016, 856, P. 188-194. ISSN 16627482. Available on: doi:10.4028/www.scientific.net/AMM.856.188

[P10] JAVIED, T., A. ESFANDYARI and J. FRANKE. Systematic energy management. A foundation for sustainable production. In: *2016 IEEE Conference on Technologies for Sustainability (SusTech). 9-11 Oct. 2016.* Piscataway, NJ: IEEE, 2016, P. 20-27. ISBN 9781509041589

[P11] TAHRIRI, F., M.R. OSMAN, A. ALI, R.M. YUSUFF and A. ESFANDIARY. AHP approach for supplier evaluation and selection in a steel manufacturing company. *Journal of Industrial Engineering and Management,* 2008, 1(2), P. 54-76

[P12] JAVIED, T., S. KREITLEIN, A. ESFANDYARI and J. FRANKE. Identification of Energy Consumption and Energy Saving Potentials of Electric Drive Systems [online]. *Applied Mechanics and Materials,* 2014, 655, P. 21-26. ISSN 16627482. Available on: doi:10.4028/www.scientific.net/AMM.655.21

[P13] ESFANDYARI, A., M.R. OSMAN, N. ISMAIL and F. TAHRIRI. Application of value stream mapping using simulation to decrease production lead time [online]. A Malaysian manufacturing case. *International Journal of Industrial and Systems Engineering,* 2011, 8(2), P. 230. ISSN 17485037. Available on: doi:10.1504/IJISE.2011.041371

[P14] TAHRIRI, F., M.R. OSMAN, R. YUSUFF and A. ESFANDYARI. A classification of multi-criteria and evaluation of supplier selection methods. In: *Proc. 37th International Conference on Computer and Industrial Engineering,* 2007, P. 20-23.

[P15] ESFANDYARI, A., M.R. OSMAN, F. TAHRIRI and R. RIEDEL. Lean production tools and techniques application toward more productivity in textile industries. . In: *Proc. 37th International Conference on Computer and Industrial Engineering,* 2007, 20-23 Oct.

Student works within the scope of the presented research topics *

[S1] KARAALIOGLU, O. C., A. ESFANDYARI and J. FRANKE. *Wärmeübergangskoeffizienten Ermittlung im SEHO Reflow-Lötofen zur Steigerung der Ressourceneffizienz.* Bachelor thesis. Erlangen, 2016

[S2] BAUDISCH, N., A. ESFANDYARI and J. FRANKE. *Lastmanagement in der Elektronikproduktion.* Project thesis. Erlangen, 2016

[S3] ACHATZ, F., A. ESFANDYARI and J. FRANKE. *Analyse und Optimierung des Prozessprofils für Seho Reflow-Lötofen.* Bachelor thesis. Erlangen, 2015

[S4] HORVATH, M., A. ESFANDYARI and J. FRANKE. *Exergie basierte Lötprofilanalyse durch Untersuchungen der Energieeffizienz für die Dampfphasenlöttechnologie.* Bachelor thesis. Erlangen, 2015

[S5] SCHWAGER, M., A. ESFANDYARI and J. FRANKE. *Energiewert-stromanalyse einer Überdruck Lötofen Anlage.* Bachelor thesis. Erlangen, 2016

[S6] WALCHER, P., A. ESFANDYARI and J. FRANKE. *Modeling and Evaluation of Thermodynamic Performance Indicators for Reflow Soldering Processes.* Bachelor thesis. Erlangen, 2016

[S7] KNOTT, C., A. ESFANDYARI and J. FRANKE. *Evaluation of the performance model for energy, quality, cost, time in an overpressure reflow soldering oven.* Project thesis. Erlangen, 2016

[S8] SATTLER, D., A. ESFANDYARI and J. FRANKE. *Entwicklung und Modellierung eines Kennzahlensystems für den Vergleich der Energieeffizienz von Lötofenanlagen.* Project thesis. Erlangen, 2016

[S9] SHWAGER, M., A. ESFANDYARI and J. FRANKE. *Optimierung des Lötprofils einer Überdruck-Lötofenanlage durch Fehleranalyse der Leiterplatten.* Project thesis. Erlangen, 2017

[S10] LANDSKRONE, T., A. ESFANDYARI and J. FRANKE. *Exergy-Based Soldering Profile Analysis in the Energy Efficiency Investigations for an overpressure Reflow Soldering Technology.* Project thesis. Erlangen, 2015

[S11] LI, J., A. ESFANDYARI and J. FRANKE. *Energy efficiency analysis of lean-based production planning for electronics production.* Master thesis. Erlangen, 2015

[S12] BAUDISCH, N., A. ESFANDYARI and J. FRANKE. *Soldering Process Optimization in Electronics Production.* Master thesis. Erlangen, 2017

* The author at the second (and third) position designates the supervisor of the student work and at the last position the chair holder.

[S13] KUYOĞLU, S., A. ESFANDYARI and J. FRANKE. Optimierung und Analyse von Temperaturprofilen an der Reflow Lötanlage durch die mathematischen Modelle. Master thesis. Erlangen, 2017

[S14] VEHABOVIC, Z., A. ESFANDYARI and J. FRANKE. Prädiktive Modellierung zur Optimierung des Stromverbrauchs im Reflow-Lötprozess. Master thesis. Erlangen, 2017

Supervised student works in other subject areas

[S15] RAITHEL, S., A. ESFANDYARI and J. FRANKE. *Wärmeübertragungssimulation eines energieeffizienten Lötprozesses in der Überdruck-Lötofenanlage.* Bachelor thesis. Erlangen, 2015

[S16] BAUER, M., A. ESFANDYARI and J. FRANKE. *Aufbau und Kontaktierung gedruckter Elektronik and Analyse des Langzeitverhaltens.* Bachelor thesis. Erlangen, 2018

[S17] REISSMANN, F., A. ESFANDYARI and J. FRANKE. *Entwicklung eines Standby-Strategie Modells für eine energieeffiziente Lötofenanlage.* Project thesis. Erlangen, 2016

[S18] DIEHM, F., A. ESFANDYARI and J. FRANKE. *Energy Efficiency of LDS-Processes for MID-Structuring.* Project thesis. Erlangen, 2016

[S19] ZILLNER, S., A. ESFANDYARI and J. FRANKE. *Energieeffizienzsteigerung eines Lötofens durch Einsatz von Wärmerohren.* Project thesis. Erlangen, 2016

[S20] RAITHEL, S., A. ESFANDYARI and J. FRANKE. *Optimierung des Temperaturprofils im Reflow Lötprozess durch künstliche neuronale Netzwerke und thermische Simulation.* Project thesis. Erlangen, 2017

[S21] KELLER, V., A. ESFANDYARI and J. FRANKE. *Implementierung eines CBR-Systems zur multiobjektiven Optimierung eines Lötofenverfahrens in der Elektronikproduktion.* Project thesis. Erlangen, 2017

[S22] XIONG, S., A. ESFANDYARI and J. FRANKE. *Ontologie-basierte Fehleranalyse von Reflow-Lötprozessen.* Master thesis. Erlangen, 2016

Reihenübersicht

Koordination der Reihe (Stand 2020):
Geschäftsstelle Maschinenbau, Dr.-Ing. Oliver Kreis, www.mb.fau.de/diss/

Im Rahmen der Reihe sind bisher die nachfolgenden Bände erschienen.

Band 1 – 52
Fertigungstechnik – Erlangen
ISSN 1431-6226
Carl Hanser Verlag, München

Band 53 – 307
Fertigungstechnik – Erlangen
ISSN 1431-6226
Meisenbach Verlag, Bamberg

ab Band 308
FAU Studien aus dem Maschinenbau
ISSN 2625-9974
FAU University Press, Erlangen

Die Zugehörigkeit zu den jeweiligen Lehrstühlen ist wie folgt gekennzeichnet:

Lehrstühle:

FAPS	Lehrstuhl für Fertigungsautomatisierung und Produktionssystematik
KTmfk	Lehrstuhl für Konstruktionstechnik
LFT	Lehrstuhl für Fertigungstechnologie
LPT	Lehrstuhl für Photonische Technologien

Band 1: Andreas Hemberger
Innovationspotentiale in der rechnerintegrierten Produktion durch wissensbasierte Systeme
FAPS, 208 Seiten, 107 Bilder. 1988.
ISBN 3-446-15234-2.

Band 2: Detlef Classe
Beitrag zur Steigerung der Flexibilität automatisierter Montagesysteme durch Sensorintegration und erweiterte Steuerungskonzepte
FAPS, 194 Seiten, 70 Bilder. 1988.
ISBN 3-446-15529-5.

Band 3: Friedrich-Wilhelm Nolting
Projektierung von Montagesystemen
FAPS, 201 Seiten, 107 Bilder, 1 Tab. 1989.
ISBN 3-446-15541-4.

Band 4: Karsten Schlüter
Nutzungsgradsteigerung von Montagesystemen durch den Einsatz der Simulationstechnik
FAPS, 177 Seiten, 97 Bilder. 1989.
ISBN 3-446-15542-2.

Band 5: Shir-Kuan Lin
Aufbau von Modellen zur Lageregelung von Industrierobotern
FAPS, 168 Seiten, 46 Bilder. 1989.
ISBN 3-446-15546-5.

Band 6: Rudolf Nuss
Untersuchungen zur Bearbeitungsqualität im Fertigungssystem Laserstrahlschneiden
LFT, 206 Seiten, 115 Bilder, 6 Tab. 1989.
ISBN 3-446-15783-2.

Band 7: Wolfgang Scholz
Modell zur datenbankgestützten Planung automatisierter Montageanlagen
FAPS, 194 Seiten, 89 Bilder. 1989.
ISBN 3-446-15825-1.

Band 8: Hans-Jürgen Wißmeier
Beitrag zur Beurteilung des Bruchverhaltens von Hartmetall-Fließpreßmatrizen
LFT, 179 Seiten, 99 Bilder, 9 Tab. 1989.
ISBN 3-446-15921-5.

Band 9: Rainer Eisele
Konzeption und Wirtschaftlichkeit von Planungssystemen in der Produktion
FAPS, 183 Seiten, 86 Bilder. 1990.
ISBN 3-446-16107-4.

Band 10: Rolf Pfeiffer
Technologisch orientierte Montageplanung am Beispiel der Schraubtechnik
FAPS, 216 Seiten, 102 Bilder, 16 Tab. 1990.
ISBN 3-446-16161-9.

Band 11: Herbert Fischer
Verteilte Planungssysteme zur Flexibilitätssteigerung der rechnerintegrierten Teilefertigung
FAPS, 201 Seiten, 82 Bilder. 1990.
ISBN 3-446-16105-8.

Band 12: Gerhard Kleineidam
CAD/CAP: Rechnergestützte Montagefeinplanung
FAPS, 203 Seiten, 107 Bilder. 1990.
ISBN 3-446-16112-0.

Band 13: Frank Vollertsen
Pulvermetallurgische Verarbeitung eines übereutektoiden verschleißfesten Stahls
LFT, XIII u. 217 Seiten, 67 Bilder, 34 Tab. 1990. ISBN 3-446-16133-3.

Band 14: Stephan Biermann
Untersuchungen zur Anlagen- und Prozeßdiagnostik für das Schneiden mit CO_2-Hochleistungslasern
LFT, VIII u. 170 Seiten, 93 Bilder, 4 Tab. 1991. ISBN 3-446-16269-0.

Band 15: Uwe Geißler
Material- und Datenfluß in einer flexiblen Blechbearbeitungszelle
LFT, 124 Seiten, 41 Bilder, 7 Tab. 1991.
ISBN 3-446-16358-1.

Band 16: Frank Oswald Hake
Entwicklung eines rechnergestützten Diagnosesystems für automatisierte Montagezellen
FAPS, XIV u. 166 Seiten, 77 Bilder. 1991.
ISBN 3-446-16428-6.

Band 17: Herbert Reichel
Optimierung der Werkzeugbereitstellung durch rechnergestützte Arbeitsfolgenbestimmung
FAPS, 198 Seiten, 73 Bilder, 2 Tab. 1991.
ISBN 3-446-16453-7.

Band 18: Josef Scheller
Modellierung und Einsatz von Softwaresystemen für rechnergeführte Montagezellen
FAPS, 198 Seiten, 65 Bilder. 1991.
ISBN 3-446-16454-5.

Band 19: Arnold vom Ende
Untersuchungen zum Biegeumforme mit elastischer Matrize
LFT, 166 Seiten, 55 Bilder, 13 Tab. 1991.
ISBN 3-446-16493-6.

Band 20: Joachim Schmid
Beitrag zum automatisierten Bearbeiten von Keramikguß mit Industrierobotern
FAPS, XIV u. 176 Seiten, 111 Bilder, 6 Tab. 1991. ISBN 3-446-16560-6.

Band 21: Egon Sommer
Multiprozessorsteuerung für kooperierende Industrieroboter in Montagezellen
FAPS, 188 Seiten, 102 Bilder. 1991.
ISBN 3-446-17062-6.

Band 22: Georg Geyer
Entwicklung problemspezifischer Verfahrensketten in der Montage
FAPS, 192 Seiten, 112 Bilder. 1991.
ISBN 3-446-16552-5.

Band 23: Rainer Flohr
Beitrag zur optimalen Verbindungstechnik in der Oberflächenmontage (SMT)
FAPS, 186 Seiten, 79 Bilder. 1991.
ISBN 3-446-16568-1.

Band 24: Alfons Rief
Untersuchungen zur Verfahrensfolge Laserstrahlschneiden und -schweißen in der Rohkarosseriefertigung
LFT, VI u. 145 Seiten, 58 Bilder, 5 Tab. 1991. ISBN 3-446-16593-2.

Band 25: Christoph Thim
Rechnerunterstützte Optimierung von Materialflußstrukturen in der Elektronikmontage durch Simulation
FAPS, 188 Seiten, 74 Bilder. 1992.
ISBN 3-446-17118-5.

Band 26: Roland Müller
CO_2 -Laserstrahlschneiden von kurzglasverstärkten Verbundwerkstoffen
LFT, 141 Seiten, 107 Bilder, 4 Tab. 1992.
ISBN 3-446-17104-5.

Band 27: Günther Schäfer
Integrierte Informationsverarbeitung bei der Montageplanung
FAPS, 195 Seiten, 76 Bilder. 1992.
ISBN 3-446-17117-7.

Band 28: Martin Hoffmann
Entwicklung einer CAD/CAM-Prozeßkette für die Herstellung von Blechbiegeteilen
LFT, 149 Seiten, 89 Bilder. 1992.
ISBN 3-446-17154-1.

Band 29: Peter Hoffmann
Verfahrensfolge Laserstrahlschneiden und –schweißen: Prozeßführung und Systemtechnik in der 3D-Laserstrahlbearbeitung von Blechformteilen
LFT, 186 Seiten, 92 Bilder, 10 Tab. 1992.
ISBN 3-446-17153-3.

Band 30: Olaf Schrödel
Flexible Werkstattsteuerung mit objektorientierten Softwarestrukturen
FAPS, 180 Seiten, 84 Bilder. 1992.
ISBN 3-446-17242-4.

Band 31: Hubert Reinisch
Planungs- und Steuerungswerkzeuge zur impliziten Geräteprogrammierung in Roboterzellen
FAPS, XI u. 212 Seiten, 112 Bilder. 1992.
ISBN 3-446-17380-3.

Band 32: Brigitte Bärnreuther
Ein Beitrag zur Bewertung des Kommunikationsverhaltens von Automatisierungsgeräten in flexiblen Produktionszellen
FAPS, XI u. 179 Seiten, 71 Bilder. 1992.
ISBN 3-446-17451-6.

Band 33: Joachim Hutfless
Laserstrahlregelung und Optikdiagnostik in der Strahlführung einer CO_2-Hochleistungslaseranlage
LFT, 175 Seiten, 70 Bilder, 17 Tab. 1993.
ISBN 3-446-17532-6.

Band 34: Uwe Günzel
Entwicklung und Einsatz eines Simulationsverfahrens für operative und strategische Probleme der Produktionsplanung und –steuerung
FAPS, XIV u. 170 Seiten, 66 Bilder, 5 Tab. 1993. ISBN 3-446-17604-7.

Band 35: Bertram Ehmann
Operatives Fertigungscontrolling durch Optimierung auftragsbezogener Bearbeitungsabläufe in der Elektronikfertigung
FAPS, XV u. 167 Seiten, 114 Bilder. 1993.
ISBN 3-446-17658-6.

Band 36: Harald Kolléra
Entwicklung eines benutzerorientierten Werkstattprogrammiersystems für das Laserstrahlschneiden
LFT, 129 Seiten, 66 Bilder, 1 Tab. 1993.
ISBN 3-446-17719-1.

Band 37: Stephanie Abels
Modellierung und Optimierung von Montageanlagen in einem integrierten Simulationssystem
FAPS, 188 Seiten, 88 Bilder. 1993.
ISBN 3-446-17731-0.

Band 38: Robert Schmidt-Hebbel
Laserstrahlbohren durchflußbestimmender Durchgangslöcher
LFT, 145 Seiten, 63 Bilder, 11 Tab. 1993.
ISBN 3-446-17778-7.

Band 39: Norbert Lutz
Oberflächenfeinbearbeitung keramischer Werkstoffe mit XeCl-Excimerlaserstrahlung
LFT, 187 Seiten, 98 Bilder, 29 Tab. 1994.
ISBN 3-446-17970-4.

Band 40: Konrad Grampp
Rechnerunterstützung bei Test und Schulung an Steuerungssoftware von SMD-Bestücklinien
FAPS, 178 Seiten, 88 Bilder. 1995.
ISBN 3-446-18173-3.

Band 41: Martin Koch
Wissensbasierte Unterstützung der Angebotsbearbeitung in der Investitionsgüterindustrie
FAPS, 169 Seiten, 68 Bilder. 1995.
ISBN 3-446-18174-1.

Band 42: Armin Gropp
Anlagen- und Prozeßdiagnostik beim Schneiden mit einem gepulsten Nd:YAG-Laser
LFT, 160 Seiten, 88 Bilder, 7 Tab. 1995.
ISBN 3-446-18241-1.

Band 43: Werner Heckel
Optische 3D-Konturerfassung und on-line Biegewinkelmessung mit dem Lichtschnittverfahren
LFT, 149 Seiten, 43 Bilder, 11 Tab. 1995.
ISBN 3-446-18243-8.

Band 44: Armin Rothhaupt
Modulares Planungssystem zur Optimierung der Elektronikfertigung
FAPS, 180 Seiten, 101 Bilder. 1995.
ISBN 3-446-18307-8.

Band 45: Bernd Zöllner
Adaptive Diagnose in der Elektronikproduktion
FAPS, 195 Seiten, 74 Bilder, 3 Tab. 1995.
ISBN 3-446-18308-6.

Band 46: Bodo Vormann
Beitrag zur automatisierten Handhabungsplanung komplexer Blechbiegeteile
LFT, 126 Seiten, 89 Bilder, 3 Tab. 1995.
ISBN 3-446-18345-0.

Band 47: Peter Schnepf
Zielkostenorientierte Montageplanung
FAPS, 144 Seiten, 75 Bilder. 1995.
ISBN 3-446-18397-3.

Band 48: Rainer Klotzbücher
Konzept zur rechnerintegrierten Materialversorgung in flexiblen Fertigungssystemen
FAPS, 156 Seiten, 62 Bilder. 1995.
ISBN 3-446-18412-0.

Band 49: Wolfgang Greska
Wissensbasierte Analyse und Klassifizierung von Blechteilen
LFT, 144 Seiten, 96 Bilder. 1995.
ISBN 3-446-18462-7.

Band 50: Jörg Franke
Integrierte Entwicklung neuer Produkt- und Produktionstechnologien für räumliche spritzgegossene Schaltungsträger (3-D MID)
FAPS, 196 Seiten, 86 Bilder, 4 Tab. 1995.
ISBN 3-446-18448-1.

Band 51: Franz-Josef Zeller
Sensorplanung und schnelle Sensorregelung für Industrieroboter
FAPS, 190 Seiten, 102 Bilder, 9 Tab. 1995.
ISBN 3-446-18601-8.

Band 52: Michael Solvie
Zeitbehandlung und Multimedia-Unterstützung in Feldkommunikationssystemen
FAPS, 200 Seiten, 87 Bilder, 35 Tab. 1996.
ISBN 3-446-18607-7.

Band 53: Robert Hopperdietzel
Reengineering in der Elektro- und Elektronikindustrie
FAPS, 180 Seiten, 109 Bilder, 1 Tab. 1996.
ISBN 3-87525-070-2.

Band 54: Thomas Rebhahn
Beitrag zur Mikromaterialbearbeitung mit Excimerlasern - Systemkomponenten und Verfahrensoptimierungen
LFT, 148 Seiten, 61 Bilder, 10 Tab. 1996.
ISBN 3-87525-075-3.

Band 55: Henning Hanebuth
Laserstrahlhartlöten mit Zweistrahltechnik
LFT, 157 Seiten, 58 Bilder, 11 Tab. 1996.
ISBN 3-87525-074-5.

Band 56: Uwe Schönherr
Steuerung und Sensordatenintegration für flexible Fertigungszellen mit kooperierenden Robotern
FAPS, 188 Seiten, 116 Bilder, 3 Tab. 1996.
ISBN 3-87525-076-1.

Band 57: Stefan Holzer
Berührungslose Formgebung mit Laserstrahlung
LFT, 162 Seiten, 69 Bilder, 11 Tab. 1996.
ISBN 3-87525-079-6.

Band 58: Markus Schultz
Fertigungsqualität beim 3D-Laserstrahlschweißen von Blechformteilen
LFT, 165 Seiten, 88 Bilder, 9 Tab. 1997.
ISBN 3-87525-080-X.

Band 59: Thomas Krebs
Integration elektromechanischer CA-Anwendungen über einem STEP-Produktmodell
FAPS, 198 Seiten, 58 Bilder, 8 Tab. 1997.
ISBN 3-87525-081-8.

Band 60: Jürgen Sturm
Prozeßintegrierte Qualitätssicherung in der Elektronikproduktion
FAPS, 167 Seiten, 112 Bilder, 5 Tab. 1997.
ISBN 3-87525-082-6.

Band 61: Andreas Brand
Prozesse und Systeme zur Bestückung räumlicher elektronischer Baugruppen (3D-MID)
FAPS, 182 Seiten, 100 Bilder. 1997.
ISBN 3-87525-087-7.

Band 62: Michael Kauf
Regelung der Laserstrahlleistung und der Fokusparameter einer CO_2-Hochleistungslaseranlage
LFT, 140 Seiten, 70 Bilder, 5 Tab. 1997.
ISBN 3-87525-083-4.

Band 63: Peter Steinwasser
Modulares Informationsmanagement in der integrierten Produkt- und Prozeßplanung
FAPS, 190 Seiten, 87 Bilder. 1997.
ISBN 3-87525-084-2.

Band 64: Georg Liedl
Integriertes Automatisierungskonzept für den flexiblen Materialfluß in der Elektronikproduktion
FAPS, 196 Seiten, 96 Bilder, 3 Tab. 1997.
ISBN 3-87525-086-9.

Band 65: Andreas Otto
Transiente Prozesse beim Laserstrahlschweißen
LFT, 132 Seiten, 62 Bilder, 1 Tab. 1997.
ISBN 3-87525-089-3.

Band 66: Wolfgang Blöchl
Erweiterte Informationsbereitstellung an offenen CNC-Steuerungen zur Prozeß- und Programmoptimierung
FAPS, 168 Seiten, 96 Bilder. 1997.
ISBN 3-87525-091-5.

Band 67: Klaus-Uwe Wolf
Verbesserte Prozeßführung und Prozeßplanung zur Leistungs- und Qualitätssteigerung beim Spulenwickeln
FAPS, 186 Seiten, 125 Bilder. 1997.
ISBN 3-87525-092-3.

Band 68: Frank Backes
Technologieorientierte Bahnplanung für die 3D-Laserstrahlbearbeitung
LFT, 138 Seiten, 71 Bilder, 2 Tab. 1997.
ISBN 3-87525-093-1.

Band 69: Jürgen Kraus
Laserstrahlumformen von Profilen
LFT, 137 Seiten, 72 Bilder, 8 Tab. 1997.
ISBN 3-87525-094-X.

Band 70: Norbert Neubauer
Adaptive Strahlführungen für CO_2-Laseranlagen
LFT, 120 Seiten, 50 Bilder, 3 Tab. 1997.
ISBN 3-87525-095-8.

Band 71: Michael Steber
Prozeßoptimierter Betrieb flexibler Schraubstationen in der automatisierten Montage
FAPS, 168 Seiten, 78 Bilder, 3 Tab. 1997.
ISBN 3-87525-096-6.

Band 72: Markus Pfestorf
Funktionale 3D-Oberflächenkenngrößen in der Umformtechnik
LFT, 162 Seiten, 84 Bilder, 15 Tab. 1997.
ISBN 3-87525-097-4.

Band 73: Volker Franke
Integrierte Planung und Konstruktion von Werkzeugen für die Biegebearbeitung
LFT, 143 Seiten, 81 Bilder. 1998.
ISBN 3-87525-098-2.

Band 74: Herbert Scheller
Automatisierte Demontagesysteme und recyclinggerechte Produktgestaltung elektronischer Baugruppen
FAPS, 184 Seiten, 104 Bilder, 17 Tab. 1998.
ISBN 3-87525-099-0.

Band 75: Arthur Meßner
Kaltmassivumformung metallischer Kleinstteile - Werkstoffverhalten, Wirkflächenreibung, Prozeßauslegung
LFT, 164 Seiten, 92 Bilder, 14 Tab. 1998.
ISBN 3-87525-100-8.

Band 76: Mathias Glasmacher
Prozeß- und Systemtechnik zum Laserstrahl-Mikroschweißen
LFT, 184 Seiten, 104 Bilder, 12 Tab. 1998.
ISBN 3-87525-101-6.

Band 77: Michael Schwind
Zerstörungsfreie Ermittlung mechanischer Eigenschaften von Feinblechen mit dem Wirbelstromverfahren
LFT, 124 Seiten, 68 Bilder, 8 Tab. 1998.
ISBN 3-87525-102-4.

Band 78: Manfred Gerhard
Qualitätssteigerung in der Elektronikproduktion durch Optimierung der Prozeßführung beim Löten komplexer Baugruppen
FAPS, 179 Seiten, 113 Bilder, 7 Tab. 1998.
ISBN 3-87525-103-2.

Band 79: Elke Rauh
Methodische Einbindung der Simulation in die betrieblichen Planungs- und Entscheidungsabläufe
FAPS, 192 Seiten, 114 Bilder, 4 Tab. 1998.
ISBN 3-87525-104-0.

Band 80: Sorin Niederkorn
Meßeinrichtung zur Untersuchung der Wirkflächenreibung bei umformtechnischen Prozessen
LFT, 99 Seiten, 46 Bilder, 6 Tab. 1998.
ISBN 3-87525-105-9.

Band 81: Stefan Schuberth
Regelung der Fokuslage beim Schweißen mit CO2-Hochleistungslasern unter Einsatz von adaptiven Optiken
LFT, 140 Seiten, 64 Bilder, 3 Tab. 1998.
ISBN 3-87525-106-7.

Band 82: Armando Walter Colombo
Development and Implementation of Hierarchical Control Structures of Flexible Production Systems Using High Level Petri Nets
FAPS, 216 Seiten, 86 Bilder. 1998.
ISBN 3-87525-109-1.

Band 83: Otto Meedt
Effizienzsteigerung bei Demontage und Recycling durch flexible Demontagetechnologien und optimierte Produktgestaltung
FAPS, 186 Seiten, 103 Bilder. 1998.
ISBN 3-87525-108-3.

Band 84: Knuth Götz
Modelle und effiziente Modellbildung zur Qualitätssicherung in der Elektronikproduktion
FAPS, 212 Seiten, 129 Bilder, 24 Tab. 1998.
ISBN 3-87525-112-1.

Band 85: Ralf Luchs
Einsatzmöglichkeiten leitender Klebstoffe zur zuverlässigen Kontaktierung elektronischer Bauelemente in der SMT
FAPS, 176 Seiten, 126 Bilder, 30 Tab. 1998.
ISBN 3-87525-113-7.

Band 86: Frank Pöhlau
Entscheidungsgrundlagen zur Einführung räumlicher spritzgegossener Schaltungsträger (3-D MID)
FAPS, 144 Seiten, 99 Bilder. 1999.
ISBN 3-87525-114-8.

Band 87: Roland T. A. Kals
Fundamentals on the miniaturization of sheet metal working processes
LFT, 128 Seiten, 58 Bilder, 11 Tab. 1999.
ISBN 3-87525-115-6.

Band 88: Gerhard Luhn
Implizites Wissen und technisches Handeln am Beispiel der Elektronikproduktion
FAPS, 252 Seiten, 61 Bilder, 1 Tab. 1999.
ISBN 3-87525-116-4.

Band 89: Axel Sprenger
Adaptives Streckbiegen von Aluminium-Strangpreßprofilen
LFT, 114 Seiten, 63 Bilder, 4 Tab. 1999.
ISBN 3-87525-117-2.

Band 90: Hans-Jörg Pucher
Untersuchungen zur Prozeßfolge Umformen, Bestücken und Laserstrahllöten von Mikrokontakten
LFT, 158 Seiten, 69 Bilder, 9 Tab. 1999.
ISBN 3-87525-119-9.

Band 91: Horst Arnet
Profilbiegen mit kinematischer Gestalterzeugung
LFT, 128 Seiten, 67 Bilder, 7 Tab. 1999.
ISBN 3-87525-120-2.

Band 92: Doris Schubart
Prozeßmodellierung und Technologieentwicklung beim Abtragen mit CO_2-Laserstrahlung
LFT, 133 Seiten, 57 Bilder, 13 Tab. 1999.
ISBN 3-87525-122-9.

Band 93: Adrianus L. P. Coremans
Laserstrahlsintern von Metallpulver - Prozeßmodellierung, Systemtechnik, Eigenschaften laserstrahlgesinterter Metallkörper
LFT, 184 Seiten, 108 Bilder, 12 Tab. 1999.
ISBN 3-87525-124-5.

Band 94: Hans-Martin Biehler
Optimierungskonzepte für Qualitätsdatenverarbeitung und Informationsbereitstellung in der Elektronikfertigung
FAPS, 194 Seiten, 105 Bilder. 1999.
ISBN 3-87525-126-1.

Band 95: Wolfgang Becker
Oberflächenausbildung und tribologische Eigenschaften excimerlaserstrahlbearbeiteter Hochleistungskeramiken
LFT, 175 Seiten, 71 Bilder, 3 Tab. 1999.
ISBN 3-87525-127-X.

Band 96: Philipp Hein
Innenhochdruck-Umformen von Blechpaaren: Modellierung, Prozeßauslegung und Prozeßführung
LFT, 129 Seiten, 57 Bilder, 7 Tab. 1999.
ISBN 3-87525-128-8.

Band 97: Gunter Beitinger
Herstellungs- und Prüfverfahren für thermoplastische Schaltungsträger
FAPS, 169 Seiten, 92 Bilder, 20 Tab. 1999.
ISBN 3-87525-129-6.

Band 98: Jürgen Knoblach
Beitrag zur rechnerunterstützten verursachungsgerechten Angebotskalkulation von Blechteilen mit Hilfe wissensbasierter Methoden
LFT, 155 Seiten, 53 Bilder, 26 Tab. 1999.
ISBN 3-87525-130-X.

Band 99: Frank Breitenbach
Bildverarbeitungssystem zur Erfassung der Anschlußgeometrie elektronischer SMT-Bauelemente
LFT, 147 Seiten, 92 Bilder, 12 Tab. 2000.
ISBN 3-87525-131-8.

Band 100: Bernd Falk
Simulationsbasierte Lebensdauervorhersage für Werkzeuge der Kaltmassivumformung
LFT, 134 Seiten, 44 Bilder, 15 Tab. 2000.
ISBN 3-87525-136-9.

Band 101: Wolfgang Schlögl
Integriertes Simulationsdaten-Management für Maschinenentwicklung und Anlagenplanung
FAPS, 169 Seiten, 101 Bilder, 20 Tab. 2000.
ISBN 3-87525-137-7.

Band 102: Christian Hinsel
Ermüdungsbruchversagen hartstoffbeschichteter Werkzeugstähle in der Kaltmassivumformung
LFT, 130 Seiten, 80 Bilder, 14 Tab. 2000.
ISBN 3-87525-138-5.

Band 103: Stefan Bobbert
Simulationsgestützte Prozessauslegung für das Innenhochdruck-Umformen von Blechpaaren
LFT, 123 Seiten, 77 Bilder. 2000.
ISBN 3-87525-145-8.

Band 104: Harald Rottbauer
Modulares Planungswerkzeug zum Produktionsmanagement in der Elektronikproduktion
FAPS, 166 Seiten, 106 Bilder. 2001.
ISBN 3-87525-139-3.

Band 105: Thomas Hennige
Flexible Formgebung von Blechen durch Laserstrahlumformen
LFT, 119 Seiten, 50 Bilder. 2001.
ISBN 3-87525-140-7.

Band 106: Thomas Menzel
Wissensbasierte Methoden für die rechnergestützte Charakterisierung und Bewertung innovativer Fertigungsprozesse
LFT, 152 Seiten, 71 Bilder. 2001.
ISBN 3-87525-142-3.

Band 107: Thomas Stöckel
Kommunikationstechnische Integration der Prozeßebene in Produktionssysteme durch Middleware-Frameworks
FAPS, 147 Seiten, 65 Bilder, 5 Tab. 2001.
ISBN 3-87525-143-1.

Band 108: Frank Pitter
Verfügbarkeitssteigerung von Werkzeugmaschinen durch Einsatz mechatronischer Sensorlösungen
FAPS, 158 Seiten, 131 Bilder, 8 Tab. 2001.
ISBN 3-87525-144-X.

Band 109: Markus Korneli
Integration lokaler CAP-Systeme in einen globalen Fertigungsdatenverbund
FAPS, 121 Seiten, 53 Bilder, 11 Tab. 2001.
ISBN 3-87525-146-6.

Band 110: Burkhard Müller
Laserstrahljustieren mit Excimer-Lasern - Prozeßparameter und Modelle zur Aktorkonstruktion
LFT, 128 Seiten, 36 Bilder, 9 Tab. 2001.
ISBN 3-87525-159-8.

Band 111: Jürgen Göhringer
Integrierte Telediagnose via Internet zum effizienten Service von Produktionssystemen
FAPS, 178 Seiten, 98 Bilder, 5 Tab. 2001.
ISBN 3-87525-147-4.

Band 112: Robert Feuerstein
Qualitäts- und kosteneffiziente Integration neuer Bauelementetechnologien in die Flachbaugruppenfertigung
FAPS, 161 Seiten, 99 Bilder, 10 Tab. 2001.
ISBN 3-87525-151-2.

Band 113: Marcus Reichenberger
Eigenschaften und Einsatzmöglichkeiten alternativer Elektroniklote in der Oberflächenmontage (SMT)
FAPS, 165 Seiten, 97 Bilder, 18 Tab. 2001.
ISBN 3-87525-152-0.

Band 114: Alexander Huber
Justieren vormontierter Systeme mit dem Nd:YAG-Laser unter Einsatz von Aktoren
LFT, 122 Seiten, 58 Bilder, 5 Tab. 2001.
ISBN 3-87525-153-9.

Band 115: Sami Krimi
Analyse und Optimierung von Montagesystemen in der Elektronikproduktion
FAPS, 155 Seiten, 88 Bilder, 3 Tab. 2001.
ISBN 3-87525-157-1.

Band 116: Marion Merklein
Laserstrahlumformen von Aluminiumwerkstoffen - Beeinflussung der Mikrostruktur und der mechanischen Eigenschaften
LFT, 122 Seiten, 65 Bilder, 15 Tab. 2001.
ISBN 3-87525-156-3.

Band 117: Thomas Collisi
Ein informationslogistisches Architekturkonzept zur Akquisition simulationsrelevanter Daten
FAPS, 181 Seiten, 105 Bilder, 7 Tab. 2002.
ISBN 3-87525-164-4.

Band 118: Markus Koch
Rationalisierung und ergonomische Optimierung im Innenausbau durch den Einsatz moderner Automatisierungstechnik
FAPS, 176 Seiten, 98 Bilder, 9 Tab. 2002.
ISBN 3-87525-165-2.

Band 119: Michael Schmidt
Prozeßregelung für das Laserstrahl-Punktschweißen in der Elektronikproduktion
LFT, 152 Seiten, 71 Bilder, 3 Tab. 2002.
ISBN 3-87525-166-0.

Band 120: Nicolas Tiesler
Grundlegende Untersuchungen zum Fließpressen metallischer Kleinstteile
LFT, 126 Seiten, 78 Bilder, 12 Tab. 2002.
ISBN 3-87525-175-X.

Band 121: Lars Pursche
Methoden zur technologieorientierten Programmierung für die 3D-Lasermikrobearbeitung
LFT, 111 Seiten, 39 Bilder, 0 Tab. 2002.
ISBN 3-87525-183-0.

Band 122: Jan-Oliver Brassel
Prozeßkontrolle beim Laserstrahl-Mikroschweißen
LFT, 148 Seiten, 72 Bilder, 12 Tab. 2002.
ISBN 3-87525-181-4.

Band 123: Mark Geisel
Prozeßkontrolle und -steuerung beim Laserstrahlschweißen mit den Methoden der nichtlinearen Dynamik
LFT, 135 Seiten, 46 Bilder, 2 Tab. 2002.
ISBN 3-87525-180-6.

Band 124: Gerd Eßer
Laserstrahlunterstützte Erzeugung metallischer Leiterstrukturen auf Thermoplastsubstraten für die MID-Technik
LFT, 148 Seiten, 60 Bilder, 6 Tab. 2002.
ISBN 3-87525-171-7.

Band 125: Marc Fleckenstein
Qualität laserstrahl-gefügter Mikroverbindungen elektronischer Kontakte
LFT, 159 Seiten, 77 Bilder, 7 Tab. 2002.
ISBN 3-87525-170-9.

Band 126: Stefan Kaufmann
Grundlegende Untersuchungen zum Nd:YAG- Laserstrahlfügen von Silizium für Komponenten der Optoelektronik
LFT, 159 Seiten, 100 Bilder, 6 Tab. 2002.
ISBN 3-87525-172-5.

Band 127: Thomas Fröhlich
Simultanes Löten von Anschlußkontakten elektronischer Bauelemente mit Diodenlaserstrahlung
LFT, 143 Seiten, 75 Bilder, 6 Tab. 2002.
ISBN 3-87525-186-5.

Band 128: Achim Hofmann
Erweiterung der Formgebungsgrenzen beim Umformen von Aluminiumwerkstoffen durch den Einsatz prozessangepasster Platinen
LFT, 113 Seiten, 58 Bilder, 4 Tab. 2002.
ISBN 3-87525-182-2.

Band 129: Ingo Kriebitzsch
3 - D MID Technologie in der Automobilelektronik
FAPS, 129 Seiten, 102 Bilder, 10 Tab. 2002.
ISBN 3-87525-169-5.

Band 130: Thomas Pohl
Fertigungsqualität und Umformbarkeit laserstrahlgeschweißter Formplatinen aus Aluminiumlegierungen
LFT, 133 Seiten, 93 Bilder, 12 Tab. 2002.
ISBN 3-87525-173-3.

Band 131: Matthias Wenk
Entwicklung eines konfigurierbaren Steuerungssystems für die flexible Sensorführung von Industrierobotern
FAPS, 167 Seiten, 85 Bilder, 1 Tab. 2002.
ISBN 3-87525-174-1.

Band 132: Matthias Negendanck
Neue Sensorik und Aktorik für Bearbeitungsköpfe zum Laserstrahlschweißen
LFT, 116 Seiten, 60 Bilder, 14 Tab. 2002.
ISBN 3-87525-184-9.

Band 133: Oliver Kreis
Integrierte Fertigung - Verfahrensintegration durch Innenhochdruck-Umformen, Trennen und Laserstrahlschweißen in einem Werkzeug sowie ihre tele- und multimediale Präsentation
LFT, 167 Seiten, 90 Bilder, 43 Tab. 2002.
ISBN 3-87525-176-8.

Band 134: Stefan Trautner
Technische Umsetzung produktbezogener Instrumente der Umweltpolitik bei Elektro- und Elektronikgeräten
FAPS, 179 Seiten, 92 Bilder, 11 Tab. 2002.
ISBN 3-87525-177-6.

Band 135: Roland Meier
Strategien für einen produktorientierten Einsatz räumlicher spritzgegossener Schaltungsträger (3-D MID)
FAPS, 155 Seiten, 88 Bilder, 14 Tab. 2002.
ISBN 3-87525-178-4.

Band 136: Jürgen Wunderlich
Kostensimulation - Simulationsbasierte Wirtschaftlichkeitsregelung komplexer Produktionssysteme
FAPS, 202 Seiten, 119 Bilder, 17 Tab. 2002.
ISBN 3-87525-179-2.

Band 137: Stefan Novotny
Innenhochdruck-Umformen von Blechen aus Aluminium- und Magnesiumlegierungen bei erhöhter Temperatur
LFT, 132 Seiten, 82 Bilder, 6 Tab. 2002.
ISBN 3-87525-185-7.

Band 138: Andreas Licha
Flexible Montageautomatisierung zur Komplettmontage flächenhafter Produktstrukturen durch kooperierende Industrieroboter
FAPS, 158 Seiten, 87 Bilder, 8 Tab. 2003.
ISBN 3-87525-189-X.

Band 139: Michael Eisenbarth
Beitrag zur Optimierung der Aufbau- und Verbindungstechnik für mechatronische Baugruppen
FAPS, 207 Seiten, 141 Bilder, 9 Tab. 2003.
ISBN 3-87525-190-3.

Band 140: Frank Christoph
Durchgängige simulationsgestützte Planung von Fertigungseinrichtungen der Elektronikproduktion
FAPS, 187 Seiten, 107 Bilder, 9 Tab. 2003.
ISBN 3-87525-191-1.

Band 141: Hinnerk Hagenah
Simulationsbasierte Bestimmung der zu erwartenden Maßhaltigkeit für das Blechbiegen
LFT, 131 Seiten, 36 Bilder, 26 Tab. 2003.
ISBN 3-87525-192-X.

Band 142: Ralf Eckstein
Scherschneiden und Biegen metallischer Kleinstteile - Materialeinfluss und Materialverhalten
LFT, 148 Seiten, 71 Bilder, 19 Tab. 2003.
ISBN 3-87525-193-8.

Band 143: Frank H. Meyer-Pittroff
Excimerlaserstrahlbiegen dünner metallischer Folien mit homogener Lichtlinie
LFT, 138 Seiten, 60 Bilder, 16 Tab. 2003.
ISBN 3-87525-196-2.

Band 144: Andreas Kach
Rechnergestützte Anpassung von Laserstrahlschneidbahnen an Bauteilabweichungen
LFT, 139 Seiten, 69 Bilder, 11 Tab. 2004.
ISBN 3-87525-197-0.

Band 145: Stefan Hierl
System- und Prozeßtechnik für das simultane Löten mit Diodenlaserstrahlung von elektronischen Bauelementen
LFT, 124 Seiten, 66 Bilder, 4 Tab. 2004.
ISBN 3-87525-198-9.

Band 146: Thomas Neudecker
Tribologische Eigenschaften keramischer Blechumformwerkzeuge- Einfluss einer Oberflächenendbearbeitung mittels Excimerlaserstrahlung
LFT, 166 Seiten, 75 Bilder, 26 Tab. 2004.
ISBN 3-87525-200-4.

Band 147: Ulrich Wenger
Prozessoptimierung in der Wickeltechnik durch innovative maschinenbauliche und regelungstechnische Ansätze
FAPS, 132 Seiten, 88 Bilder, 0 Tab. 2004.
ISBN 3-87525-203-9.

Band 148: Stefan Slama
Effizienzsteigerung in der Montage durch marktorientierte Montagestrukturen und erweiterte Mitarbeiterkompetenz
FAPS, 188 Seiten, 125 Bilder, 0 Tab. 2004.
ISBN 3-87525-204-7.

Band 149: Thomas Wurm
Laserstrahljustieren mittels Aktoren-Entwicklung von Konzepten und Methoden für die rechnerunterstützte Modellierung und Optimierung von komplexen Aktorsystemen in der Mikrotechnik
LFT, 122 Seiten, 51 Bilder, 9 Tab. 2004.
ISBN 3-87525-206-3.

Band 150: Martino Celeghini
Wirkmedienbasierte Blechumformung: Grundlagenuntersuchungen zum Einfluss von Werkstoff und Bauteilgeometrie
LFT, 146 Seiten, 77 Bilder, 6 Tab. 2004.
ISBN 3-87525-207-1.

Band 151: Ralph Hohenstein
Entwurf hochdynamischer Sensor- und Regelsysteme für die adaptive Laserbearbeitung
LFT, 282 Seiten, 63 Bilder, 16 Tab. 2004.
ISBN 3-87525-210-1.

Band 152: Angelika Hutterer
Entwicklung prozessüberwachender Regelkreise für flexible Formgebungsprozesse
LFT, 149 Seiten, 57 Bilder, 2 Tab. 2005.
ISBN 3-87525-212-8.

Band 153: Emil Egerer
Massivumformen metallischer Kleinstteile bei erhöhter Prozesstemperatur
LFT, 158 Seiten, 87 Bilder, 10 Tab. 2005.
ISBN 3-87525-213-6.

Band 154: Rüdiger Holzmann
Strategien zur nachhaltigen Optimierung von Qualität und Zuverlässigkeit in der Fertigung hochintegrierter Flachbaugruppen
FAPS, 186 Seiten, 99 Bilder, 19 Tab. 2005.
ISBN 3-87525-217-9.

Band 155: Marco Nock
Biegeumformen mit Elastomerwerkzeugen Modellierung, Prozessauslegung und Abgrenzung des Verfahrens am Beispiel des Rohrbiegens
LFT, 164 Seiten, 85 Bilder, 13 Tab. 2005.
ISBN 3-87525-218-7.

Band 156: Frank Niebling
Qualifizierung einer Prozesskette zum Laserstrahlsintern metallischer Bauteile
LFT, 148 Seiten, 89 Bilder, 3 Tab. 2005.
ISBN 3-87525-219-5.

Band 157: Markus Meiler
Großserientauglichkeit trockenschmierstoffbeschichteter Aluminiumbleche im Presswerk Grundlegende Untersuchungen zur Tribologie, zum Umformverhalten und Bauteilversuche
LFT, 104 Seiten, 57 Bilder, 21 Tab. 2005.
ISBN 3-87525-221-7.

Band 158: Agus Sutanto
Solution Approaches for Planning of Assembly Systems in Three-Dimensional Virtual Environments
FAPS, 169 Seiten, 98 Bilder, 3 Tab. 2005.
ISBN 3-87525-220-9.

Band 159: Matthias Boiger
Hochleistungssysteme für die Fertigung elektronischer Baugruppen auf der Basis flexibler Schaltungsträger
FAPS, 175 Seiten, 111 Bilder, 8 Tab. 2005.
ISBN 3-87525-222-5.

Band 160: Matthias Pitz
Laserunterstütztes Biegen höchstfester Mehrphasenstähle
LFT, 120 Seiten, 73 Bilder, 11 Tab. 2005.
ISBN 3-87525-223-3.

Band 161: Meik Vahl
Beitrag zur gezielten Beeinflussung des Werkstoffflusses beim Innenhochdruck-Umformen von Blechen
LFT, 165 Seiten, 94 Bilder, 15 Tab. 2005.
ISBN 3-87525-224-1.

Band 162: Peter K. Kraus
Plattformstrategien - Realisierung einer varianz- und kostenoptimierten Wertschöpfung
FAPS, 181 Seiten, 95 Bilder, 0 Tab. 2005.
ISBN 3-87525-226-8.

Band 163: Adrienn Cser
Laserstrahlschmelzabtrag - Prozessanalyse und -modellierung
LFT, 146 Seiten, 79 Bilder, 3 Tab. 2005.
ISBN 3-87525-227-6.

Band 164: Markus C. Hahn
Grundlegende Untersuchungen zur Herstellung von Leichtbauverbundstrukturen mit Aluminiumschaumkern
LFT, 143 Seiten, 60 Bilder, 16 Tab. 2005.
ISBN 3-87525-228-4.

Band 165: Gordana Michos
Mechatronische Ansätze zur Optimierung von Vorschubachsen
FAPS, 146 Seiten, 87 Bilder, 17 Tab. 2005.
ISBN 3-87525-230-6.

Band 166: Markus Stark
Auslegung und Fertigung hochpräziser Faser-Kollimator-Arrays
LFT, 158 Seiten, 115 Bilder, 11 Tab. 2005.
ISBN 3-87525-231-4.

Band 167: Yurong Zhou
Kollaboratives Engineering Management in der integrierten virtuellen Entwicklung der Anlagen für die Elektronikproduktion
FAPS, 156 Seiten, 84 Bilder, 6 Tab. 2005.
ISBN 3-87525-232-2.

Band 168: Werner Enser
Neue Formen permanenter und lösbarer elektrischer Kontaktierungen für mechatronische Baugruppen
FAPS, 190 Seiten, 112 Bilder, 5 Tab. 2005.
ISBN 3-87525-233-0.

Band 169: Katrin Melzer
Integrierte Produktpolitik bei elektrischen und elektronischen Geräten zur Optimierung des Product-Life-Cycle
FAPS, 155 Seiten, 91 Bilder, 17 Tab. 2005.
ISBN 3-87525-234-9.

Band 170: Alexander Putz
Grundlegende Untersuchungen zur Erfassung der realen Vorspannung von armierten Kaltfließpresswerkzeugen mittels Ultraschall
LFT, 137 Seiten, 71 Bilder, 15 Tab. 2006.
ISBN 3-87525-237-3.

Band 171: Martin Prechtl
Automatisiertes Schichtverfahren für metallische Folien - System- und Prozesstechnik
LFT, 154 Seiten, 45 Bilder, 7 Tab. 2006.
ISBN 3-87525-238-1.

Band 172: Markus Meidert
Beitrag zur deterministischen Lebensdauerabschätzung von Werkzeugen der Kaltmassivumformung
LFT, 131 Seiten, 78 Bilder, 9 Tab. 2006.
ISBN 3-87525-239-X.

Band 173: Bernd Müller
Robuste, automatisierte Montagesysteme durch adaptive Prozessführung und montageübergreifende Fehlerprävention am Beispiel flächiger Leichtbauteile
FAPS, 147 Seiten, 77 Bilder, 0 Tab. 2006.
ISBN 3-87525-240-3.

Band 174: Alexander Hofmann
Hybrides Laserdurchstrahlschweißen von Kunststoffen
LFT, 136 Seiten, 72 Bilder, 4 Tab. 2006.
ISBN 978-3-87525-243-9.

Band 175: Peter Wölflick
Innovative Substrate und Prozesse mit feinsten Strukturen für bleifreie Mechatronik-Anwendungen
FAPS, 177 Seiten, 148 Bilder, 24 Tab. 2006.
ISBN 978-3-87525-246-0.

Band 176: Attila Komlodi
Detection and Prevention of Hot Cracks during Laser Welding of Aluminium Alloys Using Advanced Simulation Methods
LFT, 155 Seiten, 89 Bilder, 14 Tab. 2006.
ISBN 978-3-87525-248-4.

Band 177: Uwe Popp
Grundlegende Untersuchungen zum Laserstrahlstrukturieren von Kaltmassivumformwerkzeugen
LFT, 140 Seiten, 67 Bilder, 16 Tab. 2006.
ISBN 978-3-87525-249-1.

Band 178: Veit Rückel
Rechnergestützte Ablaufplanung und Bahngenerierung Für kooperierende Industrieroboter
FAPS, 148 Seiten, 75 Bilder, 7 Tab. 2006.
ISBN 978-3-87525-250-7.

Band 179: Manfred Dirscherl
Nicht-thermische Mikrojustiertechnik mittels ultrakurzer Laserpulse
LFT, 154 Seiten, 69 Bilder, 10 Tab. 2007.
ISBN 978-3-87525-251-4.

Band 180: Yong Zhuo
Entwurf eines rechnergestützten integrierten Systems für Konstruktion und Fertigungsplanung räumlicher spritzgegossener Schaltungsträger (3D-MID)
FAPS, 181 Seiten, 95 Bilder, 5 Tab. 2007.
ISBN 978-3-87525-253-8.

Band 181: Stefan Lang
Durchgängige Mitarbeiterinformation zur Steigerung von Effizienz und Prozesssicherheit in der Produktion
FAPS, 172 Seiten, 93 Bilder. 2007.
ISBN 978-3-87525-257-6.

Band 182: Hans-Joachim Krauß
Laserstrahlinduzierte Pyrolyse präkeramischer Polymere
LFT, 171 Seiten, 100 Bilder. 2007.
ISBN 978-3-87525-258-3.

Band 183: Stefan Junker
Technologien und Systemlösungen für die flexibel automatisierte Bestückung permanent erregter Läufer mit oberflächenmontierten Dauermagneten
FAPS, 173 Seiten, 75 Bilder. 2007.
ISBN 978-3-87525-259-0.

Band 184: Rainer Kohlbauer
Wissensbasierte Methoden für die simulationsgestützte Auslegung wirkmedienbasierter Blechumformprozesse
LFT, 135 Seiten, 50 Bilder. 2007.
ISBN 978-3-87525-260-6.

Band 185: Klaus Lamprecht
Wirkmedienbasierte Umformung tiefgezogener Vorformen unter besonderer Berücksichtigung maßgeschneiderter Halbzeuge
LFT, 137 Seiten, 81 Bilder. 2007.
ISBN 978-3-87525-265-1.

Band 186: Bernd Zolleiß
Optimierte Prozesse und Systeme für die Bestückung mechatronischer Baugruppen
FAPS, 180 Seiten, 117 Bilder. 2007.
ISBN 978-3-87525-266-8.

Band 187: Michael Kerausch
Simulationsgestützte Prozessauslegung für das Umformen lokal wärmebehandelter Aluminiumplatinen
LFT, 146 Seiten, 76 Bilder, 7 Tab. 2007.
ISBN 978-3-87525-267-5.

Band 188: Matthias Weber
Unterstützung der Wandlungsfähigkeit von Produktionsanlagen durch innovative Softwaresysteme
FAPS, 183 Seiten, 122 Bilder, 3 Tab. 2007.
ISBN 978-3-87525-269-9.

Band 189: Thomas Frick
Untersuchung der prozessbestimmenden Strahl-Stoff-Wechselwirkungen beim Laserstrahlschweißen von Kunststoffen
LFT, 104 Seiten, 62 Bilder, 8 Tab. 2007.
ISBN 978-3-87525-268-2.

Band 190: Joachim Hecht
Werkstoffcharakterisierung und Prozessauslegung für die wirkmedienbasierte Doppelblech-Umformung von Magnesiumlegierungen
LFT, 107 Seiten, 91 Bilder, 2 Tab. 2007.
ISBN 978-3-87525-270-5.

Band 191: Ralf Völkl
Stochastische Simulation zur Werkzeuglebensdaueroptimierung und Präzisionsfertigung in der Kaltmassivumformung
LFT, 178 Seiten, 75 Bilder, 12 Tab. 2008.
ISBN 978-3-87525-272-9.

Band 192: Massimo Tolazzi
Innenhochdruck-Umformen verstärkter Blech-Rahmenstrukturen
LFT, 164 Seiten, 85 Bilder, 7 Tab. 2008.
ISBN 978-3-87525-273-6.

Band 193: Cornelia Hoff
Untersuchung der Prozesseinflussgrößen beim Presshärten des höchstfesten Vergütungsstahls 22MnB5
LFT, 133 Seiten, 92 Bilder, 5 Tab. 2008.
ISBN 978-3-87525-275-0.

Band 194: Christian Alvarez
Simulationsgestützte Methoden zur effizienten Gestaltung von Lötprozessen in der Elektronikproduktion
FAPS, 149 Seiten, 86 Bilder, 8 Tab. 2008.
ISBN 978-3-87525-277-4.

Band 195: Andreas Kunze
Automatisierte Montage von makromechatronischen Modulen zur flexiblen Integration in hybride Pkw-Bordnetzsysteme
FAPS, 160 Seiten, 90 Bilder, 14 Tab. 2008.
ISBN 978-3-87525-278-1.

Band 196: Wolfgang Hußnätter
Grundlegende Untersuchungen zur experimentellen Ermittlung und zur Modellierung von Fließortkurven bei erhöhten Temperaturen
LFT, 152 Seiten, 73 Bilder, 21 Tab. 2008.
ISBN 978-3-87525-279-8.

Band 197: Thomas Bigl
Entwicklung, angepasste Herstellungsverfahren und erweiterte Qualitätssicherung von einsatzgerechten elektronischen Baugruppen
FAPS, 175 Seiten, 107 Bilder, 14 Tab. 2008.
ISBN 978-3-87525-280-4.

Band 198: Stephan Roth
Grundlegende Untersuchungen zum Excimerlaserstrahl-Abtragen unter Flüssigkeitsfilmen
LFT, 113 Seiten, 47 Bilder, 14 Tab. 2008.
ISBN 978-3-87525-281-1.

Band 199: Artur Giera
Prozesstechnische Untersuchungen zum Rührreibschweißen metallischer Werkstoffe
LFT, 179 Seiten, 104 Bilder, 36 Tab. 2008.
ISBN 978-3-87525-282-8.

Band 200: Jürgen Lechler
Beschreibung und Modellierung des Werkstoffverhaltens von presshärtbaren Bor-Manganstählen
LFT, 154 Seiten, 75 Bilder, 12 Tab. 2009.
ISBN 978-3-87525-286-6.

Band 201: Andreas Blankl
Untersuchungen zur Erhöhung der Prozessrobustheit bei der Innenhochdruck-Umformung von flächigen Halbzeugen mit vor- bzw. nachgeschalteten Laserstrahlfügeoperationen
LFT, 120 Seiten, 68 Bilder, 9 Tab. 2009.
ISBN 978-3-87525-287-3.

Band 202: Andreas Schaller
Modellierung eines nachfrageorientierten Produktionskonzeptes für mobile Telekommunikationsgeräte
FAPS, 120 Seiten, 79 Bilder, 0 Tab. 2009.
ISBN 978-3-87525-289-7.

Band 203: Claudius Schimpf
Optimierung von Zuverlässigkeitsuntersuchungen, Prüfabläufen und Nacharbeitsprozessen in der Elektronikproduktion
FAPS, 162 Seiten, 90 Bilder, 14 Tab. 2009.
ISBN 978-3-87525-290-3.

Band 204: Simon Dietrich
Sensoriken zur Schwerpunktslagebestimmung der optischen Prozessemissionen beim Laserstrahltiefschweißen
LFT, 138 Seiten, 70 Bilder, 5 Tab. 2009.
ISBN 978-3-87525-292-7.

Band 205: Wolfgang Wolf
Entwicklung eines agentenbasierten Steuerungssystems zur Materialflussorganisation im wandelbaren Produktionsumfeld
FAPS, 167 Seiten, 98 Bilder. 2009.
ISBN 978-3-87525-293-4.

Band 206: Steffen Polster
Laserdurchstrahlschweißen transparenter Polymerbauteile
LFT, 160 Seiten, 92 Bilder, 13 Tab. 2009.
ISBN 978-3-87525-294-1.

Band 207: Stephan Manuel Dörfler
Rührreibschweißen von walzplattiertem Halbzeug und Aluminiumblech zur Herstellung flächiger Aluminiumschaum-Sandwich-Verbundstrukturen
LFT, 190 Seiten, 98 Bilder, 5 Tab. 2009.
ISBN 978-3-87525-295-8.

Band 208: Uwe Vogt
Seriennahe Auslegung von Aluminium Tailored Heat Treated Blanks
LFT, 151 Seiten, 68 Bilder, 26 Tab. 2009.
ISBN 978-3-87525-296-5.

Band 209: Till Laumann
Qualitative und quantitative Bewertung der Crashtauglichkeit von höchstfesten Stählen
LFT, 117 Seiten, 69 Bilder, 7 Tab. 2009.
ISBN 978-3-87525-299-6.

Band 210: Alexander Diehl
Größeneffekte bei Biegeprozessen- Entwicklung einer Methodik zur Identifikation und Quantifizierung
LFT, 180 Seiten, 92 Bilder, 12 Tab. 2010.
ISBN 978-3-87525-302-3.

Band 211: Detlev Staud
Effiziente Prozesskettenauslegung für das Umformen lokal wärmebehandelter und geschweißter Aluminiumbleche
LFT, 164 Seiten, 72 Bilder, 12 Tab. 2010.
ISBN 978-3-87525-303-0.

Band 212: Jens Ackermann
Prozesssicherung beim Laserdurchstrahlschweißen thermoplastischer Kunststoffe
LPT, 129 Seiten, 74 Bilder, 13 Tab. 2010.
ISBN 978-3-87525-305-4.

Band 213: Stephan Weidel
Grundlegende Untersuchungen zum Kontaktzustand zwischen Werkstück und Werkzeug bei umformtechnischen Prozessen unter tribologischen Gesichtspunkten
LFT, 144 Seiten, 67 Bilder, 11 Tab. 2010.
ISBN 978-3-87525-307-8.

Band 214: Stefan Geißdörfer
Entwicklung eines mesoskopischen Modells zur Abbildung von Größeneffekten in der Kaltmassivumformung mit Methoden der FE-Simulation
LFT, 133 Seiten, 83 Bilder, 11 Tab. 2010.
ISBN 978-3-87525-308-5.

Band 215: Christian Matzner
Konzeption produktspezifischer Lösungen zur Robustheitssteigerung elektronischer Systeme gegen die Einwirkung von Betauung im Automobil
FAPS, 165 Seiten, 93 Bilder, 14 Tab. 2010.
ISBN 978-3-87525-309-2.

Band 216: Florian Schüßler
Verbindungs- und Systemtechnik für thermisch hochbeanspruchte und miniaturisierte elektronische Baugruppen
FAPS, 184 Seiten, 93 Bilder, 18 Tab. 2010.
ISBN 978-3-87525-310-8.

Band 217: Massimo Cojutti
Strategien zur Erweiterung der Prozessgrenzen bei der Innhochdruck-Umformung von Rohren und Blechpaaren
LFT, 125 Seiten, 56 Bilder, 9 Tab. 2010.
ISBN 978-3-87525-312-2.

Band 218: Raoul Plettke
Mehrkriterielle Optimierung komplexer Aktorsysteme für das Laserstrahljustieren
LFT, 152 Seiten, 25 Bilder, 3 Tab. 2010.
ISBN 978-3-87525-315-3.

Band 219: Andreas Dobroschke
Flexible Automatisierungslösungen für die Fertigung wickeltechnischer Produkte
FAPS, 184 Seiten, 109 Bilder, 18 Tab. 2011.
ISBN 978-3-87525-317-7.

Band 220: Azhar Zam
Optical Tissue Differentiation for Sensor-Controlled Tissue-Specific Laser Surgery
LPT, 99 Seiten, 45 Bilder, 8 Tab. 2011.
ISBN 978-3-87525-318-4.

Band 221: Michael Rösch
Potenziale und Strategien zur Optimierung des Schablonendruckprozesses in der Elektronikproduktion
FAPS, 192 Seiten, 127 Bilder, 19 Tab. 2011.
ISBN 978-3-87525-319-1.

Band 222: Thomas Rechtenwald
Quasi-isothermes Laserstrahlsintern von Hochtemperatur-Thermoplasten - Eine Betrachtung werkstoff-prozessspezifischer Aspekte am Beispiel PEEK
LPT, 150 Seiten, 62 Bilder, 8 Tab. 2011.
ISBN 978-3-87525-320-7.

Band 223: Daniel Craiovan
Prozesse und Systemlösungen für die SMT-Montage optischer Bauelemente auf Substrate mit integrierten Lichtwellenleitern
FAPS, 165 Seiten, 85 Bilder, 8 Tab. 2011.
ISBN 978-3-87525-324-5.

Band 224: Kay Wagner
Beanspruchungsangepasste Kaltmassivumformwerkzeuge durch lokal optimierte Werkzeugoberflächen
LFT, 147 Seiten, 103 Bilder, 17 Tab. 2011.
ISBN 978-3-87525-325-2.

Band 225: Martin Brandhuber
Verbesserung der Prognosegüte des Versagens von Punktschweißverbindungen bei höchstfesten Stahlgüten
LFT, 155 Seiten, 91 Bilder, 19 Tab. 2011.
ISBN 978-3-87525-327-6.

Band 226: Peter Sebastian Feuser
Ein Ansatz zur Herstellung von pressgehärteten Karosseriekomponenten mit maßgeschneiderten mechanischen Eigenschaften: Temperierte Umformwerkzeuge. Prozessfenster, Prozesssimulation und funktionale Untersuchung
LFT, 195 Seiten, 97 Bilder, 60 Tab. 2012.
ISBN 978-3-87525-328-3.

Band 227: Murat Arbak
Material Adapted Design of Cold Forging Tools Exemplified by Powder Metallurgical Tool Steels and Ceramics
LFT, 109 Seiten, 56 Bilder, 8 Tab. 2012.
ISBN 978-3-87525-330-6.

Band 228: Indra Pitz
Beschleunigte Simulation des Laserstrahlumformens von Aluminiumblechen
LPT, 137 Seiten, 45 Bilder, 27 Tab. 2012.
ISBN 978-3-87525-333-7.

Band 229: Alexander Grimm
Prozessanalyse und -überwachung des Laserstrahlhartlötens mittels optischer Sensorik
LPT, 125 Seiten, 61 Bilder, 5 Tab. 2012.
ISBN 978-3-87525-334-4.

Band 230: Markus Kaupper
Biegen von höhenfesten Stahlblechwerkstoffen - Umformverhalten und Grenzen der Biegbarkeit
LFT, 160 Seiten, 57 Bilder, 10 Tab. 2012.
ISBN 978-3-87525-339-9.

Band 231: Thomas Kroiß
Modellbasierte Prozessauslegung für die Kaltmassivumformung unter Brücksichtigung der Werkzeug- und Pressenauffederung
LFT, 169 Seiten, 50 Bilder, 19 Tab. 2012.
ISBN 978-3-87525-341-2.

Band 232: Christian Goth
Analyse und Optimierung der Entwicklung und Zuverlässigkeit räumlicher Schaltungsträger (3D-MID)
FAPS, 176 Seiten, 102 Bilder, 22 Tab. 2012.
ISBN 978-3-87525-340-5.

Band 233: Christian Ziegler
Ganzheitliche Automatisierung mechatronischer Systeme in der Medizin am Beispiel Strahlentherapie
FAPS, 170 Seiten, 71 Bilder, 19 Tab. 2012.
ISBN 978-3-87525-342-9.

Band 234: Florian Albert
Automatisiertes Laserstrahllöten und -reparaturlöten elektronischer Baugruppen
LPT, 127 Seiten, 78 Bilder, 11 Tab. 2012.
ISBN 978-3-87525-344-3.

Band 235: Thomas Stöhr
Analyse und Beschreibung des mechanischen Werkstoffverhaltens von presshärtbaren Bor-Manganstählen
LFT, 118 Seiten, 74 Bilder, 18 Tab. 2013.
ISBN 978-3-87525-346-7.

Band 236: Christian Kägeler
Prozessdynamik beim Laserstrahlschweißen verzinkter Stahlbleche im Überlappstoß
LPT, 145 Seiten, 80 Bilder, 3 Tab. 2013.
ISBN 978-3-87525-347-4.

Band 237: Andreas Sulzberger
Seriennahe Auslegung der Prozesskette zur wärmeunterstützten Umformung von Aluminiumblechwerkstoffen
LFT, 153 Seiten, 87 Bilder, 17 Tab. 2013.
ISBN 978-3-87525-349-8.

Band 238: Simon Opel
Herstellung prozessangepasster Halbzeuge mit variabler Blechdicke durch die Anwendung von Verfahren der Blechmassivumformung
LFT, 165 Seiten, 108 Bilder, 27 Tab. 2013.
ISBN 978-3-87525-350-4.

Band 239: Rajesh Kanawade
In-vivo Monitoring of Epithelium Vessel and Capillary Density for the Application of Detection of Clinical Shock and Early Signs of Cancer Development
LPT, 124 Seiten, 58 Bilder, 15 Tab. 2013.
ISBN 978-3-87525-351-1.

Band 240: Stephan Busse
Entwicklung und Qualifizierung eines Schneidclinchverfahrens
LFT, 119 Seiten, 86 Bilder, 20 Tab. 2013.
ISBN 978-3-87525-352-8.

Band 241: Karl-Heinz Leitz
Mikro- und Nanostrukturierung mit kurz und ultrakurz gepulster Laserstrahlung
LPT, 154 Seiten, 71 Bilder, 9 Tab. 2013.
ISBN 978-3-87525-355-9.

Band 242: Markus Michl
Webbasierte Ansätze zur ganzheitlichen technischen Diagnose
FAPS, 182 Seiten, 62 Bilder, 20 Tab. 2013.
ISBN 978-3-87525-356-6.

Band 243: Vera Sturm
Einfluss von Chargenschwankungen auf die Verarbeitungsgrenzen von Stahlwerkstoffen
LFT, 113 Seiten, 58 Bilder, 9 Tab. 2013.
ISBN 978-3-87525-357-3.

Band 244: Christian Neudel
Mikrostrukturelle und mechanisch-technologische Eigenschaften widerstandspunktgeschweißter Aluminium-Stahl-Verbindungen für den Fahrzeugbau
LFT, 178 Seiten, 171 Bilder, 31 Tab. 2014.
ISBN 978-3-87525-358-0.

Band 245: Anja Neumann
Konzept zur Beherrschung der Prozessschwankungen im Presswerk
LFT, 162 Seiten, 68 Bilder, 15 Tab. 2014.
ISBN 978-3-87525-360-3.

Band 246: Ulf-Hermann Quentin
Laserbasierte Nanostrukturierung mit optisch positionierten Mikrolinsen
LPT, 137 Seiten, 89 Bilder, 6 Tab. 2014.
ISBN 978-3-87525-361-0.

Band 247: Erik Lamprecht
Der Einfluss der Fertigungsverfahren auf die Wirbelstromverluste von Stator-Einzelzahnblechpaketen für den Einsatz in Hybrid- und Elektrofahrzeugen
FAPS, 148 Seiten, 138 Bilder, 4 Tab. 2014.
ISBN 978-3-87525-362-7.

Band 248: Sebastian Rösel
Wirkmedienbasierte Umformung von Blechhalbzeugen unter Anwendung magnetorheologischer Flüssigkeiten als kombiniertes Wirk- und Dichtmedium
LFT, 148 Seiten, 61 Bilder, 12 Tab. 2014.
ISBN 978-3-87525-363-4.

Band 249: Paul Hippchen
Simulative Prognose der Geometrie indirekt pressgehärteter Karosseriebauteile für die industrielle Anwendung
LFT, 163 Seiten, 89 Bilder, 12 Tab. 2014.
ISBN 978-3-87525-364-1.

Band 250: Martin Zubeil
Versagensprognose bei der Prozesssimulation von Biegeumform- und Falzverfahren
LFT, 171 Seiten, 90 Bilder, 5 Tab. 2014.
ISBN 978-3-87525-365-8.

Band 251: Alexander Kühl
Flexible Automatisierung der Statorenmontage mit Hilfe einer universellen ambidexteren Kinematik
FAPS, 142 Seiten, 60 Bilder, 26 Tab. 2014.
ISBN 978-3-87525-367-2.

Band 252: Thomas Albrecht
Optimierte Fertigungstechnologien für Rotoren getriebeintegrierter PM-Synchronmotoren von Hybridfahrzeugen
FAPS, 198 Seiten, 130 Bilder, 38 Tab. 2014.
ISBN 978-3-87525-368-9.

Band 253: Florian Risch
Planning and Production Concepts for Contactless Power Transfer Systems for Electric Vehicles
FAPS, 185 Seiten, 125 Bilder, 13 Tab. 2014.
ISBN 978-3-87525-369-6.

Band 254: Markus Weigl
Laserstrahlschweißen von Mischverbindungen aus austenitischen und ferritischen korrosionsbeständigen Stahlwerkstoffen
LPT, 184 Seiten, 110 Bilder, 6 Tab. 2014.
ISBN 978-3-87525-370-2.

Band 255: Johannes Noneder
Beanspruchungserfassung für die Validierung von FE-Modellen zur Auslegung von Massivumformwerkzeugen
LFT, 161 Seiten, 65 Bilder, 14 Tab. 2014.
ISBN 978-3-87525-371-9.

Band 256: Andreas Reinhardt
Ressourceneffiziente Prozess- und Produktionstechnologie für flexible Schaltungsträger
FAPS, 123 Seiten, 69 Bilder, 19 Tab. 2014.
ISBN 978-3-87525-373-3.

Band 257: Tobias Schmuck
Ein Beitrag zur effizienten Gestaltung globaler Produktions- und Logistiknetzwerke mittels Simulation
FAPS, 151 Seiten, 74 Bilder. 2014.
ISBN 978-3-87525-374-0.

Band 258: Bernd Eichenhüller
Untersuchungen der Effekte und Wechselwirkungen charakteristischer Einflussgrößen auf das Umformverhalten bei Mikroumformprozessen
LFT, 127 Seiten, 29 Bilder, 9 Tab. 2014.
ISBN 978-3-87525-375-7.

Band 259: Felix Lütteke
Vielseitiges autonomes Transportsystem basierend auf Weltmodellerstellung mittels Datenfusion von Deckenkameras und Fahrzeugsensoren
FAPS, 152 Seiten, 54 Bilder, 20 Tab. 2014.
ISBN 978-3-87525-376-4.

Band 260: Martin Grüner
Hochdruck-Blechumformung mit formlos festen Stoffen als Wirkmedium
LFT, 144 Seiten, 66 Bilder, 29 Tab. 2014.
ISBN 978-3-87525-379-5.

Band 261: Christian Brock
Analyse und Regelung des Laserstrahltiefschweißprozesses durch Detektion der Metalldampffackelposition
LPT, 126 Seiten, 65 Bilder, 3 Tab. 2015.
ISBN 978-3-87525-380-1.

Band 262: Peter Vatter
Sensitivitätsanalyse des 3-Rollen-Schubbiegens auf Basis der Finite Elemente Methode
LFT, 145 Seiten, 57 Bilder, 26 Tab. 2015.
ISBN 978-3-87525-381-8.

Band 263: Florian Klämpfl
Planung von Laserbestrahlungen durch simulationsbasierte Optimierung
LPT, 169 Seiten, 78 Bilder, 32 Tab. 2015.
ISBN 978-3-87525-384-9.

Band 264: Matthias Domke
Transiente physikalische Mechanismen bei der Laserablation von dünnen Metallschichten
LPT, 133 Seiten, 43 Bilder, 3 Tab. 2015.
ISBN 978-3-87525-385-6.

Band 265: Johannes Götz
Community-basierte Optimierung des Anlagenengineerings
FAPS, 177 Seiten, 80 Bilder, 30 Tab. 2015.
ISBN 978-3-87525-386-3.

Band 266: Hung Nguyen
Qualifizierung des Potentials von Verfestigungseffekten zur Erweiterung des Umformvermögens aushärtbarer Aluminiumlegierungen
LFT, 137 Seiten, 57 Bilder, 16 Tab. 2015.
ISBN 978-3-87525-387-0.

Band 267: Andreas Kuppert
Erweiterung und Verbesserung von Versuchs- und Auswertetechniken für die Bestimmung von Grenzformänderungskurven
LFT, 138 Seiten, 82 Bilder, 2 Tab. 2015.
ISBN 978-3-87525-388-7.

Band 268: Kathleen Klaus
Erstellung eines Werkstofforientierten Fertigungsprozessfensters zur Steigerung des Formgebungsvermögens von Aluminiumlegierungen unter Anwendung einer zwischengeschalteten Wärmebehandlung
LFT, 154 Seiten, 70 Bilder, 8 Tab. 2015.
ISBN 978-3-87525-391-7.

Band 269: Thomas Svec
Untersuchungen zur Herstellung von funktionsoptimierten Bauteilen im partiellen Presshärtprozess mittels lokal unterschiedlich temperierter Werkzeuge
LFT, 166 Seiten, 87 Bilder, 15 Tab. 2015.
ISBN 978-3-87525-392-4.

Band 270: Tobias Schrader
Grundlegende Untersuchungen zur Verschleißcharakterisierung beschichteter Kaltmassivumformwerkzeuge
LFT, 164 Seiten, 55 Bilder, 11 Tab. 2015.
ISBN 978-3-87525-393-1.

Band 271: Matthäus Brela
Untersuchung von Magnetfeld-Messmethoden zur ganzheitlichen Wertschöpfungsoptimierung und Fehlerdetektion an magnetischen Aktoren
FAPS, 170 Seiten, 97 Bilder, 4 Tab. 2015.
ISBN 978-3-87525-394-8.

Band 272: Michael Wieland
Entwicklung einer Methode zur Prognose adhäsiven Verschleißes an Werkzeugen für das direkte Presshärten
LFT, 156 Seiten, 84 Bilder, 9 Tab. 2015.
ISBN 978-3-87525-395-5.

Band 273: René Schramm
Strukturierte additive Metallisierung durch kaltaktives Atmosphärendruckplasma
FAPS, 136 Seiten, 62 Bilder, 15 Tab. 2015.
ISBN 978-3-87525-396-2.

Band 274: Michael Lechner
Herstellung beanspruchungsangepasster Aluminiumblechhalbzeuge durch eine maßgeschneiderte Variation der Abkühlgeschwindigkeit nach Lösungsglühen
LFT, 136 Seiten, 62 Bilder, 15 Tab. 2015.
ISBN 978-3-87525-397-9.

Band 275: Kolja Andreas
Einfluss der Oberflächenbeschaffenheit auf das Werkzeugeinsatzverhalten beim Kaltfließpressen
LFT, 169 Seiten, 76 Bilder, 4 Tab. 2015.
ISBN 978-3-87525-398-6.

Band 276: Marcus Baum
Laser Consolidation of ITO Nanoparticles for the Generation of Thin Conductive Layers on Transparent Substrates
LPT, 158 Seiten, 75 Bilder, 3 Tab. 2015.
ISBN 978-3-87525-399-3.

Band 277: Thomas Schneider
Umformtechnische Herstellung dünnwandiger Funktionsbauteile aus Feinblech durch Verfahren der Blechmassivumformung
LFT, 188 Seiten, 95 Bilder, 7 Tab. 2015.
ISBN 978-3-87525-401-3.

Band 278: Jochen Merhof
Sematische Modellierung automatisierter Produktionssysteme zur Verbesserung der IT-Integration zwischen Anlagen-Engineering und Steuerungsebene
FAPS, 157 Seiten, 88 Bilder, 8 Tab. 2015.
ISBN 978-3-87525-402-0.

Band 279: Fabian Zöller
Erarbeitung von Grundlagen zur Abbildung des tribologischen Systems in der Umformsimulation
LFT, 126 Seiten, 51 Bilder, 3 Tab. 2016.
ISBN 978-3-87525-403-7.

Band 280: Christian Hezler
Einsatz technologischer Versuche zur Erweiterung der Versagensvorhersage bei Karosseriebauteilen aus höchstfesten Stählen
LFT, 147 Seiten, 63 Bilder, 44 Tab. 2016.
ISBN 978-3-87525-404-4.

Band 281: Jochen Bönig
Integration des Systemverhaltens von Automobil-Hochvoltleitungen in die virtuelle Absicherung durch strukturmechanische Simulation
FAPS, 177 Seiten, 107 Bilder, 17 Tab. 2016.
ISBN 978-3-87525-405-1.

Band 282: Johannes Kohl
Automatisierte Datenerfassung für diskret ereignisorientierte Simulationen in der energieflexibelen Fabrik
FAPS, 160 Seiten, 80 Bilder, 27 Tab. 2016.
ISBN 978-3-87525-406-8.

Band 283: Peter Bechtold
Mikroschockwellenumformung mittels ultrakurzer Laserpulse
LPT, 155 Seiten, 59 Bilder, 10 Tab. 2016.
ISBN 978-3-87525-407-5.

Band 284: Stefan Berger
Laserstrahlschweißen thermoplastischer Kohlenstofffaserverbundwerkstoffe mit spezifischem Zusatzdraht
LPT, 118 Seiten, 68 Bilder, 9 Tab. 2016.
ISBN 978-3-87525-408-2.

Band 285: Martin Bornschlegl
Methods-Energy Measurement - Eine Methode zur Energieplanung für Fügeverfahren im Karosseriebau
FAPS, 136 Seiten, 72 Bilder, 46 Tab. 2016.
ISBN 978-3-87525-409-9.

Band 286: Tobias Rackow
Erweiterung des Unternehmenscontrollings um die Dimension Energie
FAPS, 164 Seiten, 82 Bilder, 29 Tab. 2016.
ISBN 978-3-87525-410-5.

Band 287: Johannes Koch
Grundlegende Untersuchungen zur Herstellung zyklisch-symmetrischer Bauteile mit Nebenformelementen durch Blechmassivumformung
LFT, 125 Seiten, 49 Bilder, 17 Tab. 2016.
ISBN 978-3-87525-411-2.

Band 288: Hans Ulrich Vierzigmann
Beitrag zur Untersuchung der tribologischen Bedingungen in der Blechmassivumformung - Bereitstellung von tribologischen Modellversuchen und Realisierung von Tailored Surfaces
LFT, 174 Seiten, 102 Bilder, 34 Tab. 2016.
ISBN 978-3-87525-412-9.

Band 289: Thomas Senner
Methodik zur virtuellen Absicherung der formgebenden Operation des Nasspressprozesses von Gelege-Mehrschichtverbunden
LFT, 156 Seiten, 96 Bilder, 21 Tab. 2016.
ISBN 978-3-87525-414-3.

Band 290: Sven Kreitlein
Der grundoperationsspezifische Mindestenergiebedarf als Referenzwert zur Bewertung der Energieeffizienz in der Produktion
FAPS, 185 Seiten, 64 Bilder, 30 Tab. 2016.
ISBN 978-3-87525-415-0.

Band 291: Christian Roos
Remote-Laserstrahlschweißen verzinkter Stahlbleche in Kehlnahtgeometrie
LPT, 123 Seiten, 52 Bilder, 0 Tab. 2016.
ISBN 978-3-87525-416-7.

Band 292: Alexander Kahrimanidis
Thermisch unterstützte Umformung von Aluminiumblechen
LFT, 165 Seiten, 103 Bilder, 18 Tab. 2016.
ISBN 978-3-87525-417-4.

Band 293: Jan Tremel
Flexible Systems for Permanent Magnet Assembly and Magnetic Rotor Measurement / Flexible Systeme zur Montage von Permanentmagneten und zur Messung magnetischer Rotoren
FAPS, 152 Seiten, 91 Bilder, 12 Tab. 2016.
ISBN 978-3-87525-419-8.

Band 294: Ioannis Tsoupis
Schädigungs- und Versagensverhalten hochfester Leichtbauwerkstoffe unter Biegebeanspruchung
LFT, 176 Seiten, 51 Bilder, 6 Tab. 2017.
ISBN 978-3-87525-420-4.

Band 295: Sven Hildering
Grundlegende Untersuchungen zum Prozessverhalten von Silizium als Werkzeugwerkstoff für das Mikroscherschneiden metallischer Folien
LFT, 177 Seiten, 74 Bilder, 17 Tab. 2017.
ISBN 978-3-87525-422-8.

Band 296: Sasia Mareike Hertweck
Zeitliche Pulsformung in der Lasermikromaterialbearbeitung – Grundlegende Untersuchungen und Anwendungen
LPT, 146 Seiten, 67 Bilder, 5 Tab. 2017.
ISBN 978-3-87525-423-5.

Band 297: Paryanto
Mechatronic Simulation Approach for the Process Planning of Energy-Efficient Handling Systems
FAPS, 162 Seiten, 86 Bilder, 13 Tab. 2017.
ISBN 978-3-87525-424-2.

Band 298: Peer Stenzel
Großserientaugliche Nadelwickeltechnik für verteilte Wicklungen im Anwendungsfall der E-Traktionsantriebe
FAPS, 239 Seiten, 147 Bilder, 20 Tab. 2017.
ISBN 978-3-87525-425-9.

Band 299: Mario Lušić
Ein Vorgehensmodell zur Erstellung montageführender Werkerinformationssysteme simultan zum Produktentstehungsprozess
FAPS, 174 Seiten, 79 Bilder, 22 Tab. 2017.
ISBN 978-3-87525-426-6.

Band 300: Arnd Buschhaus
Hochpräzise adaptive Steuerung und Regelung robotergeführter Prozesse
FAPS, 202 Seiten, 96 Bilder, 4 Tab. 2017.
ISBN 978-3-87525-427-3.

Band 301: Tobias Laumer
Erzeugung von thermoplastischen Werkstoffverbunden mittels simultanem, intensitätsselektivem Laserstrahlschmelzen
LPT, 140 Seiten, 82 Bilder, 0 Tab. 2017.
ISBN 978-3-87525-428-0.

Band 302: Nora Unger
Untersuchung einer thermisch unterstützten Fertigungskette zur Herstellung umgeformter Bauteile aus der höherfesten Aluminiumlegierung EN AW-7020
LFT, 142 Seiten, 53 Bilder, 8 Tab. 2017.
ISBN 978-3-87525-429-7.

Band 303: Tommaso Stellin
Design of Manufacturing Processes for the Cold Bulk Forming of Small Metal Components from Metal Strip
LFT, 146 Seiten, 67 Bilder, 7 Tab. 2017.
ISBN 978-3-87525-430-3.

Band 304: Bassim Bachy
Experimental Investigation, Modeling, Simulation and Optimization of Molded Interconnect Devices (MID) Based on Laser Direct Structuring (LDS) / Experimentelle Untersuchung, Modellierung, Simulation und Optimierung von Molded Interconnect Devices (MID) basierend auf Laser Direktstrukturierung (LDS)
FAPS, 168 Seiten, 120 Bilder, 26 Tab. 2017.
ISBN 978-3-87525-431-0.

Band 305: Michael Spahr
Automatisierte Kontaktierungsverfahren für flachleiterbasierte Pkw-Bordnetzsysteme
FAPS, 197 Seiten, 98 Bilder, 17 Tab. 2017.
ISBN 978-3-87525-432-7.

Band 306: Sebastian Suttner
Charakterisierung und Modellierung des spannungszustandsabhängigen Werkstoffverhaltens der Magnesiumlegierung AZ31B für die numerische Prozessauslegung
LFT, 150 Seiten, 84 Bilder, 19 Tab. 2017.
ISBN 978-3-87525-433-4.

Band 307: Bhargav Potdar
A reliable methodology to deduce thermo-mechanical flow behaviour of hot stamping steels
LFT, 203 Seiten, 98 Bilder, 27 Tab. 2017.
ISBN 978-3-87525-436-5.

Band 308: Maria Löffler
Steuerung von Blechmassivumformprozessen durch maßgeschneiderte tribologische Systeme
LFT, viii u. 166 Seiten, 90 Bilder, 5 Tab. 2018. ISBN 978-3-96147-133-1.

Band 309: Martin Müller
Untersuchung des kombinierten Trenn- und Umformprozesses beim Fügen artungleicher Werkstoffe mittels Schneidclinchverfahren
LFT, xi u. 149 Seiten, 89 Bilder, 6 Tab. 2018. ISBN: 978-3-96147-135-5.

Band 310: Christopher Kästle
Qualifizierung der Kupfer-Drahtbondtechnologie für integrierte Leistungsmodule in harschen Umgebungsbedingungen
FAPS, xii u. 167 Seiten, 70 Bilder, 18 Tab. 2018. ISBN 978-3-96147-145-4.

Band 311: Daniel Vipavc
Eine Simulationsmethode für das 3-Rollen-Schubbiegen
LFT, xiii u. 121 Seiten, 56 Bilder, 17 Tab. 2018. ISBN 978-3-96147-147-8.

Band 312: Christina Ramer
Arbeitsraumüberwachung und autonome Bahnplanung für ein sicheres und flexibles Roboter-Assistenzsystem in der Fertigung
FAPS, xiv u. 188 Seiten, 57 Bilder, 9 Tab. 2018. ISBN 978-3-96147-153-9.

Band 313: Miriam Rauer
Der Einfluss von Poren auf die Zuverlässigkeit der Lötverbindungen von Hochleistungs-Leuchtdioden
FAPS, xii u. 209 Seiten, 108 Bilder, 21 Tab. 2018. ISBN 978-3-96147-157-7.

Band 314: Felix Tenner

Kamerabasierte Untersuchungen der Schmelze und Gasströmungen beim Laserstrahlschweißen verzinkter Stahlbleche

LPT, xxiii u. 184 Seiten, 94 Bilder, 7 Tab.
2018. ISBN 978-3-96147-160-7.

Band 315: Aarief Syed-Khaja

Diffusion Soldering for High-temperature Packaging of Power Electronics

FAPS, x u. 202 Seiten, 144 Bilder, 32 Tab.
2018. ISBN 978-3-87525-162-1.

Band 316: Adam Schaub

Grundlagenwissenschaftliche Untersuchung der kombinierten Prozesskette aus Umformen und Additive Fertigung

LFT, xi u. 192 Seiten, 72 Bilder, 27 Tab.
2019. ISBN 978-3-96147-166-9.

Band 317: Daniel Gröbel

Herstellung von Nebenformelementen unterschiedlicher Geometrie an Blechen mittels Fließpressverfahren der Blechmassivumformung

LFT, x u. 165 Seiten, 96 Bilder, 13 Tab.
2019. ISBN 978-3-96147-168-3.

Band 318: Philipp Hildenbrand

Entwicklung einer Methodik zur Herstellung von Tailored Blanks mit definierten Halbzeugeigenschaften durch einen Taumelprozess

LFT, ix u. 153 Seiten, 77 Bilder, 4 Tab.
2019. ISBN 978-3-96147-174-4.

Band 319: Tobias Konrad

Simulative Auslegung der Spann- und Fixierkonzepte im Karosserierohbau: Bewertung der Baugruppenmaßhaltigkeit unter Berücksichtigung schwankender Einflussgrößen

LFT, x u. 203 Seiten, 134 Bilder, 32 Tab.
2019. ISBN 978-3-96147-176-8.

Band 320: David Meinel

Architektur applikationsspezifischer Multi-Physics-Simulationskonfiguratoren am Beispiel modularer Triebzüge

FAPS, xii u. 166 Seiten, 82 Bilder, 25 Tab.
2019. ISBN 978-3-96147-184-3.

Band 321: Andrea Zimmermann

Grundlegende Untersuchungen zum Einfluss fertigungsbedingter Eigenschaften auf die Ermüdungsfestigkeit kaltmassivumgeformter Bauteile

LFT, ix u. 160 Seiten, 66 Bilder, 5 Tab.
2019. ISBN 978-3-96147-190-4.

Band 322: Christoph Amann

Simulative Prognose der Geometrie nassgepresster Karosseriebauteile aus Gelege-Mehrschichtverbunden

LFT, xvi u. 169 Seiten, 80 Bilder, 13 Tab.
2019. ISBN 978-3-96147-194-2.

Band 323: Jennifer Tenner

Realisierung schmierstofffreier Tiefziehprozesse durch maßgeschneiderte Werkzeugoberflächen

LFT, x u. 187 Seiten, 68 Bilder, 13 Tab.
2019. ISBN 978-3-96147-196-6.

Band 324: Susan Zöller

Mapping Individual Subjective Values to Product Design

KTmfk, xi u. 223 Seiten, 81 Bilder, 25 Tab.
2019. ISBN 978-3-96147-202-4.

Band 325: Stefan Lutz

Erarbeitung einer Methodik zur semiempirischen Ermittlung der Umwandlungskinetik durchhärtender Wälzlagerstähle für die Wärmebehandlungssimulation

LFT, xiv u. 189 Seiten, 75 Bilder, 32 Tab. 2019. ISBN 978-3-96147-209-3.

Band 326: Tobias Gnibl

Modellbasierte Prozesskettenabbildung rührreibgeschweißter Aluminiumhalbzeuge zur umformtechnischen Herstellung höchstfester Leichtbaustrukturteile

LFT, xii u. 167 Seiten, 68 Bilder, 17 Tab. 2019. ISBN 978-3-96147-217-8.

Band 327: Johannes Bürner

Technisch-wirtschaftliche Optionen zur Lastflexibilisierung durch intelligente elektrische Wärmespeicher

FAPS, xiv u. 233 Seiten, 89 Bilder, 27 Tab. 2019. ISBN 978-3-96147-219-2.

Band 328: Wolfgang Böhm

Verbesserung des Umformverhaltens von mehrlagigen Aluminiumblechwerkstoffen mit ultrafeinkörnigem Gefüge

LFT, ix u. 160 Seiten, 88 Bilder, 14 Tab. 2019. ISBN 978-3-96147-227-7.

Band 329: Stefan Landkammer

Grundsatzuntersuchungen, mathematische Modellierung und Ableitung einer Auslegungsmethodik für Gelenkantriebe nach dem Spinnenbeinprinzip

LFT, xii u. 200 Seiten, 83 Bilder, 13 Tab. 2019. ISBN 978-3-96147-229-1.

Band 330: Stephan Rapp

Pump-Probe-Ellipsometrie zur Messung transienter optischer Materialeigenschaften bei der Ultrakurzpuls-Lasermaterialbearbeitung

LPT, xi u. 143 Seiten, 49 Bilder, 2 Tab. 2019. ISBN 978-3-96147-235-2.

Band 331: Michael Scholz

Intralogistics Execution System mit integrierten autonomen, servicebasierten Transportentitäten

FAPS, xi u. 195 Seiten, 55 Bilder, 11 Tab. 2019. ISBN 978-3-96147-237-6.

Band 332: Eva Bogner

Strategien der Produktindividualisierung in der produzierenden Industrie im Kontext der Digitalisierung

FAPS, ix u. 201 Seiten, 55 Bilder, 28 Tab. 2019. ISBN 978-3-96147-246-8.

Band 333: Daniel Benjamin Krüger

Ein Ansatz zur CAD-integrierten muskuloskelettalen Analyse der Mensch-Maschine-Interaktion

KTmfk, x u. 217 Seiten, 102 Bilder, 7 Tab. 2019. ISBN 978-3-96147-250-5.

Band 334: Thomas Kuhn

Qualität und Zuverlässigkeit laserdirektstrukturierter mechatronisch integrierter Baugruppen (LDS-MID)

FAPS, ix u. 152 Seiten, 69 Bilder, 12 Tab. 2019. ISBN: 978-3-96147-252-9.

Band 335: Hans Fleischmann
Modellbasierte Zustands- und Prozessüberwachung auf Basis sozio-cyber-physischer Systeme
FAPS, xi u. 214 Seiten, 111 Bilder, 18 Tab.
2019. ISBN: 978-3-96147-256-7.

Band 336: Markus Michalski
Grundlegende Untersuchungen zum Prozess- und Werkstoffverhalten bei schwingungsüberlagerter Umformung
LFT, xii u. 197 Seiten, 93 Bilder, 11 Tab.
2019. ISBN: 978-3-96147-270-3.

Band 337: Markus Brandmeier
Ganzheitliches ontologiebasiertes Wissensmanagement im Umfeld der industriellen Produktion
FAPS, xi u. 255 Seiten, 77 Bilder, 33 Tab.
2020. ISBN: 978-3-96147-275-8.

Band 338: Stephan Purr
Datenerfassung für die Anwendung lernender Algorithmen bei der Herstellung von Blechformteilen
LFT, ix u. 165 Seiten, 48 Bilder, 4 Tab.
2020. ISBN: 978-3-96147-281-9.

Band 339: Christoph Kiener
Kaltfließpressen von gerad- und schrägverzahnten Zahnrädern
LFT, viii u. 151 Seiten, 81 Bilder, 3 Tab.
2020. ISBN 978-3-96147-287-1.

Band 340: Simon Spreng
Numerische, analytische und empirische Modellierung des Heißcrimpprozesses
FAPS, xix u. 204 Seiten, 91 Bilder, 27 Tab.
2020. ISBN 978-3-96147-293-2.

Band 341: Patrik Schwingenschlögl
Erarbeitung eines Prozessverständnisses zur Verbesserung der tribologischen Bedingungen beim Presshärten
LFT, x u. 177 Seiten, 81 Bilder, 8 Tab.
2020. ISBN 978-3-96147-297-0.

Band 342: Emanuela Affronti
Evaluation of failure behaviour of sheet metals
LFT, ix u. 136 Seiten, 57 Bilder, 20 Tab.
2020. ISBN 978-3-96147-303-8.

Band 343: Julia Degner
Grundlegende Untersuchungen zur Herstellung hochfester Aluminiumblechbauteile in einem kombinierten Umform- und Abschreckprozess
LFT, x u. 172 Seiten, 61 Bilder, 9 Tab.
2020. ISBN 978-3-96147-307-6.

Band 344: Maximilian Wagner
Automatische Bahnplanung für die Aufteilung von Prozessbewegungen in synchrone Werkstück- und Werkzeugbewegungen mittels Multi-Roboter-Systemen
FAPS, xxi u. 181 Seiten, 111 Bilder, 15 Tab.
2020. ISBN 978-3-96147-309-0.

Band 345: Stefan Härter
Qualifizierung des Montageprozesses hochminiaturisierter elektronischer Bauelemente
FAPS, ix u. 194 Seiten, 97 Bilder, 28 Tab.
2020. ISBN 978-3-96147-314-4.

Band 346: Toni Donhauser
Ressourcenorientierte Auftragsregelung in einer hybriden Produktion mittels betriebsbegleitender Simulation
FAPS, xix u. 242 Seiten, 97 Bilder, 17 Tab.
2020. ISBN 978-3-96147-316-8.

Band 347: Philipp Amend
Laserbasiertes Schmelzkleben von Thermoplasten mit Metallen
LPT, xv u. 154 Seiten, 67 Bilder
2020. ISBN 978-3-96147-326-7.

Band 348: Matthias Ehlert
Simulationsunterstützte funktionale Grenzlagenabsicherung
KTmfk, xvi u. 300 Seiten, 101 Bilder,
73 Tab. 2020. ISBN 978-3-96147-328-1.

Band 349: Thomas Sander
Ein Beitrag zur Charakterisierung und Auslegung des Verbundes von Kunststoffsubstraten mit harten Dünnschichten
KTmfk, xiv u. 178 Seiten, 88 Bilder, 21 Tab. 2020. ISBN 978-3-96147-330-4

Band 350: Florian Pilz
Fließpressen von Verzahnungselementen an Blechen
LFT, x u. 170 Seiten, 103Bilder, 4 Tab.
2020. ISBN 978-3-96147-332-8

Band 351: Sebastian Josef Katona
Evaluation und Aufbereitung von Produktsimulationen mittels abweichungsbehafteter Geometriemodelle
KTmfk, ix u. 147 Seiten, 73 Bilder, 11 Tab.
2020. ISBN 978-3-96147-336-6

Band 352: Jürgen Herrmann
Kumulatives Walzplattieren. Bewertung der Umformeigenschaften mehrlagiger Blechwerkstoffe der ausscheidungshärtbaren Legierung AA6014
LFT, x u. 157 Seiten, 64 Bilder, 5 Tab.
2020. ISBN 978-3-96147-344-1

Band 353: Christof Küstner
Assistenzsystem zur Unterstützung der datengetriebenen Produktentwicklung
KTmfk, xii u. 219 Seiten, 63 Bilder, 14 Tab.
2020. ISBN 978-3-96147-348-9

Band 354: Tobias Gläßel
Prozessketten zum Laserstrahlschweißen von flachleiterbasierten Formspulenwicklungen für automobile Traktionsantriebe
FAPS, xiv u. 206 Seiten, 89 Bilder, 11 Tab.
2020. ISBN 978-3-96147-356-4.

Band 355: Andreas Meinel
Experimentelle Untersuchung der Auswirkungen von Axialschwingungen auf Reibung und Verschleiß in Zylinderrollenlagern
KTmfk, xii u. 162 Seiten, 56 Bilder, 7 Tab.
2020. ISBN 978-3-96147-358-8

Band 356: Hannah Riedle
Haptische, generische Modelle weicher anatomischer Strukturen für die chirurgische Simulation
FAPS, xxx u. 179 Seiten, 82 Bilder, 35 Tab.
2020. ISBN 978-3-96147-367-0

Band 357: Maximilian Landgraf
Leistungselektronik für den Einsatz dielektrischer Elastomere in aktorischen, sensorischen und integrierten sensomotorischen Systemen
FAPS, xxiii u. 166 Seiten, 71 Bilder, 10 Tab.2020. ISBN 978-3-96147-380-9

Band 358: Alireza Esfandyari
Multi-Objective Process Optimization for Overpressure Reflow Soldering in Electronics Production
FAPS, xviii u. 175 Seiten, 57 Bilder, 23 Tab.
2020. ISBN 978-3-96147-382-3

Abstract

Die Surface Mount Technology (SMT) ist das primäre Verfahren, um elektronische Komponenten dauerhaft auf einem Substrat zu befestigen. Eine entscheidende Qualitätssteigerung der Verbindungstechnologien wird durch die Erhöhung der Zuverlässigkeit der Lötverbindung und eine geringere Wärmeabstrahlung erzielt. Die Lötofentechnik in Kombination mit einem Überdruckmodul ermöglicht Void-freie Lötstellen. Jedoch ist die Konfiguration des prozessbezogenen Mechanismus noch nicht vollständig untersucht. Darüber hinaus ist die auf dem Markt angebotene Methode energieintensiv, und eine eingehende Untersuchung des Ressourcenflusses in den Prozess ist zwingend erforderlich, wenn eine Minimierung des Verbrauchs erreicht werden will.

Diese Arbeit befasst sich mit einer multikriteriellen/gesamtheitlichen Optimierungslösung, die auf einem Trade-off-Modell für Qualitäts-, Energie-, Kosten- und Zeitkriterien basiert. Es ist nicht möglich eine ganzheitlich optimierte Mehrkriterienlösung zu konfigurieren jedoch lässt sich der ansatz formulieren für jedes Kriterium die optimale Lösung zu finden. Mittels Signifikanzanalyse wird ein Kriterienansatz für den Überdrucklötprozess definiert, um jedes Ziel bzw. Kriterium durch ein ANN-Modell zu maximieren oder zu minimieren. Es wurde ein Kompromissmodell entwickelt, mit dem der Entscheidungsträger in der Lage ist, das Setup-Ziel unter bestmöglicher Berücksichtigung der teilweise konträren Anforderungen zu erreichen.

Surface Mount Technology (SMT) is the primary method of permanently mounting electronic components on a substrate. A decisive improvement in the quality of the connection technologies is achieved by increasing the reliability of the solder joints and reducing heat dissipation. The soldering oven technology in combination with an overpressure module enables void-free solder joints. However, the configuration of the process-related mechanism has not yet been fully investigated. In addition, the method offered in the market is energy-intensive, and a deep understanding of the resource flow into the process is mandatory if minimization of consumption is to be achieved.

This study deals with a multi-criteria/overall optimization solution based on a trade-off model for quality, energy, cost and time criteria. The approach to find the optimal solution for each criterion is possible. However, a holistically optimized multi-criteria solution is not possible. Using significance analysis a criteria approach for the overpressure soldering process is defined to maximize or minimize each goal/criterion using Artificial Neural Network (ANN) modeling approach. A compromise model has been developed, which enables the decision maker to achieve the setup goal while considering the conflicting requirements in the best possible approach.

ISBN 978-3-96147-382-3

FAU UNIVERSITY PRESS 2020